Hydrodynamic Design of Ship Bulbous Bows Considering Seaway and Operational Conditions

vorgelegt von

Gonzalo Tampier Brockhaus

aus Chile

von der Fakultät V - Verkehrs- und Maschinensysteme
der Technischen Universität Berlin
zur Erlangung des Akademischen Grades

Doktor der Ingenieurwissenschaften
- Dr.-Ing -

genehmigte Dissertation

Promotionsausschuss:

Vorsitzender:	Prof. Dr. rer. nat. Heinz Lehr
Berichter:	Prof. Dr.-Ing. Andrés Cura Hochbaum
Berichter:	Prof. Dr.-Ing. Apostolos Papanikolaou

Tag der wissenschaftlichen Aussprache: 30. September 2010

Berlin 2011
D 83

Danksagung

Ich möchte diese Danksagung auf Deutsch schreiben, obwohl ich diese Arbeit auf Englisch verfasst habe, denn es handelt sich größtenteils um Personen, die ich mit meinem Aufenthalt in Deutschland verbinde, denen ich diese Danksagung widme.

An erster Stelle möchte ich mich bei meinem Betreuer und Hauptberichter dieser Dissertation, Prof. Dr.-Ing. Andrés Cura Hochbaum, für seine permanente Unterstützung, aktive Betreuung und wertvolle Kritik bedanken. Gerne hätte ich mir gewünscht, dass Prof. Cura seinen Dienst früher angetreten hätte und ich so seine Betreuung über eine längere Zeit hätte genießen können. Auch bei meinem Betreuer und zweiten Berichter dieser Dissertation, Prof. Dr.-Ing. Apostolos Papanikolaou, möchte ich mich für seine Unterstützung und wertvolle Kritik bedanken. Für seine Bereitschaft, jede meiner Fragen mit Geduld und praktischen Hinweisen zu beantworten bin ich ihm besonders dankbar.

An gleich wichtiger Stelle möchte ich meine Dankbarkeit an meinen langjährigen Mentor und geistigen Vater dieser Arbeit, Dr.-Ing. Alfred Kracht, zum Ausdruck bringen. Sein Glauben an meine Person, die stetige Unterstützung und die Güte, mir das Gefühl vermittelt zu haben, mit ihm für jedes Problem oder Fragestellung rechnen zu können, sind für mich über diese gesamte Zeit von größter Bedeutung gewesen.

Für die langjährige Zusammenarbeit und Unterstützung möchte ich mich auch bei Dr.-Ing. Stefan Harries und Dr.-Ing. Karsten Hochkirch bedanken. Für ihr stetes Interesse an den Fortschritten meiner Arbeit, ihre Unterstützung mit Hinweisen und Diskussionen, aber auch für die zur Verfügung gestellte Software, bin ich ihnen besonders dankbar.

Auch meinen ehemaligen Kollegen Dr.-Ing. Jörn Hinnenthal und Felix Fliege möchte ich auf diesem Weg danken. Ihr Vertrauen und ihr Einsatz ermöglichte überhaupt erst meine Ankunft an der Technischen Universität Berlin. Unsere Zusammenarbeit und wertvollen Diskussionen während der darauffolgenden Jahre werden für mich als eine der prägendsten Erinnerungen an meine Zeit an dieser Universität bleiben. Auch meinen aktuellen Kollegen und Mitarbeitern des gesamten Bereiches der Schiffs- und Meerestechnik gilt ein großes Dankeschön, insbesondere meinem Kollegen Christian Eckl für seine Unterstützung und großartige Zusammenarbeit in der letzten Zeit.

Auch bei meinen Freunden und bei meiner Familie, sowohl hier in Deutschland als auch in Chile, möchte ich mich herzlichst für jede einzelne kleine und große Hilfestellung bedanken.

Zuletzt schulde ich die größte Dankbarkeit meiner geliebten Ehefrau Andrea Sacher. Diese Arbeit ist zu einem großen Teil auch ihre Arbeit, denn die gleiche Energie, die ich für diese Arbeit eingesetzt habe, und die damit verbundenen Stunden der physischen und geistigen Abwesenheit, hat sie mit viel Verständnis, Geduld und Stärke für unsere Familie und mit Begeisterung, Optimismus und Freude für unsere gemeinsamen Projekte

eingesetzt.

Meinen Söhnen, Anton und Bruno, widme ich in diesem Sinne nicht die Inhalte dieser Arbeit, sondern vielmehr alle positiven Auswirkungen, die diese Arbeit und dieser Abschluss für unser gemeinsames Familienleben haben mögen.

Berlin, August 2010 – Gonzalo Tampier B.

Contents

List of Figures

List of Tables

Nomenclature

WCS	:	world coordinate system	–
SCS	:	ship coordinate system	–
ICS	:	inertial coordinate system	–
HCS	:	hybrid coordinate system	–
g	:	gravitational constant ($g = 9.81$)	m^2/s
ρ	:	water density	kg/m^3
ρ_A	:	air density	kg/m^3
B	:	ship breadth	m
L_{PP}	:	length between perpendiculars	m
L_{WL}	:	waterline length	m
T	:	mean draft	m
T_{AP}	:	draft at aft perpendicular	m
T_{FP}	:	draft at forward perpendicular	m
∇	:	displacement volume	m^3
Δ	:	displacment force (buoyancy)	N
m	:	mass	kg
I	:	inertia tensor	m^4
S	:	wetted surface	m^2
A_{WL}	:	waterplane area	m^2
$\overline{GM}_T$	:	transversal metacentric height	m
$\overline{GM}_L$	:	longitudinal metacentric height	m
C_B	:	block coefficient	–
C_P	:	prismatic coefficient	–
C_{WP}	:	waterplane coefficient	–
C_M	:	midship section coefficient	–
x_{CB}	:	longitudinal center of bouyancy	m
z_{CB}	:	vertical center of bouyancy	m
λ	:	scaling factor	–
F_n	:	Froude number	–
R_n	:	Reynolds number	–
C_W	:	wave resistance coefficient	–
C_R	:	residual resistance coefficient	–
C_p	:	pressure resistance coefficient	–
C_F	:	frictional resistance coefficient	–
C_{PV}	:	pressure viscous resistance coefficient	–
C_{T0}	:	total calm water resistance coefficient	–
C_{AW}	:	dimensionless added resistance in waves	–
C_{Ap}	:	appendage resistance coefficient	–

C_{AA}	:	wind resistance coefficient	–
C_{St}	:	resistance coefficient due to steering	–
C_A	:	model-ship correlation factor	–
Δc_{AR}	:	resistance coefficient for roughness increase due to fouling	–
C_{TS}	:	total resistance coefficient under service conditions	–
R	:	resistance (indexes as for resistance coefficients)	N
V_S	:	ship speed	$^{\mathrm{m}}/_{\mathrm{s}}$
K_T	:	thrust coefficient	–
K_Q	:	torque coefficient	–
J	:	propeller advance ratio	–
η_0	:	propeller open water efficiency	–
η_R	:	relative rotative efficiency	–
η_H	:	hull efficiency	–
$H_{1/3}$	:	significant wave height	m
T_1	:	mean wave period	s
T_p	:	peak wave period	s
T_e	:	encounter wave period	s
ψ	:	ship course	$^\circ$
ξ_m	:	mean wave direction	$^\circ$
μ	:	encounter wave direction	$^\circ$
ω	:	wave frequency	s^{-1}
ω_e	:	encounter wave frequency	s^{-1}
λ_w	:	wave length	m
ζ_a	:	wave amplitude	m
V_u, V_v	:	wind velocity components	$^{\mathrm{m}}/_{\mathrm{s}}$
V_{WA}	:	apparent wind velocity	$^{\mathrm{m}}/_{\mathrm{s}}$
α_{WA}	:	apparent wind angle	$^\circ$
η_1	:	surge motion	m
η_2	:	sway motion	m
η_3	:	heave motion	m
η_4	:	roll motion	m
η_5	:	pitch motion	m
η_6	:	yaw motion	m
AAC	:	average annual costs	$^{\$}/_{\mathrm{year}}$
CF	:	annual fuel costs	$^{\$}/_{\mathrm{year}}$
CO	:	annual fixed operational costs	$^{\$}/_{\mathrm{year}}$
P	:	invested capital	\$
CR	:	capital recovery factor	year^{-1}
W_{PL}	:	design payload	t
MC	:	annual mean cargo	$^{\mathrm{t\cdot nm}}/_{\mathrm{year}}$

RFR	:	required freight rate	$^{\$}/_{\mathrm{tnm}}$
FEC	:	fuel equivalent costs	$^{\$}/_{\mathrm{tnm}}$
k_f	:	fuel costs coefficient	$^{\$}/_{\mathrm{tnm}}$
n	:	rate of revolutions	s^{-1}
rpm	:	rate of revolutions per minute	min^{-1}
MCR	:	maximum continuous rating	kW
mep	:	mean effective pressure	Pa
$sfoc$	:	specific fuel oil consumption	$^{\mathrm{g}}/_{\mathrm{W\cdot h}}$

Abstract

In the present work, long-term operational simulations within a hydrodynamic ship design procedure were conducted, in which specifically the hydrodynamic design of bulbous bows is explored. In this approach, the operation of the ship considering aspects such as weather, routing and cargo, is simulated over a time period considered statistically representative for the lifetime of the ship. Simulations are finally evaluated on the basis of economic criteria.

In particular, different bulbous bow variants, for different ship sizes and different routes, are systematically studied by the presented approach, and obtained results are assessed within the formulated design procedure. For the simulations, a central aspect is the evaluation of the responses and, in particular, of the added resistance of the ship in waves. For this purpose, an Open Source CFD code is adapted to the needs of the present work and obtained results are compared with available experimental data. Thereafter, further designs are generated by means of parametric variation and are evaluated numerically by the above mentioned CFD code. Obtained results are assessed, showing the dependence in ship size, simulated route and simulational approach, leading to the ranking of the economic indexes of the investigated bulbous bow configurations. The advantage of considering the operational life of the ship within ship design is highlighted and discussed.

Kurzdarstellung

Diese Arbeit zeigt die Anwendung von Langzeitsimulationen für den hydrodynamischen Schiffsentwurf, insbesondere für die Auslegung von Bugwülsten. Die vorgestellte Methodik vereint mehrere beteiligte Aspekte in einer zentralen Entwurfsplattform mit Simulationen, die u.a. Routen, Wetter-, und Beladungszustände mit berücksichtigen, über einen für das Betriebsleben des Schiffes als statistisch repräsentativ ansehbaren Zeitraum. Simulationsergebnisse werden nachfolgend über ökonomische Kriterien bewertet.

Unterschiedliche Bugwulstkonfigurationen, für unterschiedliche Schiffsgrößen und Hochseerouten, werden mit diese Entwurfsmethode untersucht und bewertet. Ein zentraler Punkt für eine gute Vergleichbarkeit zwischen den unterschiedlichen untersuchten Fällen ist eine zuverlässige Methode für die Ermittlung des Verhaltens der Schiffe im Seegang, insbesondere des Zusatzwiderstandes im Seegang. Für diesen Zweck wird ein Open Source CFD-Verfahren an die Erfordernisse dieser Arbeit angepasst und mit verfügbare experimentelle Daten verglichen und validiert. Nachfolgend werden mit einer parametrischen Methode neue Varianten generiert und mit numerischen Verfahren errechnet. Anschließend werden auch für diese Varianten Betriebssimulationen durchgeführt und die erzielten Ergebnisse miteinander verglichen. Die Abhängigkeiten zwischen Schiffsgröße, gefahrener Route und Simulationsmethodik werden aufgezeigt, um die Rangfolge der Wirtschaftlichkeit der untersuchten Varianten zu diskutieren. Schließlich werden die Vorteile der Berücksichtigung des Schiffsbetriebes über die gesamte Lebenszeit im Entwurf herausgestellt und diskutiert.

1. Introduction

1.1. Background

In the present day, keen business competition in a characteristically global maritime market and the growing awareness about the need of reducing global emissions encourages the ship designer to seek for innovative techniques to improve the design of ships and offshore structures. While seeking larger economic profit, greater safety and reduced emissions, the handling of complex tasks in early design stages becomes mandatory attempting, in this way, to find improvements and solutions to a wide range of possible problems which may appear in future design stages or during operation. Normally, these tasks (e.g. hull form optimization, seakeeping performance calculations or general arrangement) have been handled separately and have often been considered as almost independent from each other. The integration of many of these tasks is a promising approach to achieve the desired profit surplus.

Within all aspects of ship design, the development of different numerical and experimental techniques in the field of hydrodynamics in the last decades has made a more in-depth study of many detail aspects possible. For example, the application of CFD (*computational fluid dynamics*) techniques has become a standard tool in industry, and new computational methods are expected to do so in a near future.

The answers provided by these highly specialized techniques alone do not always lead to better designs; integrating these answers into a more global context can, in some cases, be very advantageous. Holistic design, simulation-based design, life cycle design or predictive engineering are some of the many terms used to name this principle, applied in each case slightly differently, but in general terms with many similarities.

In the present work, *simulation-based design* will be applied to improve the transport efficiency of ships, attempting to integrate aspects which are usually considered separately at an early design stage. Rising fuel costs over the last years increase considerably the importance of these within the total costs. Particularly, the influence of fuel in operational costs when considering *off-design* conditions will be studied here. Off-design conditions are defined within this document as loading conditions, service speeds and weather conditions which are different to the design loading condition, design or contract speed and calm weather.

Nowadays, hydrodynamic design of ships is, in many cases, still undertaken for a single design condition with a specified speed, trim and draft and for calm weather, i.e. without considering either wind or waves. These conditions are also normally applied for the optimization of the ship geometry, leading to optimum designs which might potentially have a suboptimal performance outside their design specifications, leading subsequently

to an economic loss. Since most ships operate for considerable amounts of time outside these specified conditions, it can be expected that considering them can be advantageous. This paper presents a procedure which includes relevant operational factors at an early design stage and can thus provide the designer with important informations to achieve an optimum ship design. A simulation environment is implemented and employed for the hydrodynamic design of the bulbous bow of a merchant vessel, modeling environmental, operational and technical characteristics of its operational life and quantifying its performance by an economic index.

1.2. State of the Art

Simulation techniques, especially those where many different tasks are integrated into one system and the performance evaluation process occurs often within an optimization strategy, have experienced a ceaseless development since electronic computers became available for engineering purposes and have found many applications in ship design. For a discussion of the state of the art in this field, one can distinguish between the simulation methods for modeling the operational life of the ship itself and the underlying (*partial simulation*) methods involved, such as those for structural analysis, ship resistance or ship propulsion. Additionally, the integration of these methods into an optimization strategy plays a role in many cases also, a short discussion about this task being appropriate. From this three elements (partial simulations, operational performance assessment and optimization), a design methodology can be defined. The present state of the art will refer to hydrodynamic design methodologies, specifically those considering the effect of off-design conditions (and to a great extent the influence of weather factors). For a more general state of the art in marine design methodology, the reader is referred to the recent publication of Nowacki [86].

A detailed hydrodynamic model for performing an operational simulation needs to consider resistance, propulsion and seakeeping aspects. From these aspects, special attention shall be paid to the added resistance in waves. This has two main reasons: firstly, it is (at least for conventional ships) the largest resistance component not considered accurately in the design conditions (for which, else, very accurate estimations and measurements are undertaken) and, secondly, the commonly applied methodologies are in many cases not accurate enough for the qualitative or even quantitative comparison of design variants[1], or, if then, more accurate but of very recent date, being not enough experience with them to be applied in ship design. For the evaluation of the added resistance in irregular waves over longer time periods, reliable weather information has to be available. This kind of information was first available in the late sixties and, together with the availability of the necessary hydrodynamic and statistical theory, an increased amount of investigations about added resistance in waves could be observed in the following decade. Probably the most important contributions to this theoretical background were strip theory, presented by Grim in 1953 [37], and the probabilistic model of ship motions in irregular seas,

[1]This matter will be discussed in more detail further in section 2.6

presented by St. Denis and Pierson in the same year [107]. Several authors have presented approximation methods for the calculation of added resistance in regular waves, remarking the contributions of Maruo [80] in 1957, Joosen [61] in 1966, Boese [18] in 1970, Gerritsma and Beukelmann [33] in 1972, Salvesen [99] in 1978 and Faltinsen [29] in 1980. All these methods are based on potential theory and contain, to a greater or lesser extent, some of the assumptions made in strip theory[2]. In Pedersen [96], an exhaustive comparison of some of the mentioned methods is performed and critically discussed. In 1986, in a theoretical work, Sakamoto and Baba [98] performed a hull form optimization for minimal added resistance in *short waves*. Although the approximations undertaken were questionable for practical purposes [42], it was shown that optimal hull forms can be designed for minimal added resistance in short waves. In 1998, Matsumoto et al. [81] presented a so-called "beak bow" for full ships such as bulk carriers, obtaining a reduction of the added resistance in waves between 20% to 30% in an experimental investigation. This study also proposed a theoretical formulation for the calculation of the added resistance to take indirect account of the above-water shape of the ship, consisting of simple modifications to linear theory. The method agrees well with experiments for the example shown, but its applicability to a wider range of ship types is questionable.

The development of 3D potential panel codes for seakeeping in the 1970's and 1980's (e.g. Papanikolaou [95], Sclavounos et al. [103], Kring et al. [71], Bertram et al. [12]) brought new perspectives for the prediction of added resistance in waves. For seakeeping calculations solved by nonlinear, time-domain panel codes as presented by Sclavounos et al. [103], results of added resistance fall out directly from seakeeping calculations with an - at least from a theoretical point of view - inherently higher accuracy than linear methods. Nevertheless, two-dimensional methods still remained as a standard tool in industry and have been developed continuously until now. As an example, Kihara et al. [63] [64] presented in 2000 a two-dimensional nonlinear method, calculating in his work the influence of the above-water bow form on the added resistance in waves.

In the late nineties, first investigations on seakeeping with RANS CFD methods were presented, which were followed by many more during the next decade. In 1998, Wilson et al. [111] presented RANS calculations for a Wigley hull and a surface combatant in regular waves, without motions. In 1999, Gentaz et al. [32] showed results for forced oscillation motions in waves from RANS calculations for a Series 60 ship and different wave frequencies and in the same year, Sato et al. [100] calculated ship motions in regular head waves with forward speed. In 2002, Cura Hochbaum et al. [26] calculated the seakeeping characteristics of two ships, showing results of motions and forces (also added resistance in waves), with a RANS-Method. Results were in good agreement with experiments, even for the coarsest grids presented. In 2003, Orihara and Miyata [92] evaluated the added resistance in head waves for a ship with an overlapping grid system. Of special interest is that the authors modified the above-water bow shape to reduce the added resistance in waves of a medium-speed tanker. The calculations were compared with experiments, showing good agreement and demonstrating the ability of complex CFD calculations to be used as a design tool in this field. In 2005, Weymouth et al. [110] calculated the

[2] A short description of strip theory is given in section 2.6.2

motions and forces of a Wigley hull in waves, validating their work extensively with both experimental and potential theory results and in 2006, Xing-Kaeding [112] showed simultaneous simulations of seakeeping and manoeuvring including appendages and a body force model for the propeller. Carrica et al. [23] [22] presented in 2006 and 2007 CFD calculations for ships in waves using a dynamic overset grid, making large amplitude motions possible. In 2007, Luquet et al. [77] presented the application of a SWENSE (Spectral Wave Explicit Navier Stokes Equations) method to study motions and loads of floating bodies in regular and irregular waves, including a calculation example for a Wigley hull in head waves. The achieved progress in this field has lead to the need of extensive validation and verification and the comparison of results between different authors. Of special interest in this matter was the CFD Workshop 2005 in Tokyo [44], where for the first time a ship in waves was considered as a benchmark case[3]. The participants showed the ability of calculating a ship in regular, head waves with their CFD solvers, collecting a detailed validation and verification with experimental data and providing a good overview of the achievable quality with viscous CFD solvers.

As previously mentioned, the integration of different hydrodynamic tasks in the design process is a focal point of this investigation, especially when considering the influence of waves, ship motions and/or the resistance increase due to this. Of special interest is the combination of such methods with systematic hull form variations or optimization strategies.

In the early eighties, Blume (HSVA - Hamburgische Schiffsversuchsanstalt) [16] and Kracht (VWS Berlin - Versuchsanstalt für Wasserbau und Schiffbau) [68] carried out a considerable amount of model tests to investigate the influence of the bulbous bow on the propulsive performance of ships in waves. Both researchers conducted self-propulsion tests in head waves for different ships, considering thrust increase and also separate measurements for speed loss. Blume undertook experiments for three base ships and a total of eleven variants, and after combining his experimental results with strip theory calculations for other wave angles, he superposed these with representative statistical weather data from the North Atlantic to carry out an estimation of the ship performance under service conditions in this region. This approach can be considered as an early operational simulation approach and shows clearly the importance of this task even thirty years ago. Blume concludes that it is probable that extreme bulbous bows with very good calm-water performance can lead to significant speed losses and/or power increase under service conditions. Kracht, in Berlin, undertook similar experiments, although for two families of ships, for which the bulbous bows were variated systematically. The ship lines represent a fast cargo liner (model 2388) and a full ship (model 2389), e.g. a tanker, and were designed at VWS for research purposes only. The generated ship models had an interchangeable bow and were fitted each with:

- a bulbless bow, considered as base ship (2388.0 and 2389.0),
- an implicit, small bulbous bow (2388.1 and 2389.1),

[3]This benchmark case, a surface naval combatant, will be used for the validation of the CFD solver implemented within this investigation

- an additive, small bulbous bow (2388.2 and 2389.2),
- an additive, larger bulbous bow (2388.3 and 2389.3).

The combination of systematic hull form variation and the investigation of the performance of bulbous bows in waves is unique and was apparently not repeated in any other research project since then. Both authors together published their results in [17].

In the following years, different authors studied the hydrodynamic performance of ships considering seakeeping aspects. Of special interest are those including a shape variation approach and will be therefore mentioned here. In 1990, Nowacki et al. [87] presented a systematic computational design study for an innovative hull form (SWATH), including both ship resistance and seakeeping aspects for design assessment by means of potential theory. In 2003, Zaraphonitis et al. [113] presented an optimization study for a high speed vessel considering powering and wash by a potential flow method. The two objective functions, namely total resistance and wave wash, were optimized with a multi-objective genetic algorithm and a Pareto-front was obtained. In 2006, Boulougouris et al. [19] presented an investigation on hull form optimization, specifically a bulbous bow optimization considering calm water resistance and motions in head waves. The calm water resistance calculations were performed with a nonlinear potential CFD code and seakeeping calculations with the potential, linear 3D seakeeping code *NEWDRIFT*. The bulbous bow geometry was defined by a total of nine form parameters, from which geometry variants were generated. First results dealt in some cases with numerical instabilities, and a thorough investigation was made to overcome this problem and finally find an optimal design.

In 2006, Campana et al. [21] presented an hydrodynamic hull optimization making use of RANS CFD methods for the calculation of the total resistance in calm water. The authors considered, as a design constraint, the motion amplitudes of the ship in regular head waves. These were calculated by a means of strip theory. A detailed validation and verification of the RANS CFD calculations was undertaken. Unfortunately, this was not the case for the linear seakeeping calculations.

The development of fuel prices and the subsequent interest of many ship owners to have a deeper insight into the economic performance of ship designs under real-life conditions have impulsed the development of new performance assessment methods, some of them by means of operational simulations. In 2004, Dallinga et al. [27] presented operational simulations considering the in-service performance of ships under different scenarios considering the influence of weather and prudent seamanship. For this purpose, the authors developed a simulation platform in a very similar manner to the one to be presented in this thesis. The hydrodynamic performance is evaluated by means of a "ship behavior database" which can be fed with existing data from numerical calculations or model tests. The authors showed different examples of operational simulations including speed loss, accelerations and added resistance in waves calculated by linear, frequency domain methods. Additionally, an example showing the effect of bow flare on trip duration based on experimental data was presented. Unfortunately, neither advanced hydrodynamic methods (e.g. nonlinear-potential or RANS methods) nor systematic form variations were

investigated in this study.

Hollenbach et al. published different papers discussing the performance of ships in off-design conditions. In [47] and [48], different measures to design more fuel efficient ships are discussed, under which the "optimization for off-design conditions" is treated and a hull optimization considering those conditions is performed. For the calculation of the calm water resistance, a potential CFD method was used. Although the authors define "off-design conditions" as four different floating conditions and three operation speeds without considering the effect of weather at all, it shows that the consideration of off-design speed and off-design floating conditions is gaining importance too. The numerical optimization was validated with model tests and showed good agreement. In a similar manner, Hochkirch and Bertram (2009) [45] presented a bulbous bow and fore ship optimization for slow steaming. In this optimization, normal and reduced service speed are considered, reaching optimized designs which perform well in both conditions. In 2008, Naito [83] presented a novel method for calculating the propulsive performance of a ship under given environmental conditions, assessing the power increase in actual seas. Results were compared to on-board measurements making use of behind-cast simulations by the method presented by Minoura and Naito [82]. For the assessment of the added resistance, an enhanced linear method is proposed, showing good results for ships with a blunt bow, such as tankers and bulk carriers. In 2009, Greitsch et al. [35] [34] presented an innovative approach applying long-term operational simulations. Considering weather data for a given route, rudder cavitation risk is assessed and different design variants are compared.

From the presented current information, it can be concluded, firstly, that viscous CFD methods are finding more and more applicability as a design tool in ship hydrodynamic problems when considering local hull form variations (like the form variation of a bulbous bow) and that they are very well suited for the calculation of added resistance in waves and, secondly, that the consideration of operational factors for the assessment of the economic performance of ships is becoming more and more important. Finally, it can be remarked that none of the investigations made in the past combined viscous CFD seakeeping calculations with complex operational simulations as will be made in this study, and only one investigation (Dallinga et al. [27]) presented an approach for operational simulations comparable to the one to be presented here.

1.3. Objectives and Outline

The main objective of this investigation is the development of a practical hydrodynamic design and performance assessment methodology considering real operational conditions specially applied to bulbous bows, but extendable to other design parameters of interest. Different computational approaches (e.g. numerical seakeeping analysis, computational fluid dynamics) are integrated into a single simulation platform to achieve this. The routes, weather conditions and trim/draft of a ship in a given period are computationally simulated and different geometric parameters of the bulbous bow are varied systematically to minimize operational costs, attempting to maintain seakeeping performance as better

or equal.

For the correct assessment of operational costs, an accurate prediction of the added resistance in waves is mandatory. In this work, the comparison of different bulbous bow variants leads to even higher accuracy requirements in this matter, since the influence of relatively small, local shape variations must be taken into account. For this purpose, the application of a viscous CFD method proved to be a suitable approach. Thus, development and application of the required CFD solver for seakeeping problems is another of the main objectives of this thesis.

The author's hypothesis is, in this context, that assessing the system's performance with the presented methodology can lead, within an optimization approach, to a different optimal design compared to the one obtained when only a single condition (calm weather, design trim & draft and design speed) is considered. Thus, the presented work attempts to demonstrate the feasibility of applying such a design methodology and the economic advantages of designs which were conceived specifically for their operational profile.

In general terms, the integration of different design aspects playing a role in hydrodynamic design are presented and demonstrated for the hydrodynamic design of the bulbous bow of a vessel. In chapter 2, the main principles and methodologies applied in this study are described, discussing their applicability for design purposes at an early design stage. In chapter 3, the integration of these methods into an operational simulation platform is outlined, describing the most relevant characteristics of the resultant implementation `SimOship`. In the following chapter (chapt. 4), a special application case is presented; namely the operational simulation of a ship is undertaken for which - opposite to the usual case in early design stages - experimental data is available for validation of numerical results. The main purpose of this chapter is to present the functionality of the presented operational simulations, giving a discussion about the different simulational approaches themselves rather than about the achieved results. In chapter 5, a general application case is presented, describing the operational simulation of a ship where no experimental data is available. This application case is of central relevance since it represents the reality in an early ship design stage. A systematic shape variation is included and some recommendations for the design of bulbous bows are given. Final remarks about the results and an outlook are presented in chapter 6.

In summary, the present thesis deals with a design methodology which differs from the common practice in hydrodynamic ship design. Instead of considering a single design condition for the performance assessment of a design, an increased number of operational factors which influence the performance assessment are considered, integrating all these factors by means of an operational simulation representing the whole operational life of the ship. For the successful application of this approach to the design of bulbous bows, the applied methodologies, specially the assessment of the added resistance in waves with viscous CFD methods and the influence of the most relevant operational factors, sea state and operational conditions, are of great importance. These aspects will be elaborated and discussed in detail during the entire course of the presented thesis.

2. Basic Principles

2.1. Overview

In this chapter, basic principles of the most relevant methodologies applied within this work will be depicted. Due to the high number of different tasks integrated in this investigation, the principles described in this section might not appear to be related to each other at a first glance. For this reason, an introductory explanation appears to be necessary.

In this study, simulations for the performance assessment of the operational life of a ship are performed. In section 2.2, simulations are defined from a general point of view and in section 2.3, operational simulations are defined in more detail. Within these operational simulations, several hydrodynamic and ship design techniques are integrated. The common coordinate system for all these techniques is described in section 2.4.

The main hydrodynamic tasks which are studied within this work are ship resistance and seakeeping. A detailed description of the methods applied within this work in these two fields is found in sections 2.5 and 2.6. As previously mentioned, the use of a viscous CFD method for the evaluation of the seakeeping performance of ships plays a central role, especially when considering that a solver was implemented for this purpose. Due to the fact that the mentioned solver is presented for a first time here, a more detailed description and a thorough validation for two different benchmark cases is presented in section 2.7.

The ship design technique described thereafter is a partial parametrical approach for the geometric variation of the bulbous bow, which will take place to elaborate operational simulations for different ship subvariants. A detailed description of this form variation approach is described in section 2.8 .

2.2. Simulational Approach

Simulation (def.):

> Scientific method in industry, science, and education, a research or teaching technique that reproduces actual events and processes under test conditions. (Encyclopædia Britannica)

Within this investigation, a *simulation* will be meant specifically as a computer simulation for engineering and/or design purposes. Since this specific definition of simulation covers also a very ample field in engineering and design applications, it will be proper to explain and categorize simulations more accurately.

Simulation techniques are becoming very popular for the investigation or the improvement of the performance of processes or systems along their design process. They are inherently inexpensive (compared to model or full scale tests) and allow the evaluation of complex tasks with many different variants. In many engineering problems, the simulation of the system's performance consists of the addition of different, fully isolated methodologies into a representative value which can be compared to other design variants. As an example, one could consider the total resistance of a ship in the following fictive case: The wave resistance of the naked hull is calculated by a potential CFD method, the frictional resistance and the resistance of the appendages by empirical formulae and the added resistance in waves by means of strip theory, neglecting all other possible resistance components. In this example, and also in a very general context, each mentioned method could even be considered as a restricted *simulation method* itself[1]. Under these simulation methods, the numerical solution of fluid flow problems is of special interest, considering in this context the mentioned potential CFD methods (including strip theory) but also viscous CFD methods. For the described case, for example, only a single viscous CFD simulation would be necessary (including free surface, incoming waves and appendages), from which the system's performance (e.g. total resistance) can be evaluated. With this example, the multiple character of simulations, which can be in some cases a very partial reproduction of the actual process or system to be modeled, is shown.

Considering that the system's performance has been evaluated for a single operational condition (or for instance for a set of n selected conditions), the question if this or these conditions are representative for the operational life of the system arises. Obtaining the relationship between these conditions and the actual performance of the system over its complete lifetime becomes a logical, further step to undertake. This step will be defined here as an *operational simulation*. In a simplest approach, the application of a security factor (e.g. service factor) would roughly fulfill this purpose. This common practice for many engineering applications is mostly done when information about the operational life of the system is to a large extent not available or is too difficult to obtain.

A more robust approach is the application of statistical methods, which permit a much deeper insight into the stochastic character of the operational life of the system. In the case of the operational life of a ship, an essential component is long term weather data for the region where the ship operates. This data, superposed with ship response functions, can be used to obtain representative statistical information, from mean values up to probability distribution functions over the ship's lifetime. The reliability of this approach depends on a correct statistical model (e.g. representative sea spectra) and the quality and applicability of the input data (e.g. parameters used to define a sea state).

For more detailed results, deterministic, time domain simulations of the operation of the system under realistic conditions become necessary. For this purpose, time histories for the unknown environmental (i.e. weather) or boundary conditions are needed. These can be obtained from representative data from past experience (e.g. behind-cast weather data) or

[1]It can be matter of discussion if the calculation of e.g. a force by means of a semi-empirical formula can be interpreted as a simulation or not, i.e. for which level of complexity an algebraic formula can be defined as a simulation model. A deeper discussion on this matter is out of scope in this study.

generated from statistical data. Different categories of detail level (e.g. different time step sizes) can be identified for this kind of simulation. The time domain simulation of every phenomenon involved in the operation of the system would represent the highest level of detail. In this case, the detail level (e.g. time step) of the simulation is limited by the phenomenon with the highest detail requirement (e.g. smallest time step requirement). In many cases, this leads to an extremely high simulation effort which is not always compensated by the improvement in the results when compared to simpler methods. In order to reduce the computational effort, simulational approaches in the time domain including a statistical approach for those phenomenon which would be problematic to solve (when considering the necessary computational effort) have shown to be a good compromise for many engineering applications. For numerical flow simulations (CFD), the popularity of RANS methods with statistically based turbulence models are an example of this. In the case of the simulation of the operational life of a ship, this approach shows itself to be advantageous too. While certain aspects of the operation (e.g. route, ship position, cargo or bunkering) are simulated in the time domain, other aspects are simulated by a statistical approach (e.g. ship responses by means of short-term statistics). A complete description of the operational simulation approach presented in this study will be given in detail in the following section.

2.3. Operational Simulations: a Short Introduction

Within this study, reference will be made to operational simulations as a *computational simulation attempting to model the operation of a system*. For industrial applications, this model must be as realistic as possible, within a limited, given amount of resources. This can be only achieved with:

- realistic input data (the interaction of the system with its exterior),
- proven, robust and qualitatively accepted methods and
- validated output data.

Operational simulations are intended to aid the designer and/or engineer within the design process, bringing answers about complex, interrelated processes which act together in a system. Additionally, a deep insight into the operation mechanisms of the system is made possible, revealing problems which might not yet have been recognized as such by the designer. Normally, operational simulations are undertaken at an early design stage where these answers cannot be obtained by any other means without excessive costs and/or risks.

2.3.1. Operational Simulations for Ships

The *operational simulation of a ship* implies synthesizing the operational life of a ship as a system. This system acts according to certain rules and a given input. For a merchant

ship, this is done simulating not only the ship as such. The system to be evaluated is its *operational life*. This synthesized operational life has two main components: a *ship* and an *environment*. In this way, an important part of the classical input is treated now as part of the simulation.

Simulation of the Environment

The environment of a typical merchant ship during its operation has two main components: the first component groups all aspects which can be considered as known. It comprises a known amount of time to carry a known amount of cargo between a known amount of known places. The second component groups all unknown aspects, viz., all other factors which can influence the operation of the ship during its lifetime. Leaving aside extreme situations such as damage by any means, system failures or force majeure (piracy, war, etc.), the most characteristic and permanent unknown environment factor is weather. Within all weather factors (meteorologists distinguish about 55 different weather parameters), waves, wind, currents, sight (e.g. fog) and tides are key-role players within the operation of ships.

At an early design stage, realistic weather information can be only retrieved from the past, selecting a convenient amount of time so that it can be considered representative for the ship's lifetime. For this purpose, weather data from the *European Centre for Medium-Range Weather Forecasts* (ECMWF) were used. The ERA-40 database from ECMWF provides weather data for a period from 1957 to 2002 in six-hour steps. Providing data points every 1.5° latitude and longitude, this data is only suitable for long voyages and long distances. Details about the ECMWF weather data will be discussed in section 3.2.2 on page 56.

Simulation of the Ship

An exhaustive simulation of all ship's systems, their interaction among each other and with the environment must be seen, for the presented design methodology, as impossible. For the purposes of this investigation, the simulation of the propulsion and the motions of the ship for any given condition is sufficient. To model this, appropriate information about floating condition, total resistance, seakeeping and machinery characteristics are necessary.

Considering the six-hour periods of the available weather data, the propulsion is considered as stationary for each time period and its simulation will be made according to the ITTC'78 Performance Prediction Method. The seakeeping simulation will be made for each 6 hrs. period by means of short time statistics, considering a sea- and a response spectrum from which representative data can be derived.

Here, the selection of the methods for obtaining the required information for these simulations plays a crucial role: considering an early design stage, most of this information will not be available or can be estimated with limited reliability. On the other hand, information which is believed to play a significant role within the simulation or for the evaluation of different design variants must be obtained by methods which are able to

indicate the differences between the evaluated variants with enough accuracy. In the case of the present investigation, it will be shown that the ship's calm water resistance and its seakeeping characteristics, especially the added resistance in waves, play an important role. Different state-of-the-art techniques which were used during the course of this investigation for these two tasks will be discussed in sections 2.5 and 2.6.

2.4. Coordinate Systems

Three main coordinate systems are defined: a world coordinate system (WCS), a ship coordinate system (SCS) and an inertial coordinate system (ICS).

The WCS is defined in degrees of latitude and longitude, with its origin in the equator, and the Greenwich meridian. West longitudes and north latitudes are positive and east longitudes and south latitudes negative. The heading angle of the ship, ψ, is defined as usual with 0°for north heading, with positive angles in clockwise direction. This coordinate system is mainly used for the global weather data and for the definition of the routes.

The SCS is defined in ship coordinates. Origin is the intersection between midship plane, main section and base line. x is defined positive in forward direction, y to port side and z upwards. The ICS follows the ship with its steady forward velocity and its origin coincides with the time-averaged position of the SCS. X is parallel to the intersection between the calm water (horizontal) plane and the longitudinal center plane, positive in forward direction. Y is parallel to the calm water plane, pointing to port side and Z points upwards, normal to the calm water plane. The WCS and the ICS are also shown in fig. 2.2. From the ICS, the three translations of the origin of the SCS represent the linear motions of the ship (surge η_1, sway η_2 and heave η_3). Since rotations occur around more than one axis, and considering the non-commutativity of such an operation, it is convenient to adhere to the established convention in aeronautics and ship dynamics using a modified set of Euler angles (DIN 9300). Considering that the ship axes will be initially parallel to the inertial axes, the rotation of the ship axes is obtained by the following consecutive rotations:

1. A yaw η_6 around the Z axis: $X, Y, Z \rightarrow x', y', Z$
2. A pitch η_5 around the temporary y' axis: $x', y', Z \rightarrow x, y, z'$. Note that this axis is parallel to the intersection between the calm water plane and the y-z plane.
3. A roll η_4 around the ship x axis: $x, y, z' \rightarrow x, y, z$

The six defined motions are summarized in table 2.1.

The transformation from the ship to the inertial coordinate system is given by:

$$\begin{pmatrix} X \\ Y \\ Z \end{pmatrix} = \begin{pmatrix} \eta_1 \\ \eta_2 \\ \eta_3 \end{pmatrix} + \mathbf{T} \cdot \begin{pmatrix} x \\ y \\ z \end{pmatrix} \tag{2.1}$$

Translations		Rotations	
surge:	η_1	roll:	η_4
sway:	η_2	pitch:	η_5
heave:	η_3	yaw:	η_6

Table 2.1.: Definition of translational and rotational ship motions

with the transformation matrix $\mathbf{T}$:

$$\mathbf{T} = \left(\begin{array}{c|c|c} \cos\eta_6 \cdot \cos\eta_5 & \cos\eta_6 \cdot \sin\eta_5 \cdot \sin\eta_4 - \sin\eta_6 \cdot \cos\eta_4 & \cos\eta_6 \cdot \sin\eta_5 \cdot \cos\eta_4 + \sin\eta_6 \cdot \sin\eta_4 \\ \hline \sin\eta_6 \cdot \cos\eta_5 & \sin\eta_6 \cdot \sin\eta_5 \cdot \sin\eta_4 + \cos\eta_6 \cdot \cos\eta_4 & \sin\eta_6 \cdot \sin\eta_5 \cdot \cos\eta_4 - \cos\eta_6 \cdot \sin\eta_4 \\ \hline -\sin\eta_5 & \cos\eta_5 \cdot \sin\eta_4 & \cos\eta_5 \cdot \cos\eta_4 \end{array}\right) \tag{2.2}$$

A schematic view of the defined Euler angles and the relation between the ICS and the SCS is shown in fig. 2.1.

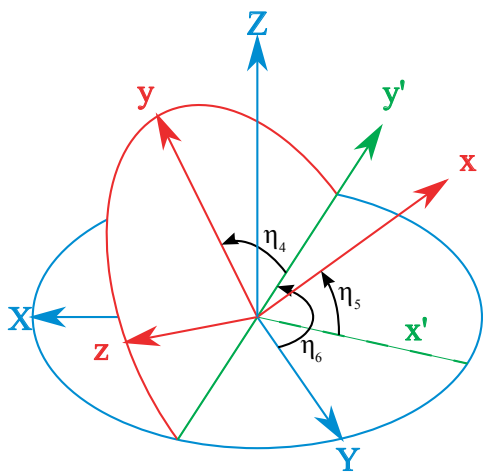

Figure 2.1.: Defined Euler angles and relationship between ICS and SCS when no translations are present (Based partly on a figure from Juan Sempere, Creative Commons License)

Additionally, it was found to be convenient to define a hybrid coordinate system HCS for the calculation of ship motions with CFD methods (details in section 2.6). This hybrid coordinate system has its origin at the center of gravity of the ship $\vec{x}_G$. The axes x^h, y^h and z^h are respectively parallel to the axes X, Y and Z from the ICS, the rotations in this system being equal to the rotations defined for the ICS. The transformation from SCS to HCS is given by:

$$\begin{pmatrix} x^h \\ y^h \\ z^h \end{pmatrix} = \mathbf{T} \cdot \begin{pmatrix} x - x_G \\ y - y_G \\ z - z_G \end{pmatrix} \tag{2.3}$$

or alternatively in terms of the ICS:

$$\begin{pmatrix} x^h \\ y^h \\ z^h \end{pmatrix} = \begin{pmatrix} X \\ Y \\ Z \end{pmatrix} - \begin{pmatrix} \eta_1 \\ \eta_2 \\ \eta_3 \end{pmatrix} - \mathbf{T} \cdot \begin{pmatrix} x_G \\ y_G \\ z_G \end{pmatrix} \tag{2.4}$$

For the rates of change of the Euler angles $\dot{\eta}_4$, $\dot{\eta}_5$ and $\dot{\eta}_6$, a relationship to the angular velocity $\vec{\omega^h}$ around the hybrid coordinate system can be established by relating unit vectors along the Euler rotation axes, resulting in the relationship:

$$\vec{\omega^h} = \begin{pmatrix} 1 & 0 & 0 \\ 0 & 1 & 0 \\ -\sin\eta_5 & 0 & 1 \end{pmatrix} \cdot \begin{pmatrix} \dot{\eta}_4 \\ \dot{\eta}_5 \\ \dot{\eta}_6 \end{pmatrix} \tag{2.5}$$

Finally, it has been considered convenient to define the direction of the wave propagation (which will be recalled here as *wave direction*) in the different coordinate systems. In the WCS, the wave direction is defined by the angle χ, with 0°for wave propagation in north direction, with positive angles in clockwise direction. From the ICS (or alternatively from the HCS), the direction of the wave propagation (to be recalled further on as *wave encounter angle*) is defined by the angle μ, with 0°for wave propagation in X-direction, also positive in counter-clockwise direction (i.e. μ=180°for head seas). The relation between both angles is given by:

$$\mu = 180 - \psi + \chi \tag{2.6}$$

For all rotations and moments in all defined coordinate systems, the right-hand rule is considered.

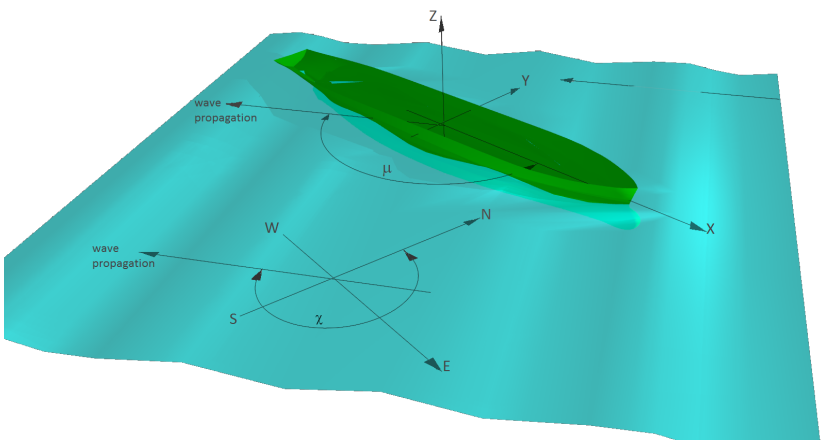

Figure 2.2.: World- and inertial coordinate systems

2.5. Resistance

2.5.1. Resistance Prediction in Ship Design: an Overview

The resistance of a ship advancing in water with constant speed has an important meaning during the complete ship design process. Different methodologies are applied within different design stages to estimate it and it is a permanent challenge for the designer to achieve an optimal (minimum resistance) value.

During a preliminary design phase (normally in a conceptual, very early stage), the use of simple estimation methods based on statistical data, similar ships or systematic series may appear to be suitable. Typical representants of methods based on statistical data, especially suitable for merchant vessels, are the methods of Holtrop and Mennen [50], [49] and Hollenbach [46]. The limitations of these approaches have been amply discussed in literature and textbooks (e.g. [70]) and will not be discussed here.

At a later design stage (normally at the beginning of the preliminary design stage), potential CFD methods can be applied to calculate the wave resistance of a wide range of design variants, often within an automatized optimization process. Potential CFD methods can be seen as a good compromise between computational resources and accuracy for such a task, especially when the performance assessment is done comparatively. The absolute values of resistance provided by potential CFD must always be interpreted with care, and model tests are usually performed to confirm final results. These model tests represent the maximal level of accuracy in the prediction of the resistance of the ship during its design. Their almost contractual character[2], the use of world-wide conventions (which is owed to a great extent to the ITTC conferences over the last half century) and the long experience of ship model basins are also additional reasons for the special importance of resistance model tests.

Additionally, RANSE CFD solvers can be used for the prediction of ship resistance or for the improvement of wake characteristics and/or the analysis of appendages. Due to the high requirement of computational resources for an acceptable accuracy, a high meshing effort and a still not completely satisfactory turbulence modeling, RANSE CFD methods are rarely applied for this task for practical (industrial) applications. Nevertheless, RANSE methods are expected to gain more and more acceptance as the development of innovative numerical methods, new physical (e.g. turbulence) models and more powerful hardware become available.

2.5.2. Resistance Model Tests

Since for practically every ship a *resistance model test* is carried out, it is convenient to describe it briefly and apply similar conventions to post-process results from numerical calculations. In this study, the latest recommendations of the ITTC [55] will be used. For

[2]since they are used for the ship speed prediction at sea trials, which *have* contractual character between shipyard and shipowner

convenience, all resistance formulas will be shown in dimensionless form by:

$$c_X = \frac{R_X}{\frac{1}{2}\rho V^2 S} \tag{2.7}$$

c_X being an arbitrary resistance coefficient, R_X an arbitrary resistance component and V and S a reference speed and a reference area, respectively.

In a model test, the total model resistance is measured for different model speeds. On the basis of Froude's hypothesis, the total model resistance is broken down into:

$$c_{TM} = c_{FM}(1+k) + c_R \tag{2.8}$$

with:

$$c_{FM} = \frac{0.075}{(log(R_n) - 2)^2} \tag{2.9}$$

$$R_n = \frac{v \cdot L}{\nu} \tag{2.10}$$

where c_{FM} is the frictional resistance coefficient of the model according to the ITTC 1957 friction line with the Reynolds number R_n, k represents Prohaska's form factor as recommended by the ITTC in 1978 and c_R the residual resistance coefficient, being its main component the wave resistance coefficient c_W. For equal Froude numbers (Froude's similitude law), the residual resistance coefficient of the model is assumed to be equal to the residual resistance coefficient of the ship. Detailed descriptions of the similarity laws applied and the theoretical background can be found e.g. in Lewis [75], Kracht [70] and many others.

For a ship in calm waters, without appendages and neglecting air resistance, the total ship resistance coefficient c_{TS0} is represented by the sum:

$$c_{TS0} = c_{FS}(1+k) + c_R + c_A \tag{2.11}$$

where c_{FS} is the frictional resistance coefficient of the ship according to ITTC 1957 friction line and c_A the model-ship correlation allowance. According to the ITTC 1978 procedure, c_A can be estimated as:

$$c_A = \left[105\left(\frac{k_S}{L_{WL}}\right)^{1/3} - 0.64\right] \cdot 10^{-3} \tag{2.12}$$

The hull roughness k_S for a new ship, if no better information is available, can be assumed to be $k_S = 150 \cdot 10^{-6}$m.

In service conditions, many additional components are added to calm water resistance, so that the total ship resistance coefficient in service conditions c_{TSS} is the sum (according to Kracht [70]):

$$c_{TSS} = c_{TS0} + c_{AW} + c_{AP} + c_{AA} + c_{ST} + c_{PAR} + \Delta c_{AR} \tag{2.13}$$

where c_{AW} represents the added resistance in waves coefficient, c_{AP} the appendage resistance coefficient, c_{AA} the wind resistance coefficient, c_{ST} the resistance coefficient due to steering and Δc_{AR} the roughness increase in service conditions, mainly due to fouling. For convenience, the parasitic resistance coefficient c_{PAR}, e.g. due to openings in the hull, will be hereinafter included in the appendage resistance coefficient.

2.5.3. Resistance Calculation with Potential CFD Methods

For many decades, potential theory has been used to calculate the wave resistance of ships. Today, nonlinear potential panel codes are widely used in industry and provide fast calculations for ship wave resistance (e.g. as presented in [97], [60], [59] and [72]). Most of these codes make use of the same principles and assumptions, superposing a set of singularities over the discretized boundary field of a domain of interest (the wetted part of the hull and a free surface region) in form of a Boundary Value Problem (BVP).

Since in potential theory the fluid is assumed to be inviscid, incompressible and irrotational, the velocity vector $\vec{u}$ can be determined from the gradient of a scalar quantity, the *potential* ϕ as follows:

$$\vec{u} = \nabla\phi \tag{2.14}$$

The fundamental equation to be solved is the Laplace equation, a linear partial differential equation. Beginning from mass conservation:

$$\frac{\partial\rho}{\partial t} + \nabla\cdot(\rho\vec{u}) = 0 \tag{2.15}$$

when $\rho = const$:

$$\nabla\cdot\vec{u} = 0 \tag{2.16}$$

Combined with eq. 2.14, it leads to the Laplace equation:

$$\nabla^2\phi = 0 \tag{2.17}$$

On the other hand, for momentum conservation in an inviscid flow, the Euler equation is taken:

$$\rho\left(\frac{\partial\vec{u}}{\partial t} + (\vec{u}\cdot\nabla)\vec{u}\right) = \mathbf{f} - \nabla p \tag{2.18}$$

with $\mathbf{f}$ representing body forces (e.g. gravitation, Coriolis force, etc.). From this equation, the generalized Bernoulli equation for irrotational flow can be obtained:

$$\frac{\partial\phi}{\partial t} + \frac{(\nabla\phi)^2}{2} + \frac{p}{\rho} + gz = const. \tag{2.19}$$

These fundamental equations are used to obtain the solution of the potential flow problem. For this purpose, the potential field ϕ must be found.

Due to the linear character of the Laplace equation, the potential can be assumed as the superposition of different components, i.e. the undisturbed flow potential ϕ_∞, waves potential and/or the potential of a perturbation caused by a body:

$$\phi = \phi_\infty + \phi_1 + \phi_2 + ... \tag{2.20}$$

To solve this equation, boundary conditions on the body, free surface, bottom and at infinity must be considered.

The body condition defines a tangential flow on the wetted part of the hull. This can be written:

$$\left(\nabla\vec{u} - \vec{V_b}\right) \cdot \vec{n} = 0 \tag{2.21}$$

where $\vec{n}$ is the unitary normal vector at a given position of the body and $\vec{V_b}$ the velocity of the body at this position. This condition implies that no particles will flow through the body.

The steady kinematic free surface boundary condition on the water surface ($z = \zeta$) can be written:

$$\nabla\phi \cdot \nabla\zeta - \frac{\partial\phi}{\partial z} = 0 \tag{2.22}$$

This condition implies that the movement of particles at the water surface must be parallel to the perturbed free surface, i.e. no water particle leaves the free surface.

The steady dynamic free surface boundary condition implies atmospheric pressure at the free surface. For $z = \zeta$, this can be written in the form:

$$gz + \frac{1}{2}\left(\nabla\phi\right)^2 - \frac{1}{2}U^2 = 0 \tag{2.23}$$

Different discretization methods and numerical techniques are available today for solving flow problems with potential theory. Most panel codes make use of Rankine panels and an iterative approach for the relocation of the discretized free surface. The geometry and the free surface domain are discretized by quadrilateral elements and, at each of these, a Rankine-source is placed. These sources can be of first or higher order and are normally located slightly behind the defined panel. A *collocation point* is defined, normally at the center of the panel, where the boundary conditions are to be fulfilled. A similar, but in certain aspects different method has been proposed by Söding [105] and is known as *patch method*, making use of shifted point-sources and the fulfillment of the boundary conditions as an averaged value over the whole patch instead of at the collocation point only. Both methods solve therefore the potential flow problem by finding the source strength distribution for which the respective residuals become zero.

The iterative approach, correcting both the wave elevations and the dynamic floating condition of the ship at each step, is finalized when changes between iterations become small, obtaining finally the nonlinear wave field and the pressure distribution over the hull. From the integration of this pressure distribution, the wave resistance R_W of the ship is obtained, being usually added to the viscous resistance (obtained e.g. from the frictional resistance according to the ITTC'57 and an estimated form factor k) to estimate the total resistance of the ship.

Potential flow methods, when disregarding their evident drawbacks, provide valuable results in early stages of ship design, representing a good trade-off between required computational resources and accuracy of results.

2.5.4. Resistance Calculation with RANS CFD Methods

The application of *Computational Fluid Dynamics* (CFD) by means of solving the Reynolds-Averaged Navier Stokes Equations by numerical means has become an important component of the available tools for solving ship hydromechanics problems. Specifically, their application to the prediction of ship resistance will be discussed here, including relevant basic principles which apply to other application fields too.

The reports from the resistance committee of the ITTC conferences show the advances of CFD in resistance prediction over the last decades (e.g. in [53], [54], [56] and [57]), being the increased presence of RANSE CFD since the beginning of the nineties evident. Another important mirror of the developments of each period have been the CFD workshops, e.g. Tokyo 1994 (Kodama [65]), Gothenburg 2000 (Larsson [73], [74]) and Tokyo 2005 (Hino [44]). Beginning from simple applications solving single-phase fluid problems without turbulence, the application of turbulence models in the beginnings of the nineties were an important step for further, more realistic applications in ship hydrodynamics. At that time, an important trend could be observed: the prevalence of finite volume methods compared to finite differences and finite element methods. Later on, the development of free surface techniques could be observed, the techniques of Volume of Fluid, Level Set and Surface Tracking becoming the most widespread for this purpose. Later developments for unsteady simulations, grid motion and further advances in numerics and physical modeling, hand in hand with the ceaseless development of hardware and massive parallelization make the future of RANSE CFD even more promising.

Governing Equations

The number of governing equations depends of the problem to be solved, and considering that a continuum mechanics problem is handled here, mass and momentum conservation are always present. Thermal and/or chemical energy balance and additional scalar transport equations such as turbulent kinetic energy or phase fraction (e.g. in the Volume of Fluid Method) are typical exponents of additional transport equations which are usually solved together with the basic conservation equations. For mass conservation:

$$\frac{\partial \rho}{\partial t} + \nabla \cdot (\rho \vec{u}) = 0 \tag{2.24}$$

and for momentum conservation:

$$\rho \left(\frac{\partial(\vec{u})}{\partial t} + (\vec{u} \cdot \nabla)\, \vec{u} \right) = \mathbf{f} - \nabla p + \nabla \mathbb{T} \tag{2.25}$$

where $\mathbf{f}$ are body forces (e.g. gravitation, Coriolis force, etc.) and $\mathbb{T}$ is the stress tensor defined by:

$$\mathbb{T} = \mu \left(\nabla \vec{u} + (\nabla \vec{u})^T - \frac{2}{3}(\nabla \cdot \vec{u})\mathbb{I} \right) \tag{2.26}$$

where $\mathbb{I}$ represents a 3x3 identity matrix. For an incompressible flow, the stress tensor can be simplified, leading to:

$$\rho\left(\frac{\partial(\vec{u})}{\partial t}+(\vec{u}\cdot\nabla)\,\vec{u}\right)=\mathbf{f}-\nabla p+\mu\nabla^2\vec{u} \tag{2.27}$$

For engineering problems, the application of the *Reynolds Averaged Navier-Stokes Equations* for turbulent flows represents a good trade-off between computational effort and quality of the results. In this approach, the small scales of the unsteadiness of the flow are averaged (by means of time averaging for statistically steady flows or ensemble averaging for unsteady flows), permitting the solution of the problem with a much larger spatial and temporal discretization as when turbulence is calculated totally (e.g. direct numerical simulations, DNS) or partially (e.g. large eddy simulations, LES) with numerical methods. Due to the non-linearity of the Navier-Stokes equation, time-averaging causes the appearance of an additional term, the *Reynolds stress tensor* $\mathbf{R}$, writing for the RANS equations:

$$\rho\left(\frac{\partial(\overline{\vec{u}})}{\partial t}+\left(\overline{\vec{u}}\cdot\nabla\right)\overline{\vec{u}}\right)=-\nabla\overline{p}+\mu\nabla^2\overline{\vec{u}}+\mathbf{f}-\nabla\mathbf{R} \tag{2.28}$$

with $\mathbf{R}$ (in index notation):

$$\mathbf{R}_{i,j}=\rho\overline{u_i'u_j'} \tag{2.29}$$

and considering $\overline{\vec{u}}$ as the average velocity and $\vec{u'}$ the fluctuation of it. Since the equation is not closed anymore, the Reynolds stress tensor must be modeled by means of a *turbulence model*. For ship hydrodynamics problems, two-equation turbulence models are the most widespread ones and, among these, to mention but some of them, the k-ϵ, the k-ω and the the k-ω-SST models are quite popular ones. A common characteristic of the mentioned models is that the Reynolds stresses are collected into the shear stress term $\mu\nabla^2\overline{\vec{u}}$ by means of replacing μ by the effective viscosity $\mu_{eff}=\mu+\mu_t$. Each of the mentioned models applies a different approach for the estimation of the turbulent viscosity μ_t. These details will not be discussed here; a reading of Ferziger and Peric [30] is recommended.

An additional matter of interest for ship hydrodynamic problems is the treatment of the free surface. A widespread method, which has also been applied in this investigation work, is the Volume of Fluid method (VoF). This methodology, an *interface capturing method*, determines the shape of the free surface in a fixed mesh allocating for each cell a scalar quantity, the *phase fraction* γ, and solving the correspondent transport equation:

$$\frac{\partial\gamma}{\partial t}+\nabla\cdot(\gamma\vec{u})=0 \tag{2.30}$$

The phase fraction has a value of $\gamma=0$ for total absence of a definite phase in a cell and $\gamma=1$ for a completely filled cell. For two-phase problems (in ship hydrodynamics applications normally water and air), the second phase has a phase fraction equal to $1-\gamma$ (see also [30]).

Discretization and Solution Techniques

For engineering purposes, and for ship hydrodynamics applications almost without exception, the discretization of the equations to be solved is done by the *finite volume method* (FVM). This method makes use of the governing equations in integral form for a set of control volumes (CVs) which constitute the computational mesh where the flow simulation is to be undertaken. The discretization by the finite volume method includes the approximation of volume integral quantities, the use of numerical interpolation and differencing schemes between control volumes and the proper selection of boundary conditions.

For the treatment of the boundaries of the domain (viz. for the treatment of CVs in vicinity of these boundaries), the definition of physically correct boundary conditions plays a central role. These conditions must either be known (Dirichlet boundary conditions) or must be expressed in dependency of interior values, e.g. by means of a given gradient (Neumann boundary condition) or by the combination of a gradient and a known quantity. For all these alternatives, this means that boundary conditions do not introduce new unknowns into the problem, and further means that each boundary condition requires a different treatment for the discretization of governing equations of CVs affected to these conditions.

The governing equations, when discretized, are represented by the summation of each of the approximations and assumptions made and the corresponding source terms leading, for an arbitrary control volume, to an algebraic equation. This algebraic equation relates the unknown in the CV (e.g. phase fraction γ) to the unknowns from its neighbors. For the complete computational domain, this leads into a sparse system of n algebraic equations, being n the number of control volumes of the computational domain. Written in matricial form, the equation system can be defined as:

$$A\phi = \mathbf{Q} \tag{2.31}$$

with A representing an $n \times n$ coefficient matrix, ϕ an n-dimensional vector representing the quantity to be solved (e.g. the phase fraction γ) and $\mathbf{Q}$ an n-dimensional vector containing source terms. This system of equations, as previously mentioned, is inherently sparse and can be solved by different computational methods. The most widespread solution methods for engineering purposes, and specially those suited for the governing equations of interest, have been extensively discussed in Ferziger and Peric [30].

For the calculation of the resistance of a ship, an appropriate computational domain representing the region of interest must be defined, i.e. providing adequate resolution of the ship geometry and adequate overall dimensions in order to avoid undesired effects such as blockage or wave reflection. This step is followed by the careful definition of all necessary boundary conditions, numerical schemes, solution strategies and an appropriate turbulence model. For ship hydrodynamics problems, valuable recommendations on these matters are given from the EU-Thematic Network "MARNET-CFD" [8]. Once calculations have been performed successfully, the ship total resistance is obtained by the integration of the resultant normal and shear stresses over the wetted surface of the ship, resulting for the first the total pressure forces and, for the second, the total frictional

forces over the ship. In section 2.7.3, an example of the described steps is given for an application case.

2.6. Seakeeping

2.6.1. Prediction of Seakeeping Performance: an Overview

The seakeeping performance of a ship plays a decisive role for its operation, this aspect being often underestimated during early stages of the design process. This section will describe general aspects of three different methods for the estimation of ship responses: strip theory, panel methods and viscous CFD methods. The two methods applied during this investigation, strip theory and viscous CFD, will be discussed in more detail.

The calculation of the motions of a rigid body in waves is a complex phenomenon, including many different forces and the interaction of them. The rigid body, in our case a ship, is assumed to move in six degrees of freedom in the time domain (with motions as defined in sect. 2.4). This results in a nonlinear system of six equations which must be defined and solved. At a first instance, the calculation of these motions in regular waves appears to be a convenient approach, reducing the computational effort considerably. By superposing the evaluated responses in regular waves with a sea spectrum, the responses of the ship in irregular waves can be obtained (Details on the superposition principle for seakeeping will be given in section 3.2.2).

Different methods, most of them developed in the second half of the 20th century, apply several assumptions to linearize the problem of the ship in regular waves and thus be able to solve it easily. Frequency domain methods consider both waves and the resulting motions as harmonic functions, eliminating in this manner the time-dependency of the problem. Additionally, motions are often linearized, being considered as small enough for this purpose in calm to moderate seas, and equations are partially uncoupled, considering the usual symmetry of the ship. Many strip theory methods and linear potential methods apply these linearizations to a greater or lesser extent (see sect. 2.6.2). Time-domain methods, on the other hand, are able to consider those nonlinearities being, however, confronted with a much higher computational effort. The equations of motion can thus be solved directly from the resulting flow, making this a clear advantage since also responses in irregular waves can be directly considered. For a deeper insight into the different established methods Söding et al. [106] is also recommended. The time-domain calculation of ship responses in combination with viscous CFD methods, as it was done in this study, represents the highest level of complexity for practical applications today. This approach will be explained further in sect. 2.6.3.

2.6.2. Potential Theory Methods for Seakeeping

In the same manner as defined in 2.5.3 for the wave resistance, inviscid, incompressible and irrotational flow is assumed and a potential of the velocity vector field is defined. In practice, potential flow methods are widely used for the calculation of ship responses in

waves due to their low requirement of computational resources, making the calculation of a large amount of calculations possible (e.g. for different wave angles and wave encounter frequencies).In this section, potential flow methods for the calculation of linear ship responses in the frequency domain will be discussed first, paying special attention to strip theory. Due to the widely known drawbacks of strip theory, especially for certain wave conditions or for atypical geometries, 3D-potential methods have become a practical tool for this purpose over the past few decades. Under these methods, frequency domain and time domain methods can be distinguished and for each of those, linear and (quasi-) nonlinear approaches for the wave elevations are possible. These approaches will be also described briefly here.

For all methods described in this section, the linearized equation of motion in six degrees of freedom in the inertial coordinate system ICS has the form:

$$\vec{F} = \mathbf{M} \cdot \ddot{\vec{\eta}} \tag{2.32}$$

with:

$$\vec{F} = (F_1, F_2, F_3, F_4, F_5, F_6)^T \tag{2.33}$$

$$\mathbf{M} = \begin{pmatrix} m & 0 & 0 & 0 & mz_G & -my_G \\ 0 & m & 0 & -mz_G & 0 & mx_G \\ 0 & 0 & m & my_G & -mx_G & 0 \\ 0 & -mz_G & my_G & I_{44} & -I_{45} & -I_{46} \\ mz_G & 0 & -mx_G & -I_{45} & I_{55} & -I_{56} \\ -my_G & mx_G & 0 & -I_{46} & -I_{56} & I_{66} \end{pmatrix} \tag{2.34}$$

$$\vec{\eta} = (\eta_1, \eta_2, \eta_3, \eta_4, \eta_5, \eta_6)^T \tag{2.35}$$

where $\vec{F}$ is the six-component vector of total forces and moments, $\mathbf{M}$ being the generalized inertia matrix and $\vec{\eta}$ the six-component vector of motions. For the generalized inertia matrix, m represents the mass of the ship, I_{ij} the inertial moment of the ship around the j-th axis when rotated around the i-th axis and (x_G, y_G, z_G) the three coordinates of the centre of gravity of the body in ship coordinates. The lower-right quarter of the matrix represents the moment of inertia tensor $\mathbf{I}$ in ship coordinates. Note that, for small motion amplitudes, $(x_G, y_G, z_G) \approx (X_G, Y_G, Z_G)$ and $(\dot{\eta}_4, \dot{\eta}_5, \dot{\eta}_6) \approx (\vec{\omega^i}) \approx (\vec{\omega^s})$ are considered, where ω^i and ω^s represent the angular velocities in the ICS and SCS, respectively.

Strip Theory Method

Since $\vec{\eta}$, as defined in eq. 2.35, is a function of time and sinusoidal waves of length λ_W are considered, the motion vector can be written as a harmonic function:

$$\vec{\eta} = \Re(\hat{\eta} e^{i\omega_e t}) \tag{2.36}$$

where $\hat{\eta}$ is the six-component complex amplitude vector and ω_e the encounter wave frequency:

$$\omega_e = \omega - k \cdot V_S \cos(\mu) \tag{2.37}$$

with wave frequency ω, wave number $k = 2\pi/\lambda_W$ and wave encounter angle μ, defined as the angle between the X-axis and the direction of wave propagation (i.e. $\mu = 180$ represents head seas).

From the defined complex motion amplitudes, velocities and accelerations are found:

$$\hat{\dot{\eta}} = i\omega_e\hat{\eta} \tag{2.38}$$

$$\hat{\ddot{\eta}} = -\omega_e^2\hat{\eta} \tag{2.39}$$

It is assumed that the total force can be split in an *excitation* and a hydrodynamic *radiation* force component, that is:

$$\vec{F} = \vec{F_E} + \vec{F_R} \tag{2.40}$$

The hydrodynamic radiation force $\vec{F_R}$, when linearized, can be obtained from forced motions in calm waters and can be expressed as the sum of parts directly proportional to the displacements, the velocities and the accelerations, respectively, and can be written as:

$$\vec{F_R} = -\left[\mathbf{A}\cdot\vec{\ddot{\eta}} + \mathbf{B}\cdot\vec{\dot{\eta}} + \mathbf{C}\cdot\vec{\eta}\right] \tag{2.41}$$

or alternatively in complex amplitudes as:

$$\widehat{F}_R = \left[-\omega_e^2\cdot\mathbf{A} + i\omega_e\cdot\mathbf{B} + \mathbf{C}\right]\cdot\hat{\eta} \tag{2.42}$$

where $\mathbf{A}$ is the matrix of the hydrodynamic added mass coefficients, $\mathbf{B}$ the matrix of damping coefficients and $\mathbf{C}$ the matrix of hydrostatic restoring force coefficients, which can be written for a symmetric ship as:

$$C = \begin{pmatrix} 0 & 0 & 0 & 0 & 0 & 0 \\ 0 & 0 & 0 & 0 & 0 & 0 \\ 0 & 0 & \rho g A_{WL} & 0 & -\rho g A_{WL} x_{CF} & 0 \\ 0 & 0 & 0 & mg\overline{GM}_T & 0 & 0 \\ 0 & 0 & -\rho g A_{WL} x_{CF} & 0 & mg\overline{GM}_L & 0 \\ 0 & 0 & 0 & 0 & 0 & 0 \end{pmatrix} \tag{2.43}$$

where A_{WL} is the waterplane area, x_{CF} the center of flotation and $\overline{GM}_T$ and $\overline{GM}_L$ the transversal and longitudinal metacentric height, respectively. An empirical value for the steering force of the rudder when keeping course can be assumed as a restoring force coefficient C_{66}, as described by Söding [104]. From eq. 2.32, 2.40 and 2.41, the equation of motion can be rewritten as:

$$\vec{F_E} = (\mathbf{M} + \mathbf{A})\cdot\vec{\ddot{\eta}} + \mathbf{B}\cdot\vec{\dot{\eta}} + \mathbf{C}\cdot\vec{\eta} \tag{2.44}$$

or with complex amplitudes, taking eq. 2.42:

$$\widehat{F}_E = \left[-\omega_e^2(\mathbf{M} + \mathbf{A}) + i\omega_e\mathbf{B} + \mathbf{C}\right]\hat{\eta} \tag{2.45}$$

For the solution of this equation, hydrodynamic forces and consequently the values of $\mathbf{A}$, $\mathbf{B}$, $\mathbf{C}$ and $\widehat{F}_E$ must be computed.

The excitation forces $\widehat{F}_E$ are split into two components: an exciting force component due to the pressure distribution of the undisturbed incident wave, also called the Froude-Krylov force, and a component due to the waves diffracted by the ship.

The main difficulty is to calculate the added mass, damping and the diffraction force. Restoring forces can be calculated directly as shown in eq. 2.43 and the Froude-Krylov force by integrating the wave pressure over the hull using potential theory (details explained e.g. in Lewis [75]).

For the estimation of the radiation force (eq. 2.42), wave radiation is assumed to occur only in transversal direction, which can be acceptable for slender bodies and relatively high motion frequencies. For the radiation force at lower frequencies, the hydrostatic restoring force becomes dominant, being a false estimation of hydrodynamic forces (added mass and damping) acceptable for the estimation of the radiation force. For the estimation of the diffraction exciting force, diffraction waves are expected to propagate in a similar direction to the incident wave, being longitudinal velocity components no longer being negligible. Within strip theory, only the two-dimensional flow around a finite number of cross sections is computed, corrections for wave diffraction being necessary to achieve more accurate results at high frequencies. The computation of the two-dimensional flow can be made by different methods and, among these, conformal mapping (e.g. Lewis-form sections, see Lewis [76]) and boundary element methods can be distinguished[3]. To obtain the total effect on the ship, the calculated results of each section are integrated over the longitudinal coordinate. In this study, the boundary element method presented by Söding (and described by Bertram et al. [13]), applied in the open source strip theory program PDSTRIP was used. In the applied method, point singularities are distributed on the section contour and a system of equations is solved to fulfill the zero normal flow boundary condition over the contour of the section to obtain the solution of the problem.

The Method of Gerritsma and Beukelmann for the Estimation of the Added Resistance in Waves

For linear motion computations, second order forces like drift or added resistance are not present, since they are proportional to higher terms of the wave amplitude. Nevertheless, these forces can be estimated from known linear parameters. Typical exponents of these methods were mentioned in section 1.2. The method of Gerritsma and Beukelmann [33] was implemented in the strip theory program PDSTRIP for the purpose of this investigation, making a short explanation appropriate. In this method, the energy radiated by the heave and pitch motions of the ship in head seas over one period is considered to contribute to a resulting force over the ship, representing the drift force F_x. This simple

[3]The advantages and disadvantages of these two different approaches in strip theory will not be discussed here, and a general overview can be found e.g. in Ogilvie [90]

relationship leads to the formula:

$$F_x = \frac{\pi \omega_e}{L_W} \int_0^L b(x) \left| \hat{\dot{\xi}}_{3,R} \right|^2 (x) dx \tag{2.46}$$

with

$$b(x) = b_{33} - V_S \frac{d\left(a_{33}(x)\right)}{dx} \tag{2.47}$$

where the terms b_{33} and a_{33} represent the damping and added mass in pure vertical motion for a 2D section, respectively. The term $\hat{\dot{\xi}}_{3,R}$ represents the complex amplitude of the vertical relative velocity between the ship and the water surface at a given cross section. Neglecting wave diffraction and radiation (considering the wave as undisturbed), linearizing eq. 2.2 for small rotations and assuming that $z = 0$, the complex amplitude of the relative vertical motion is expressed:

$$\hat{\xi}_{3,R} = \hat{\eta}_3 - x\hat{\eta}_5 + y\hat{\eta}_4 - \zeta_a e^{-ik(x \cos\mu + y \sin\mu)} \tag{2.48}$$

The value of the velocity amplitude is thereafter obtained according to eq. 2.38.

For application purposes, the longitudinal drift force at zero speed is considered to be equal to the added resistance in waves $R_{AW} = F_x$ and will be hereinafter recalled as such when provenient from strip theory computations. Considering the inherent deficiencies of this approach (which have been amply discussed in the past, see e.g. [96], [99]), it appears obvious that the accuracy of the results will be limited. Nevertheless, the wide application of this method over decades and for many test cases has shown robustness and acceptable quality of results for rough estimations. In chapter 3, the application of the method of Gerritsma and Beukelmann within this investigation will be described, remarking its valuability when combined with results from viscous CFD computations.

Panel Methods

Panel methods represent a good trade-off for the calculations of ship responses in waves, being positioned between strip theory and RANSE CFD methods both in their accuracy and resource requirements. The most widespread methodology, namely the Rankine Singularity Method (RSM), makes use of the same principles described in section 2.5.3. Within this method, frequency and time domain methods can be distinguished. An in depth review on existing implementations and methods was given by Bertam et al. [14] in 1996.

Frequency domain panel methods are able to consider important aspects which are (in most cases) completely neglected in strip theory. The advance speed of the ship, its steady wave profile or its dynamic trim and sinkage are some of these aspects which, depending on the implementation, can be included or not. In the same manner as for strip theory, the linearization of incoming waves and motions leads to the consequence that second order forces such as added resistance in waves may be estimated from known first-order quantities. A description of such an approach is given in Bertram [15]. In his

paper, the author emphasizes the advantage of the consideration of the fully nonlinear steady wave field for seakeeping calculations, showing, for the estimation of motions, good agreement with experimental results. For the the added resistance in waves, the need of estimative methods is certainly a considerable drawback (especially for the purpose of this investigation), although a deeper validation of these estimative methods would be desirable to demonstrate or refute this statement [11]. Further research in this field is being undertaken by Papanikolaou [94].

Time domain panel methods might probably offer, at least from a theoretical point of view, the best trade-off between accuracy of results and computational effort. These methods can account for the nonlinearities of both the steady and the unsteady wave field and are also able to perform calculations in irregular waves. Regrettably, only a few implementations presented so far have reached enough maturity for industrial applications. The group around Sclavounos (Massachusets Inst. of Technology - MIT) and their commercial RSM solver SWAN (ShipWaveANalysis) [71],[84],[103] can be considered as the most advanced one in this field (as surveyed by Bertram et al. [14]).

A time domain nonlinear potential RSM code, such as the previously mentioned code SWAN, would have certainly been of great advantage, especially in order to perform a large amount of calculations for different variants. However, no such code was available and all attempts to obtain a time-domain code fulfilling the requirements for the intended analysis did not succeed. Considering the free availability of a general purpose, open source field solver for CFD applications (OpenFOAM) and the author's experience with similar codes, the decision of applying a viscous CFD method was enforced, despite the higher computational resources required by such a method. The result of following this approach lead to the adaption and partial reimplementation of a CFD solver for seakeeping problems, `TUBsixDOFFoam`.

2.6.3. Application of RANS CFD Methods for Seakeeping

As previously mentioned in section 1.2, the simulation of motions and forces of a ship in waves solving the Navier-Stokes equations in the time domain is a promising approach. Here, all described discretization and solution approaches as described in section 2.5.4 for the calculation of the calm water resistance with viscous CFD methods apply. Additionally, the solution of the equations of motion for rigid bodies becomes necessary, making also a mesh motion approach necessary (to be described later on in this section). Special care has also to be taken in the time discretization approach in order to achieve good results.

Analogous to the calculation of the calm water resistance with RANSE CFD methods, the total resistance in waves is obtained by the integration of the resultant normal and shear stresses over the wetted surface of the ship. The subtraction of the calm water resistance leads to the added resistance in waves for a given time step. In regular waves, the *mean* value of the added resistance in waves is of special interest, assuming that the periodic character of added resistance over a defined number of wave periods can be assured. The calculation of the added resistance for different wave lengths, wave

encounter angles and/or wave heights leads to a large number of calculations, especially when different geometry variants are to be studied. Practical examples of the application of a viscous CFD method for a ship in regular waves will be given in section 2.7 (for validation purposes) and in chapter 5 (main application case).

In the following, the main principles of the implemented solver `TUBsixDOFFoam` will be described.

TUBsixDOFFoam

In the present investigation, the OpenFOAM (Open Source Field Operation and Manipulation) toolbox [6] has been used to implement the CFD solver `TUBsixDOFFoam`. The OpenFOAM toolbox is a collection of open source C++ libraries released under the general public license (GPL) which can be used to build numerical solvers specially (but not uniquely) for continuum mechanics problems. Additionally, this toolbox includes several pre-configured solvers and utilities intended to solve specific engineering problems, especially in the field of CFD. For a detailed description of general characteristics of these OpenFOAM solvers, Jasak [58] is recommended. The constitution of the presented solver is very similar to any standard OpenFOAM-solver for multiphase flows, differing in the ability of considering rigid body motions and some resultant minor issues. All of these will be described in the following.

The presented solver has been based on the existing solver `shipFoam` [24], and multiple additions, corrections and improvements have been done. The outcome of this is a finite volume solver for multiphase laminar flows permitting solid body motions in six degrees of freedom (6-DoF) by grid deformation. Its multiphase ability is realized by the Volume of Fluid (VoF) method and the solid body motions by means of the explicit solution of the equations of motion. The base solver `shipFoam` is based itself on other existing solvers, and is intended for laminar flows (i.e. no turbulence models are available for this solver). This means that results from `TUBsixDOFFoam` will consider laminar flows only, i.e. shear stresses are not being correctly represented for turbulent flows. Since the main force components for the correct prediction of motions and forces in waves are pressure forces, this aspect does not represent a significant problem for the presented application cases. Nevertheless, newer versions of OpenFOAM present approaches for including turbulence models in combination with moving meshes, making the possibility of including turbulence models in a future reimplementation of `TUBsixDOFFoam` possible.

The equation of motion to be solved is defined in the hybrid coordinate system (HCS) and is presented here separately for translational (eq. 2.49) and rotational (eq. 2.50)

motions:

$$\begin{pmatrix} F_1 \\ F_2 \\ F_3 \end{pmatrix} = m \cdot \begin{pmatrix} \ddot{\eta}_1 \\ \ddot{\eta}_2 \\ \ddot{\eta}_3 \end{pmatrix} \tag{2.49}$$

$$\begin{pmatrix} F_4 \\ F_5 \\ F_6 \end{pmatrix} = \frac{d}{dt}\left(\mathbf{I^h} \cdot \vec{\omega^h}\right) \tag{2.50}$$

$$\mathbf{I}^h = \mathbf{T} \cdot \mathbf{I} \cdot \mathbf{T}^T = \begin{pmatrix} {I_{44}}^h & -{I_{45}}^h & -{I_{46}}^h \\ -{I_{45}}^h & {I_{55}}^h & -{I_{56}}^h \\ -{I_{46}}^h & -{I_{56}}^h & {I_{66}}^h \end{pmatrix} \tag{2.51}$$

The force vector $\vec{F} = (F_1, F_2, F_3, F_4, F_5, F_6)^T$ represents the total force and is obtained directly from the solution of the RANS equations by integration over the body surface, adding the weight force of the body in vertical direction. Due to the usage of an hybrid coordinate system, the moment of inertia tensor I in ship-fixed coordinates must be transformed to the moment of inertia tensor I^h in the HCS as shown in eq. 2.51, with $\mathbf{T}$ from eq. 2.2. The main drawback of this approach is the time dependency of I^h, being the solution for rotational motions only in its generalized form possible (eq. 2.50). Considering motions without yaw and a symmetric geometry where $I_{45} = 0$ and $I_{56} = 0$, the inertial moments for the remaining matrix elements are:

$$\begin{aligned} I^h_{44} &= I_{44}\cos^2\eta_5 - 2I_{46}\cos\eta_4\cos\eta_5\sin\eta_5 + I_{55}\sin^2\eta_4\sin^2\eta_5 + \\ &\quad + I_{66}\cos^2\eta_4\sin^2\eta_5 \end{aligned} \tag{2.52}$$

$$I^h_{55} = I_{55}\cos^2\eta_4 + I_{66}\sin^2\eta_4 \tag{2.53}$$

$$\begin{aligned} I^h_{46} &= I_{46}\cos\eta_4\left(2\sin^2\eta_5 - 1\right) - I_{44}\cos\eta_5\sin\eta_5 + \left(I_{55}\sin^2\eta_4 + \right) \\ &\quad \left(+I_{66}\cos^2\eta_4\right)\cos\eta_5\sin\eta_5 \end{aligned} \tag{2.54}$$

The field and matrix operation abilities of the OpenFOAM toolkit permit the implementation of the coordinate transformation in matricial form, reducing the necessary programming effort considerably. Note that, since the calculations performed in this study will include only pitch and heave motions, the presented equations can be simplified even more, and the equations of heave and pitch can be then rewritten:

$$\ddot{\eta}_3 = \frac{F_3}{m} \tag{2.55}$$

$$\dot{\omega}^h_y = \ddot{\eta}_5 = \frac{F_5}{I_{55}} \tag{2.56}$$

The equations of motion can be subsequently solved by an explicit Euler method or alternatively by a Runge-Kutta method to obtain the velocity and displacement vectors $\dot{\vec{\eta}}$ and $\vec{\eta}$, respectively. From these, the mesh is updated by an automatic mesh motion solver, firstly for the translations and then, for the rotations. This solver makes use of a simplified mesh motion equation in the form of a Laplace equation with variable diffusivity:

$$\nabla \cdot (k\nabla\mathbf{q}) = 0 \tag{2.57}$$

where $\mathbf{q}$ represents the mesh deformation velocity and k the variable diffusivity. This diffusivity can be chosen to be related to the distance l from the moving boundary or, alternatively, based on the quality of the resulting mesh. For the first, the diffusivity coefficient is proportional to $1/l^a$, representing $a = 1$ an inverse proportional relation. In the original implementation, only $a = 1$ and $a = 2$ are available. This has been extended for any value of a, providing an increased flexibility and better chances to avoid larger mesh deformations in regions placed near to the ship.

Due to the explicit handling of the motion equations, an additional outer iteration for each time step has been implemented in the solver, in a similar manner as presented by Schmode et al. [101]. In this approach, resulting forces from the actual outer iteration are compared with the forces from the last outer iteration, repeating the iteration until a desired convergence is achieved (see also fig. 2.3). For each time step t, resultant forces are first guessed by means of a damped extrapolation:

$$F_{t,guess} = (1-r)F_{t-1} + rF_{t-2} + (1-r)\frac{F_{t-1} - F_{t-2}}{dt_{t-1}}dt_t \tag{2.58}$$

with r representing a force damping factor and the subindexes t, $t-1$ and $t-2$ representing last three time steps of the simulation. The damping factor r can be controlled by the user and is reduced automatically if the force guessing of previous iterations was not successful. With the guessed force, motions are calculated, the mesh is updated and the flow calculations, including the pressure-velocity correction, are performed. After this, the new resultant forces at the ship are calculated and are compared to the initial guess as previously mentioned. The process is repeated until a given convergence is achieved, being in most cases, specially for slow motions, only a single outer iteration necessary. In figure 2.3, a flowchart including all the mentioned solver steps is shown.

The mentioned outer iteration is intended to undergo force peaks, caused by numerical instabilities, especially when high force gradients are encountered. Compared to the initial solver implementation without the mentioned outer iteration, this approach has shown to provide a higher stability during calculations and a higher accuracy when high force gradients arise (e.g. slamming events), without increasing the required computational resources significantly.

2.7. Validation of CFD Solver

2.7.1. Background

The quality of results from CFD calculations plays an important role for the successful application of this technique for the assessment of added resistance in waves within this investigation. For this purpose, and considering that the presented solver `TUBsixDOFFoam` has a very short history, several benchmark calculations were undertaken. To guarantee appropriate conditions for these calculations, a two-dimensional wave tank was studied in order to test different numerical and solution schemes, validating attained results with the underlying analytical description of the inlet wave. After this preliminary step, an

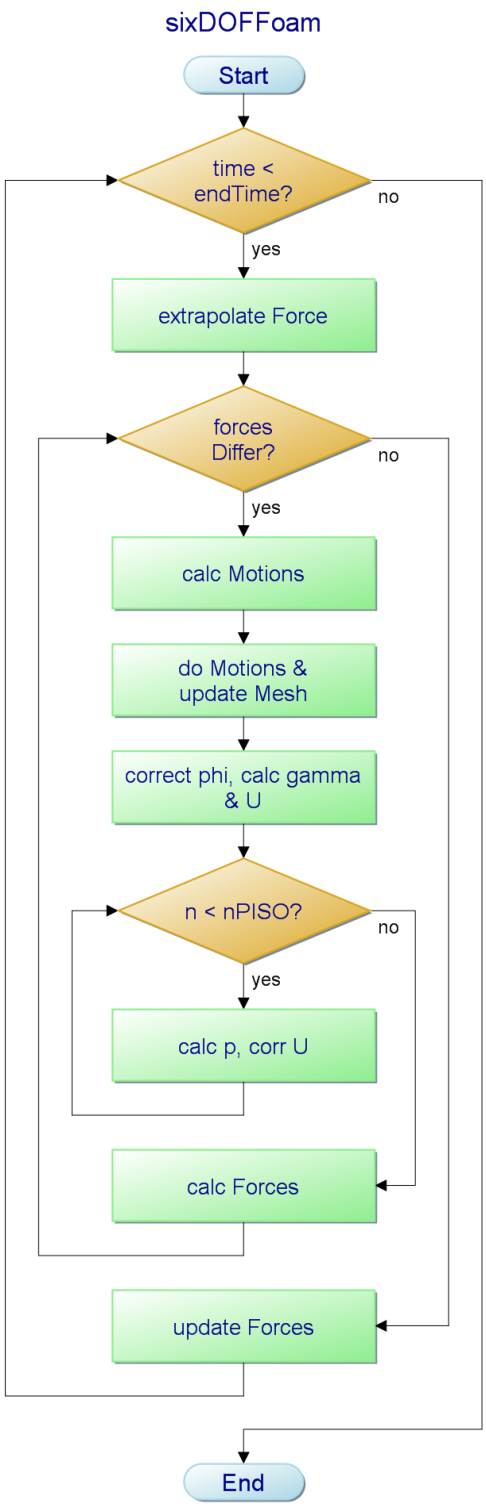

Figure 2.3.: Flowchart of TUBsixDOFFoam

exhaustive validation of OpenFOAM is undertaken with a ship geometry where accurate experimental data and results from other authors using similar solvers are available. This lead to the choice of the surface combatant model 5415 from the David Taylor Model Basin (DTMB5415), including the validation of the calm water resistance and its performance in waves.

Measurements from IIHR [4] (Iowa Institute of Hydraulic Research) for DTMB model 5512 (a 3.05m geosim model of the 5.72m 5415 model) were taken for the intended validation, making use of the same benchmark cases from the CFD Workshop Tokyo 2005 [44]. The usage of the DTMB combatant model within the CFD workshop in Gothenburg (2000) [73] and the mentioned workshop in Tokyo (2005) [44] permits a comparison of the presented OpenFOAM solver with other, well established CFD codes from the participants these CFD workshops.

2.7.2. 2D Wave Tank

The inlet condition of every CFD setup for seakeeping applications, providing a regular wave in a moving frame (equal to advance speed), showed to be a sensitive task within the setup of the solver. This applies not only for the implemented solver, but also for all other multiphase solvers provided by OpenFOAM. To attain the desired wave shape quality, a 2D wave tank case was studied and different numerical setups were tested and compared to the analytical solution. A complete description of each tested setup is out of scope, but the final setup will be discussed here.

Grid Generation, Boundary Conditions and Numerical Setup

To avoid wave reflection from the outlet boundary, appropriate boundary conditions must be chosen (non-reflective boundary conditions, sponge layers and similar solutions have been discussed by many authors). Since the OpenFOAM toolkit does not provide such a boundary condition for multiphase problems, a simple solution was applied. By extremely coarsening the grid at the outlet region, especially in longitudinal direction, the reflection disappears completely and zero-gradient outlet boundary conditions can be used without difficulties. It must be recalled that this solution is valid for the head waves condition, and is in many cases not possible to apply e.g. for manoeuvring simulations. For the wave tank case, a Cartesian 2D grid with the mentioned coarseness at the outlet region is required. A finer grid with 29120 cells and a coarser grid with 7280 (half number of cells in longitudinal and vertical direction) were generated.

A special treatment is required for the inlet boundary: since a regular wave must be defined, a time-variable inlet is needed. In most of commercial CFD applications, this is done by user coding, which must be compiled additionally and linked to the executable file. In the present case, a directly interpreted boundary condition named `groovyBC` is used. This condition permits the input of formulas, datasets and many other variables into the boundary condition. In the present case, the inlet boundary defines a second-order,

regular Stokes wave. The wave deflection for a wave of amplitude ζ_A is defined:

$$\zeta(t) = \zeta_A \cdot cos\,(k\,x - \omega_e\,t) + 0.5\zeta_A^2 \cdot cos\,(2\,(k\,x - \omega_e\,t)) \tag{2.59}$$

and is taken to check whether a cell is located below or above the water surface, and thus the boundary conditions for the longitudinal and vertical components u and w of water velocity and for the phase fraction γ can be defined:

$$\gamma(z,t) = \begin{cases} 1 & \forall \quad z \leq \zeta(t) \\ 0 & \forall \quad z > \zeta(t) \end{cases} \tag{2.60}$$

$$u(z,t) = \begin{cases} V_A + \zeta_A \cdot \omega \cdot e^{k\,z} \cdot \cos(k\,x - \omega_e\,t) & \forall \quad z \leq \zeta(t) \\ V_A & \forall \quad z > \zeta(t) \end{cases} \tag{2.61}$$

$$w(z,t) = \begin{cases} \zeta_A \cdot \omega \cdot e^{k\,z} \cdot \sin(k\,x - \omega_e\,t) & \forall \quad z \leq \zeta(t) \\ 0 & \forall \quad z > \zeta(t) \end{cases} \tag{2.62}$$

$$\tag{2.63}$$

The outlet boundary is defined by a zero-gradient condition, the bottom boundary by a slip-wall condition and the top-wall by an atmospheric condition. A detailed description of the boundary conditions for calculations considering ships, including the boundaries mentioned here, is given in the next section (2.7.3).

The selection of appropriate numerical schemes to solve the governing equations is a task where intensive testing was necessary. Since the OpenFOAM toolkit neither provides a detailed documentation nor general guidelines on this, testing of practically every physically and numerically reasonable scheme was necessary. A detailed description of these is considered outside the scope of this work. The final numerical setup applied for all calculations is given in tables 2.2 and 2.3.

Results

As a known fact, the diffusion or loss of wave height along the computational domain an issue of matter, especially for coarser grids, when making use of the VoF method for capturing the free surface. This fact arose in this validation case too, showing a wave height diffusivity along the computational domain. Figure 2.4 shows this phenomenon comparing both test cases. Additionally, the steadiness of the harmonic cycles was tested by comparing the wave elevation after different numbers of wave periods. This is shown in figure 2.5, being compared to an analytical, second order Stokes wave as given in the inlet boundary condition.

Although results obtained show a certain loss in wave height along the domain, slope, phase and shape match the analytical definition adequately.

2.7.3. DTMB5415 Surface Combatant

The DTMB surface combatant model 5415 is a widely known benchmark model for both experimental and numerical investigation on ship flows and has been explicitly recommended by the ITTC [54] for this purpose. This model was conceived as a preliminary

	Item	Symbol	Keyword	Description
1	First and second time derivatives	$\frac{\partial}{\partial t}$	`Euler`	First order, bounded, implicit
2	Gradient	∇	`faceLimited leastSquares 0.5`	Limited, second order least squares
3	Divergence (velocity terms)	$\nabla \cdot \vec{u}$	`Gauss vanLeerV`	Second order Gaussian integration, van Leer interpolation for face centres
4	Divergence (phase fraction terms)	$\nabla \cdot \gamma$	`Gauss vanLeer01`	As 3, strictly bounded between 0 and 1
5	Laplacian	∇^2	`Gauss linear corrected`	Second order, Gaussian integration, linear interpolation for face centres, conservative
6	Point-to-point interpolation		`linear`	Linear interpolation for general fields
7	Gradient component normal to face	∇_{SN}	`corrected`	Explicit non-orthogonal correction

Table 2.2.: Numerical schemes for CFD calculations

design of a surface combatant for the US navy in the early eighties. The main dimensions and the geometry of the hull can be found in table 2.4 and figure 2.6, respectively. The available experimental data provided by IIHR covers model tests both in calm water and in waves, with and without motions. The model tests for the validation consider a single speed ($F_n = 0.280, R_n = 4.860 \cdot 10^6$) and measurements in waves a single wave length ($\lambda_W / L_{PP} = 1.50$). Detailed measurements of the nominal wake field, wave elevations and global quantities such as motions, forces and moments are also available from this institution.

Grid Generation

The grid generation is undertaken by the OpenFOAM-utility `snappyHexMesh`, a script-driven, unstructured grid generator. `snappyHexMesh` generates meshes containing hexaedra and split-hexaedra, opposite to most of commercially or freely available automatic grid generators which generate mainly tetrahedral meshes. Since only poor documentation is available, a short discussion, specially for its application in meshing ship hulls, is given in appendix A.

Four refinement levels (80k, 200k, 500k and 2M cells approx.) and two additional grids for calculations without free surface (using the topologies from the 200k and 2M meshes) were generated. These are summarized in table 2.5. The four meshes for free surface

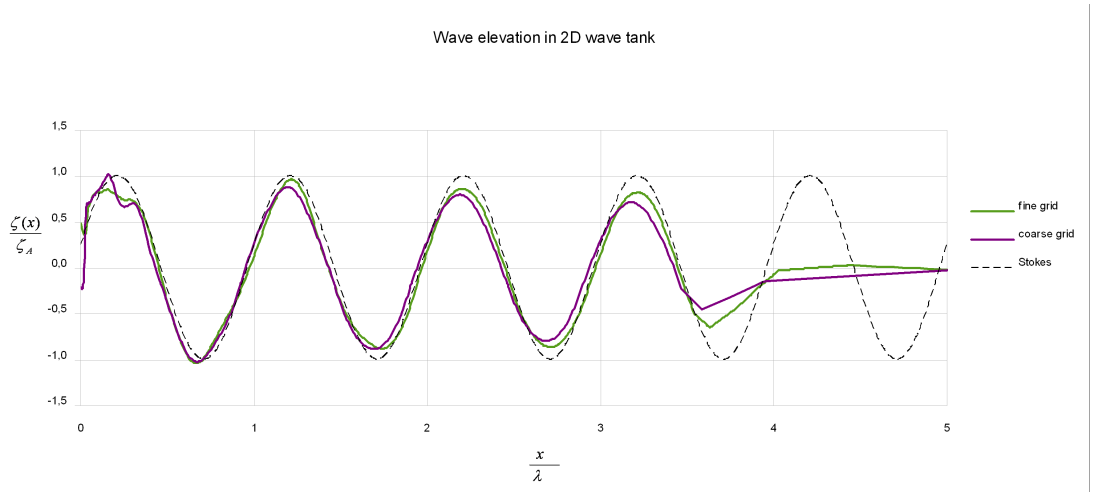

Figure 2.4.: Wave elevation for two different grids (fine, with 29120 cells and coarse with 7280 cells)

calculations are also shown in figure 2.7 in p. 42.

Boundary Conditions

A typical box-shaped arrangement of the calculation domain was chosen and, since the problem can be treated as symmetrical along the xz-plane, only a half-hull is considered. A physically reasonable boundary condition was assigned to each boundary of the domain, considering the `groovyBC` condition described in last section for the inlet, a zero-gradient pressure outlet, slip walls for top, side and bottom boundaries and a wall condition for the ship hull. These boundary conditions are summarized in table 2.6.

Calm Water and Double-Body Calculations

In a first instance, steady state turbulent simulations without free surface (double-body flow), were undertaken. These simulations were undertaken with the standard, steady state OpenFOAM solver `simpleFoam`, making use of the $k-\omega-SST$ turbulence model. Although neither experimental nor numerical data is available for comparison, these simulations were intended to complement results with free surface in calm water and permit the identification of single resistance components, namely the viscous pressure and the wave resistance (i.e. its coefficients c_{PV} and c_W).

Simulations with free surface represent the benchmark case 1.2 of the Tokyo CFD workshop [44], considering the fixed dynamic sinkage given there (at FP: -0.0028L_{PP}, AP: -0.0009L_{PP}). These simulations were undertaken with the transient, turbulent solver `interFoam`, being all settings equal to the previous simulation without free surface. Results of the resistance components for the different meshes are shown in tab. 2.7.

In figure 2.8, a longitudinal cut of the free surface is compared to the experimental data from IIHR [91] for all mesh refinement levels. In figure 2.9, the wave elevation field is com-

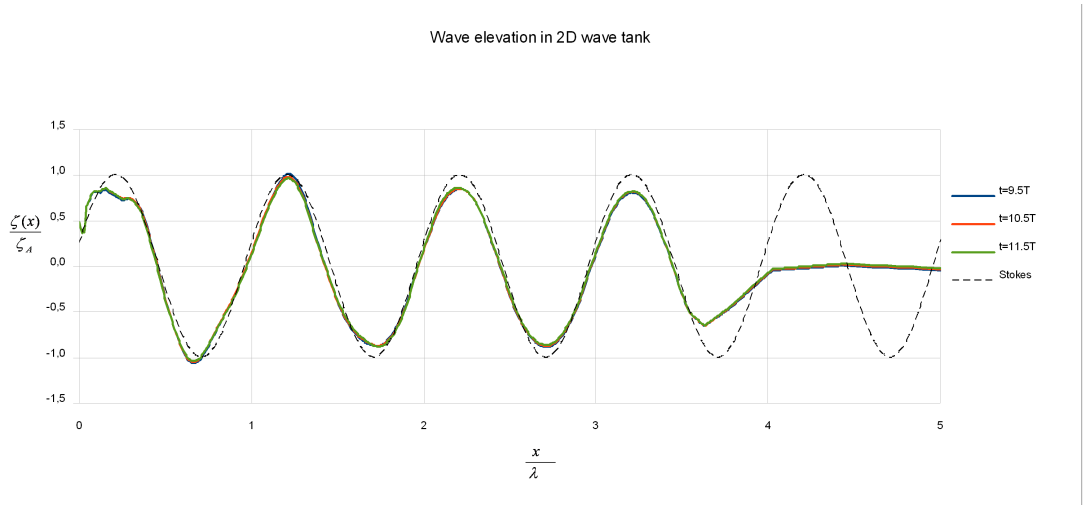

Figure 2.5.: Wave elevation at three different time steps (after 9.5, 10.5 and 11.5 wave phases)

Figure 2.6.: DTMB 5415 (5512) model (Source: Hino [44])

pared with experiments. In both figures, the better agreement between the finer meshes and experiments can be observed, except for the finest grid (2M grid): here, wave elevations are overpredicted in some regions, which can have been caused by different numerical problems. During the calculations of the finest mesh, a secondary wave advancing against flow direction was observed. The causes of this phenomenon are not clear, but reflections from the outlet boundary or numerical instabilities are possible causes. Nevertheless, the agreement for much coarser grids is very encouraging and has a much higher significance for the further application of the solver with rather coarse grids. When comparing the achieved results with the three best results submitted by participants of the CFD Workshop in Gothenburg 2000 [73], the attained results can be clearly ranked among the best of them. For the purpose of this investigation, the presented results in calm water fulfill the needed requirements and confirm the suitability of the applied solution method for ship hydrodynamics in calm water.

Simulations in Waves without Motions

The "diffraction" benchmark case no. 4 from the CFD workshop in Tokyo [44] consider the ship without appendages in head waves ($\lambda_W/L_{PP} = 1.50$, wave steepness $A_k = 2\pi\zeta_A/\lambda_W = 0.025$) and without motions. CFD calculations with the previously mentioned solver `interFOAM` were undertaken for three meshes (80k, 200k and 500k), and results of wave elevations and force amplitudes are compared to experiments carried at IIHR (ref. [38] and [39]). In figure 2.10, the unsteady wave elevations at $t/T_e = 0.00, 0.25, 0.50$ and

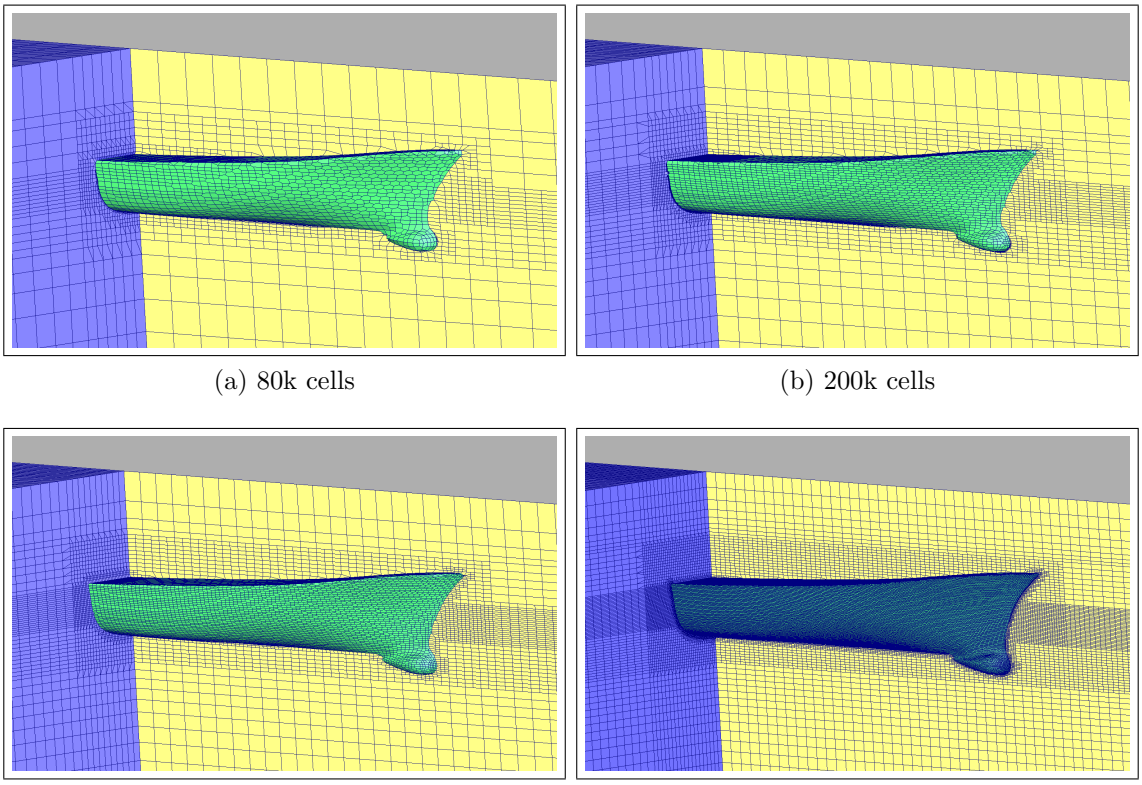

(a) 80k cells (b) 200k cells

(c) 500k cells cells (d) 2M cells

Figure 2.7.: Grids generated with `snappyHexMesh`

0.75 are presented for the 200k and 500k grids (upper half of each plot) and are compared to experimental results (lower half of each plot). The wave elevations show, especially for the 500k grid, good agreement with experiments. In figure 2.11, the time history of the longitudinal force in waves is compared to experiments. The force amplitude, in the same manner as the calm water resistance for coarser meshes, is overestimated for all meshes considered. The influence of grid fineness is not comparable to the calm water case, being the observed overprediction practically independent of the fineness of the grid. Since the role of hydrostatic forces is significant in comparison to calculations in calm water, the good agreement of results from very coarse meshes can be expected. The attained results also agree well with results submitted by participants of the CFD Workshop Tokyo 2005 (see e.g. Cura Hochbaum et al. [25]), showing the suitability of the presented solution method for ship hydrodynamic problems in waves.

Simulations in Waves with Motions

The main objective of the application of CFD in this study is the simulation of ship motions in head waves, and calculations were made for three grids (80k, 200k and 500k grids) with the implemented solver `TUBsixDOFFoam`. Considering the architecture of any

OpenFOAM solver, it must be emphasized that not only every solution setting, but also the solution approach and main structure of the solver are identical to the previous validation cases using the VoF solver `interFoam`. The main difference between both solvers is the non-availability of turbulence models and the inclusion of rigid-body motions in `TUBsixDOFFoam`, as described previously in sect. 2.6.3.

The experiments carried out by IIHR were made for the same conditions described for the diffraction case ($\lambda_W/L_{PP} = 1.50, A_k = 0.025$). Time histories for the heave and pitch motions from experiments (EFD) and CFD are presented in figures 2.12a and 2.12b, respectively. The agreement in amplitude, phase and steepness for the heave motion is good. For the pitch motion, an overprediction of the amplitude can be observed, probably due to the restrained surge motion of the CFD calculations. Phase and steepness of the pitch time history show, analogous to the heave motions, good agreement with experiments. For the simulations in waves with motions, no force measurements are available yet. The coming CFD workshop in Gothenburg 2010 will include this benchmark case and new measurements including forces are been undertaken for this purpose. Notwithstanding to this, the comparison of the motions with the experiments are encouraging and, considering the agreement of the diffraction benchmark case, the suitability of the presented code for the intended evaluation of the seakeeping performance of ships in head waves can be considered as satisfactory. Since, as for the calculations from the previous case, hydrostatic forces play an important role, good agreement is attained even for very coarse meshes, as observed in the presented example. Similar observations have been made by Schmode et al. [101]. This aspect will show to be of advantage for the purpose of this investigation.

In chapter 5, further results from the presented solver for different ship geometries and wave lengths will be presented and their importance for the application of the presented design methodology will be discussed.

Field	Task	Solver	Description
Pressure, corr. pressure `pd`	solver	`PCG`	Preconditioned conjugate gradient solver
	preconditioner	`GAMG`	Generalised geometric-algebraic multi-grid
Velocity `U`	solver	`PBiCG`	Preconditioned bi-conjugate gradient solver
	preconditioner	`DILU`	Diagonal incomplete-LU
cell motion `cellMotionU`	solver	`PCG`	Preconditioned conjugate gradient solver
	preconditioner	`DIC`	Diagonal incomplete-Cholesky

Table 2.3.: Solution algorithms for CFD calculations

Description		Ship	Model
Scale factor	λ	-	46.59
Length between perpendiculars	L_{PP} (m)	142	3.048
Waterline Length	L_{WL} (m)	142	3.048
Breadth	B (m)	18.9	0.406
Draft	T (m)	6.16	0.132
Water density	ρ (t/m^3)	1.025	1.000
Displacement	Δ (t)	8636	0.08332
Volume	∇ (m^3)	8425.4	0.08332
Wetted surface	S_W (m^2)	2949.5	1.359
Length to Breadth ratio	L_{PP}/B (-)	7.53	
Breadth to depth ratio	B/T (-)	3.091	
Block coefficient	C_B (-)	0.506	
Prismatic coefficient	C_P (-)	0.613	

Table 2.4.: Main dimensions of DTMB5512 model

Category name	With FS No. of cells	Without FS No. of cells
`very coarse grid`	84520	-
`coarse grid`	228228	145948
`medium grid`	517128	-
`fine grid`	2245406	1138528

Table 2.5.: Mesh refinement levels

Field	Name	Velocity	Phase fraction	Pressure
		`U`	`gamma`	`pd`
Inlet	`minX`	groovyBC	groovyBC	zero gradient
Outlet	`maxX`	zero gradient	zero gradient	zero gradient
Symmetry plane	`minY`	symmetry	symmetry	symmetry
Side wall	`maxY`	slip wall	zero gradient	zero gradient
Bottom wall	`minZ`	slip wall	zero gradient	zero gradient
Top wall	`maxZ`	zero gradient	zero gradient	fixed value (0)
Ship	`ship`	moving wall	zero gradient	zero gradient

Table 2.6.: Boundary fields. The groovyBC condition has been decribed in section 2.7.2

	80k	200k	500k	2M	EFD
C_F	2.53E-03	2.61E-03	2.86E-03	3.11E-03	2.89E-03
e(%)	-12.38%	-9.77%	-0.88%	7.70%	
C_P	3.12E-03	2.65E-03	1.88E-03	1.35E-03	1.35E-03
e(%)	130.65%	95.83%	39.13%	-0.11%	
C_T	5.65E-03	5.25E-03	4.74E-03	4.46E-03	4.24E-03
e(%)	33.27%	23.93%	11.89%	5.21%	

Table 2.7.: Results of CFD calculations in calm water for DTMB model 5512 compared to experiments. Since experimental data was only available for DTMB 5415 model, Reynolds-dependent CFD results for DTMB 5512 model were scaled accordingly

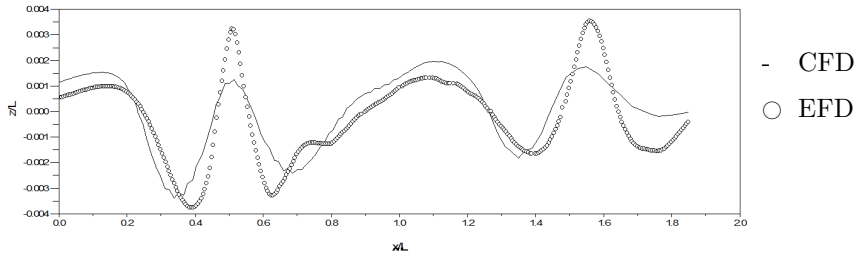

(a) 80k cells

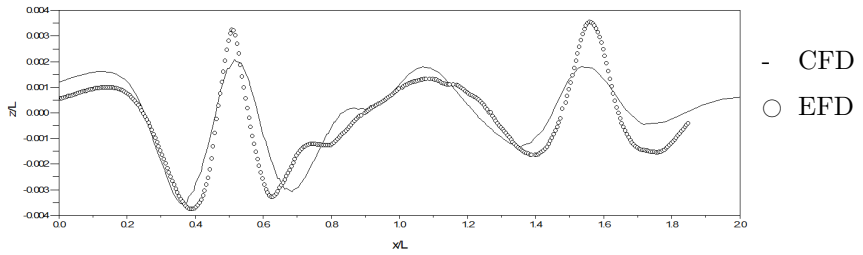

(b) 200k cells

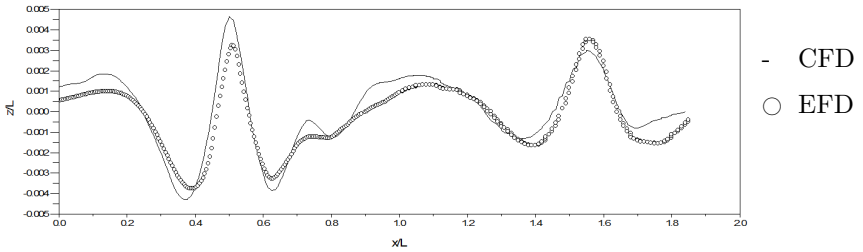

(c) 500k cells cells

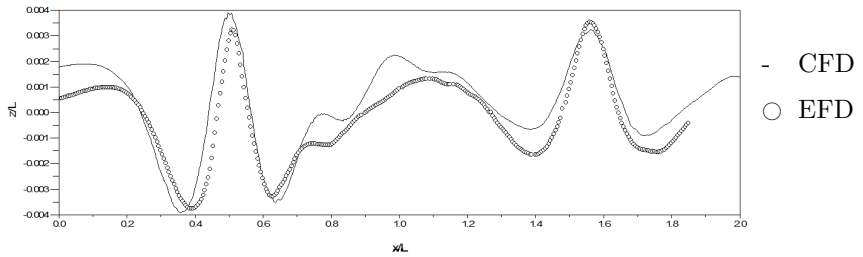

(d) 2M cells

Figure 2.8.: Wave elevation at y/L=0.172 from experiments and CFD calculations

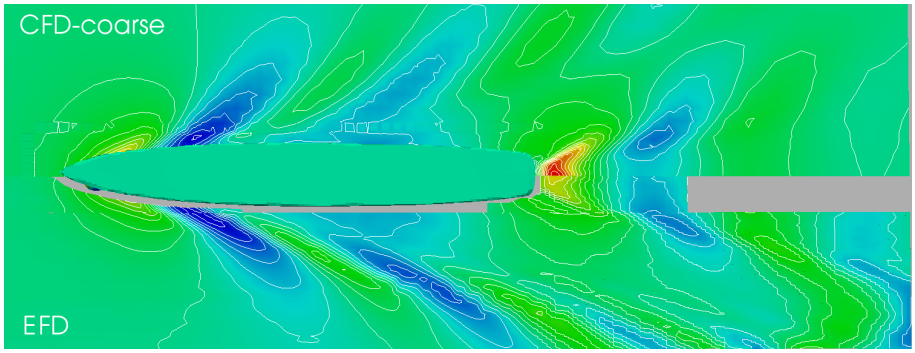

(a) 80k cells

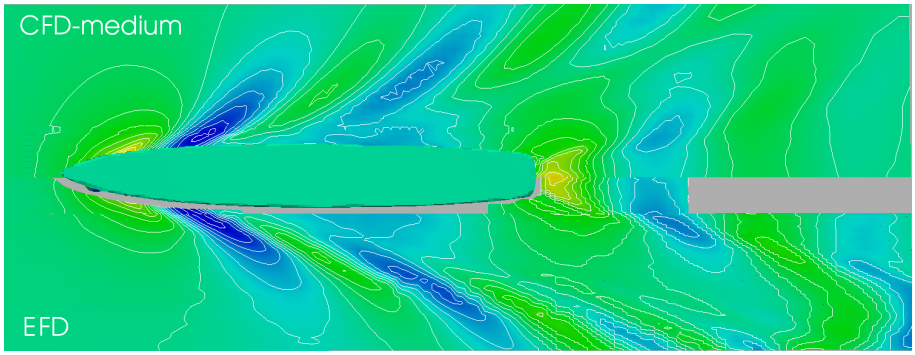

(b) 200k cells

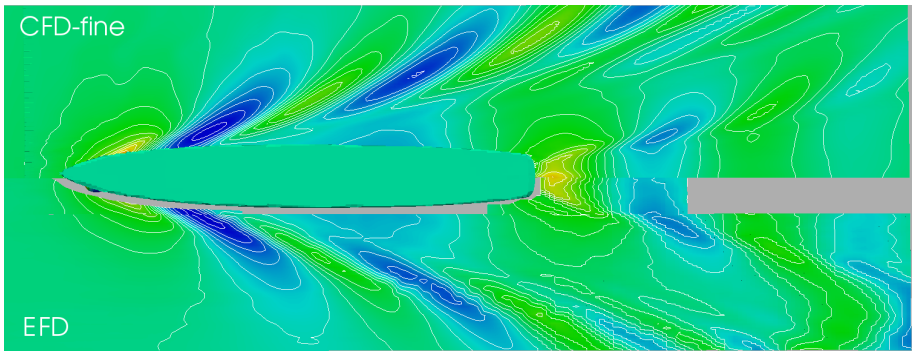

(c) 500k cells cells

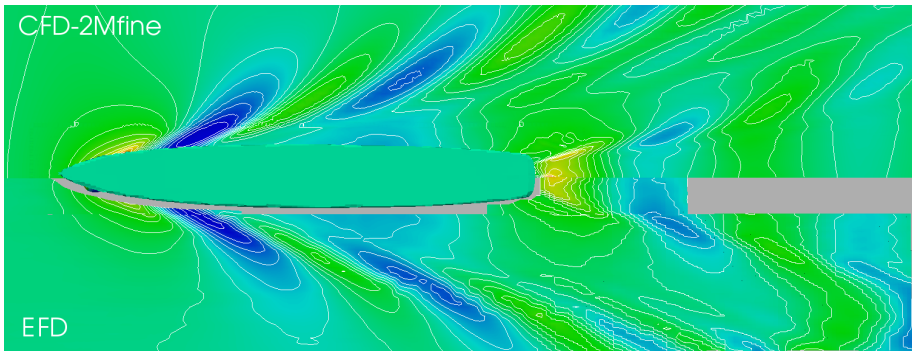

(d) 2M cells

Figure 2.9.: Wave elevations from CFD calculations (upper half of each plot) and experiments (EFD, lower half of each plot)

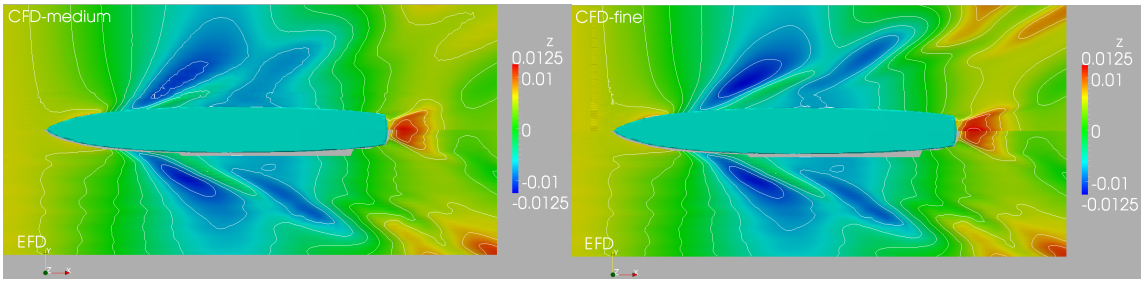

(a) t/T=0.00

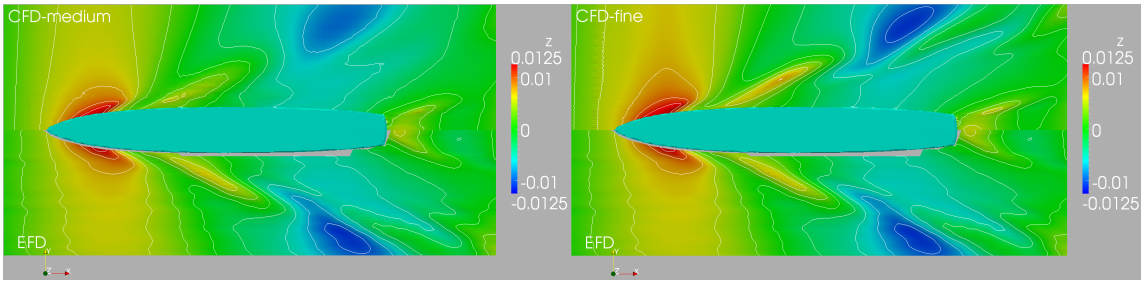

(b) t/T=0.25

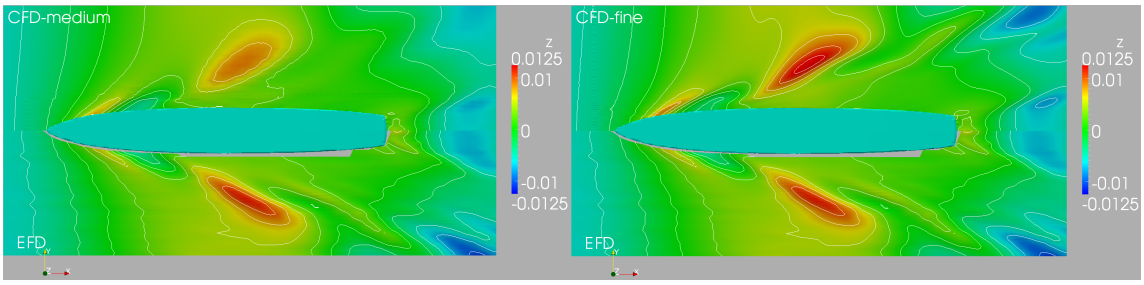

(c) t/T=0.50

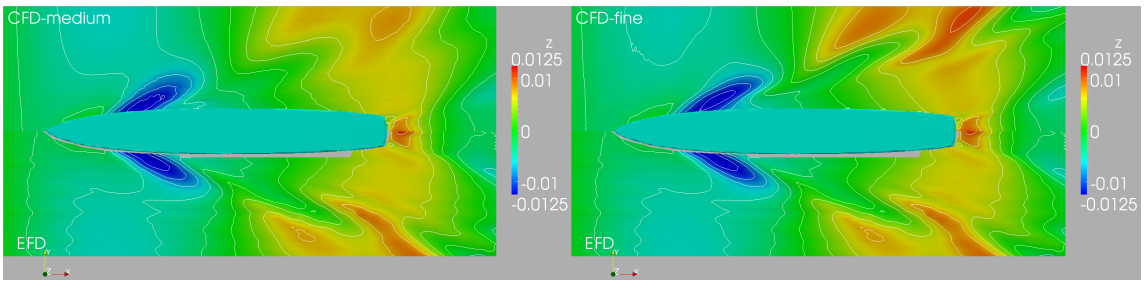

(d) t/T=0.75

Figure 2.10.: Wave elevations of ship in waves, without motions, calculated with 200k (left) and 500k (right) grid compared to experiments (EFD, lower half of each plot)

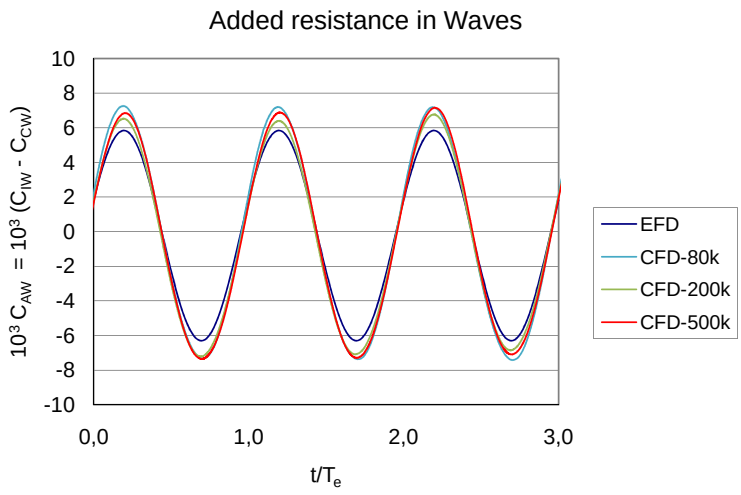

Figure 2.11.: Heave and pitch motion time histories from CFD calculations (200k grid) and experiments [51]

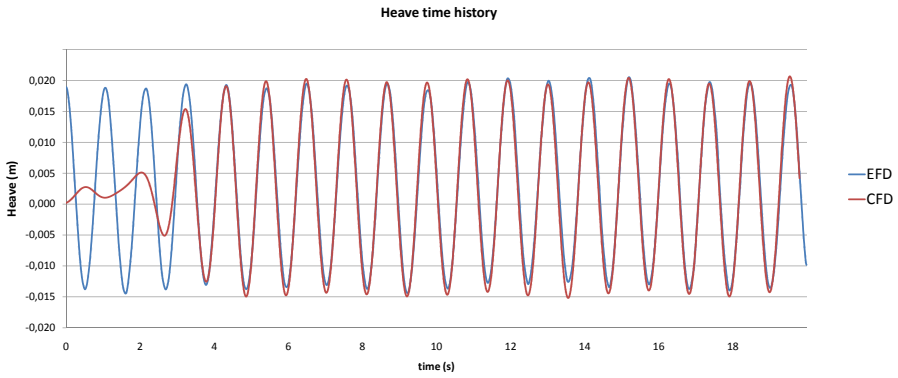

(a)

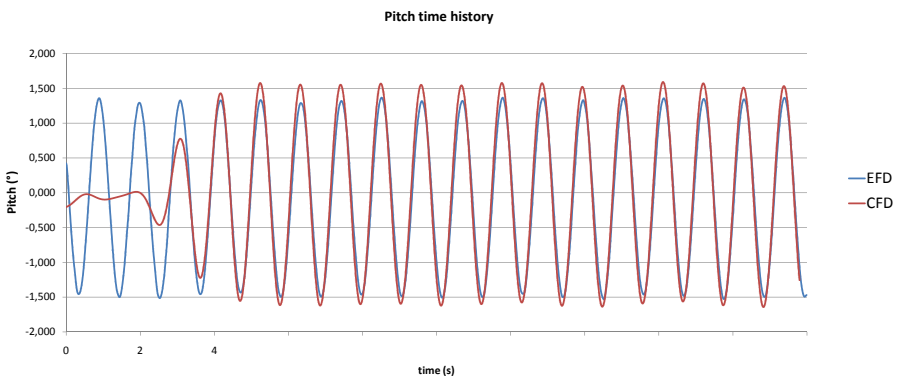

(b)

Figure 2.12.: Heave and pitch motion time histories from CFD calculations (200k grid) and experiments [51]

2.8. Partially Parametric Approach for Geometry Variation

Within this investigation work, the search for better, new bulbous bow configurations, is a field of special interest. The ships with these new, modified bulbous bows will be studied in detail in chapter 5. For the variation of the bulbous bows, a simple approach has been developed and will be presented here.

2.8.1. General Aspects

The partially parametric approach for geometry variations is often a good compromise between full parametric methods and standard geometry definition methods. In 1998, Harries [40] presented a novel technique for full parametric geometry definition. Since 2006, Harries et al. [41] and Abt et al. [9] have presented a series of publications discussing new possibilities for partial parametric methods, pointing out the clear advantages of this method for existing geometries. In 2009, Hochkirch [45] presented a similar method within an application example.

The method for the modification of bulbous bows which will be described here has clear drawbacks compared to more complex methods and is only suitable for small, global modifications of the bulbous bows, thus providing a fast and reliable solution for most needs.

2.8.2. Bulbous Bow Transformation Parameters

Following transformations for the sections of the bulbous bow and its vicinity have been defined and implemented:

Translations

- x tip translation (δx_{tt}, see fig. 2.13 left)
- x inner translation (δx_{ti}, see fig. 2.13 right)
- z tip translation (δz_{tt}, see fig. 2.14 left)

The translations for the both affected coordinates (x- and z-coordinates) are defined as follows:

$$x_t = x + \delta x_{tt} \cdot \frac{x - x_{FP}}{L_{bb}} + \delta x_{ti} \cdot \left(\frac{-1}{(1-d)^2} \left(\frac{x - x_{FP}}{L_{bb}} - d \right)^2 + 1 \right) \tag{2.64}$$

$$z_t = z + \delta z_{tt} \cdot \left(\frac{x - x_{FP}}{L_{bb}} \right)^2 \tag{2.65}$$

x_t: translated x-coordinates
z_t: translated z-coordinates
L_{bb}: length of the (base) bulb
x_{FP}: longitudinal pos. of the forward perpendicular
d: point of max. inner shift. Must be < 0.5, when $d = 0$, this point is at FP, when $d = 0.5$, neither the tip nor the FP section are shifted.

Radial Scaling

For the radial scaling, each section is transformed into a local radial 2D coordinate system, with its origin at the center of area of the bulbous part of the section considered.

$$r = \sqrt{x^2 + y^2} \tag{2.66}$$

$$\theta = \begin{cases} 0 & \text{if } x = 0 \text{ and } y = 0 \\ \arcsin(\frac{y}{r}) & \text{if } x \geq 0 \\ -\arcsin(\frac{y}{r}) + \pi & \text{if } x < 0 \end{cases} \tag{2.67}$$

The defined radial scaling is realized by a radial scaling factor S_r (see fig. 2.14, right). The scaled radial coordinates are transformed as follows:

$$r_s = r + r \cdot (S_r - 1) \cdot f_r \cdot f_a \tag{2.68}$$

$$f_r = \begin{cases} 1 & \text{for } r < r_{FP} \\ \exp\left(\frac{-\left(1-\frac{r}{r_{FP}}\right)^2}{2 \cdot c_1^2}\right) & \text{for } r >= r_{FP} \end{cases} \tag{2.69}$$

$$f_a = \begin{cases} 1 & \text{for } x >= x_{FP} \\ \exp\left(\frac{-x_{FP}^2}{2(c_2 \cdot S_r \cdot L_{bb})^2}\right) & \text{for } x < x_{FP} \end{cases} \tag{2.70}$$

with

r_s: scaled radial coordinates
r: radial coordinate of offsets
f_r: radial influence factor. The scaling is gradually decreased for points positioned outside an imaginary cylinder with the shape of the bulbous bow at the FP
f_a: aft position influence factor. The scaling is gradually decreased for points positioned aft of the FP
d: point of max. inner shift. Must be $d \leq 0.5$, when $d = 0$, this point is at FP, when $d = 0.5$, neither the tip nor the FP section are shifted.
c_1: tuning factor. A value of $c_1 \approx 0.5$ is recommended
c_2: tuning factor. A value of $c_2 \approx 0.15$ is recommended

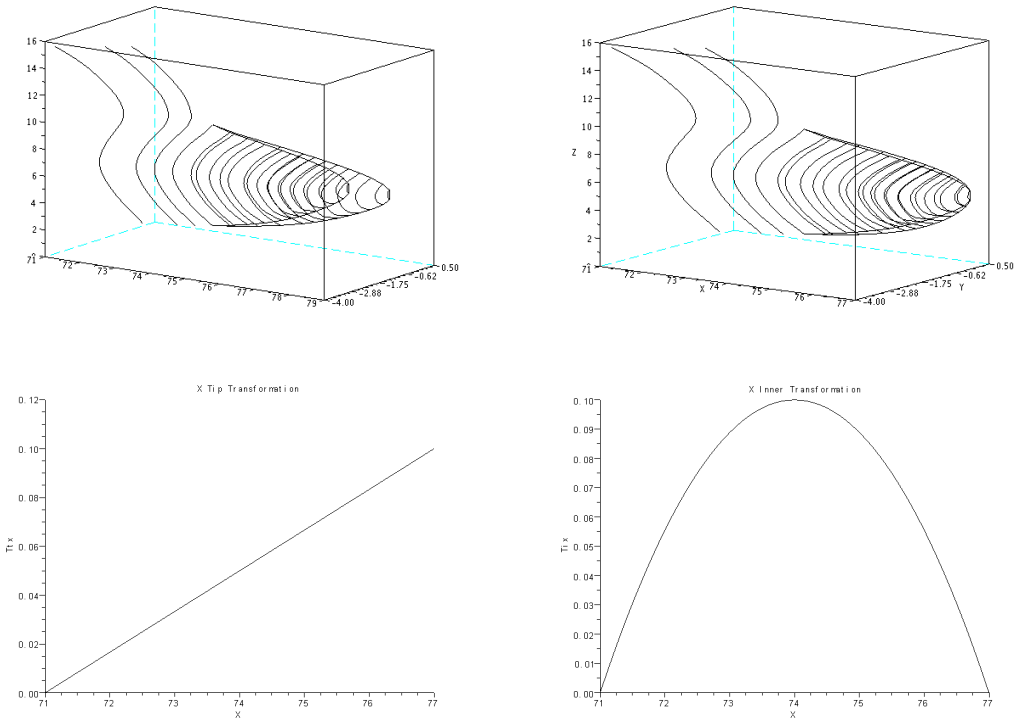

Figure 2.13.: x-tip shifting (left) and x-inner shifting (right)

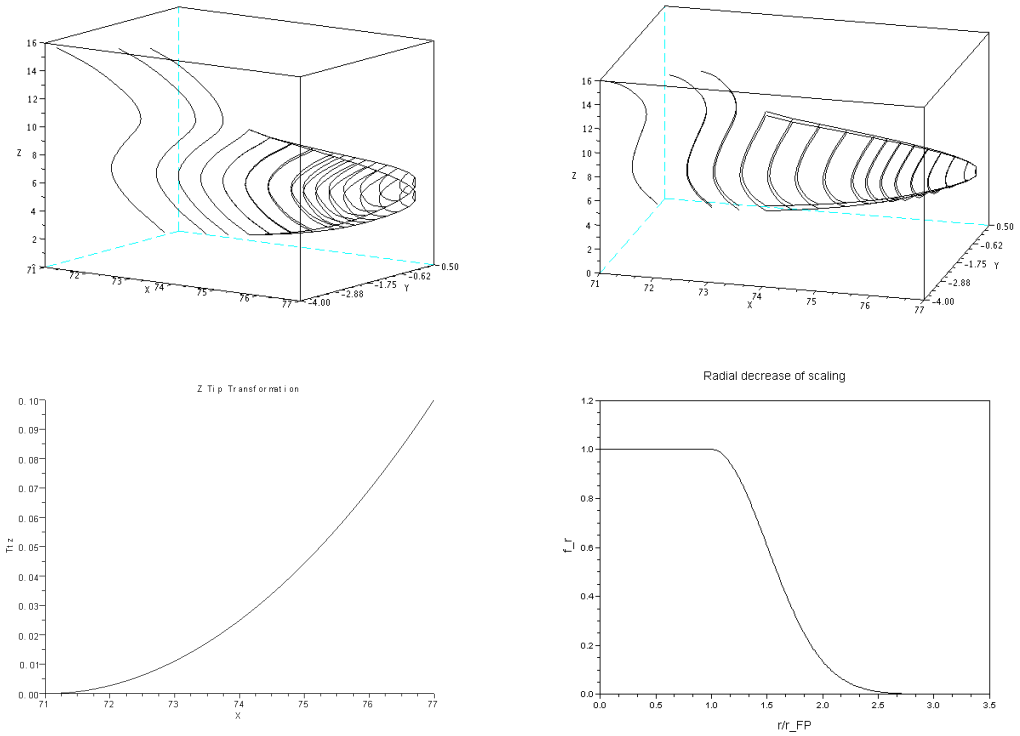

Figure 2.14.: z-tip shifting (left) and radial scaling (right)

3. Modeling of Ship Operation

3.1. General Aspects

In this chapter, the model applied for the operational simulations will be described. As previously introduced in section 2.3.1 (p. 15), two main components, an *environment model* and a *ship model* can be distinguished. In the following, these two main components will be described in detail. Finally, a brief description of the implemented simulation platform `SimOship` will be given (sect. 3.5). It must be mentioned that all descriptions apply for the simulation of the operation of a cargo vessel.

3.2. Environment Model

As mentioned in section 2.3.1, the environment model contains all aspects which are not inherently part of the ship, being two main components distinguished, the operation of the ship and the influence of weather. These will be described here in the form as they were modeled within this study.

3.2.1. Operational Model

The operational model will be defined as all aspects belonging to the environment of the ship which can be considered as known for the purpose of the simulation, mainly those of logistic/strategic nature. These aspects will be considered as constants within this design study and will remain constant for each design variant.

Routes

Routes are defined as the path to be sailed by a ship between a given number of geographic points. In oceanic navigation, the shortest line between two points over a sphere is an orthodromic curve (details see e.g. Dunlap [28]), and routes are subsequently defined as such. Special treatment is needed for routes, whose orthodromic curves lead over land. In this case, the orthodromic route must be considered as unfeasible, but as a basis route for a further modification. This basis route can be approximated by a spline, which is defined by control points. Except of the starting and the ending point, the remaining control points can be shifted–perpendicular to the course of the route–by a *perturbance vector*. This perturbance vector can be varied until the route is feasible. A more straightforward alternative is to apply an optimization strategy to solve this problem, finding the shortest feasible route in a very short time. This has been applied within this work with a simple,

deterministic quasi-Newton algorithm. An example of this approach is shown in figure 3.1.

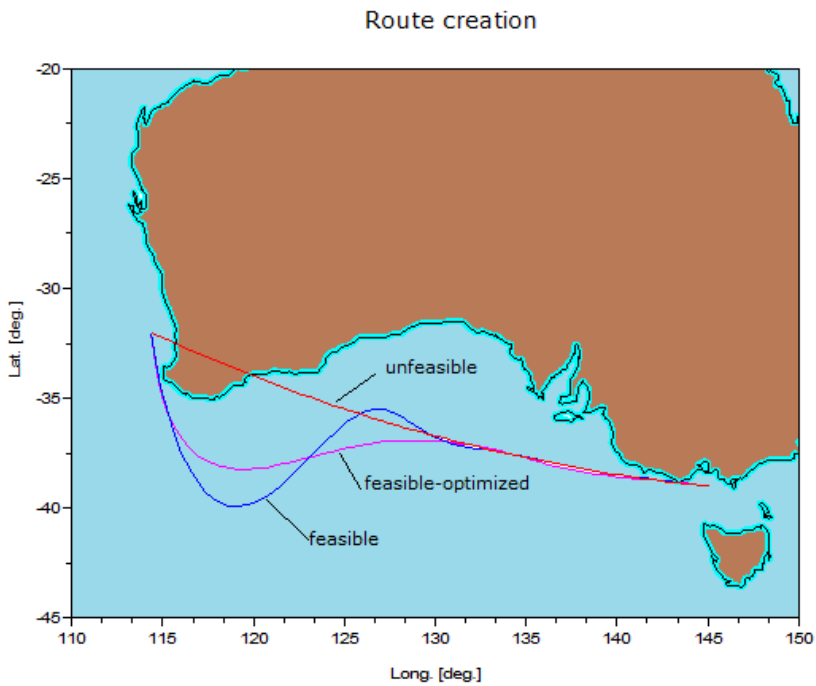

Figure 3.1.: Example of a route creation starting with an unfeasible route. Note that the optimum (shortest) route quality depends of the number of control points

Cargo

Cargo modeling is a task where no certainty of the assumptions made is given. Theoretically, different scenarios can be considered to show the sensitivity of the results due to this task. Nevertheless, and in the same way as for many other aspects within these simulations, simplified approaches will be necessary. Within this study, cargo will be considered as known for each trip made, modeled simply as a mass and a corresponding centre of gravity. In a similar way, ballast and fuel can be treated here as special cargo, considering bunkering after certain mileages or when arriving at a certain port. In this study, fuel and ballast water will be simply added to the total cargo mass.

3.2.2. Weather Model

The modeling of weather is an extremely complex task, which cannot be modeled without simplifications making use of statistical information, especially in the case of a practical application such as an operational simulation representative for the complete lifetime of the ship. In this case, depending on the available resources, weather can be modeled in different complexity levels, such as:

- Arbitrarily defined "worst case conditions", "mean" conditions and comparable approaches

- Global statistical information, such as long-term statistics, e.g. for a region of interest

- Local statistical information (short term statistics), for a defined route and a defined period of time

- Local statistical information, (short term statistics), for different locations in a defined region and a defined period of time

The latter modality will be applied here, since it provides maximum flexibility and permits the consideration of additional features such as route optimization, circumnavigation of rough weather regions, etc. Although these features will not be applied here, further investigations are applying (Balloch [10]) or will apply these using the simulation platform presented here.

The presented operational simulations are performed with existing weather data over a past period of time, so-called *behind-casts*. The ERA-40 database from the European Centre of Medium Range Weather Forecasts (ECMWF) was employed for this purpose [2]. This database contains reanalyzed weather data for a period from 1956 to 2002 in six-hour steps for each 1.5°latitude and longitude. An example of this data for the significant wave height is shown in fig. 3.2. For each six-hour period, a statistical representation of the weather needs to be undertaken. Following information is recalled from the ERA-40 database:

- Significant wave height $H_{1/3}$ [m]

- Mean wave period T_1 [s]

- Mean wave direction χ_m [°]

- Wind velocity components V_u (west-east) and V_v (south-north) [m/s]

With this information, an 1D-spectrum for the sea can be calculated. Such a wave spectrum can be modeled using different formulations; typical wave spectrum formulations are Pierson-Moskovitz, JONSWAP and Bretschneider. In this study, the mean JONSWAP spectrum was used according to the formulation of the ITTC'78 for fetch limited situations [52]:

$$S_\zeta(\omega) = \frac{172.8 \cdot H_{1/3}^2}{T_1^4} \cdot \omega^{-5} \cdot exp\left\{\frac{-691.2}{T_1^4} \cdot \omega^{-4}\right\} \cdot A \cdot \gamma^B \tag{3.1}$$

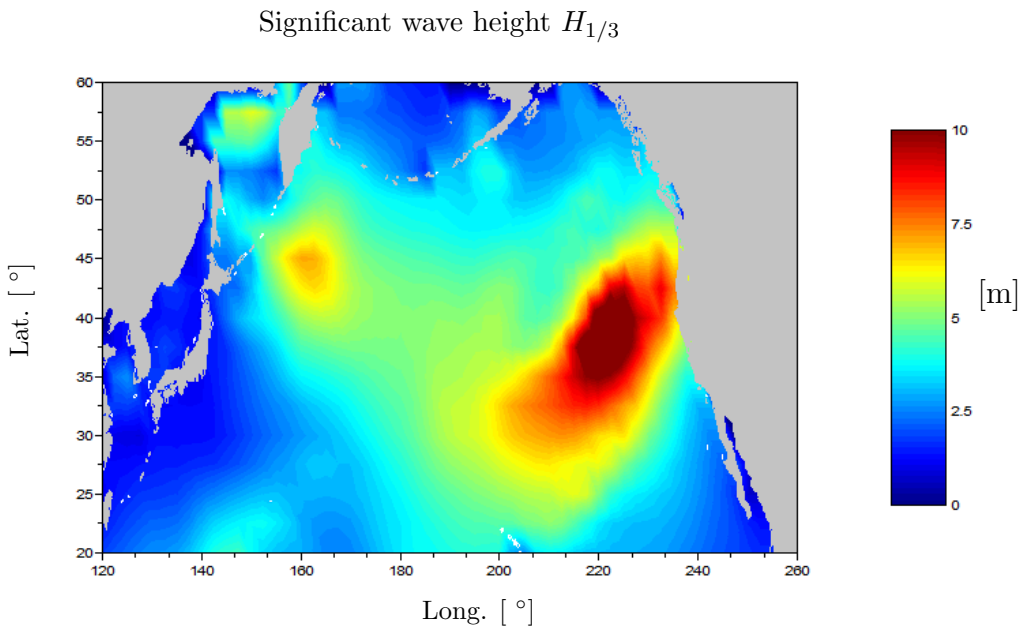

Figure 3.2.: Example of a ERA-40 dataset: significant wave height in the north Pacific

with:

$$A = 0.658 \tag{3.2}$$

$$B = \exp\left\{-\left(\frac{\frac{\omega}{\omega_p} - 1.0}{\sigma \cdot \sqrt{2}}\right)^2\right\} \tag{3.3}$$

$$\gamma = 3.3 \quad \text{(peakedness factor)} \tag{3.4}$$

$$\omega_p = \frac{2\pi}{T_p} \quad \text{(circular frequency at spectral peak)} \tag{3.5}$$

$$\sigma = 0.07|0.09 \quad \text{for } :\omega < \omega_p \,|\, \omega >= \omega_p \tag{3.6}$$

where T_p represents the peak period, which can be approximated by $T_p = 0.772T_1$, according to Journee [62].

The remaining variables, the wind speed components and the wave direction are simply treated as mean values for the six-hour period.

Encounter Weather

The weather description made above is defined in world coordinates (WCS). Since the ship coordinate system (SCS), besides having a different orientation, is also a moving point, all weather information must be recalled in "encounter" form. Proper coordinate transformations (world coordinates to ship coordinates) must be applied here. For the

wave spectrum, an encounter wave spectrum is defined:

$$S_{\zeta,e}(\omega, V_S, \mu) = \frac{S_\zeta(\omega)}{1 - (2\omega V_S/g) \cdot cos\,\mu} \tag{3.7}$$

For the wind, the wind speed and the wind angle must be transformed firstly into the SCS (into true wind speed V_{WT} and true wind angle α_{WT}), and then be made relative to the ship considering its advance velocity, leading to the apparent wind speed V_{WA} and the apparent wind angle α_{WA} as follows:

$$V_{WT} = \sqrt{V_u^2 + V_v^2} \tag{3.8}$$

$$\alpha_{WT} = \arccos\left(\frac{V_v}{\sqrt{V_u^2 + V_v^2}}\right) \cdot \frac{V_u}{|V_u|} - \psi \tag{3.9}$$

$$V_{WA} = \sqrt{(V_{WT} \cdot \sin(\alpha_{WT}))^2 + (V_{WT} \cdot \cos(\alpha_{WT}) - V_S)^2} \tag{3.10}$$

$$\alpha_{WA} = \arccos\left(\frac{V_{WT} \cdot \cos(\alpha_{WT}) - V_S}{V_{WA}}\right) \tag{3.11}$$

From this data, ship responses in irregular waves and ship resistance due to wind are obtained. This will be discussed in sections 3.3.3 and 3.3.4.

3.3. Ship Model

Modeling the ship accurately is an important factor for the success of an operational simulation, and it shall represent a good compromise between accuracy and simplicity while considering available computational resources and existing information about the ship. Due to the focus on hydrodynamics in the present investigation, all aspects related to this task were modeled as accurately as possible, considered from the point of view of an early design stage. These aspects will be described in the present section.

3.3.1. Geometry and Hydrostatics

The geometry of the hull is discretized in form of offsets from which the necessary hydrostatic characteristics are calculated. These offsets are comprised by a variable number of cross sections and a longitudinal contour. From these, hydrostatic data for a matrix of aft and forward drafts T_{AP} and T_{FP} is calculated. Following parameters are calculated:

- Displacement volume ∇
- Longitudinal center of buoyancy x_{CB}
- Vertical center of buoyancy z_{CB}
- Wetted surface S

- Waterline length L_{WL}
- Waterline breadth B_{WL}
- Waterplane area A_{WL}
- Main section area A_{MS}
- Transom area A_{Tr}
- Bulbous bow area A_{bb}

These can be recalled within the simulations to find the floating condition for any given cargo. This is done given the ship's total weight $W = g\Delta$ and the longitudinal centre of gravity x_{CG} by solving a two equation system, with T_{AP} and T_{FP} as unknowns and considering static equilibrium ($\Delta = \rho\nabla$ and $x_{CG} = x_{CB}$). This can be formulated:

$$\nabla(T_{AP}, T_{FP}) = \Delta/\rho \tag{3.12}$$

$$x_{CB}(T_{AP}, T_{FP}) = x_{CG} \tag{3.13}$$

The solution is solved numerically and the actual floating condition is obtained. This will be addressed by all simulation modules where this is relevant, especially for ship resistance and seakeeping.

3.3.2. Calm Water Resistance

Different options have been considered for the modeling of calm water resistance. Flexibility must be provided here, since, as a tool intended to be used during an early design stage, different methods must be available. As usual, if no model test data is available, the determination of the wave resistance coefficient c_W and the form factor k are the main points of interest. The remaining coefficients are estimated according to the ITTC as described in section 2.5.

Holtrop & Mennen's Method

The estimation of the ship's resistance by statistically based methods is always a good starting point in the iterative process of ship design. The method of Holtrop and Mennen (1982, [50] and 1984, [49]) has been made available in the simulation platform `SimOship`. All necessary hydrostatic information is addressed from the hydrostatics calculations and total calm water resistance is calculated for all floating conditions defined. This add-on only has value for very preliminary computations or to compare CFD or experimental results with it.

Potential Flow CFD Method

In ship design, a typical step, while comparing different design variants, is the calculation of the wave resistance with potential CFD methods. This is especially advantageous when combined with formal optimization methods, as discussed in section 1.2. Compared to RANSE CFD methods, potential CFD methods are much less time consuming but, when calculating a great amount of variants and for a great amount of velocities and floating conditions, the required computational effort should not be underestimated. For this reason, a response surface method has been applied here to interpolate wave resistance for any floating condition addressed from the hydrostatics module, being only a comparatively small number of input points (i.e. potential CFD calculations) necessary. Fig. 3.3 shows an example of such a response surface for a Froude number $F_n = 0.250$. Details and results will be shown in chapters 4 and 5.

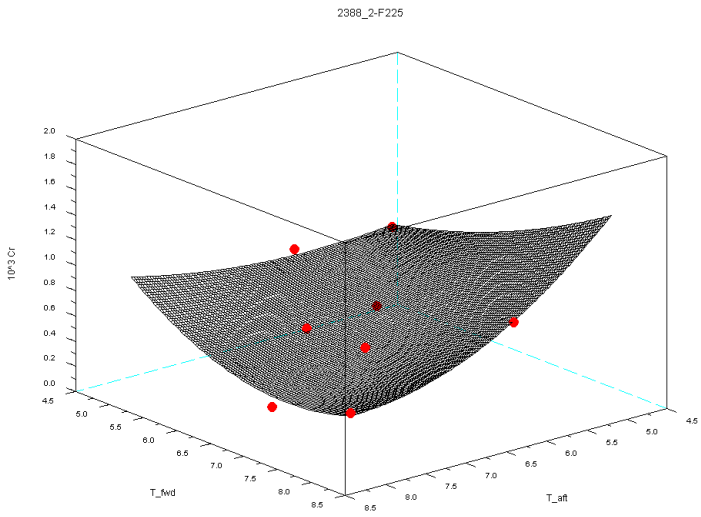

Figure 3.3.: Example of a response surface for wave resistance

Experimental Data

Experimental data can be directly addressed into the simulation platform `SimOship`. The principles involved have been explained in section 2.5.

3.3.3. Ship Motions and Added Resistance in Waves

The modeling of the seakeeping characteristics is performed in the frequency domain. Response amplitude operators (RAO's) for the motions and forces of interest are superposed upon the encounter sea spectrum to obtain the response spectrum, from which e.g. mean responses are derived. This data is presented summarized in non dimensional form

considering unitary wave amplitude $\zeta_a = 1$, re-writing the motions notation as follows:

$$|\hat{\eta}| = \frac{|\hat{\eta}|}{\zeta_a} \tag{3.14}$$

Analogous to this, local motion amplitudes $\left|\hat{\xi}\right|$ and local, relative motion amplitudes $\left|\hat{\xi}_R\right|$ will be rewritten in the same form. For the added wave resistance, its dimensionless form is defined:

$$C_{AW} = \frac{R_{AW}}{\rho \cdot g \cdot \frac{B^2}{L} \cdot \zeta_a^2} \tag{3.15}$$

Both the experiments carried out by Kracht in the VWS and the viscous CFD computations have been made only for head seas and regular waves, for different wave lengths and ship speeds. This appears to be a suitable solution for saving resources, and an approach to make use of this data is presented here, as applied also by Blume [16]. A discussion on this approach will be given after its description.

For encounter angles between μ =90°and μ =180°, the dimensionless added resistance in waves is assumed as follows [16]:

$$C_{AW}(\omega, \mu) = C_{AW}(\omega, 180) \cdot \cos(180 - \mu) \tag{3.16}$$

For encounter angles between 0°and 90°, the added wave resistance is taken from strip theory calculations. The heave and pitch motion amplitudes available for head seas from experiments or RANS-CFD calculations ($|\hat{\eta}_{head}|$) are complemented with data computed using strip theory ($|\hat{\eta}_{strip}|$) for encounter angles between 90°and 180°with a squared cosine function:

$$|\hat{\eta}_3(\omega, \mu)| = |\hat{\eta}_{3,strip}(\omega, \mu)| + \left\{|\hat{\eta}_{3,head}(\omega)| - |\hat{\eta}_{3,strip}(\omega, \mu)|\right\} \cdot \cos^2(\mu) \tag{3.17}$$

$$|\hat{\eta}_5(\omega, \mu)| = |\hat{\eta}_{5,strip}(\omega, \mu)| + \left\{|\hat{\eta}_{5,head}(\omega)| - |\hat{\eta}_{5,strip}(\omega, \mu)|\right\} \cdot \cos^2(\mu) \tag{3.18}$$

In this form, head seas (μ =180°) motions correspond to experimental measurements or viscous CFD calculations, with a decreasing influence up to beam seas (μ =90°), using from this angle until μ =0°(following seas) the results from strip theory calculations directly.

As it will be explained in chapters 4 and 5, the operational simulations to be undertaken are intended to compare the performance of different bulbous bow variants with very similar shapes. Preliminary results of added resistance in waves and motions from strip theory calculations showed practically no sensitivity to the small shape variations between bulbous bow variants, which is opposite to the tendency shown by results from more accurate methods such as viscous CFD computations or from experiments (a discussion of these results will be given in sect. 4.4.2). For the presented approach, this means that the main differences between the seakeeping performance of different bulbous bow variants

will be originated from differences in the results in head seas obtained from viscous CFD calculations (or alternatively experimental data if available) and the influence of these results for wave angles until 90°(as defined by eqs. 3.16 to 3.18). This also means that, for the comparison between results obtained from operational simulations, the relevance of the seakeeping results for following seas, where no influence of CFD or experimental data is given, is negligible.

The assumption from eq. 3.16, as presented by Blume, has its origin in linear theory and implies that no added resistance in beam seas ($\mu = 90°$) would be present. This is, from a general point of view, not correct. To confirm this, CFD calculations of a ship (which will be presented in chapter 4 as parent ship) in regular waves ($T_e = 1.20$s) for different heading angles were performed. In fig. 3.4, results of added resistance from these calculations are shown, normalized by the added resistance in head seas. These results are compared to a cosine function representing the approach presented by Blume. While CFD results confirm the incorrectness of the assumption made for $\mu = 90°$, they also show the practicability of this assumption for the remaining angles. Due to the high uncertainty about the influence of the intended small shape variations into the added resistance in *beam* seas, the validity of the curve shape from CFD results for all ships considered within this investigation is questionable. Additionally, it must be recalled that the wave-angle dependency studied with CFD has been made for a single encounter wave period ($T_e = 1.20$s). Therefore, the influence of the encounter frequency into the shape of this curve is unknown [1]. For these reasons, and due to the comparative nature of the present study, the assumption presented by Blume will be applied in all operational simulations presented.

As a matter of fact, it would be desirable to count with viscous CFD or experimental results for each of the ships considered and for all wave angles, being this one of the drawbacks which must be acquainted with when interpreting results from the operational simulations presented in the following. Nevertheless, the presented approach appears to be convenient, especially when considering the significantly lower required computational resources, and when accounting that the influence of strip theory calculations in following seas (and the significant deficiencies of the method for these heading angles) is minimized since only relative results, and not absolute values, are of interest within this study. The relativeness of results is therefore always supported by the fact that they were originated from viscous CFD or experimental results in head seas.

In a similar manner as for the wave angles, floating conditions where no viscous CFD or experimental data is available must be considered in the operational simulations. Therefore, added resistance and ship motion amplitudes are corrected with the help of strip theory. For this purpose, the ratio between the seakeeping results of the actual and the design floating condition obtained from strip theory is multiplied with the wave-direction corrected results from the design floating condition. In the same manner as for the corrections for the wave angles, this causes an uncertainty in the quality of final results which

[1] In Grigoropoulos et al. [36], this influence is studied with strip theory for a Series-60 ship for different encounter frequencies. Results of wave angle dependency of the added resistance in waves show for most cases curve shapes very similar to a cosine function

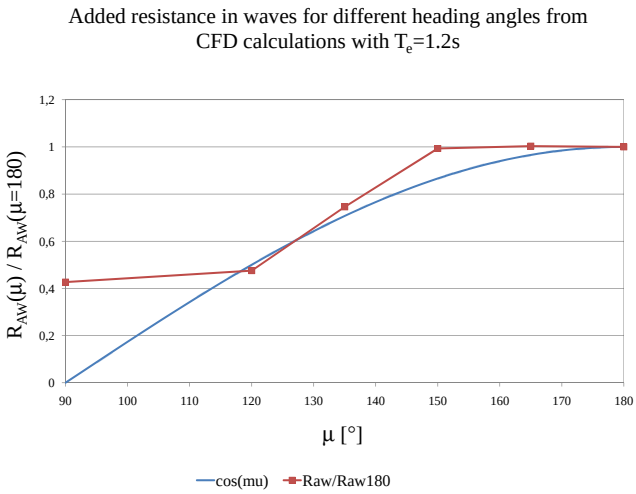

Figure 3.4.: Added resistance in waves for different heading angles

shall be kept under consideration.

For the operational simulations, the seakeeping data generated in the described manner for different wave lengths, wave directions, ship velocities and floating conditions is stored, being superposed, for each time step, to a wave spectrum for the evaluation of ship responses in irregular waves.

The wave spectrum (described in sect. 3.2.2), obtained at each time step of the operational simulation, and the described seakeeping responses of the ship are superposed to obtain the encounter spectra in irregular waves:

$$S_3(\omega,\mu) = \left|\hat{\eta}_3(\omega,\mu)\right|^2 \cdot S_\zeta(\omega,\mu) \tag{3.19}$$

$$S_5(\omega,\mu) = \left|\hat{\eta}_5(\omega,\mu)\right|^2 \cdot S_\zeta(\omega,\mu) \tag{3.20}$$

from which the *spectral moments* are calculated:

$$m_n = \int_0^\infty \omega^n \cdot S_\zeta(\omega) d\omega. \tag{3.21}$$

These spectral moments are used for the calculation of statistical information of the motions, such as mean and peak values and slamming probabilities for each time step of the operational simulation. In the following, only a short definition for the method applied for slamming assumption and added resistance in waves will be given. General definitions and a more complete derivation on spectral moments can be found, for example, in Lewis [75].

Slamming

For the consideration of slamming, the criterion of Ochi [89] has been applied. This criterion considers a point 10% behind the forward perpendicular as a reference point. As

a first condition for slamming occurrence, emergence of this point must happen. This is the case when the vertical motion amplitude at this point is greater than the local draft d_{bow} (the use of d for draft instead of T has been selected in this section to avoid confusion with periods, also defined by T). The probability of occurrence of such an emergence is:

$$P_{\xi,em} = \exp\left\{\frac{-{d_{bow}}^2}{2 \cdot m_{0,rb}}\right\} \tag{3.22}$$

where $m_{0,rb}$ represents the 0th spectral moment ($n = 0$ in eq. 3.21) of the relative vertical motion at the reference point 10% behind the forward perpendicular of the ship.

The second condition for slamming occurrence is the exceedance of a critical local velocity at the reference point. Ochi presented in his work a threshold relative velocity of 12 feet per second for a 520 feet ship. In non-dimensional form, this critical relative velocity writes:

$$\dot{\xi}_{bow,cr} = 0.0928 \cdot \sqrt{g \cdot L_{PP}} \tag{3.23}$$

The probability of occurrence of local relative velocities higher than the critical value is:

$$P_{\dot{\xi},cr} = \exp\left\{\frac{-{\dot{\xi}_{bow,cr}}^2}{2 \cdot m_{2,rb}}\right\} \tag{3.24}$$

where $m_{2,rb}$ represents the 2nd spectral moment of the relative motions at the reference point at the bow of the ship, which is equal to the 0th spectral moment of the relative velocity at this point $m_{0,rv}$.

From these two probabilities, the total slamming probability is defined:

$$P_{Slamming} = P_{\dot{\xi},crit} \cdot P_{\xi,em} \tag{3.25}$$

$$= \exp\left\{\frac{-{d_{bow}}^2}{2 \cdot m_{0,rb}} + \frac{-{\dot{\xi}_{bow,cr}}^2}{2 \cdot m_{2,rb}}\right\} \tag{3.26}$$

Additionally, the slamming events per hour

$$N_{Slamming} = \frac{3600}{T_{0,rb}} \cdot P_{Slamming} \tag{3.27}$$

can be obtained with a zero-upcrossing period:

$$T_{0,rb} = 2\pi\sqrt{\frac{m_{0,rb}}{m_{2,rb}}} \tag{3.28}$$

Added Resistance in Irregular Waves

The mean added resistance in irregular waves $\overline{R_{AW}}$ for a given wave spectrum S_ζ is calculated from:

$$\overline{R_{AW}} = 2\int_0^\infty S_\zeta(\omega) \cdot R_{AW}(\omega) d\omega \tag{3.29}$$

with R_{AW} in regular waves obtained from CFD computations or experimental data combined with strip theory results, as previously explained.

3.3.4. Total Resistance, Propulsion and Machinery

The total ship resistance in service conditions R_{TS} is modeled as:

$$R_{TS} = R_{TS0} + R_{AW} + R_{AA} + \Delta R_{AR} \tag{3.30}$$

with total ship resistance in calm waters R_{TS0}, added resistance in waves R_{AW}, wind resistance R_{AA}, and increased roughness resistance ΔR_{AR} (considering fouling). Ship resistance in calm waters and added resistance in waves are available from experiments or numerical flow simulations (CFD) as described in sections 3.3.2 and 3.3.3, wind resistance is calculated using the Wilson drag coefficients (in [75]) and fouling resistance is estimated using a fouling diagram for a five year period provided by International Marine Co. [5] for a self polishing copolymer coating[2]. Other resistance components, as mentioned in section 2.5, have not been considered for the simulations, since they are constants and not of interest for comparative purposes.

The propulsion of the ship is modeled according to the ITTC 1978 recommended procedures [55] using an open water diagram for the full-scale propeller and considering thrust identity. For this purpose, model data for resistance (resistance model test), propeller characteristics (open water mode test) and propulsion (self-propulsion test) should be available. If this is not the case, appropriate estimations can be made.

For the open water diagram, propeller thrust T and torque Q are represented in dimensionless form:

$$K_T = \frac{T}{\rho n^2 D^4} \tag{3.31}$$

$$K_Q = \frac{Q}{\rho n^2 D^5} \tag{3.32}$$

and are plotted over the propeller advance velocity J:

$$J = \frac{V_A}{nD} \tag{3.33}$$

where ρ is the water density, n the propeller rate of revolutions, D the propeller diameter and V_A the advance speed of the propeller. An example of such an open water diagram is shown in fig. 3.5. The correlation between model- and full-scale is made as recommended by the mentioned procedure (ITTC 1978). The working point of the propeller is found defining:

$$\frac{K_T}{J^2} = \frac{R_{TS}}{(1-t)\cdot(1-w_{eS})^2 \cdot V_S^2 D^2 \rho} \tag{3.34}$$

with R_{TS} from eq. 3.30, the thrust deduction factor t from a thrust variation test (or alternatively as recommended by ITTC 1978 [55]) and the effective wake fraction of the

[2]The choice of this coating is arbitrary and represents a typical modern, TBT-free antifouling coating. The data presented by International Marine Co. originates from the monitoring of over 70.000 ships and over 30 years

ship w_{eS} from the full-scale corrections of the effective wake fraction of the model (w_{eM}) as recommended by the ITTC 1978 procedure. A detailed description of the involved model test procedures and detailed definitions about the mentioned propulsive factors (thrust deduction and wake factors) have been amply discussed in several textbooks (e.g. Kracht [70]) and will not be discussed here.

When multiplying the resultant term of eq. 3.34 with the range of J^2, a curve for the required thrust is obtained. The intersection of this curve with the thrust coefficient curve K_T shows the propeller working point. An example is outlined in fig. 3.5. For this working point, the required propeller torque coefficient K_{QS}, the open water efficiency η_{0S} and advance ratio J_S are obtained. From these, and considering the relative rotative efficiency η_R as known (assuming thrust identity and available open water and self-propulsion tests), the propeller rate of revolutions,

$$n = \frac{V_S(1 - w_{eS})}{J_S D_S} \tag{3.35}$$

the delivered power,

$$P_D = 2\pi\rho n^3 D^5 \frac{K_{QSB}}{\eta_R} \tag{3.36}$$

and the engine brake power by considering a given mechanical efficiency η_M

$$P_B = \frac{P_D}{\eta_M} \tag{3.37}$$

are obtained and can be taken as input for the engine operation diagram.

The main engine characteristic is defined by an engine layout diagram. In this diagram, the engine manufacturer defines the power and speed combination points L_1, L_2, L_3 and L_4. Additionally, the specific fuel oil consumption *sfoc* is given for each layout point. From these points, several lines are defined, which themselves define the permitted operation area of the main engine and conform the engine layout diagram. An exemplar engine layout diagram is shown in figure 3.6. According to the marine engine manufacturer MAN B&W [78], the main engine can be thus defined by following lines:

- an engine overload line, caused by the limited achievable charge pressure of the turbo compressor at lower rates of revolutions. This line is also known as "turbo bound" and is approximately proportional to the square of the rate of revolutions n.

- a line between layout points L_1 and L_3 defining the maximum *mean effective pressure* (*mep*) allowable for continuous operation.

- a line between layout points L_2 and L_4 defining a constant mean effective pressure (values vary depending of the engine). This line is used as an orientation for the choice of the engine [78], being engine operation below and above this line allowed. This line also represents approximately the region with lowest specific fuel oil consumption of the engine.

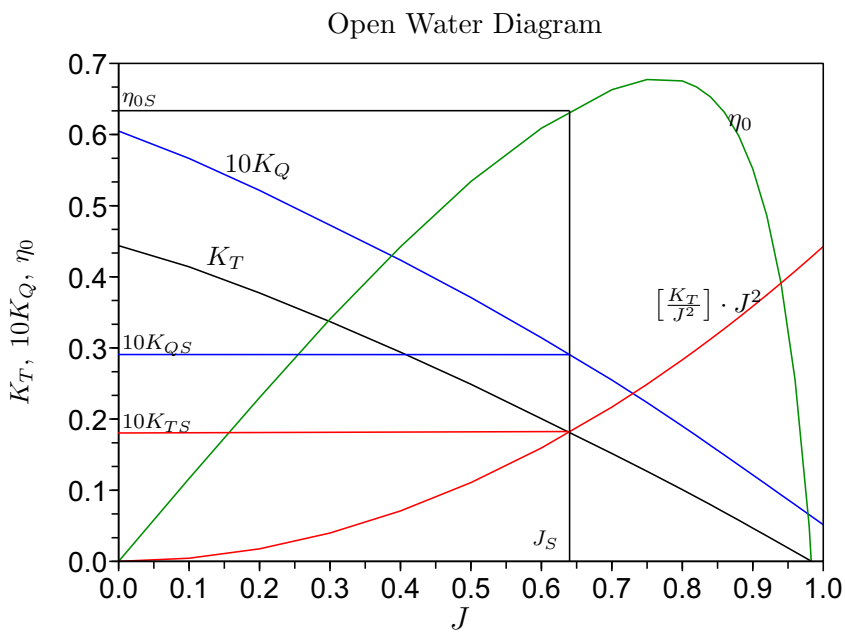

Figure 3.5.: Open water diagram and propeller working point

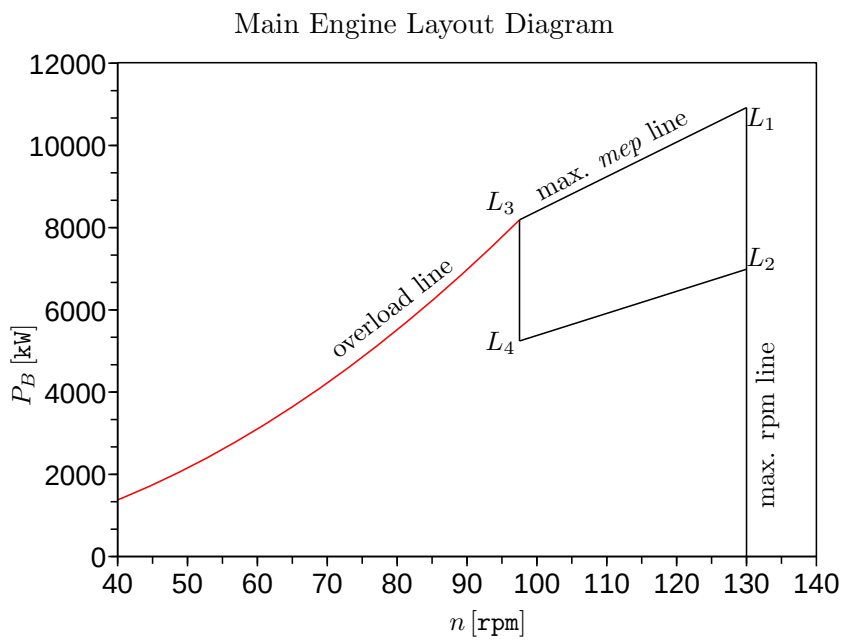

Figure 3.6.: Example of main engine layout diagram

- a maximum rate of revolutions line (100% to 105% of max. rpm)

Entering the brake power from eq. 3.37 with the corresponding rate of revolutions in the engine layout diagram, the feasibility of the attempted working point can be controlled. Subsequently, the specific fuel oil consumption can be obtained from the manufacturer (normally as function of the mean effective pressure *mep*) and at last, the fuel oil consumption for a time period Δt can be obtained:

$$FOC = P_B \cdot \Delta t \cdot \text{sfoc} \tag{3.38}$$

This fuel oil consumption is, within the simulations, added over the total simulation time to obtain the fuel oil consumption during the total time period.

3.4. Measure of Merit

To compare different design variants within a design study, and especially for optimization purposes, a measure of merit must be defined. This measure of merit must identify clearly the aspect to be compared between all variants simulated. In most of the cases, the direct comparison of economic profit is a very suitable measure of merit when enough reliable and detailed information of all aspects involved is available. If this is not the case, a typical established economic measure of merit can be used. Most of these measures of merit define the *average annual costs* **AAC** (normally in US$) as follows:

$$AAC = CF + CO + CR \cdot P \tag{3.39}$$

where CF are the annual fuel costs, CO are the annual fixed operating costs and $CR \cdot P$ the annual capital costs, defined themselves by the capital recovery factor CR and the invested capital P in US$. A widespread exponent of an economic measure of merit is the *required freight rate* **RFR**:

$$RFR = \frac{AAC}{MC} = \frac{CF + CO + CR \cdot P}{k_c \cdot W_{PL} \cdot D} \tag{3.40}$$

where MC is the annual transport volume (in tons-nmi per year), k_c is a service factor for the cargo (i.e. ratio of mean transported cargo to design payload), W_{PL} the design payload (in t) and D the covered distance per year (in nmi). For further information see e.g Nowacki (1985, [85]).

For this study, a comparative measure would be of special interest, to identify differences between the bulbous bow variants for each region and scaling factor investigated, as it will be described in chapters 4 and 5. For this purpose, ships will be compared within *groups*. A group is a set of ships of similar characteristics (e.g. different bulbous bow variants but equal main dimensions) and normally covering the same route. This reflects the typical evaluation made by shipping companies when deciding between different variants, vendors or concepts for a transport task.

For this purpose, a *fuel equivalent cost* **FEC** will be defined, i.e. a measure of economic merit relatively comparable to annual fuel costs. In this approach, only fuel oil costs are considered as variable, while all other operating and capital costs remain equal (for ships of the same group, e.g. same size). This is expressed in terms of an assumed relationship between the mean fuel costs within a group and the *average annual costs* valid for each ship of this group. This relationship is expressed by a fuel costs coefficient k_f as follows:

$$CF_{mean} = k_f \cdot AAC \tag{3.41}$$

Applying this fuel costs coefficient into eq. 3.40, it can be written:

$$RFR = \frac{CF_S + \frac{1-k_f}{k_f} \cdot CF_{mean}}{MC_S} \tag{3.42}$$

where CF_S are the annual fuel oil costs of the ship (in US$), CF_{mean} the average fuel oil costs of all ships of the group considered (in US$) and MC_S the annual transport volume of the ship (in t-nmi/year). The value of k_f, viz., the relationship between fuel costs and average annual costs is of special interest and depends on many parameters, especially of fuel prices and global economy and must be set according to realistic shipping costs. A detailed discussion about shipping costs can be found in Buxton [20]. Additionally, different scenarios with different values for k_f can be studied and thus establish a profitability range (a discussion on this aspect will be given for an application case in sect. 4.6.3 , p.96). In this study, the input of realistic values for k_f is attempted by means of simple estimations and actual fuel prices.

The different annual transport volume MC_S of each ship within a group also plays an important role. A ship being able to achieve a higher mean speed can, at least theoretically, complete more voyages per year increasing its transport capacity. Alternatively, this ship can decrease its mean speed and thus save considerable fuel costs[3]. Taking eq. 3.40 and decomposing the fixed costs component ($\frac{CO+CR \cdot P}{MC_S}$) into a component which is common to all ships and a difference value, the required freight rate can be rewritten:

$$RFR = \left\{\frac{CF}{MC}\right\}_S + \{CO + CR \cdot P\} \left[\frac{1}{MC_{mean}} + \delta \frac{1}{MC_S}\right] \tag{3.43}$$

The fuel equivalent costs attempt to consider all costs which are not common for each ship within a group and are defined as:

$$FEC = \left\{\frac{AAC}{MC}\right\}_S - \left\{\frac{CO + CR \cdot P}{MC}\right\}_{mean} = \left\{\frac{CF}{MC}\right\}_S + \left\{\delta \frac{CO + CR \cdot P}{MC}\right\}_S \tag{3.44}$$

In this form, fuel equivalent costs show the fuel costs of the ship and the costs difference due to the different transport efficiency of the ship and the mean transport efficiency value for the group. All values represent the costs of the transportation of one tonne cargo over

[3] A short discussion on this task for an application case is given in section 4.6.4 "Slow Steaming Simulations"

a nautical mile. If W_{PL} and k_c as defined in eq. 3.40 are equal for all ships, FEC can be rewritten as:

$$FEC = \left[\frac{CF_S}{D_S} + \frac{1-k_f}{k_f} \cdot CF_{mean} \left\{ \frac{1}{D_S} - \frac{1}{D_{mean}} \right\} \right] \cdot \frac{1}{k_c \cdot W_{PL}} \tag{3.45}$$

The second summand can be thus interpreted as "penalty costs" due to less navigated miles or alternatively "cost savings" due to more navigated miles. The most important advantage of this definition, compared to RFR, is that the magnitude of the value remains similar to pure fuel costs (per mile and cargo tonne), being able to be easily compared to these. Additionally, no information about capital or further operational costs is needed. Since fuel prices are always known and fuel consumption (e.g. per year) is often calculated during ship design, the described *fuel equivalent costs per mile and tonne* can be advantageous for comparison purposes, despite the slightly higher complexity of its definition.

3.5. Implementation of the Simulation Platform

The presented components modeling the ship operaion have been implemented into the program `SimOship` by means of the SciLab interpreted language. SciLab [7] is an open source project and the language attempts an easy handling of complex matricial operations, including several pre-implemented functions for this purpose. The implementation of `SimOship` was started for the simulation of the operation of wind assisted ships (Tampier [109]), and has been applied successfully for different purposes within several degree theses (Geittner [31], Oschmann [93], Balloch [10]) under the guidance of the author. The main characteristics of the implemented simulation environment are:

- Easy usability (both for the programmer and the end-user). This is centered in two features: a graphical user interface (GUI) and the ability to be run fully automatized by scripts.

- Modular. Functions are generalized and usable for and from any other modules or programs

- Strict separation between code and simulation data. This means, the program can be used for any ship, in any region of the world and any simulation time. It is not constrained to the performed examples nor code modifications have to be undertaken to simulate new cases.

- Flexible. Several data import functionalities have been implemented, specially for the geometry (offsets as generated by DelftShip or NAPA), for hydrodynamic data (e.g. PDSTRIP-Import) and for weather data from the ECMWF (`grib-` and `nc-`data).

- Optimized. When possible, code has been optimized in order to reduce computational time (iterations, interpolations, file operations have been conveniently implemented for this purpose).
- Open. Chosen modules have been contributed to other projects (e.g. Scilab, PDSTRIP) as Open Source Code.

Briefly described, the program simulates the operation of merchant ships from the information collected in a *case* (case file), which declares further files which describe all aspects of the two main components of the simulation: a *ship* and an *environment*. These files contain information about ship geometry, hydrostatics, resistance, propeller, seakeeping, machinery but also environment information about the route, cargo and weather, among others. A complete description can be found in the program manual (SimOship - General Description and Usage) [108]. The full program structure is depicted in fig. 3.7. From the structure of the program, four important tasks will be described in more detail: *Preprocessing*, *Simulation modes*, *Trip evaluation* and *Time step evaluations*.

Preprocessing

The preprocessing for each simulation case (marked in yellow in fig. 3.7) consists of the collection of all necessary information for the execution of an operational simulation. This includes the previously mentioned descriptions of *ship* and *environment*, including the possibility of feasibility checks (e.g. cargo check for realistic floating conditions). All steps within preprocessing are done with a graphical user interface (GUI).

Simulation Modes

The simulations can be realized in four different modes (marked in pale red in fig. 3.7), as it will be shown for the application cases in chapters 4 and 5:

- Full simulation mode: for simulations with variable speed and variable floating condition
- Fixed trim simulation mode: for simulations with variable speed but fixed floating condition
- Target speed simulation mode: full or fixed simulations where speed is adjusted dynamically to achieve a target mean speed over the simulation time
- Simple simulation mode: for simulations with fixed service speed and fixed floating condition.

Operational Simulation

For the given time period, the ship undertakes the programmed trips repeatedly (this trips can be also combinations of different routes or round-trips) including, if needed,

port and/or dock time periods. For each trip, following steps are realized (marked in pale purple in fig. 3.7):

- Processing of route, departure time and estimated time of arrival
- Loading of given cargo, re-filling of tanks if required and calculation of resulting floating condition
- Determination of the hydrodynamic characteristics of the ship in the departure floating condition (by means of response surfaces, interpolation or look-up tables)
- Operational simulation of the trip

Time Step Evaluations

For each time step of the operational simulation, following tasks are considered (marked in pale grey in fig. 3.7):

- Local weather conditions according to sect. 3.2.2
- Calculation of ship responses, total resistance and propulsion characteristics according to sect. 3.3.4
- Feasibility check leading to voluntary or involuntary speed loss and the repetition of the previous tasks until a feasible condition is reached

Post-processing

Results can be processed for a single ship (e.g. total fuel consumption, mean service speed, encounter weather) or compared with other ships (e.g. FEC for several design variants). Results for the application cases will be shown in detail in chapters 4 and 5.

3.5.1. Integration and Automatization for Design Purposes

A central feature of the presented implementation and the underlying design methodology is a high automatization grade, intending to make design studies with a large number of design variants possible and, if required, the application of formal optimization techniques. Especially the integration of the presented simulation environment into an optimization process including automatic geometry generation, automatically executed numerical flow calculations (CFD) and automatic full data analysis are mayor issues which were not possible to realize. Notwithstanding to this, all steps were conceived in order to do so in the future, in case of further studies applying the proposed methodology. The lack of full automatization is justified by following aspects:

- Since many methodologies had to be coordinated to work together for a first time, the error probability in single steps is very high. A rigorous control of all data fluxes, intermediate results and programming issues (mainly code optimization and debugging) was imperative.

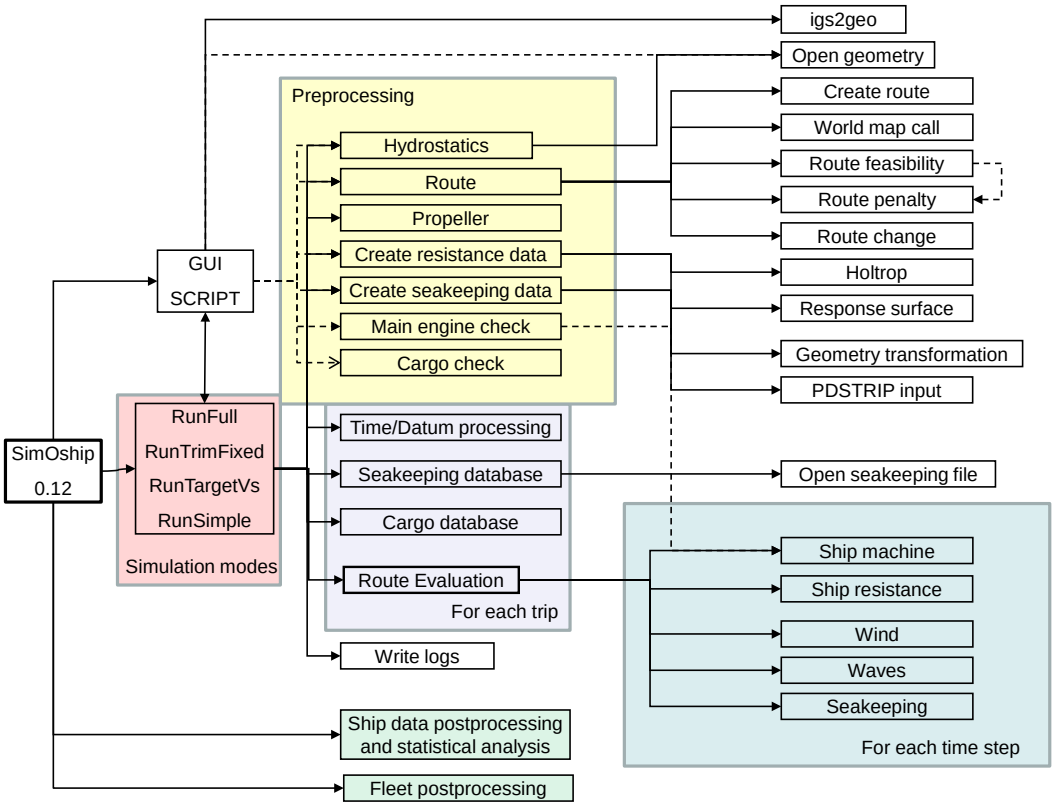

Figure 3.7.: SimOShip 0.12 Program Structure

- The parametric model used for the creation of subvariants has been kept very simple and does not include any surface quality control mechanism. For this reason, the manual control of each subvariant generated was necessary.

- One of the goals of this investigation was to use a minimum of proprietary software. This was successfully achieved, with the drawback of a higher implementation effort for different format or data converters and (small) software limitations. Some of these tools would have required further refinement to be able to work in a fully automatic mode. A major issue in this context was the implementation of `TUBsixDOFFoam`.

4. Special Application Case Exploiting Experimental Data

4.1. Introduction

In this chapter, the application of operational simulations is shown by means of a practical example. This example - the simulation of the operational life of a ship - makes use of available experimental data to model seakeeping performance (motions and added resistance) and calm water resistance of the ship in question.

From a general point of view, the ship operation model presented in the previous chapter, intended to simulate the operational life of a merchant vessel, can be applied recalling data from any available source. Keeping in mind that, in a preliminary design stage, experimental data is rarely available, the example presented in this chapter represents the rather unusual case of some experimental data being available.

Since the application of operational simulations in the manner as it is presented in this study is not a widespread technique yet, it has been considered convenient to discuss some detail aspects about these operational simulations with the help of an example case where relevant hydrodynamic data relies on experiments. Since the uncertainty of those central hydrodynamic aspects is minimal (at least when compared to numerical data), they can be excluded from the discussion about the presented simulational approaches themselves (i.e. the *simulation modes* presented in sect. 3.5). This special application case is therefore intended to discuss about aspects of the operational simulations more than about the results of each of the studied design variants and the consequences of the application of this methodology for the design of bulbous bows. These aspects, of central meaning for the outcome of this investigation, are discussed in chapter 5, where a general application case, recalling numerical data only and thus representing the usual situation of no experimental data being available, is presented. Since some of the operational simulations presented in this chapter have been performed with experimental data both for seakeeping and ship resistance, results will serve also as a validation for further results from operational simulations where numerical results are addressed partially or totally.

The presented application case will make use of the experimental data provided by the investigation of Kracht [68]. This dataset, which can be recalled as *model data*, is extrapolated with different scaling factors λ and simulations are executed for different routes over a given time period. For all simulations undertaken within this study, a simulation period of five years was chosen, considering it as statistically representative for the operational life of the ship. This decision was made after comparing the results from simulations over one, two, five and ten years of duration, showing that simulations

over periods shorter than five years are subjected to large variations in their results when simulations are started with weather data from different years.

The different simulation modes presented in section 3.5 have been tested and will be discussed accordingly, beginning from very simple (and unrealistic) simulations with fixed speed and fixed floating condition up to more complex simulations considering these parameters as variable.

4.2. Simulation Routes

For the presented application case, five different routes have been considered, following the hypothesis that different routes will lead to different best bulbous bow configurations. These routes intend to be representative for typical world shipping paths, and special attention was paid to choose routes where comparatively quiet weather is to be expected and routes where comparatively rough weather is to be expected. These routes are:

- Le Havre (France) - Paranaguá (Brazil)
- Le Havre (France) - Charleston (USA)
- Valparaiso (Chile) - Yokohama (Japan)
- San Francisco (USA) - Yokohama (Japan)
- Melbourne - Perth (both Australia) - Djibouti (Djibouti, Gulf of Aden).

All routes have been defined as orthodromic routes when possible, applying the methodology defined in section 3.2.1 if such a route was not feasible. The routes are plotted in figs. 4.1a, 4.1b and 4.1c. It must also be mentioned that, particularly, the route between Melbourne and Djibouti is intended to represent only a part of a typical shipping route between Oceania/Asia and a Mediterranean port. Since practically almost no weather influence is to be expected in the Red Sea and the Mediterranean, this part of the route has been left aside and can be, if required, considered by simple addition of fuel consumption in calm weather conditions and an estimated small service factor. In the presented operational simulations, this assumption was not made and results shown will comprise only the mentioned partial route.

4.3. Parent Geometry

The ship geometry taken for this application case has its source from the mentioned investigation from Kracht. As outlined in section 1.2, different bulbous bows were attached to a parent model. The model in question (VWS 2388 model) was considered with three different bows, resulting into variants 2388.0, 2388.2 and 2388.3. These variants represent ships with a bulbless bow (variant 2388.0), a small bulbous bow (variant 2388.2) and a moderate bulbous bow (variant 2388.3). The ship model (Mod. 2388) and its variants

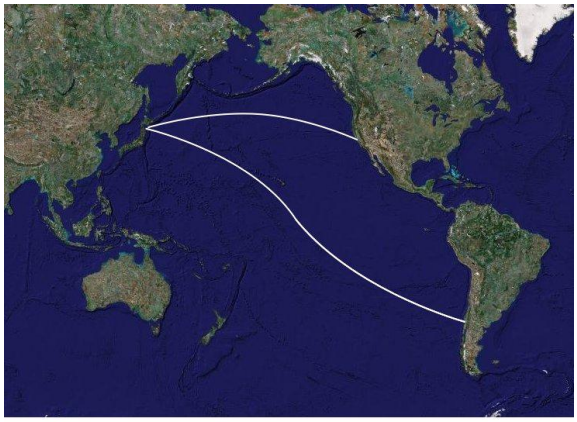

(a) Routes San Francisco - Yokohama and Valparaiso - Yokohama

(b) Routes Le Havre - Charleston and Le Havre - Paranaguá

(c) Route Melbourne - Djibouti

Figure 4.1.: Simulated routes in the Pacific, Atlantic and Indic Oceans (source: Google Maps)

Model:		2388		
Variant:		0	2	3
L_{PP}	(m)		5.8500	
B	(m)		0.9750	
T	(m)		0.3250	
L_{WL}	(m)	5.7506	5.7769	5.7792
L_{OS}	(m)	5.7506	5.9256	6.0076
S_{Total}	(m^2)	6.6391	6.7825	6.8548
∇	(m^3)	1.1690	1.1786	1.1866
c_B	(-)	0.6306	0.6358	0.6401
c_P	(-)	0.6454	0.6507	0.6551
c_{WP}	(-)	0.7218	0.7224	0.7236
bulbous bow parameters:				
c_{ABT}	(-)	-	0.0768	0.1251
c_{ABL}	(-)	-	0.0947	0.1610
$c_{\nabla PR}$	(-)	-	0.1945	0.4908
c_{LPR}	(-)	-	0.0260	0.0401
c_{BB}	(-)	-	0.1327	0.1754
c_{ZB}	(-)	-	0.6129	0.5720

Table 4.1.: Main dimensions of investigated ships in model scale

were designed for investigation purposes only, and should represent a fast cargo liner of the 1970's decade. The bulbless variant 2388.0, considered as parent model within Kracht's investigation, will be considered here only for comparison purposes and it will be shown, already in early results, that such a variant is economically not viable for any operational profile. For this reason, model 2388.2 (moderate bulb) will be used here as parent geometry for all comparisons and results throughout this work. Additionally, further subvariants will be generated from variant 2388.2 later, as it will be outlined in the next chapter (chap. 5). In table 4.1, the main particulars and the bulbous bow parameters of the variants are shown. The meaning of the bulbous bow parameters is sketched in table 4.2. Figures 4.2, 4.3 and 4.4 show the ship's lines of the considered variants.

Within the investigations of Kracht, a (fictive) scaling factor of $\lambda = 25$ was chosen to represent a full scale ship. For the operational simulations presented here, different ships were "designed" from model scale and variants with different (fictive) scaling factors were created. In this way, the model, initially with a scaling factor of $\lambda = 25$, was scaled also for three further factors $\lambda = 17$, 33, 50, as to obtain an idea of the influence of ship size into the results obtained from operational simulations. The considered scaling factors were chosen to address similar main dimensions of typical categories of actual container ships. Nevertheless, these ships are not intended to represent exactly modern ships, but they can be useful for orientation purposes. The classification of the differently scaled ships into typical container ship classes together with a selection of main parameters is

Breadth parameter	$c_{BB} = \frac{B_B}{B_{MS}}$	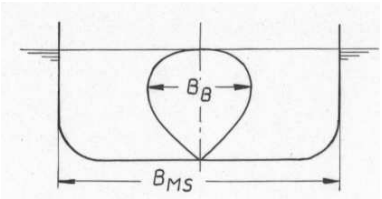
Length parameter	$c_{LPR} = \frac{L_{PR}}{L_{PP}}$	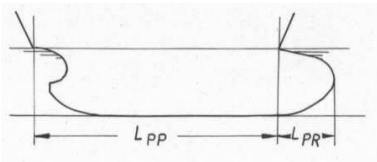
Depth parameter	$c_{ZB} = \frac{z_B}{T_{FP}}$	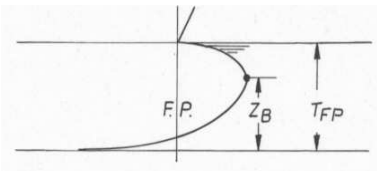
Cross area parameter	$c_{ABT} = \frac{A_{BT}}{A_{MS}}$	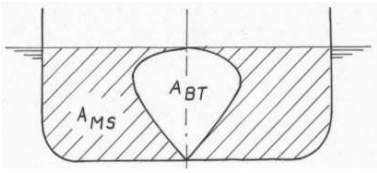
Length area parameter	$c_{ABL} = \frac{A_{BL}}{A_{MS}}$	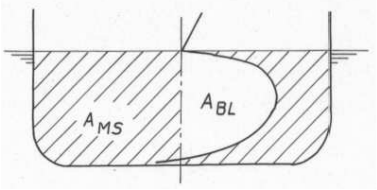
Volumetric parameter	$c_{\nabla PR} = \frac{\nabla_{PR}}{\nabla_{WL}}$	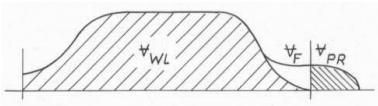

Table 4.2.: Dimensionless bulbous bow parameters as defined by Kracht [67]

λ	17	25	33	50
Category	small coaster	medium coaster	panamax	post-panamax
L_{PP} (m)	99,45	146,25	193,00	292,50
B (m)	16,58	24,38	32,18	48,75
T (m)	5,53	8,13	10,73	16,25
Δ_0(t)	12731	18723	24714	37445
Δ_2(t)	12836	18876	24917	37753
Δ_3(t)	12923	19005	25086	38009
V_S (kn)	15,2	18,4	21,1	26,0

Table 4.3.: Main dimensions of investigated ships. Displacements are given for each bulbous bow variant. Note that categories are intended only as an orientation

shown in table 4.3.

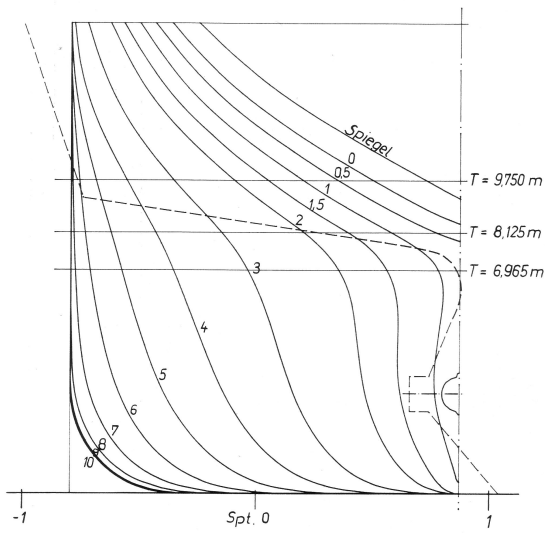

Figure 4.2.: Aft hull lines of ship 2388.0, 2388.1. 2388.2 and 2388.3 [68]

4.4. Hydrodynamic Characteristics of Variants

4.4.1. Calm Water Resistance of Variants

The calm water resistance has been determined depending of the available data. The experimental data provided by Kracht [68] included, additionally to the thrust in regular waves, the thrust in calm waters for five different velocities for a single (design, i.e. full loaded) floating condition. A later investigation from Kracht [69] measured thrust in calm waters for the same model for an additional, lower draft. Since no resistance model tests were performed within both investigations, no better experimental data is available for

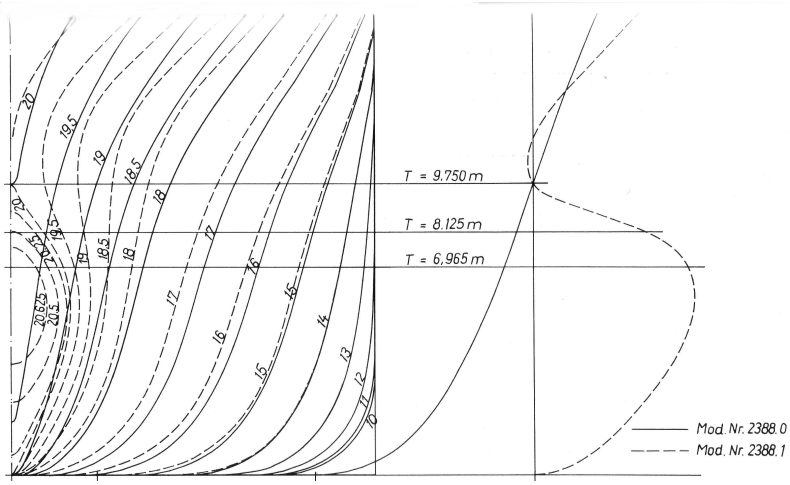

Figure 4.3.: Fwd hull lines of ship 2388.0 and 2388.1 [68]

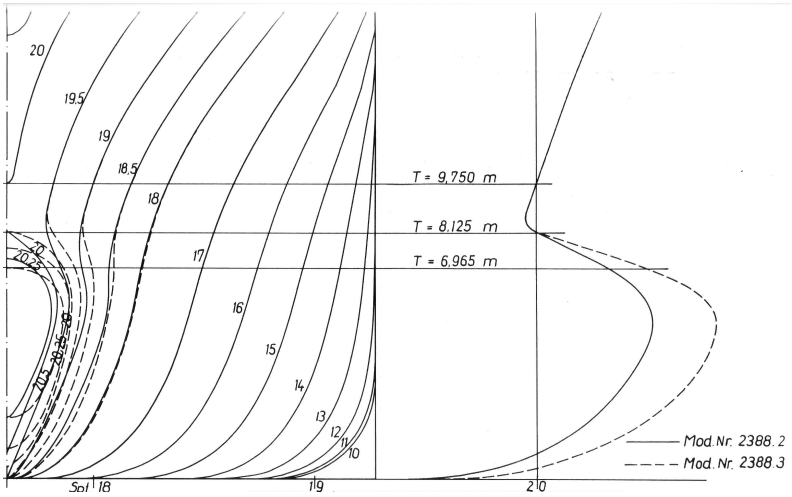

Figure 4.4.: Fwd hull lines of ship 2388.2 and 2388.3 [68]

this purpose. A thrust deduction factor t must be thus estimated to obtain a total model resistance in the form:

$$R_{TM} = (1 - t)\, T_M \tag{4.1}$$

According to the estimation formula of Holtrop [50] a thrust deduction factor $t = 0.19$ was estimated for all models. Regardless of the statements of Kracht [66] and Schneekluth [102], remarking that a bulbous bow can induce changes in the propulsive factors (effective wake w_e and thrust deduction t), this influence was left consequently aside to reduce the number of variables affecting directly the final results. This experimental data will be used for all simulations where only one floating condition was considered. For all considered scaling factors ($\lambda = 17, 25, 33, 50$), the resistance is extrapolated according to section 2.5.2 and recalled within the simulations.

As introduced in section 4.3, variant 2388.2 will be used as parent geometry throughout this work. Consequently, all diagrams with simulation results will be normalized by dividing actual values by the parent values. Figure 4.5 shows such normalized results for the total fuel oil consumption in calm water at $F_n = 0.250$ for all three variants and all four scaling factors. This figure will serve as comparison with further simulation results. It shall be noticed that the increase in the differences between the variants for larger scaling factors is simply originated by the lower viscous resistance fraction due to the higher Reynolds numbers.

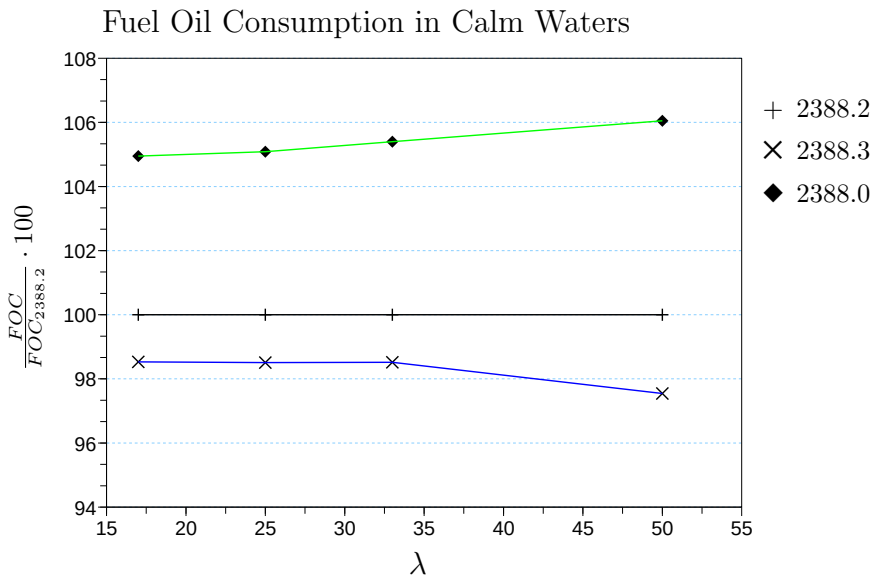

Figure 4.5.: Relative fuel consumption in calm waters

For certain operational simulations, the calm water resistance for additional floating conditions was required. Each floating condition is labeled in the form T_{ab}, with a indexing the aft perpendicular draft and b the forward perpendicular draft. These indexes are summarized, for the different scaling factors, in table 4.4. Table 4.5 summarizes the resulting trim angles for each combination of floating condition indexes a and b. The

Index a or b	Description	B/T	$T_{AP}(a)$ or $T_{FP}(b)$ in m			
			17	25	33	50
1	scantling	2.5	6.630	9.750	12.870	19.500
2	design	3.0	5.525	8.125	10.725	16.250
3	partial high	3.5	4.736	6.964	9.193	13.929
4	partial med.	4.0	4.144	6.094	8.044	12.188
5	partial low	4.5	3.683	5.417	7.150	10.833
6	ballast	5.0	3.315	4.875	6.435	9.750

Table 4.4.: Designation of draft indexes for resistance calculations

Trim angle θ [°]		$b(T_{FP})$					
		1	2	3	4	5	6
$a(T_{AP})$	1	**0.000**	0.637	1.091	1.432	1.697	1.909
	2	-0.637	**0.000**	0.455	0.796	1.061	1.273
	3	-1.091	-0.455	**0.000**	0.341	0.606	0.818
	4	-1.432	-0.796	-0.341	**0.000**	0.265	0.478
	5	-1.697	-1.061	-0.606	-0.265	**0.000**	0.212
	6	-1.909	-1.273	-0.818	-0.478	-0.212	**0.000**

Table 4.5.: Trim angles θ for each combination of floating condition indexes a and b

experimental data for thrust from Kracht [69] is therefore available for floating conditions T_{22} and T_{33}. For these two floating conditions, results of residual resistance from experiments (obtained from measured thrust, an estimated thrust deduction factor and the subtraction of the viscous resistance component), wave resistance from the potential CFD code FS-Flow[1] (considering it approximately equal to the residual resistance when applying the ITTC 1978 method) and, for comparison purposes, the estimated residual resistance from the method of Holtrop and Mennen [49] are shown in figure 4.6. It can be observed that, especially for variants 2388.2 and 2388.3, the agreement between experiments and potential CFD is good. Figure 4.8 shows exemplarily the wave elevations from potential CFD calculations at design draft and design speed for all three variants.

Since the two mentioned floating conditions were not sufficient for undertaking realistic operational simulations, additional numerical calculations for other floating conditions were required. For this purpose, the wave resistance was calculated with potential CFD, adding the viscous resistance according to the ITTC 1978 method with an estimated form factor k according to Holtrop [49], obtaining the total calm water resistance of the ship as defined in section 2.5 (eqs. 2.8 to 2.11).

The eight to ten floating conditions for which the calm water resistance was calculated are summarized in table 4.6, making use of the draft indexes a and b from table 4.4. Obtained potential CFD results are summarized in figure 4.7. The figure shows, as expected from the discussed experimental results, that variant 2388.3 (largest bulb) has only for

[1] FutureShip GmbH

		$b(T_{FP})$					
		1	2	3	4	5	6
$a(T_{AP})$	1						
	2		x	x	*		
	3			x	x		*
	4		x		x		x
	5						
	6						x

Table 4.6.: Selection of floating conditions for potential CFD wave resistance calculations (fields marked with * for $F_n = 0.250$ only)

the design draft T_{22} and the higher velocities (eq. to $F_n = 0.225$ and 0.250) a lower wave resistance. For lower drafts (e.g. T_{34}, T_{46} or T_{66}), significant differences between both bulbous bows can be observed.

Instead of limiting the simulations to the calculated floating conditions, a more generalized and flexible handling is obtained by determining response surfaces by regression (least square fit) methods. For each calculated velocity, a response surface is defined as a function of aft and forward drafts T_{AP} and T_{FP}, providing the wave resistance coefficient for any floating condition as a polynomial surface. Consequently, the error of this approach outside the bounds of the calculated floating conditions must be acquainted and handled with care. A description of the exact coefficients and response surfaces will be given in appendix B, figs. B.1, B.2 and B.3 and table B.1. In table B.1, the wave resistance coefficients C_W shown in figure 4.7 are presented in tabular form.

4.4.2. Seakeeping and Added Resistance in Waves of Variants

The simulations discussed in this chapter will recall the ship responses and the added resistance in waves as described in section 3.3.3 using the head seas data from the experiments undertaken by Kracht. As previously mentioned, the results of the experiments are available for a single floating condition and different velocities. The added resistances in regular waves for the three variants studied are shown in figure 4.9 for different Froude numbers.

In order to complement results in head seas from experiments, strip theory calculations were made for the remaining heading angles, velocities and floating conditions[2]. Figure 4.10 compares added resistance from strip theory (calculated with the implemented method of Gerritsma and Beukelmann in PDSTRIP) with experimental data in head seas. The figure states evidently the previously discussed non-suitability of strip theory to compare such similar variants (see sect. 3.3.3). This lies to a great extent in the inherent limitations of the linearity assumption of strip theory and in the limitations of the implemented method of Gerritsma and Beukelmann (both discussed in section 2.6.2)

[2]this approach will be applied in the same manner in the next chapter, complementing results in head seas from viscous CFD computations

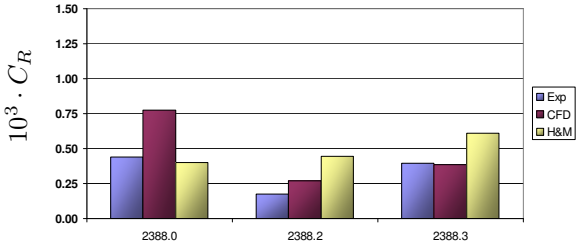

Variants

(a) Wave resistance at $F_n = 0.200$, T_{22}

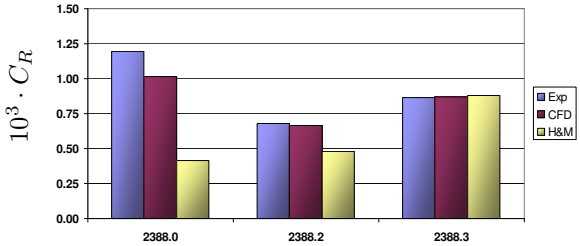

Variants

(b) Wave resistance at $F_n = 0.200$, T_{33}

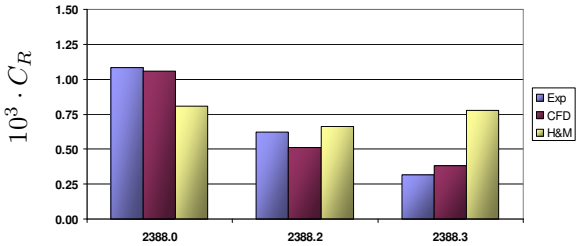

Variants

(c) Wave resistance at $F_n = 0.225$, T_{22}

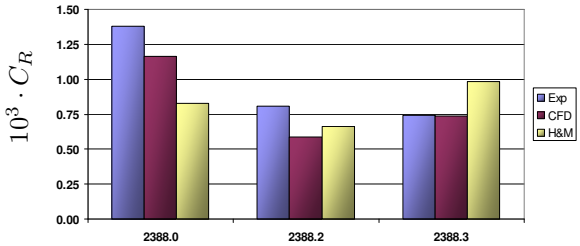

Variants

(d) Wave resistance at $F_n = 0.225$, T_{33}

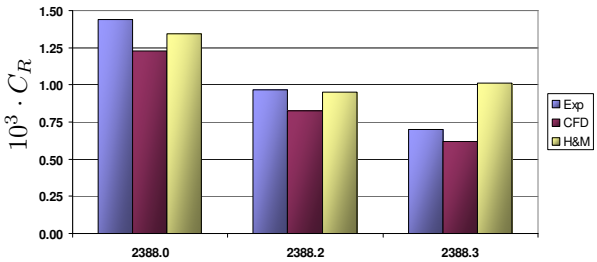

Variants

(e) Wave resistance at $F_n = 0.250$, T_{22}

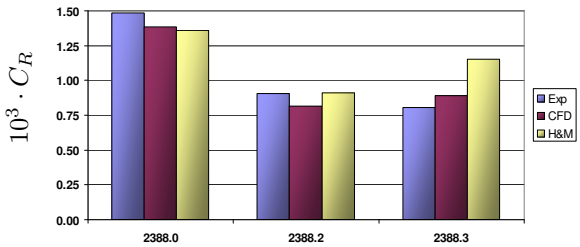

Variants

(f) Wave resistance at $F_n = 0.250$, T_{33}

Figure 4.6.: Comparison of residual/wave resistance coefficients from experiments, potential CFD and Holtrop & Mennen for full loaded condition (left) and partially loaded condition (right)

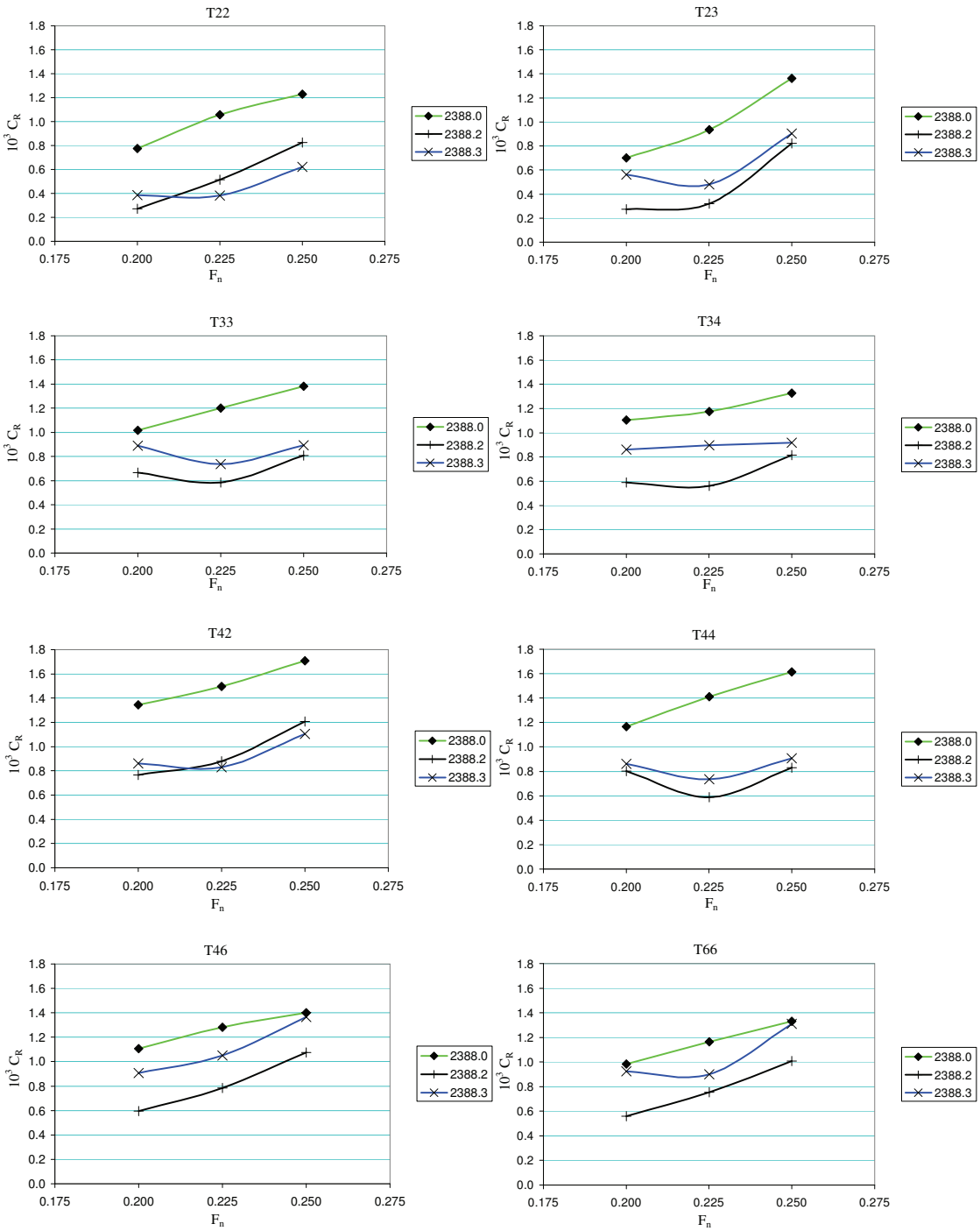

Figure 4.7.: Residual/wave resistance coefficients of considered floating conditions from potential CFD calculations

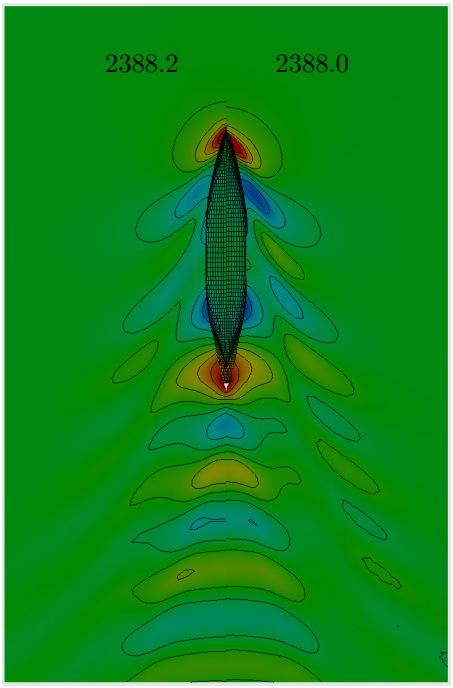

(a) 2388.2 (left) and 2388.0 (right)

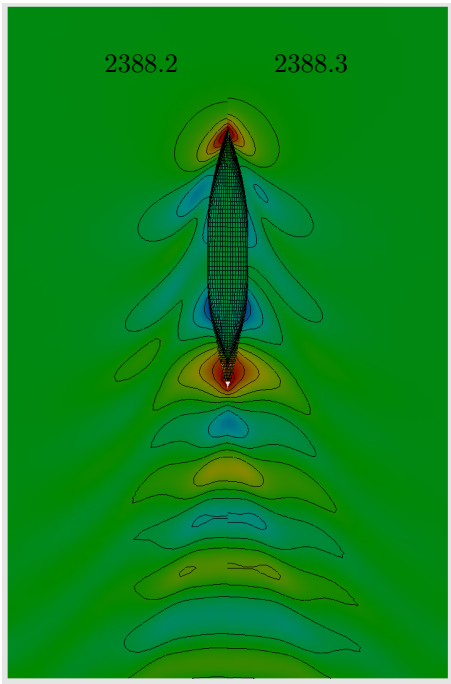

(b) 2388.2 (left) and 2388.3 (right)

Figure 4.8.: Compared wave elevations between parent geometry (2388.2) and variants 2388.0 and 2388.3

which, among other aspects, takes account only of the undisturbed wave field instead of the diffraction wave field. As previously discussed in section 3.3.3, strip theory will be therefore only applied, with proper corrections from experimental or viscous CFD results, to fill missing data needed to perform the operational simulations.

4.5. Preliminary Operational Simulations with Fixed Speed and Fixed Floating Condition

4.5.1. Simulation Setup

In a first attempt to identify the main dependencies between the different routes, bulbous bow configurations and scaling factors, extremely simple operational simulations were undertaken. These simulations include fixed values for:

- Ship speed V_S (design service speed, with $F_n = 0.250$)
- Floating condition (design draft T_{22})
- Propulsive efficiency ($\eta_D = 0.70$)
- Specific fuel consumption ($sfoc = 0.180 \left[\frac{\mathtt{kg}}{\mathtt{kWh}}\right]$)

The simulations were undertaken for a five-year period recalling weather data from ECMWF from the years 1997 to 2001 and considering the ships as in continuous operation, with 12 hours at each port visited and without any additional stops.

The main purpose of these simulations was to have a first insight on main dependencies. Results from them can be thus addressed as a comparison when discussing results from more complex simulation modes. An important aspect is to discuss if this approach makes sense for comparison purposes or to be embedded into an optimization strategy.

4.5.2. Results

For each simulation, all relevant information (e.g. added resistance, brake power, fuel consumption, sea state parameters and many others) are logged for the five-year period and mean values are obtained. An example of this data is shown for the route San Francisco - Yokohama in figure 4.11. Significant seasonal, as well as yearly differences can be observed in this figure. Especially for the significant wave height, the seasonal variation is remarkably high in this route. The fuel oil consumption diagram shows this tendency as well, and differences between the different years can also be observed.

In figures 4.12a to 4.12e (pp.92), the mean values of the added resistance in waves R_{AW} of the different variants are shown as a function of ship size, represented by the scaling factor λ, for the different routes. Figure 4.12f shows the average of all five routes simulated. The expected influence of ship size, with decreasing added resistances for increasing ship size, can be observed for all routes. The ranking between the three bulbous bow variants

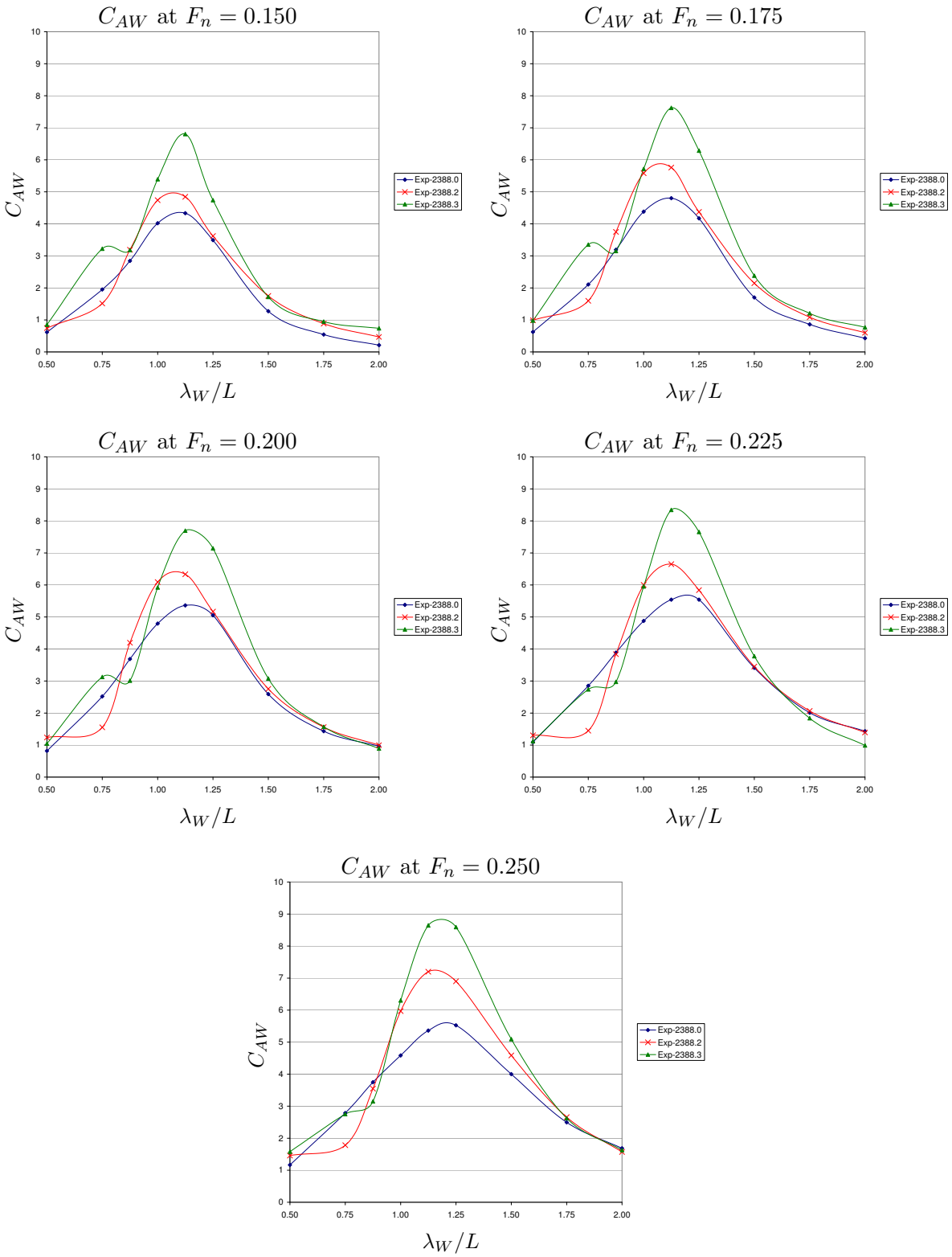

Figure 4.9.: Dimensionless added resistance in waves from experiments for different Froude numbers [68]

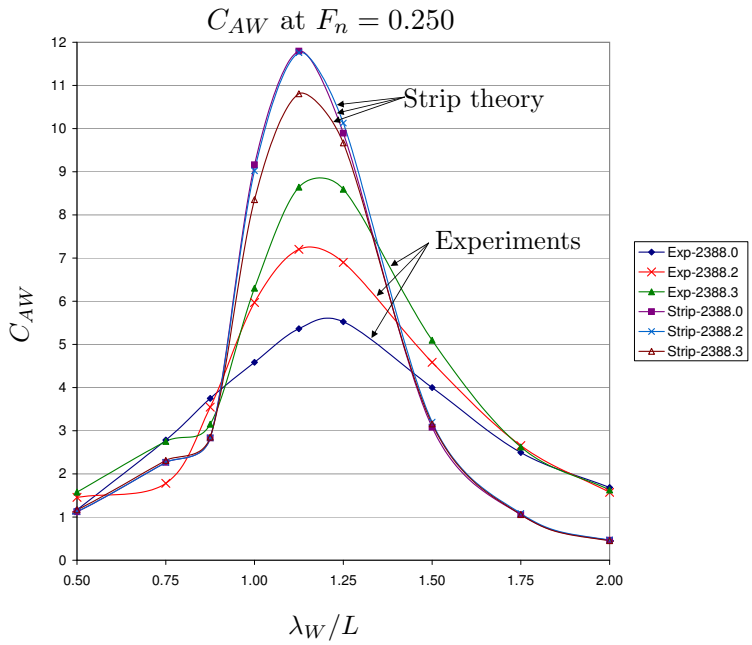

Figure 4.10.: Added resistance in waves (dimensionless) for models 2388.0, 2388.2 and 2388.3 from experiments and strip theory calculations

are in accordance with the trend observed from the added resistance in regular waves from experiments and can be distinguished for all routes, with the lowest values for the bulbless variant 2388.0 and highest for variant 2388.3. Additionally, differences between the routes can be observed, reflecting the typical sea state character of the regions where the routes are placed. These can be categorized into two groups: routes, where predominantly calm weather is found (routes Le Havre - Paranaguá and Valparaiso - Yokohama) and routes where predominantly rough weather is found (routes Le Havre - Charleston, San Francisco - Yokohama and Melbourne - Djibouti).

Since velocity is considered constant, the measure of merit, FEC, is equal to the fuel oil consumption FOC. For the different routes, the FOC of the different variants is shown as a function of ship size in fig. 4.13 (pp. 93). The figure shows the relative fuel consumption for each of the simulated routes compared to the fuel consumption of the parent geometry (model 2388.2) for the different scaling factors considered (λ = 17, 25, 33, 50). Small differences between the simulated routes can be observed, but the general trend is that the larger bulbous bow (2388.3) performs better in almost every route and scaling factor, similar to the fuel oil consumption in calm water, as seen in fig. 4.5 (p. 82). Results from more complex simulation modes presented in sections 4.6 and 4.7 will show the importance of not performing such simple simulations for design purposes. Especially, the approach of neglecting speed loss has shown to be not suitable for a proper prediction of the economical performance of a design. This aspect will be illustrated when comparing the present results with results obtained from simulations with variable ship speed.

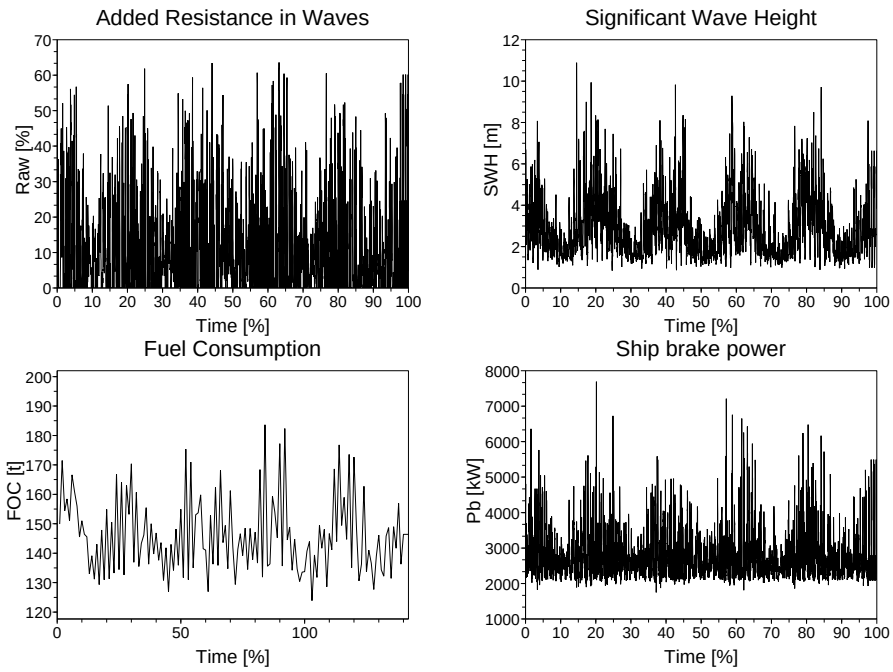

Figure 4.11.: Log summary from operational simulation of ship 2388.2 with $\lambda = 17$ in route San Francisco - Yokohama. Added resistance in waves is represented as percentage of calm water resistance.

4.6. Operational Simulations with Variable Speed and Fixed Floating Condition

4.6.1. Simulation Setup

For a more realistic simulation, voluntary and involuntary speed loss must be considered. For the voluntary speed loss, the relative motions at bow and the subsequent slamming probability according to Ochi [88] and maximum accelerations at the bridge have been considered as described in section 3.3.3. The speed is reduced until the slamming probability has a value lower than 3% and vertical significant accelerations lower than $0.15g$. This threshold has been taken from the investigation within the European Union research project SEAROUTES, as recalled by Hinnenthal [43]. For the involuntary speed losses, the propeller and machine working points are considered as described in section 3.3.4. For this purpose, an additional module is called within the simulations using the open water characteristics of the test propeller (with ITTC'78 extrapolation to full scale) and the layout diagram of each main engine. In this case, the speed is reduced until the power requirement is feasible within the engine layout diagram described in section 3.3.4.

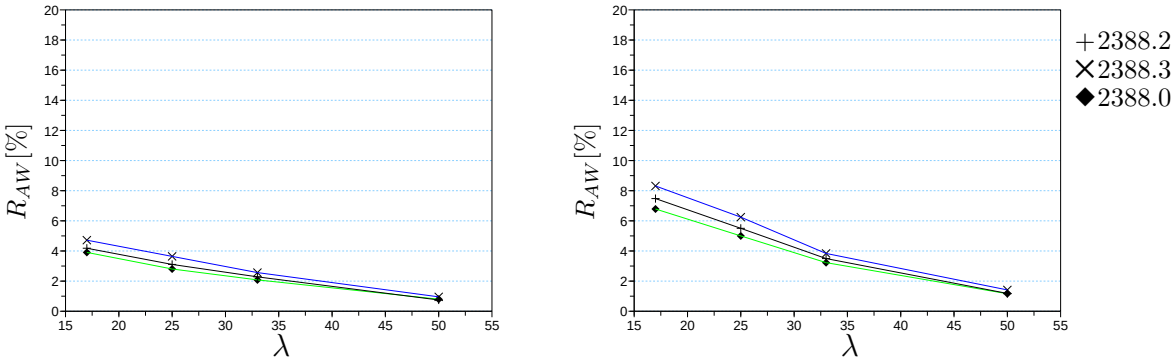

(a) mean R_{AW} (Le Havre - Paranaguá)

(b) mean R_{AW} (Le Havre - Charleston)

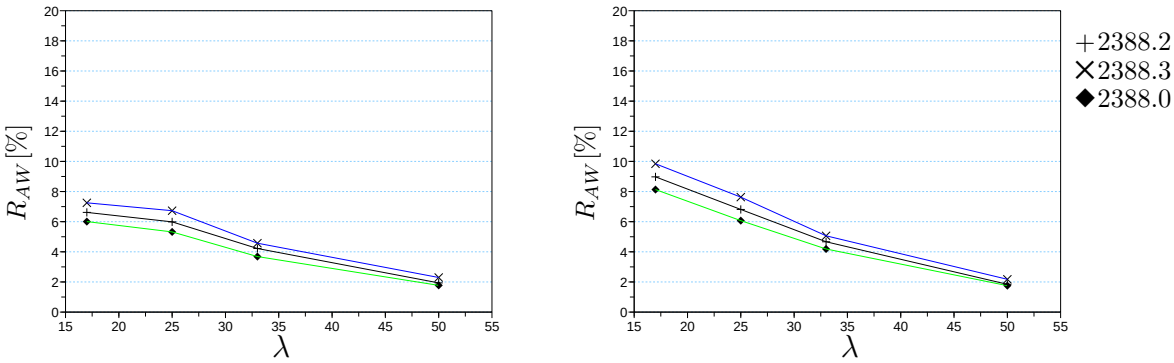

(c) mean R_{AW} (Valparaiso - Yokohama)

(d) mean R_{AW} (San Francisco - Yokohama)

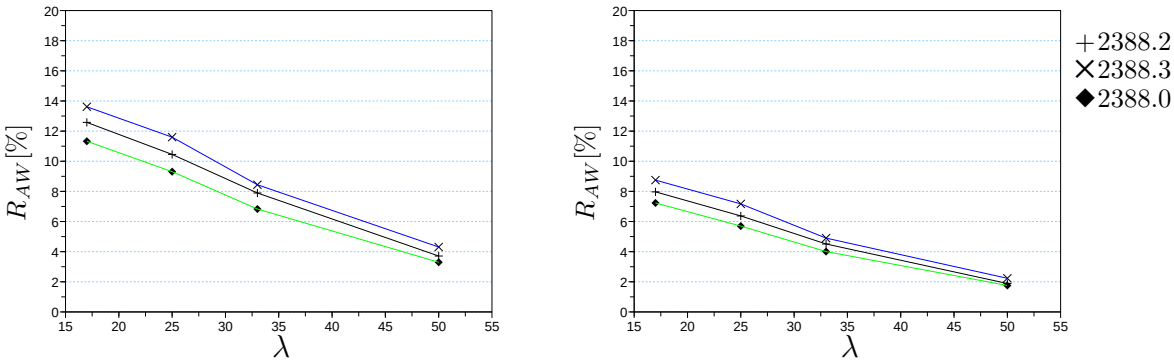

(e) mean R_{AW} (Melbourne - Djibouti)

(f) mean R_{AW} for all routes

Figure 4.12.: Mean R_{AW} (as percentage of R_{TS}) for Mod. 2388 with different bulbous bows for all considered routes and mean relative mean R_{AW} of all routes as function of the scaling factor λ from operational simulations with fixed speed and fixed floating condition

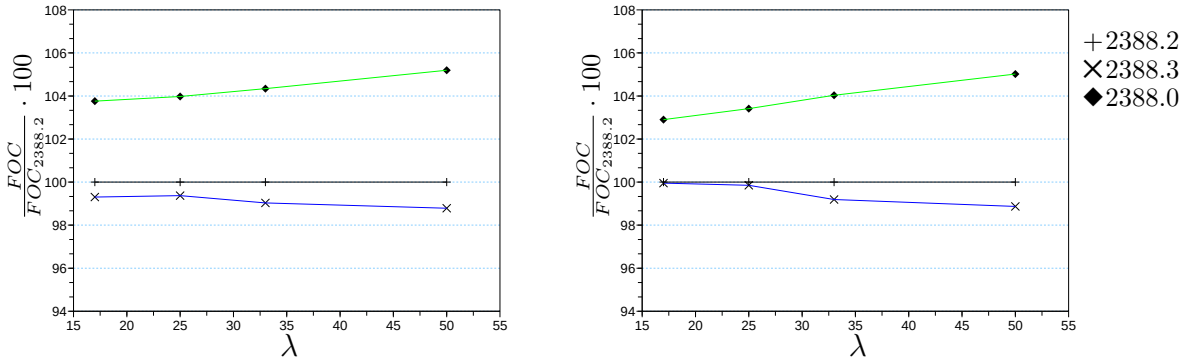

(a) FOC for route Le Havre - Paranaguá

(b) FOC for route Le Havre - Charleston

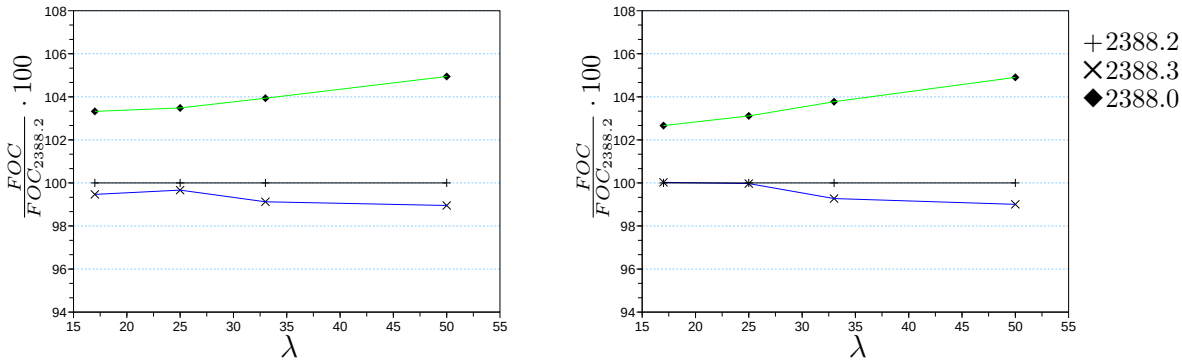

(c) FOC for route Valparaiso - Yokohama

(d) FOC for route San Francisco - Yokohama

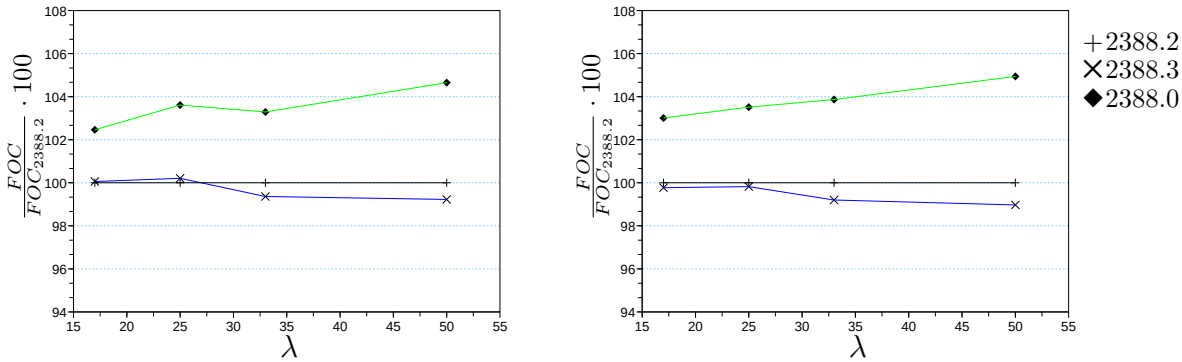

(e) FOC for route Melbourne - Djibouti

(f) mean FOC of all routes

Figure 4.13.: Relative FOC variants 2388.0, .2 and .3 with fixed speed and fixed floating condition for all considered routes and mean relative FOC of all routes as function of the scaling factor λ from operational simulations with fixed speed and fixed floating condition

Engine Characteristic

First computations were performed recalling engine characteristics from the product range of the engine manufacturer MAN B&W [79]. Since it was not always possible to obtain an adequate engine for each ship studied, engine margins differed significantly in some cases, making the comparability of the results very difficult. To avoid this problem in this design study, "fictive engines" were declared. Each of these engines operates at its MCR with an added resistance of 25% (equivalent to a sea margin of the same value), obtaining also the same *specific fuel oil consumption* **sfoc** for each ship of the same size. These *sfoc*'s were taken from *reference engines* of similar characteristics. The remaining layout points (2, 3 and 4) were made proportional to the MCR, using the ratios from reference engines of similar size from the manufacturer's product range. An example of this is shown in fig. 4.14. Table D.1 in appendix D summarizes the power characteristics of the fictive and reference engines used in this chapter.

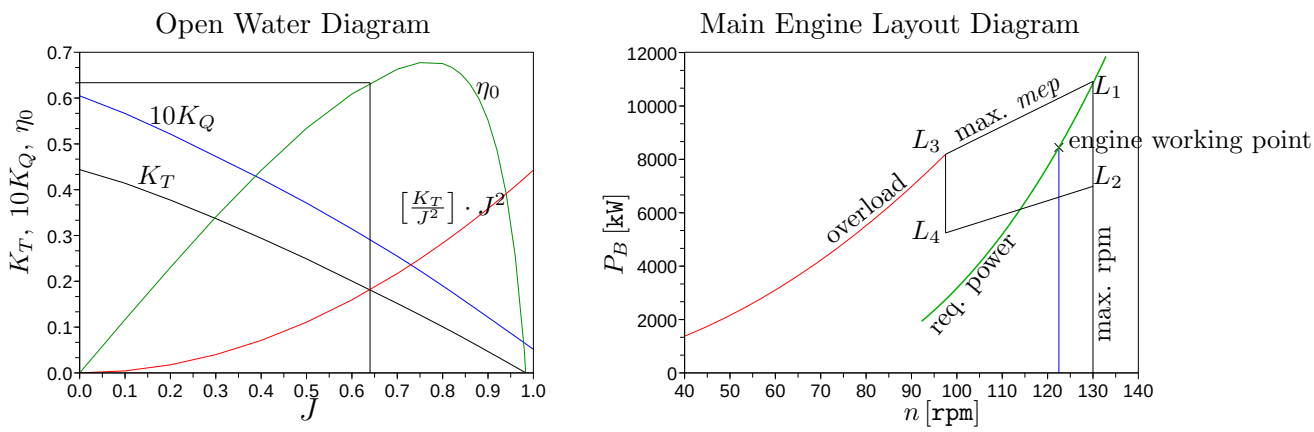

(a) Open water diagram (b) Main engine layout diagram

Figure 4.14.: Open water diagram with propeller working point and main engine layout diagram, with engine working point

Measure of Merit

When considering variable speed in the simulations, the fuel consumption alone cannot be taken as a comparison measure as made in section 4.5, due to the evident fact that ships cover different distances over the five-year period. The measure of merit described in section 3.4, the *Fuel Equivalent Costs* FEC will be applied here.

As discussed previously, an important task for addressing realistic fuel equivalent costs FEC is the choice of the fuel costs coefficient k_f. The choice of this value will certainly depend on the operational profile of the ship, its service speed, size, the actual and the estimated future fuel costs and, at last, the development of global economy during the period of interest. For the application case presented here, very little information about all these tasks is available, and for the purely comparative nature of this work, a unitary

and rather conservative value of $k_f = 0.25$ for all ship groups (as defined in sect. 3.4) will be applied. Based in the discussion presented by Buxton [20], fuel costs can make up from 10% to 50% of the operational costs of a ship. Indeed, the high dependency of the bunker prices is evident, being the higher values of k_f reached when bunker prices explode. A short example of the influence of k_f into the results will be discussed in section 4.6.3.

4.6.2. Results

The Fuel Equivalent Costs FEC obtained from the operational simulations with variable speed and fixed floating condition for each of the considered routes are shown in figures 4.15a to 4.15f (p.97). The shown Fuel Equivalent Costs FEC in US$ consider a fuel price of US$500 per tonne [3]. The clear influence of ship size into the final costs is evident and depicts clearly the advantages of large ships. This aspect is not of interest here, since only relative differences between the variants are important for a proper ranking and a subsequent design decision. For this reason, results presented in the following are normalized by the results from the parent model 2388.2. In figures 4.16a to 4.16f (p.98), the normalized FEC is shown for the presented simulations. A certain similarity to the results of Fuel Oil Consumption FOC shown in the previous section can be observed. Notwithstanding to this similarity, the present results show cases where the smaller bulbous bow (2388.2) has a better performance than the larger one (2388.3), contrary to the prediction in calm water and the largest part of the results shown in the previous section. For the smaller ship sizes ($\lambda = 17, 25$), this applies for almost every route.

The differences between results from the routes Le Havre - Paranaguá (moderate weather route) and Melbourne - Djibouti (rough weather route) are notorious. For the first route (Le Havre - Paranaguá), a small influence of weather factors can be observed, being results very similar to the ranking of FOC in calm waters. The second route (Melbourne - Djibouti) shows an evidently larger influence of weather factors, being in this case the Fuel Equivalent Costs of the larger bulbous bow (2388.3) up to 4% higher than for the parent ship (2388.2). This confirms the hypothesis made in chapter 1, showing that the best bulbous bow configuration, when considering weather factors, can be different to the one in calm waters.

It shall be recalled that differences in the FEC from all three variants are caused not only by different fuel consumptions, but also by the achieved mean service speed, viz. the total covered distance over the five-year period. Diagrams for this data (fuel oil consumption and mean service speed) and for the added resistance in waves are shown in appendix D, in figures D.1, D.2 and D.3. These results show an important dependency not only in the parameters of interest (region and bulbous bow), but also on ship size. The direct relation between ship size and R_{AW} is predominant, but other factors, such as characteristic wave length or periods in the different regions certainly play a role.

Since the operational simulations presented in this section are the only ones including experimental data both for seakeeping and calm water resistance, results obtained here

[3] IFO 180, representative for the years 2008 and 2009

are of special relevance for the validation of operational simulations including numerical data only. This aspect will be discussed in detail in chapter 5 (sect. 5.4, pp. 121).

4.6.3. Variation of Fuel Costs Coefficient k_f

As previously mentioned, the impact of the value of the fuel costs coefficient k_f will be treated here by means of two examples, namely the routes Le Havre - Paranaguá and Melbourne - Djibouti. Additionally to the shown diagrams of FEC with $k_f = 0.25$, diagrams with values of $k_f = 0.1$, 0.5, 1.0 are shown in figures 4.17a to 4.17f (p.99) for the mentioned routes. These values of k_f represent scenarios of very low fuel prices ($k_f = 0.10$) and very high fuel prices ($k_f = 0.50$), showing with $k_f = 1.00$ pure fuel costs (or disabled "punishment" costs according to the definition of FEC) as a reference.

For the calm weather route between Le Havre and Paranaguá, only small changes can be observed in the FEC for the different values of k_f. Nevertheless, these small changes lead for $k_f = 0.10$ to a different best configuration at $\lambda = 17$ (variant 2388.2). In the case of the second route (Melbourne - Djibouti), the influence of k_f is significantly higher. Specifically for smaller ship sizes ($\lambda = 17$, 25), the relatively higher influence of weather factors, especially when leading to speed loss, causes large differences in the results. For $k_f = 0.10$, these large differences are caused to a great extent due to the higher influence of the achieved mean speed (i.e. speed loss). The similarity between the results with $k = 0.50$ and $k = 1.00$ show that, for higher fuel prices, a low fuel oil consumption is more advantageous than a high mean achieved speed. Interestingly, the better performance of variant 2388.2 is, for smaller ship sizes, almost independent of the chosen value of k_f. The application of the presented *Fuel Equivalent Costs* permit, in this manner, the evaluation and comparison of different fuel price scenarios, making a subsequent decision for a representative value of k_f much easier. It shall be remarked that this decision is relevant for design purposes and should be confirmed at a later design stage by a more detailed economical study.

4.6.4. Variation of Service Speed: Slow Steaming Simulations

To illustrate the impact of the different bulbous bows in a simple manner, a slightly different approach can also be chosen and will be shortly described here: by decreasing the service speed of the ships in order to obtain the same mean velocity for all ships within a group, which is equal to the mean speed of the slowest ship (over the five year period) in the group, the fuel costs can be compared directly, i.e., costs surplus of the voluntary speed loss for the faster ships can be acquainted. These simulations will be recalled here as *slow steaming simulations*.

For the present application case, variant 2388.3 achieved the lowest mean speed, without exception, for all routes and for all ship sizes studied. For this reason, the design service speed of variants 2388.0 and 2388.2 was adjusted in order to obtain the same mean speed than variant 2388.3 over the five-year period. This was achieved by an additional routine which changes therefore service speed dynamically until this equality condition is reached.

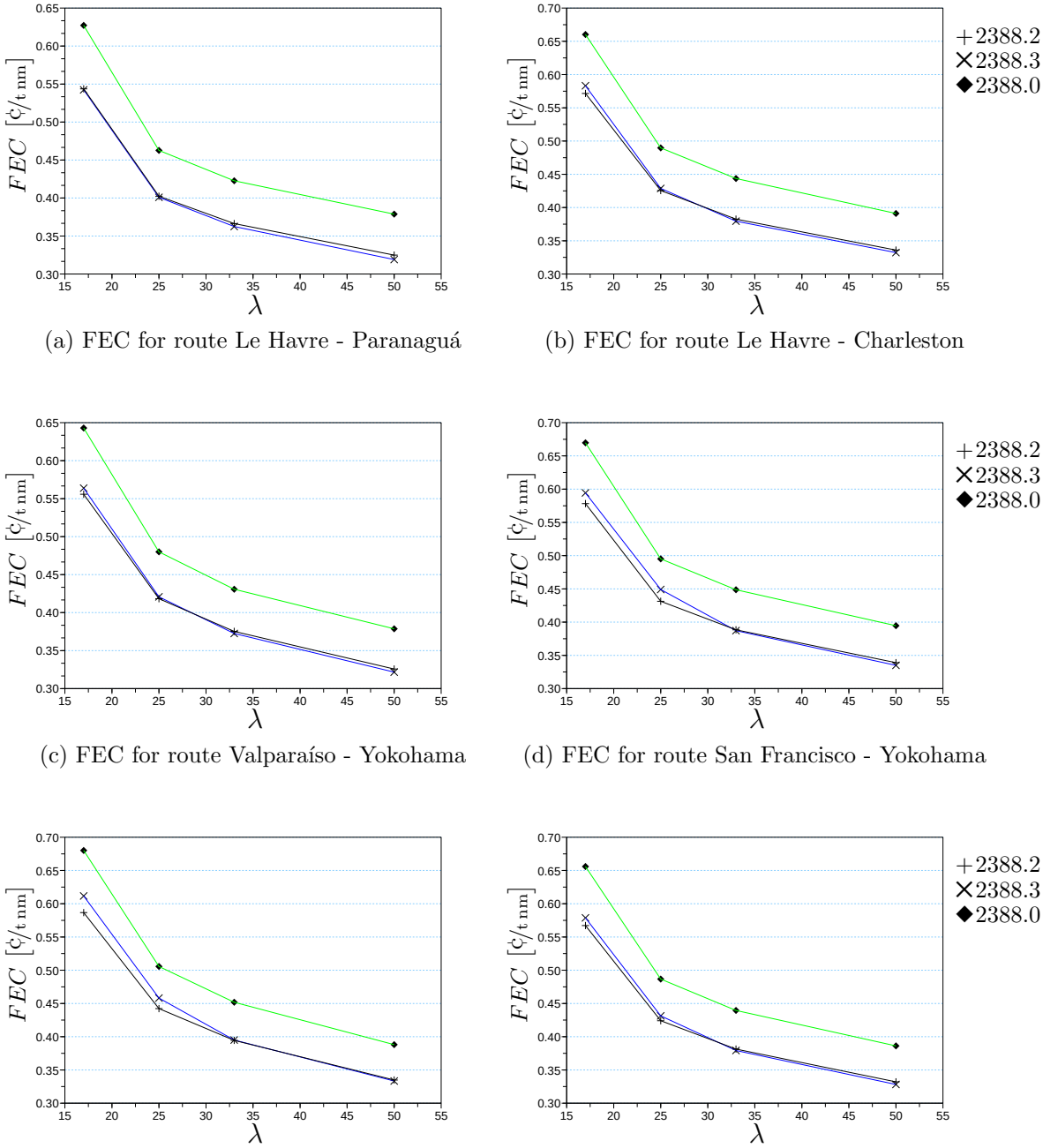

(a) FEC for route Le Havre - Paranaguá

(b) FEC for route Le Havre - Charleston

(c) FEC for route Valparaíso - Yokohama

(d) FEC for route San Francisco - Yokohama

(e) FEC for route Melbourne - Djibouti

(f) mean FEC of all routes

Figure 4.15.: FEC (in US$ cent/nmi t) of variants 2388.0, .2 and .3 with fixed floating condition for all considered routes and mean FEC as function of the scaling factor λ

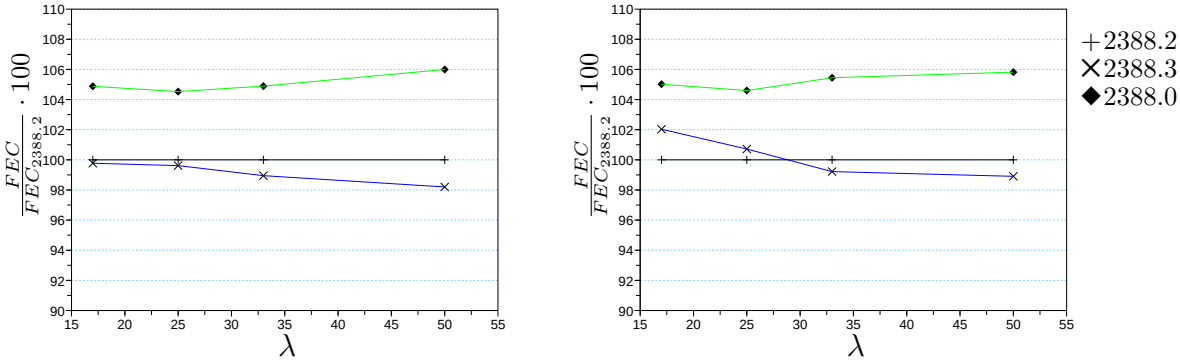

(a) FEC for route Le Havre - Paranaguá

(b) FEC for route Le Havre - Charleston

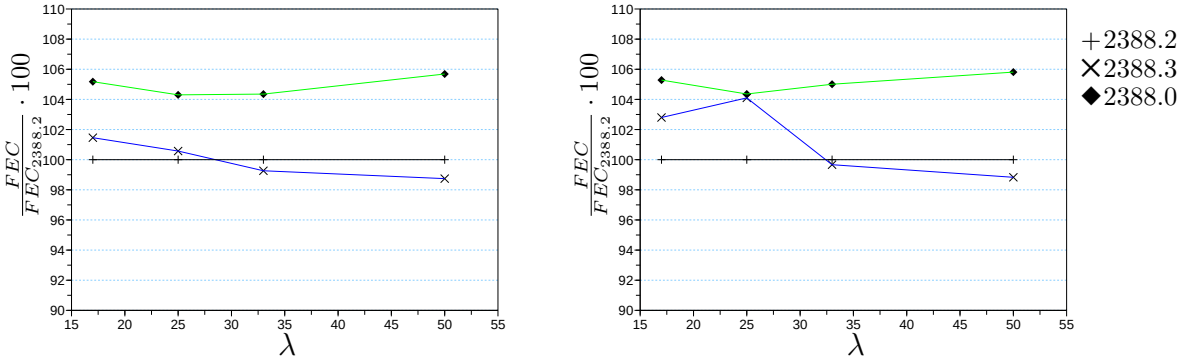

(c) FEC for route Valparaíso - Yokohama

(d) FEC for route San Francisco - Yokohama

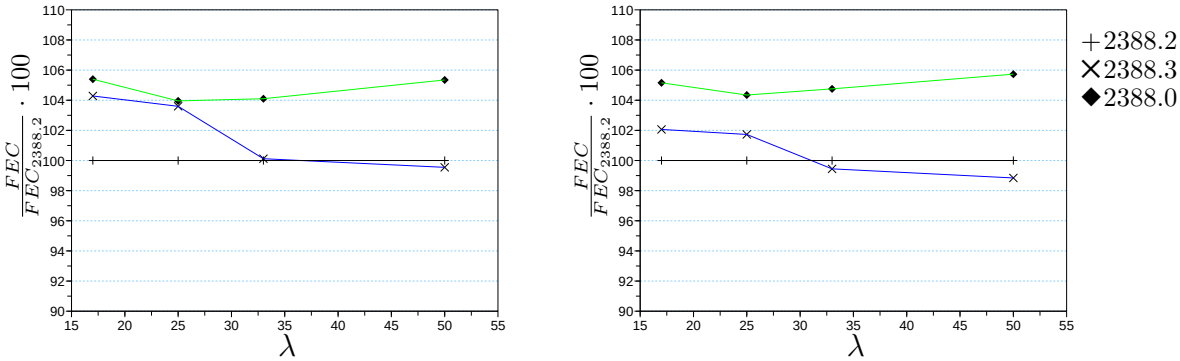

(e) FEC for route Melbourne - Djibouti

(f) mean FEC of all routes

Figure 4.16.: Relative FEC of variants 2388.0, .2 and .3 with fixed floating condition for all considered routes and mean relative FEC as function of the scaling factor λ

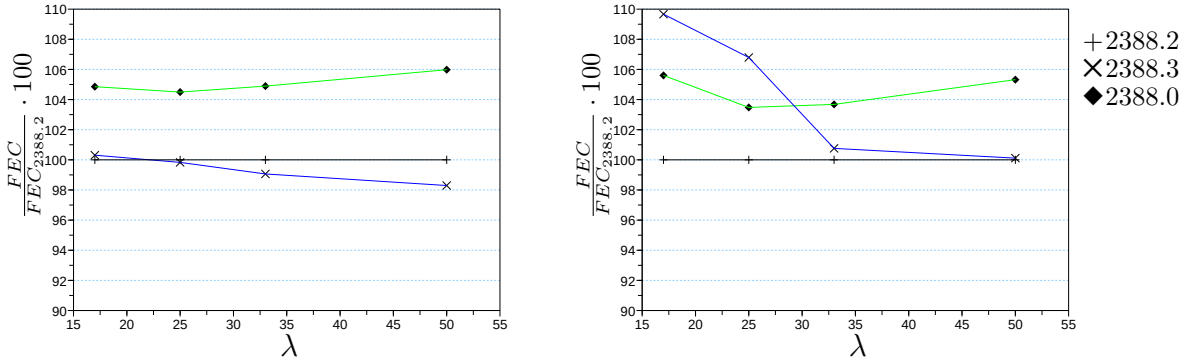

(a) FEC with $k_f = 0.10$ (Le Havre - Paranaguá) (b) FEC with $k_f = 0.10$ (Melbourne - Djibouti)

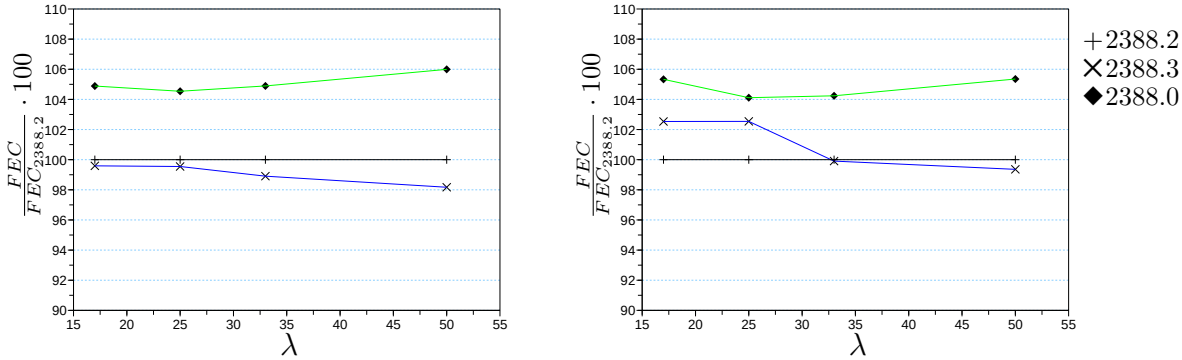

(c) FEC with $k_f = 0.50$ (Le Havre - Paranaguá) (d) FEC with $k_f = 0.50$ (Melbourne - Djibouti)

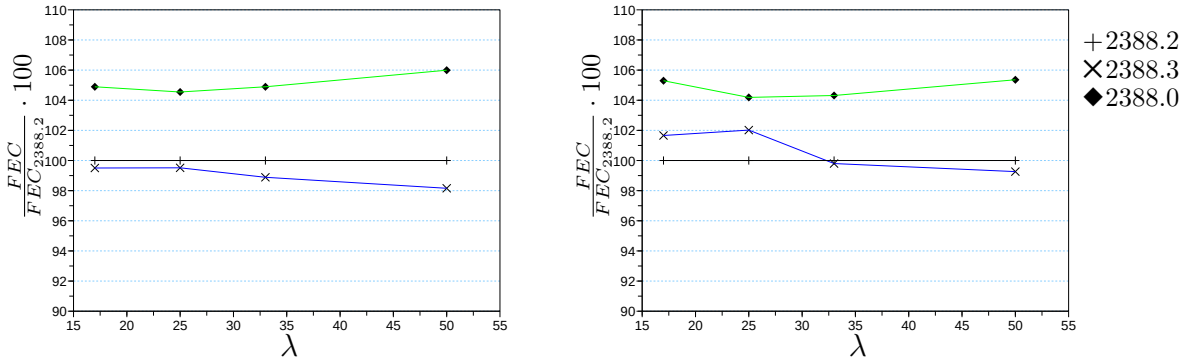

(e) FEC with $k_f = 1.00$ (Le Havre - Paranaguá) (f) FEC with $k_f = 1.00$ (Melbourne - Djibouti)

Figure 4.17.: Variation of the fuel costs coefficient k_f. Relative FEC of variants 2388.0, .2 and .3 with fixed floating condition for all considered routes as function of the scaling factor λ

In figures 4.18a to 4.18f (p.101), results for the fuel oil consumption FOC for the different routes are shown. In contrast to the previous simulations, the advantage of variant 2388.2 is considerably higher, even for the largest scaling factors $\lambda = 50$. Variant 2388.3, with the best resistance in calm waters, remains even in calm weather routes with results of the same order of magnitude than the bulbless variant 2388.0. This trend decreases for larger scaling factors, but in no single case the fuel oil consumption of variant 2388.3 becomes lower than the one of variant 2388.2.

This simulations with lowered service speed can be considered as a valuable alternative for the designer to compare different variants. On the other side, it depends of the philosophy of the ship operator and of many other factors if the decision of operating at slightly lower speeds is advantageous or not. Further possibilities for this approach would be the declaration of a "target mean service speed", for which the engine power and the propulsion unit is adjusted for each ship until this mean speed is reached. This approach will not be followed in this study, and further comparisons will be made with the proposed measure of merit FEC.

4.7. Operational Simulations with Variable Speed and Variable Floating Condition

4.7.1. Simulation Setup

As a further and last step of complexity, attempting to model ship operation as realistic as possible, simulations with variable floating condition were undertaken. It can be considered as a fact that practically every cargo ship operates, over significant amounts of time, in partially loaded or in fully unloaded (ballast) conditions, so-called *off-design floating conditions*. As previously discussed, the consequence of the operation under these conditions, for which the ship was neither designed nor optimized for, can lead to a subsequent economic loss, making the consideration of these of particular interest in this study.

Floating Conditions

The floating condition of the ship is found, for every single trip, given an amount of cargo, fuel and ballast with their respective centers of gravity. This is done as described in section 3.3.1.

For the purpose of this investigation, three different floating conditions were alternated for each trip, in order to obtain the same conditions for all ships studied. The selection of a total of three conditions ensures, for the period of five simulation years, that each trip, in each direction, will be undertaken with almost equal amounts of each floating condition. These conditions, namely full loaded, partially loaded and ballast, are summarized in table 4.7. The generalized approach of the implementation permits no limitations on this and further loading conditions, recalling statistical data from shipping companies, can be included without restrictions.

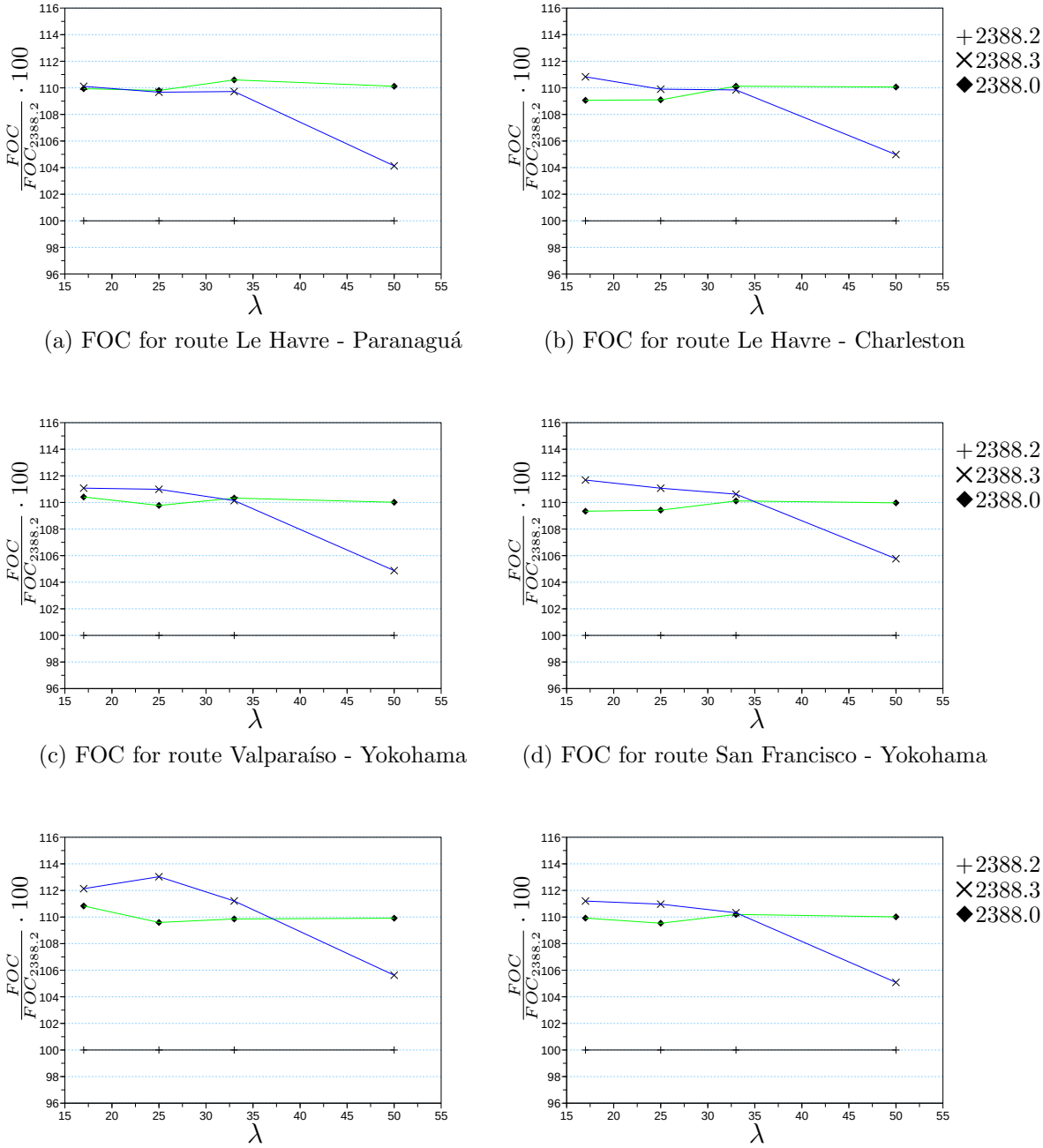

(a) FOC for route Le Havre - Paranaguá

(b) FOC for route Le Havre - Charleston

(c) FOC for route Valparaíso - Yokohama

(d) FOC for route San Francisco - Yokohama

(e) FOC for route Melbourne - Djibouti

(f) mean FOC of all routes

Figure 4.18.: Relative FOC of slow steaming simulations for variants 2388.0, .2 and .3 with fixed floating condition for all considered routes and mean relative FOC as function of the scaling factor λ

Description	Cargo [t]	$\overline{x}_{cargo}$ [m]	T_{AP} [m]	T_{FP} [m]
full loaded	8700	2.5	8.1132	8.0884
partially loaded	4000	0	6.8254	5.7306
ballast	0	0	5.1088	4.224

Table 4.7.: Loading conditions. Example for ships with $\lambda = 25$

4.7.2. Results

In the same manner as in the previous sections, results for the measure of merit (FEC) are summarized in figures 4.19a to 4.19f. Additional results for R_{AW} and achieved speed V_S can be found in appendix D, figs. D.4 and D.5 respectively.

As expected from the resistance in calm waters for off-design floating conditions, variant 2388.2 performs better in almost every route and scaling factor of the comparison. The results show also the influence of weather on the relative ranking between the variants: especially for $\lambda = 25$ a change in the relative values can be observed for almost every route. A statistical analysis presented in the next section (sect. 4.8) for the encountered sea states in the considered routes attempts to give an answer to this finding.

The differences in the fuel equivalent costs between calm and rough weather routes are here partially damped by the equally relevant influence of the partial and ballast floating conditions. Nevertheless, differences of up to 5% between the parent ship and variant 2388.3 can be observed for the route Melbourne-Djibouti (fig. 4.19e) for $\lambda = 25$, being these a few percent smaller (2%) for the route between Le Havre and Paranaguá (fig. 4.19a).

This insight shows again the importance of considering all components of the operational profile of the ship for the selection of the most adequate variant including, additionally to weather factors, realistic assumptions about the (expected) floating conditions during the operational life of the ship.

4.8. Conclusions about Simulation Modes

For the presented operational simulations exploiting existing experimental data, different simulation modes were tested. The first and simplest setup, with fixed speed and fixed floating condition, was in a first instance expected to correlate with variable speed simulations. This would have shown that, in an early design stage, such simulations can be useful for the comparison between variants and thus help the designer to choose the economically most profitable one. Since this was not the case, this simulation setup cannot be recommended for design purposes.

The simulations with variable speed and fixed floating condition demonstrated their applicability. They showed the importance of the consideration of machinery and propulsion unit, causing the subsequent involuntary speed loss, variable specific fuel oil consumptions and propeller efficiencies. Also the further consideration of slamming events and accelerations at the bridge causing voluntary speed loss played an important role, especially for

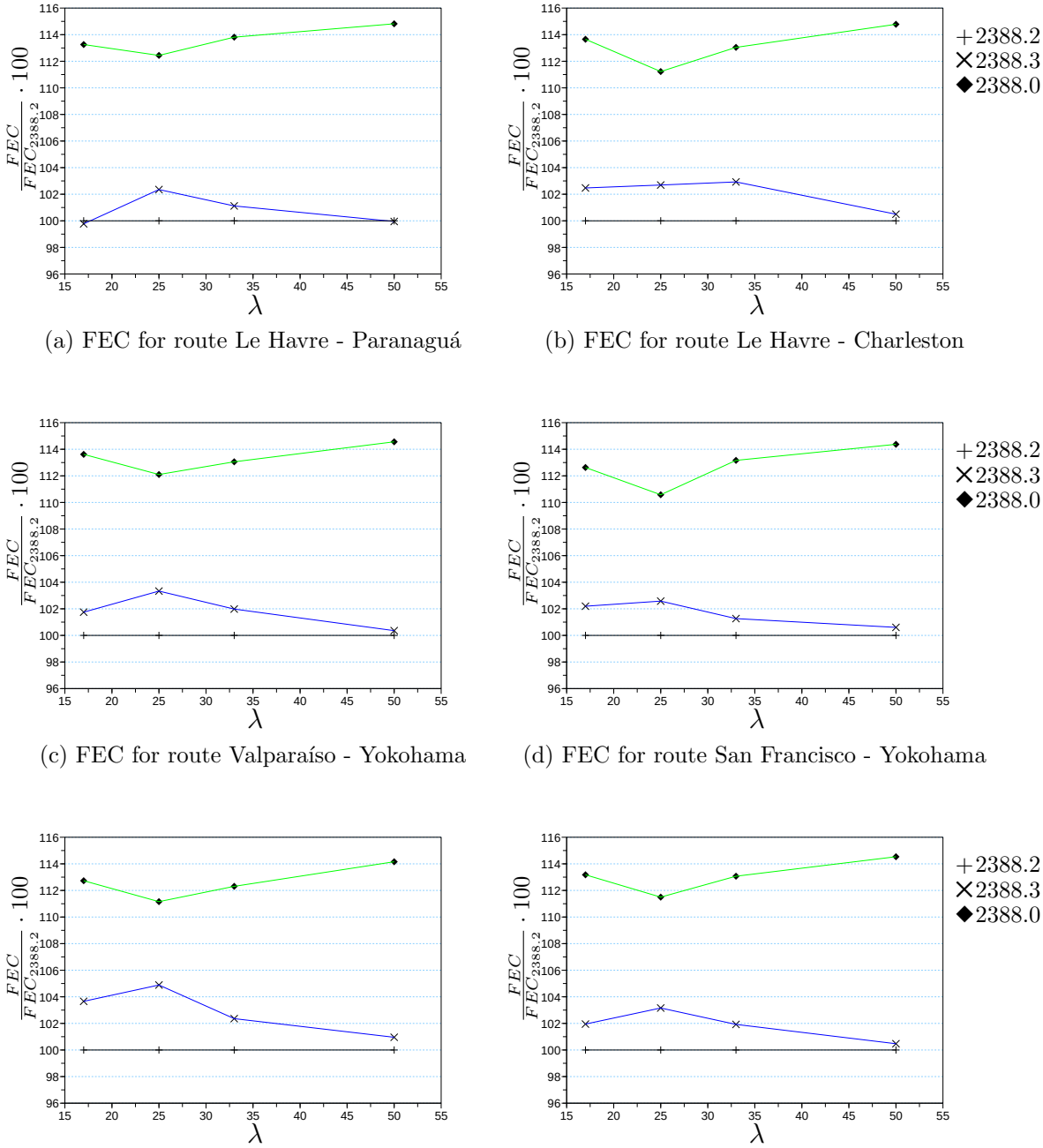

(a) FEC for route Le Havre - Paranaguá

(b) FEC for route Le Havre - Charleston

(c) FEC for route Valparaíso - Yokohama

(d) FEC for route San Francisco - Yokohama

(e) FEC for route Melbourne - Djibouti

(f) mean FEC of all routes

Figure 4.19.: Relative FEC of variants 2388.0, .2 and .3 with variable floating condition for all considered routes and mean relative FEC as function of the scaling factor λ

ships of smaller size. The measure of merit presented, the Fuel Equivalent Costs FEC, showed its robustness for different fuel costs factors k_f.

The simulations with variable speed and variable floating condition show, despite the simple cargo profile applied, the significance of off-design floating conditions into the performance assessment of a design. Especially for ships operating significant amounts of time in ballast conditions, the application of such simulations is mandatory for the correct identification of the most convenient design variant. As previously mentioned, the higher uncertainty regarding the seakeeping characteristics considered in these simulations must be considered when interpreting these results.

As mentioned in the previous section, a change in the relative values of FOC for $\lambda = 25$ can be observed for almost every route in both simulation modes. To understand the causes of this phenomenon, the encountered weather factors from all simulations performed were collected, classified and analyzed, generating occurrence probability functions of sea state parameters for each of the routes considered. In figure 4.20, occurrence probabilities of mean encounter wave direction, significant wave height, mean wave period and mean wave length are presented. This information is gained from the encountered weather of all ships simulated over the five-year period and is therefore representative, over this time period, for each of the considered routes. Of special interest is figure 4.20d for the mean wave length: the peak values of these curves are found for mean wave lengths between 100m and 170m approx., decreasing drastically for larger wave lengths. This leads, to a certain extent, to the change in the trend of the curves of relative FEC (considering that for $\lambda = 25$, $L_{PP} = 146.25$m). The final outcome of the values of FEC also depend of the encountered wave angles and significant wave heights, but also of the added resistance in regular waves and ship motions, leading to a complex interdependency between them. For the wave encounter angles (fig 4.20a), clear differences can be observed between the different routes. It shall be remarked that the weather data was collected in both directions (outward and return), which takes account for the symmetry of the occurrences. While beam seas are slightly predominant for the routes Le Havre-Paranaguá and Valparaíso-Yokohama, head and following seas are slightly predominant for the remaining routes. From the occurrence probability of significant wave heights, the previous classification of calm weather and rough weather routes can be confirmed. Particularly, the considerably higher occurrence probability of large wave heights can be observed for rough weather routes (this tendency is observed especially for significant wave heights of approx. 3 m and greater). Considering the quadratic relation between wave height and wave energy, the relevance of these significant wave heights is considerable.

From the presented special application case exploiting existing experimental data, it can be concluded that the presented operational simulations should be performed considering voluntary and involuntary speed loss, that different routes and ship sizes lead to different ship performances and that certain sea state characteristics have special influence for certain ship lengths (in the present case for $\lambda = 25$). Considering these aspects, the presented method will be applied in the next chapter for a design study including new designs and recalling the hydrodynamic characteristics of these designs from numerical methods, representing the general form of application of the presented design methodology.

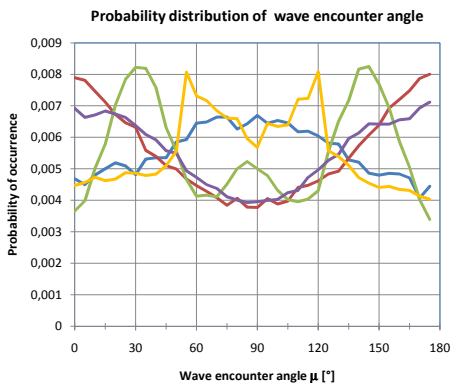

(a) Mean encounter wave direction

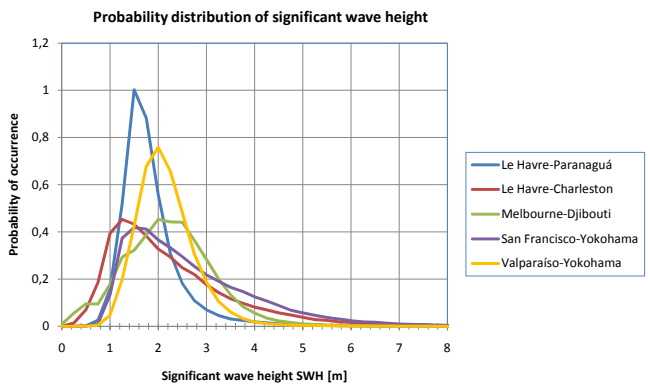

(b) Significant wave height

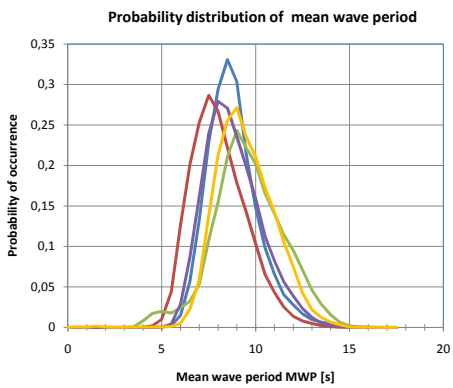

(c) Mean wave period

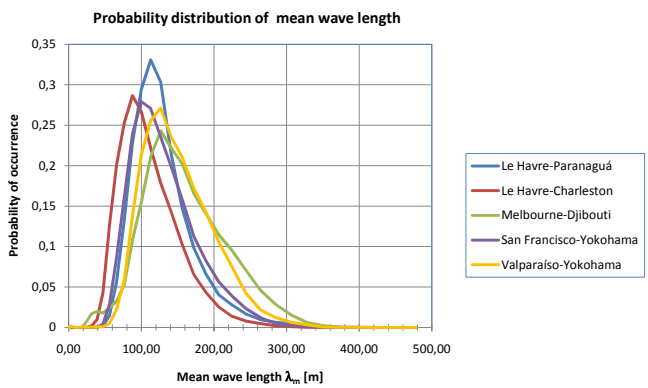

(d) Mean wave length

Figure 4.20.: Probability distributions of wave direction, significant wave height, mean wave period and mean wave length

5. General Application Case

5.1. Introduction

In this chapter, the application of operational simulations for design purposes is presented by means of a second practical example. Opposite to the application case discussed in the previous chapter, the hydrodynamic characteristics of the ships in question are obtained from numerical calculations only, including potential and viscous CFD methods. New geometries, generated by a partially parametric approach with model 2388.2 as parent form, are also included in the presented practical example. In this manner, an attempt to reproduce normal conditions in an early design stage, being experimental data not available and studying a large number of variants, is made. All of these aspects make the example presented in this chapter of central relevance for this investigation, demonstrating the applicability of the presented methodology for design purposes in early design.

In a first stage, 36 different subvariants (differing only in their bulbous bow and in some cases slightly in their foreships) have been generated from the parent geometry (model no. 2388.2). For these geometries, wave resistance calculations with a potential CFD solver were undertaken for different floating conditions and advance speeds.

From these subvariants, after studying potential CFD results, four of them have been selected to undertake further viscous CFD calculations in regular waves with the OpenFOAM-solver `TUBsixDOFFoam`. Additionally, the same viscous CFD calculations were undertaken for the ships studied in chapter 4 (with exception of the bulbless variant 2388.0), validating results from these calculations with the available experimental results.

In a similar manner as in chapter 4, operational simulations were carried out for the considered routes, making use of the same environment conditions (weather, routes and cargo) from the previous chapter. For convenience, simple simulations with fixed speed and fixed floating condition (as presented in section 4.5) were omitted, considering therefore only variable speed simulations.

The attained results from the operational simulations are discussed, and the variants providing best economic profit are identified for each route and ship size, showing that the magnitude of the achieved economic surplus is, in most cases, worth to be considered. Finally, a short discussion considering certain design aspects of bulbous bows is given.

Transformation		Index	1	2	3
Tip translation	$\delta x_{tt}/L_{PR}$	i	0.00	0.15	0.30
Inner translation	$\delta x_{ti}/L_{PR}$	j	0.00	0.15	-
Vertical translation	$\delta z_{tt}/L_{PR}$	k	0.00	0.25	-
Radial scaling	S_r/∇_{PR}	l	1.00	1.05	1.10

Table 5.1.: Parameter variation for subvariants

5.2. Generation of Subvariants

5.2.1. Parent Geometry and Overview of Calculations

As already mentioned, the parent geometry considered was variant 2388.2, due to its good performance in the undertaken operational simulations described in chapter 4. From this geometry, 36 different *subvariants* were generated, applying different combinations of the bulbous bow form parameters defined in section 2.8 (to avoid confusion, *variants* are models 2388.0, 2388.2 and 2388.3, *subvariants* are further variations of any of these variants). The wave resistance of all these subvariants has been calculated for three different floating conditions and three different velocities with the potential CFD solver FS-Flow. The results from these calculations have been analyzed and four of these subvariants have been selected. With these selected subvariants, together with variants 2388.2 and 2388.3, viscous CFD calculations in regular head waves have been undertaken for the determination of responses and added resistance in waves, making use of the procedure described in chapter 3 for the evaluation of wave angles different to 180°and floating conditions different to the design floating condition T_{22}.

5.2.2. Design Space Exploration for Wave Resistance with Potential CFD Method

Parameters for Form Variation Approach

The exploration of the design space is normally a task where special care is required in the extent and number of subvariants to be analyzed. In this case, it was intended to consider a minimal number of subvariants, since the computational effort is not negligible. Nevertheless, all bulbous bow geometric parameters defined in sect. 2.8 were varied (as shown in table 5.1), and all combinations of these parameters were calculated, making 36 different geometries. The subvariants are identified by the model number (2388), variant index (2) and a four-digit subvariant index $ijkl$, according to table 5.1 (e.g. subvariant 2388.2_3121 denotes a subvariant based in variant 2388.2, with a bulbous bow enlarged 30% ($i = 3$), without inner section shifting ($j = 1$), a dimensionless vertical tip translation of 25% ($k = 2$) and without radial scaling ($l = 1$)).

Description	Index	T_{AP} (m)	T_{FP} (m)
Design draft	T_{22}	8.125	8.125
Partially loaded	T_{34}	6.964	6.094
Ballast	T_{46}	6.094	4.875

Table 5.2.: Drafts considered into calculations

Potential CFD Calculations with FS-Flow

For each geometry, three different floating conditions (T_{22}, , T_{34} and T_{46}), as defined in table 5.2, and three different speeds (equivalent to $F_n = 0.200$, 0.225, 0.250) were calculated, making a total of 324 potential flow calculations. All calculations were made within an automatized batch routine and results were extracted automatically.

Results and Choice of Subvariants for further RANSE-CFD Seakeeping Calculations

The wave resistance of each of the subvariants is shown, normalized by the wave resistance of the parent hull, in figures 5.1 ($F_n = 0.200$), 5.2 ($F_n = 0.225$) and 5.3 ($F_n = 0.250$) for the three considered floating conditions (T_{22}, T_{34}, T_{46}). Additional data (bulbous bow parameters and results in tabular form), can be found in appendix C, tables C.1, C.2 and C.3 (pp. 156-159).

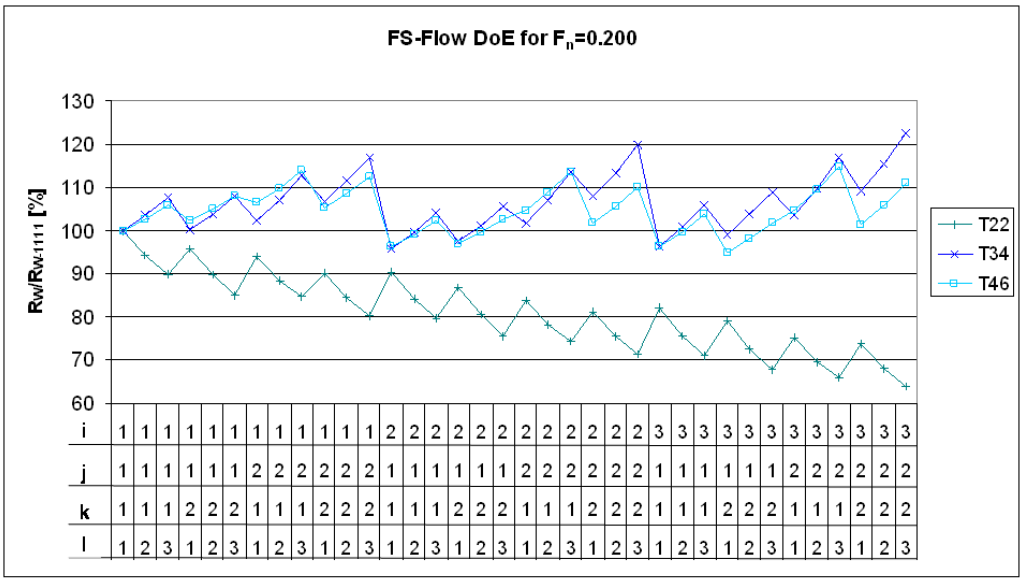

Figure 5.1.: Wave resistance (as percentage of parent hull wave resistance) of subvariants for $F_n = 0.200$

Clear differences can be observed in figs. 5.1 to 5.3 between the three different floating conditions calculated:

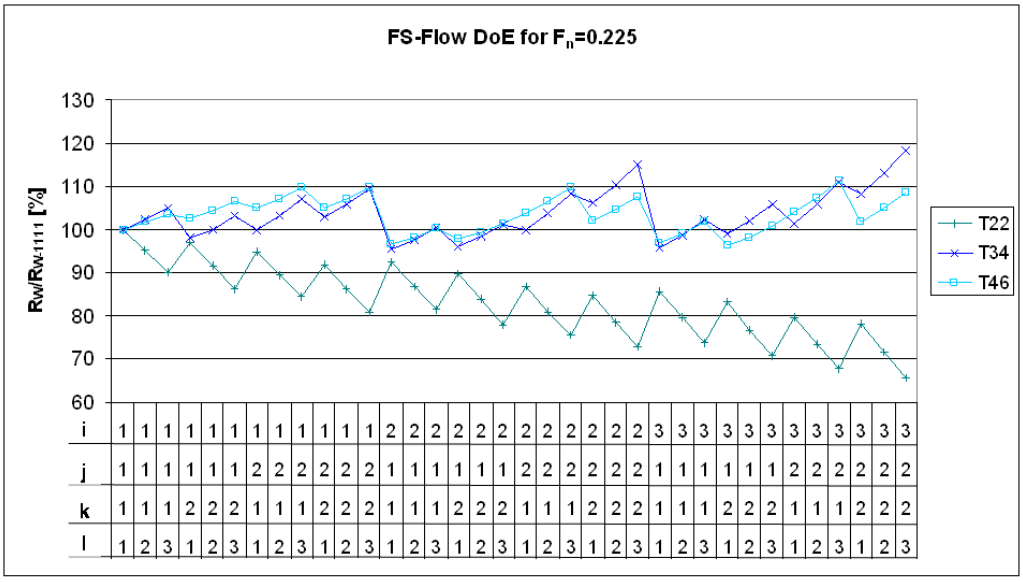

Figure 5.2.: Wave resistance (as percentage of parent hull wave resistance) of subvariants for $F_n = 0.225$

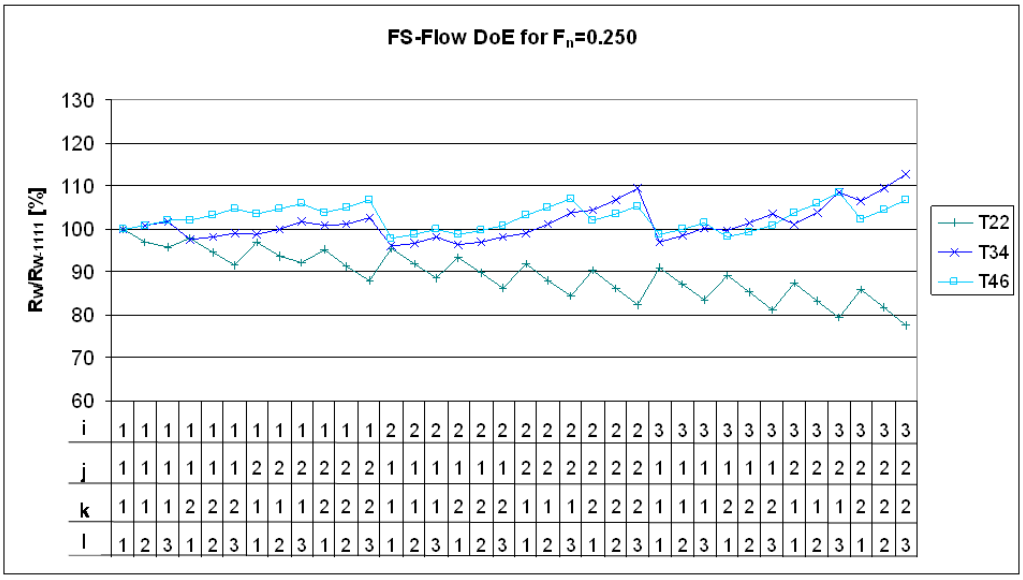

Figure 5.3.: Wave resistance (as percentage of parent hull wave resistance) of subvariants for $F_n = 0.250$

- For the design floating condition (T_{22}), subvariant 2388.2_3223 has the lowest wave resistance at all three speeds calculated.

- For the partially loaded condition (T_{34}), the same subvariant shows for the lower velocities one of the highest, for $F_n = 0.250$ the highest wave resistance. Lowest resistances are obtained for this floating condition with rather conservative designs, such as subvariants 2388.2_2111 or 2388.2_3111.

- For the ballast condition (T_{44}), subvariant 2388.2_3223 (lowest resistance at design draft T_{22}) has the highest wave resistance at all calculated speeds. For this floating condition, lower values of wave resistance can be found for subvariants 2388.2_2111 and 2388.2_3121, depending of speed.

These differences can give a clear idea of the danger of not considering off-design velocities and off-design floating conditions when making such a design space exploration, especially within a non-interactive, automatized optimization approach.

From all 36 subvariants, only a few can be chosen for calculations of seakeeping characteristics with viscous CFD. It was considered important to choose from the whole spectrum of variants, and not only those with a good performance in calm waters. In this context, subvariants 2388.2_2111, _3121, _3211 and _3223 were chosen for further calculations with `TUBsixDOFFoam` and to undertake the different operational simulations with `SimOship`. Figures 5.4, 5.5 and 5.6 show the resistance characteristic of the chosen subvariants within the design space exploration over the bulbous bow volume parameter $C_{\nabla PR}$. The foreship sections of the selected subvariants are shown in figures 5.7a to 5.7e and are shown, rendered, in fig. C.4 in appendix C (pp. 156).

5.3. Viscous CFD Calculations

5.3.1. Overview

Since the computational resources required for calculating the selected subvariants with different velocities, floating conditions, wave lengths and wave directions were not available and would go beyond the scope of this investigation (and any other design study in a preliminary design stage), only a few of these parameters can be varied. Analogous to the available experimental data described in the previous chapter, only head waves, one velocity (design speed, $F_n = 0.250$) and a single floating condition (design draft T_{22}) were considered. Different wave lengths λ_w were chosen also analogous to the experimental setup ($\lambda_w/L_{PP} = 0.750$, 1.000, 1.125, 1.250, 1.500, 1.750) for a single wave amplitude $\zeta_a = 0.05$[m] in model scale. The unsteady CFD calculations were undertaken for several wave periods in order to correlate results with harmonic motions by means of a linear regression.

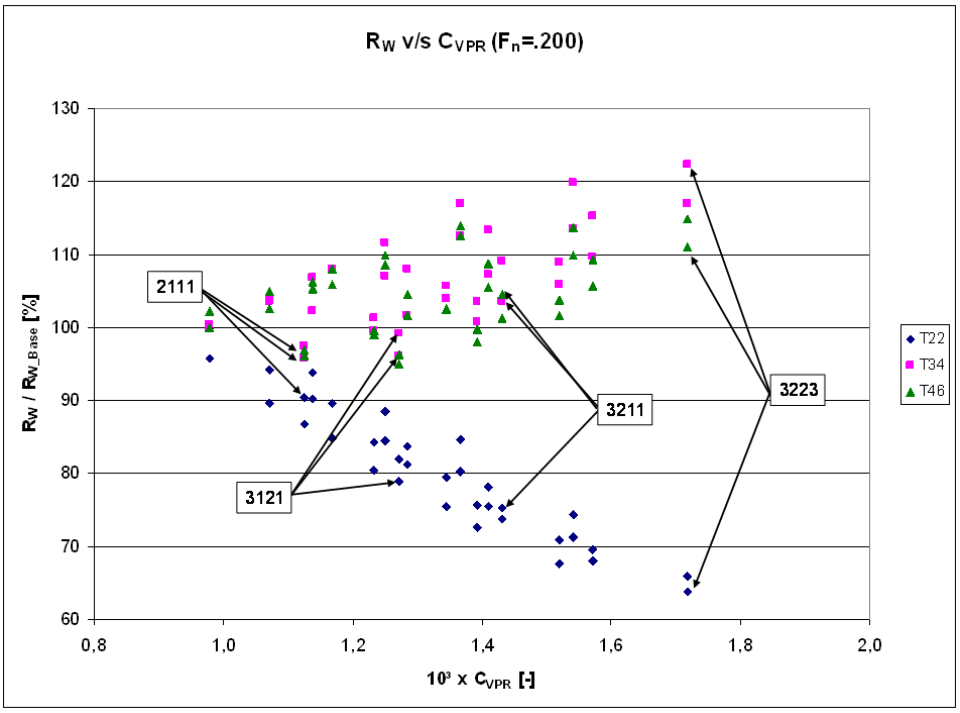

Figure 5.4.: Wave resistance (as percentage of parent hull wave resistance) over bulb volume parameter $C_{\nabla PR}$ for $F_n = 0.200$

5.3.2. Solver, Boundary Conditions and Numerical Setup

For the purpose of calculating ship motions and forces in regular waves, the OpenFOAM-solver `TUBsixDOFFoam` was developed. A brief description of the solver has been given in section 2.6.3. The selected boundary conditions and numerical setup are identical to the setup presented for the validation case with the DTMB5512 surface combatant model, as described in section 2.7.3.

5.3.3. Grid Generation

The grid generation was made with the OpenFOAM-utility `snappyHexMesh` in the same manner as for the mentioned validation case (DTMB5512 model) described in section 2.7.3.

For each of the four selected subvariants, several meshes with different levels of refinement were generated. The total number of cells is given in table 5.3. The first refinement level shown in the table, called *development*, was used for testing purposes during the development phase of the solver. Figures 5.8a to 5.8d show the meshed hulls and give also an overview of the mesh refinement levels studied. Additional figures showing the mesh at the free surface can be also found in appendix A, figures A.7a to A.7d (pp.151-151).

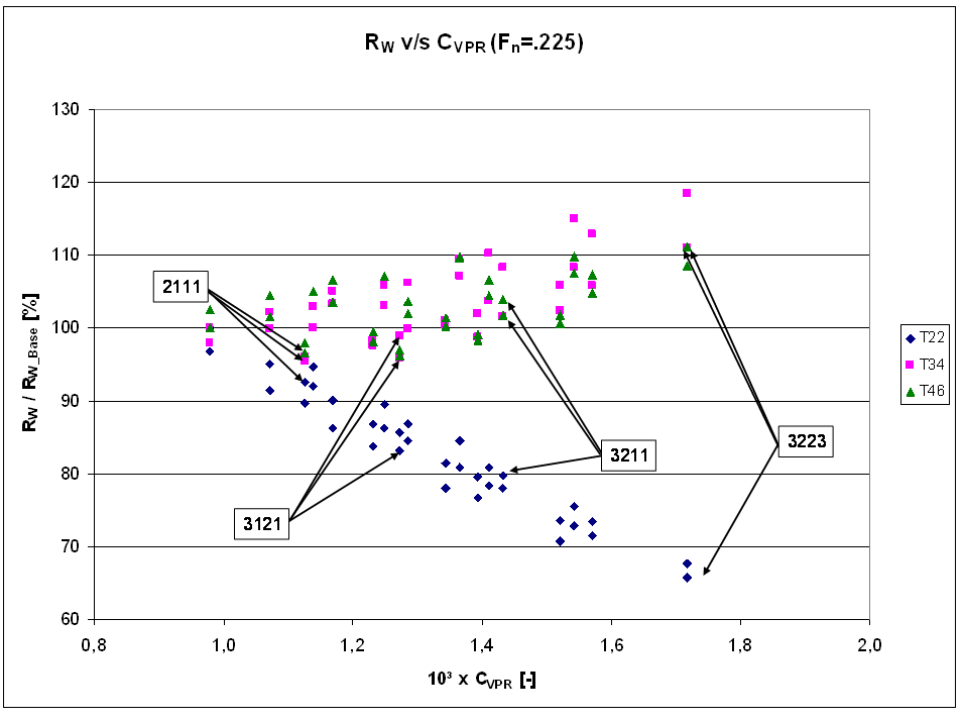

Figure 5.5.: Wave resistance (as percentage of parent hull wave resistance) over bulb volume parameter $C_{\nabla PR}$ for $F_n = 0.225$

5.3.4. Calculations

Hardware

A large number of calculations was undertaken during the different phases of the development and final use of `TUBsixDOFFOAM`, starting from initial tests up to final calculations with fine grids. This was done making use of different hardware setups available during this study and, due to their special characteristics, they will be shortly described here:

- Initial calculations during the development of `TUBsixDOFFoam`, both for coarse and medium grids, were made, when possible, in available machines from the departments *dynamics of maritime systems* and *design and operation of maritime systems*. When this was not sufficient, additional resources were booked from Amazon Web

Category name	No. of cells
`development`	16628
`evencoarser`	82183
`coarser`	187666
`standard`	365216
`finer`	791319

Table 5.3.: Mesh refinement levels

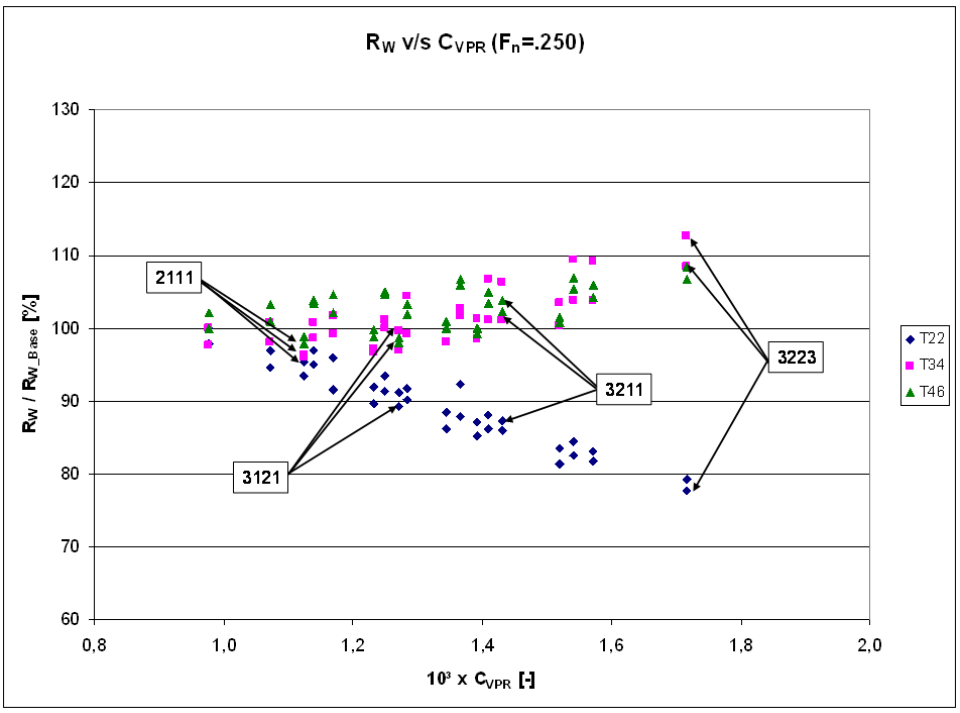

Figure 5.6.: Wave resistance (as percentage of parent hull wave resistance) over bulb volume parameter $C_{\nabla PR}$ for $F_n = 0.250$

Services™[1]. AWS is a cloud-based platform of remote computing resources, offering the possibility of practically unlimited on-demand resources. In the case of this investigation work, high performance hardware was purchased, at hourly rates and only when more resources were needed than locally available. One of the decisive advantages of this principle is the possibility of storing complete machine configurations, being those ready-to-use when needed. For general use in ship design, on-demand computing services can be of significant advantage for computationally intensive or time-sensitive projects, when the acquisition of additional hardware is not a cost-effective solution.

- Final calculations, for the complete range of meshes, were made at the large cluster of the North-German Supercomputing Alliance (*Norddeutscher Verbund zur Förderung des Hoch- und Höchstleistungsrechnens* - HLRN [3]). This alliance offers, free of charge for academic investigation projects, full access to the complete range of computational resources for a given amount of *credits*, billed for each hour and processor used. Since the number of credits is limited, only small to medium projects can be undertaken in this modality, which can be attractive e.g. for master theses. Additional resources for large investigation projects can also be booked for a fee.

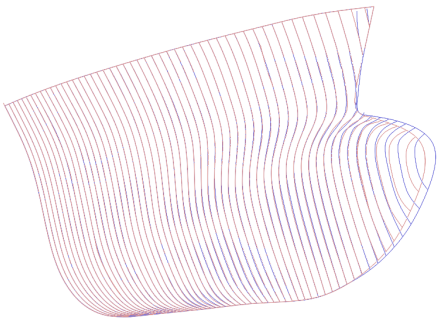

(a) 2388.2-1111 (red) and 2388.2-2111 (blue)

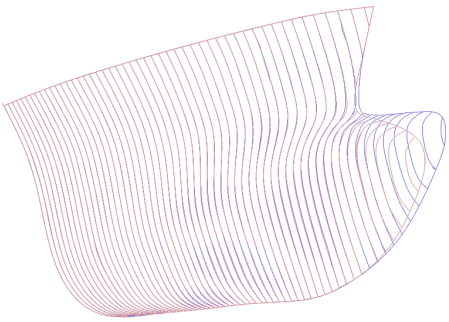

(b) 2388.2-1111 (red) and 2388.2-3121 (blue)

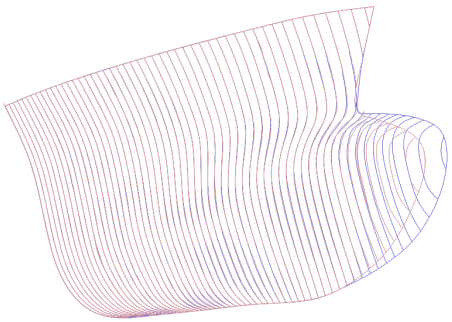

(c) 2388.2-1111 (red) and 2388.2-3211 (blue)

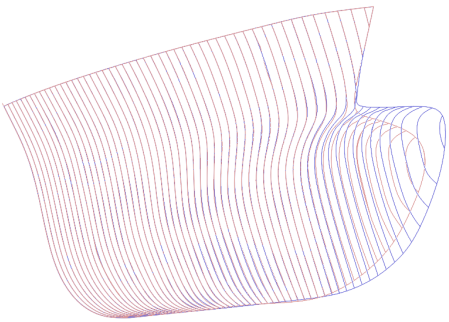

(d) 2388.2-1111 (red) and 2388.2-3223 (blue)

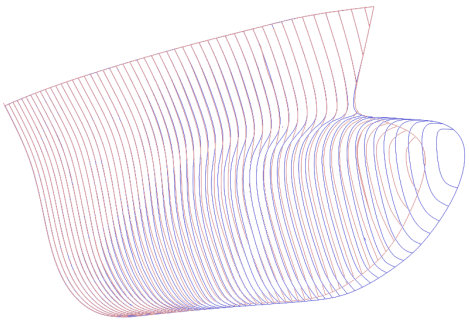

(e) 2388.2-1111 (red) and 2388.3-1111 (blue)

Figure 5.7.: Foreship sections of selected subvariants compared to parent hull 2388.2-1111

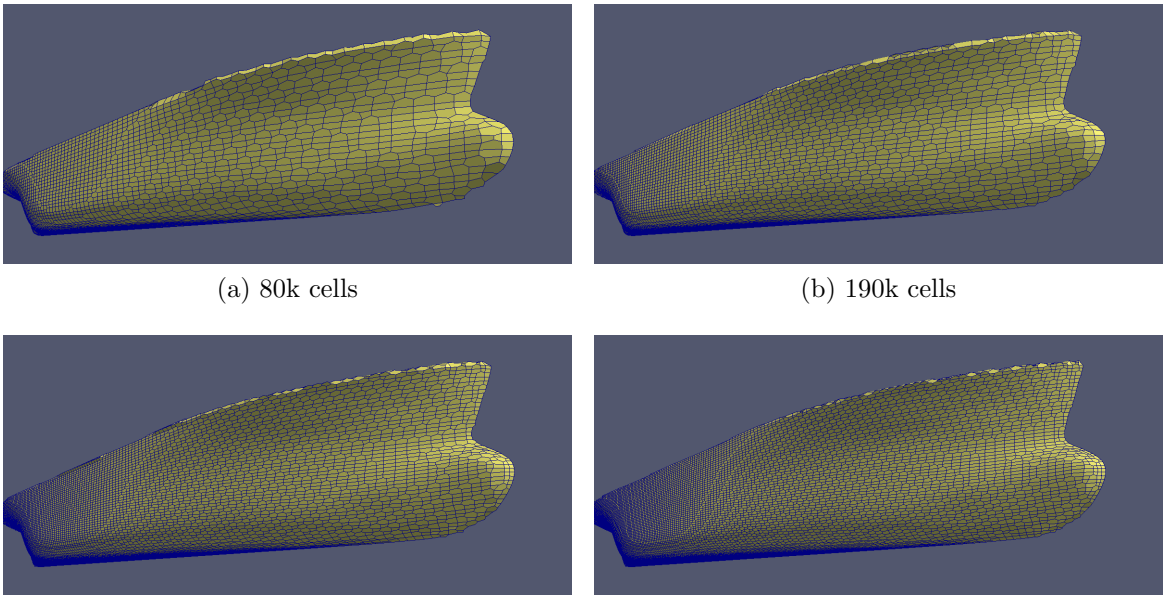

(a) 80k cells (b) 190k cells

(c) 370k cells (d) 800k cells

Figure 5.8.: Meshes with different refinement levels

Parallelization

The OpenFOAM toolkit offers parallelization features for practically every solver. Unfortunately, due to a known bug in the used version of OpenFOAM (v. 1.5.x) for dynamic meshes, calculations decomposed into more than four domains were unstable and crashed almost without exception. It is to expect that this problem has been solved in the meantime, but the present version of `TUBsixDOFFOAM` still makes use of the old dynamic mesh libraries. Due to the large amount of calculations, and additionally due to the small memory requirement of coarser meshes, it was in many cases more convenient to run many single-processor calculations at the same time instead of single, highly parallelized calculations sequentially.

Execution and Convergence

The calculations were run for a simulation time of a total of 20 to 30 seconds, a time in which for each wave length an harmonic steady state could be identified. In figure 5.9, the convergence and continuity progression is shown exemplarily for a calculation with 20s simulation time.

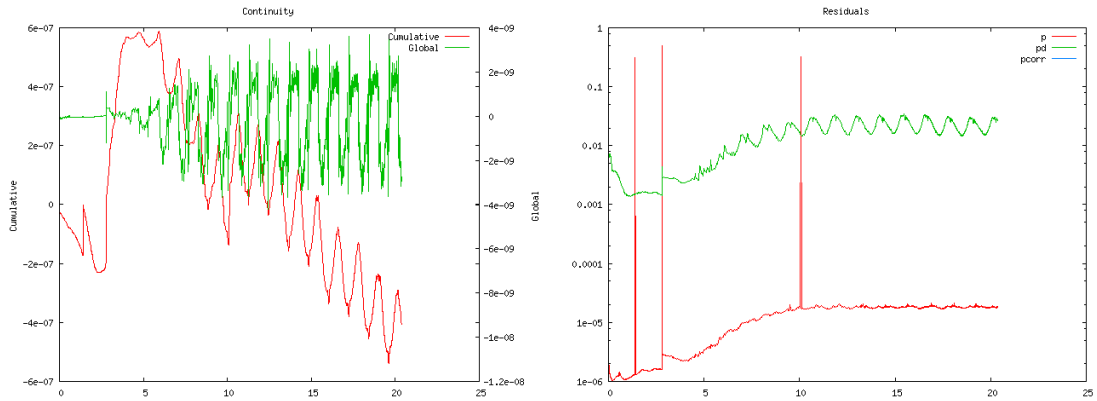

(a) Continuity (b) Residuals

Figure 5.9.: Diagrams of continuity and residuals

5.3.5. CFD Results of Variants and Comparison with Experimental Data

Grid Sensitivity Study

The grids described in section 5.3.3 (also summarized in table 5.3, p. 113) were studied for a single variant (parent model 2388.2) and a wave-to-ship length ratio $\lambda_W/L = 1.0$ for all described refinement levels. The results, shown in figure 5.10, indicate the total mean resistance in waves, equal to the force component in x-direction. As it can be expected, a considerable difference can be observed for the coarsest mesh, which was intended to be used only for fast testing and code development purposes. For the remaining four mesh refinement levels, these differences are considerably smaller and, for the same reason, the 80k (`evencoarser`) grid has been chosen for the study of the further variants. It must be certainly emphasized that both the comparative nature of this study and the proof of suitability of the method in an early design stage, considering a great amount of variants, motivated this decision.

Calm Water Resistance

Although it is not intended to use extensively a viscous CFD solver for the calculation of calm water resistance, such calculations are necessary to obtain the added resistance in waves. It is a known issue that a considerable difficulty of these calculations lies on the dynamic floating condition. Without considering dynamic trim and sinkage, results cannot be used for practical purposes. Also the usage of a floating condition from potential CFD calculations is not always a straightforward approach. Making use of the same equations of motion and the dynamic mesh motion principle applied later for seakeeping calculations, this problem can be overcome. In this case, the unsteady calm water simulation is performed until a steady state of the ship motions is achieved. Despite this approach can seem to be very straightforward at a first glance, an equilibrium condition in steady state

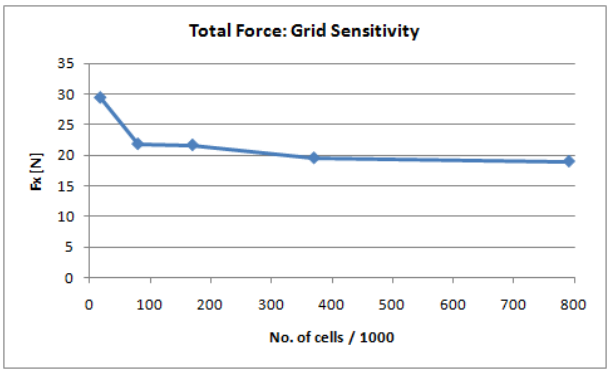

Figure 5.10.: Results of total longitudinal force in waves for different mesh refinement levels ($\lambda_W/L = 1.00$, $\zeta_A = 0.05$)

appears to be very difficult to find. One can expect that such small motions dissipate energy through very short waves. These waves, if present, would not be resolved by the calculations due to the insufficient transversal and longitudinal discretization of the free surface, being therefore the energy dissipation of these waves not present. Additionally, small numerical disturbances (such as reflections of long, narrow waves from the domain boundaries) make considerably longer CFD simulation times necessary in order to achieve the pursued steady state. By means of an artificial damping constant for the heave and pitch motions of the ship, the first of these difficulties is partially overcome, although the adjustment of this constant requires previous testing and simulation times are not reduced considerably. In figure 5.11, the time histories of total resistance, trim and sinkage are shown for an example case. A long total simulation times and the large oscillations show the mentioned difficulties which were dealt with.

Added Resistance and Motions in Waves

The main purpose of the application of the presented CFD tool is the prediction of motions and added resistance in waves in regular head waves, as outlined in section 5.3.1. For this purpose, unsteady simulations of 20s to 30s (of simulation time) have been performed. The achieved results were considered adequate when a minimum of five full periods are simulated successfully. From these results, mean values for the forces (e.g. total resistance in waves) were obtained. Additionally, a least square regression was made to identify the amplitude and phase of motions and forces. An example of the time histories of motions and forces, including fitted harmonic functions, are shown in figures 5.13 and 5.14. The mean value of the force was therefore obtained from the maximal number of full periods available from the CFD calculations. These results are processed for every variant and subvariant for the mentioned wave lengths ($\lambda_w/L_{PP} =$ 0.750, 1.000, 1.125, 1.250, 1.500, 1.750).

The mean added resistance in waves obtained for variants 2388.2 and 2388.3 is compared to the experimental results from Kracht. Figure 5.15 shows both the experimental and numerical results in dimensionless form for the mentioned variants. The accordance between

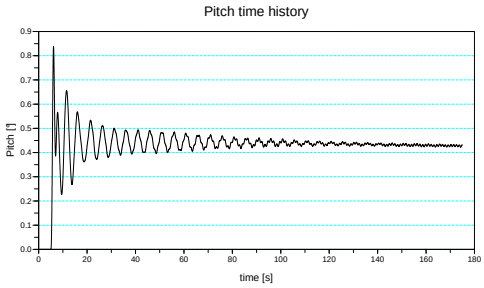

(a) Pitch

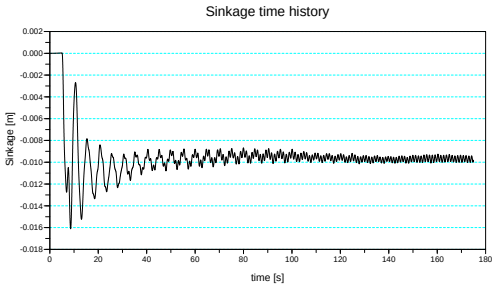

(b) Sinkage

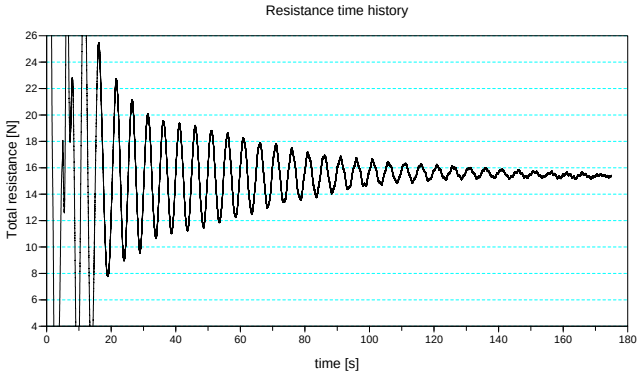

(c) Resistance

Figure 5.11.: Time histories of pitch, sinkage and total resistance in calm water

experimental and numerical results is especially good at the peak region ($\lambda_W/L = 1.125$ to 1.250), while differences for larger and longer waves are higher. In a certain manner, the numerical results seem to be "shifted", being forces for shorter waves underestimated and for longer waves overestimated. The exact origin of this effect remains unclear. Nevertheless, considering that experiments were carried out for a self-propelled model, the neglection of the surge motion and the propulsion unit in the calculations are most probably the main factors contributing to these differences. Notwithstanding to this, the relative differences between the variants correlate with the differences observed in the experiments in an acceptable manner, being well suited for the comparison of different variants.

For the heave and pitch motions, differences between numerical and experimental results appear to be considerably smaller. Figures 5.16a and 5.16b show these results for the heave and pitch motions respectively. While the accordance with experimental results is here for all frequencies given, differences between the variants could practically not be observed. Nevertheless, the results for the motions are considered just as well as valid for the purpose of this investigation.

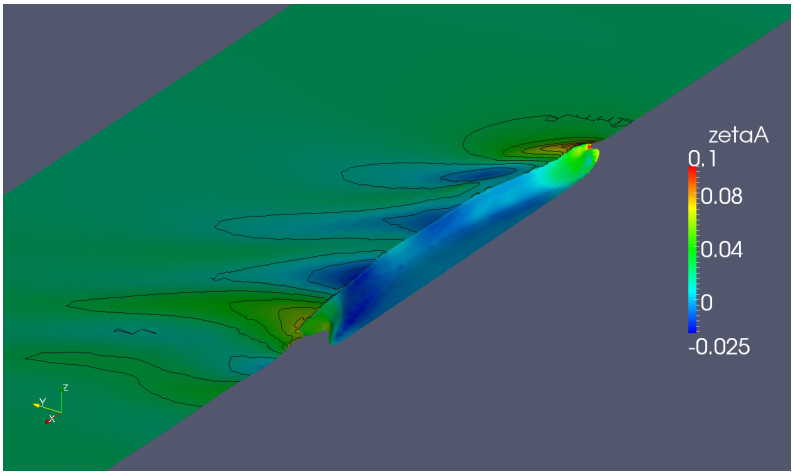

Figure 5.12.: Wave elevation in calm waters for variant 2388.2

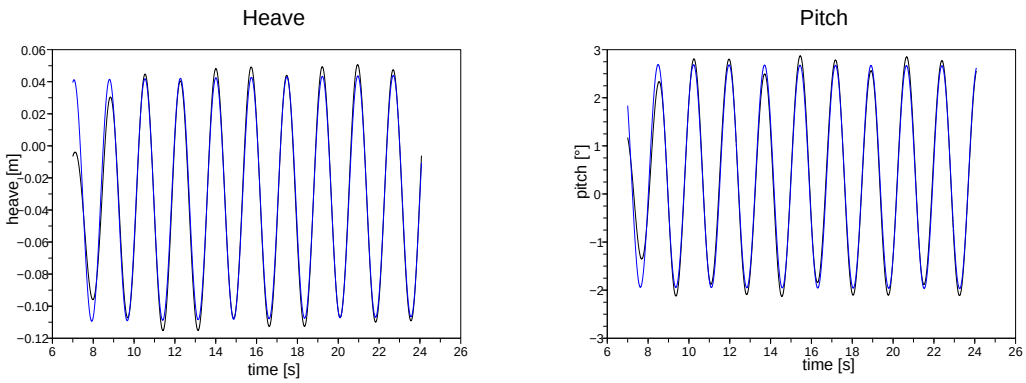

(a) Heave time history

(b) Pitch time history

Figure 5.13.: Heave and pitch time histories for parent hull, $\lambda_W/L = 1.750$ (black) and least square fitted harmonic function (blue)

5.3.6. CFD Results of Subvariants

Added Resistance and Motions in Waves

After the comparison of numerical and experimental results from the main variants 2388.2 and 2388.3, calculations in regular head waves for the remaining subvariants were undertaken. For this purpose, the same setup and meshing approach presented previously was applied, to ensure absolute comparability of final results. Calculations for the same seven wave lengths, a single velocity and a single floating condition were performed.

Results of added resistance in waves for all variants are shown in fig. 5.17. The results show clear differences between subvariants, demonstrating the ability of the presented CFD calculations to reflect such slight geometrical differences in the results.

As it could be expected, results for variant 2388.3, having the most pronounced bulbous bow, show the highest added resistance in the same way as experimental results do.

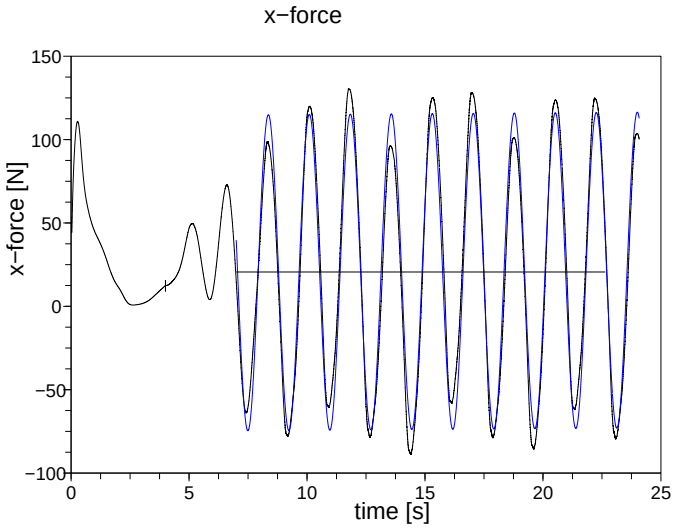

Figure 5.14.: Longitudinal force time history for parent hull, $\lambda_W/L = 1.750$ (black) and least square fitted harmonic function (blue)

Subvariants 2388.2_2111 and 2388.2_3211 show the lowest values here. Considering that subvariant 2388.2_3211 has also a good performance in calm water (see e.g. fig. 5.6), good performance within the operational simulations can be expected for this subvariant.

5.4. Operational Simulations with Variable Speed and Fixed Floating Condition

5.4.1. Simulation Setup

The less useful results from preliminary simulations with fixed speed and fixed floating condition presented in the previous chapter (sect. 4.5) encouraged the decision of omitting these for the presented general application case. Thus, operational simulations for a fixed floating condition (design draft T_{22}) with variable speed and simulations with variable speed and floating condition will be presented in this chapter. The first are presented in this section.

All assumptions, general setup, routes and measure of merit are identical to the application case in the homonymous section of the previous chapter (sect. 4.6). The importance of the operational simulations presented in this section is enforced by the fact that viscous CFD seakeeping calculations were made for the design floating condition as well.

The fictive engine characteristics of the studied subvariants have been defined in the same manner as in the previous chapter. Their characteristics are summarized in table E.1 in appendix E.

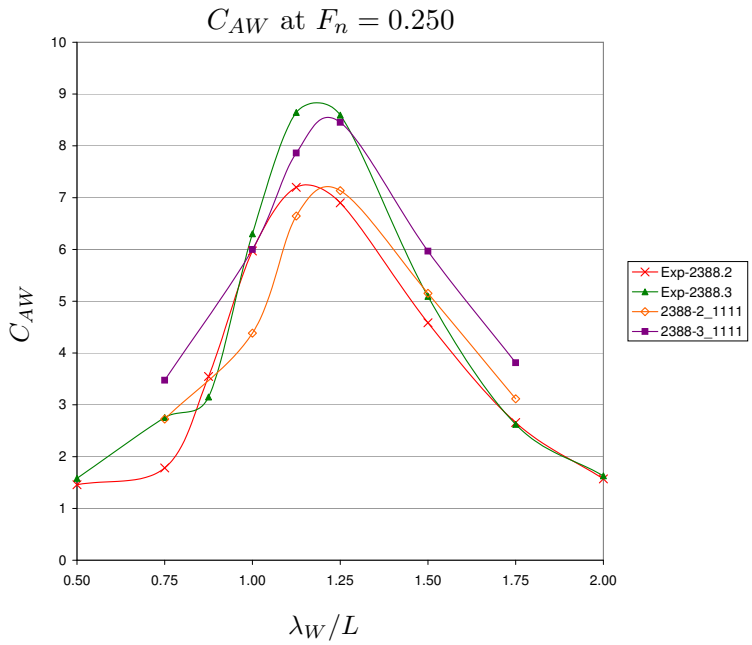

Figure 5.15.: Added resistance in waves for variants 2388.2 and 2388.3 from experiments and RANSE CFD calculations

5.4.2. Comparison with Results Recalling Experimental Data

The results from the operational simulations obtained for subvariants 2388.2_1111 and 2388.3_1111 are compared with results for the same ships from the operational simulations recalling experimental data (from section 4.6). Figures 5.18a to 5.18f show the normalized Fuel Equivalent Costs FEC as obtained from operational simulations with experimental and numerical data. In these diagrams, "experimental" and "numerical" results are normalized separately by their respective parent ship results. Differences are evidently present and can be expected when comparing numerical and experimental results for calm water resistance and added resistance in waves. Notwithstanding to this, the comparative ranking between variants shows consistency in all diagrams, particularly in the location of crossings between the curves.

Considering all aspects mentioned here, the applicability of operational simulations recalling only numerical data is demonstrated for design purposes, making their usage for the evaluation of new designs (in our case the presented subvariants) a further, logical step to undertake.

5.4.3. Results of Subvariants

The operational simulations with variable speed and fixed floating condition play a central role in this investigation. The design exploration by means of a performance assessment for selected subvariants, including the usage of advanced numerical methods and the

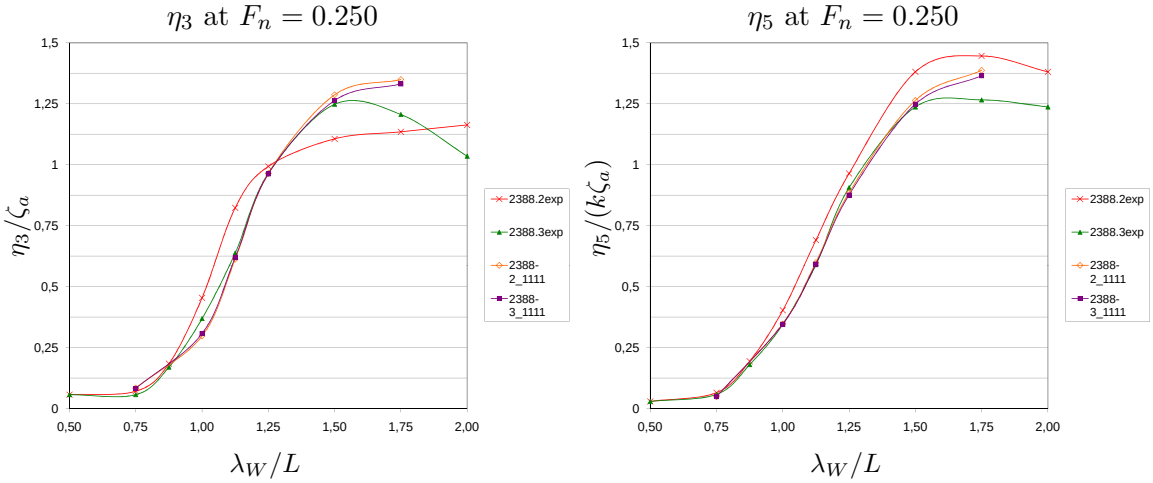

(a) Heave responses from CFD and experiments

(b) Heave responses from CFD and experiments

Figure 5.16.: Responses in head waves for variants 2388.2 and 2388.3 from experiments and RANSE CFD calculations

simulation of the operational life of these designs has been one of its main purposes. As for the results presented in the previous chapter for simulations with variable speed and fixed floating condition, results presented here have the advantage of addressing added resistance and motions in waves from the CFD calculations without additional corrections for floating condition from strip theory calculations.

The obtained results for fuel equivalent costs FEC are shown in figure 5.19 (p.127) for each subvariant as function of the scaling factor λ for all considered routes. Additional results for R_{AW} and achieved speed V_S can be found in appendix E, figs. E.1 and E.2 respectively.

In general terms, similar tendencies as discussed in chapter 4 (sect. 4.6) can be observed:

- Routes can be categorized here into calm weather routes (Le Havre-Paranaguá and Valparaíso-Yokohama) and rough weather routes (Le Havre-Charleston, San Francisco-Yokohama and Melbourne-Djibouti) as in the previous chapter
- In calm weather routes, subvariant 2388.2_3223 (purple line) shows the best performance for larger ship sizes ($\lambda = 33$, 50)
- In rough weather routes, subvariant 2388.2_3211 (red line) shows the best performance, except for the greatest length class with $\lambda = 50$
- Specifically in the route Melbourne - Djibouti (fig. 5.19e), this subvariant (2388.2_3211) shows the best performance for all length classes
- Again, a peak in the influence of added resistance in rough weather routes for $\lambda = 25$ can be observed.

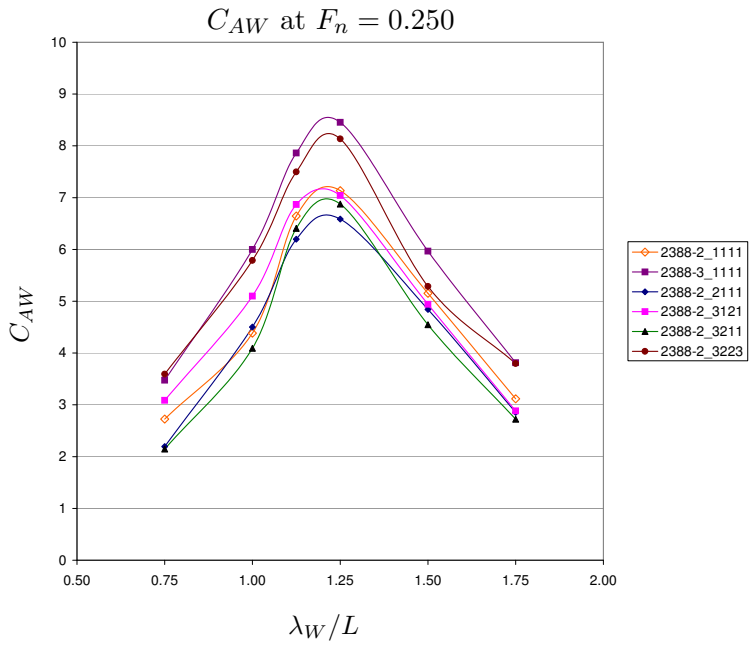

Figure 5.17.: Added resistance in waves for variants 2388.2 and 2388.3 and subvariants from RANSE CFD calculations

A short discussion will be made for the results with $\lambda = 25$, since this scaling factor represents the ship as it was originally designed.

First, results of (sub-)variants 2388.2 (2388.2_1111) and 2388.3 (2388.3_1111) will be discussed. Recalling only the fuel oil consumption in calm water (see. fig. 4.5. p.82), an advantage of less than 2% is obtained for the larger bulbous bow (here 2388.3_1111) when compared to the parent ship (here 2388.2_1111). This would have probably lead a designer to choose the larger bulbous bow for his design if no further information would have been available for his decision. After the accomplishment of the operational simulations presented here, this advantage becomes for some routes the opposite: for the route Melbourne-Djibouti, for example, the larger bulbous bow is now more than 5% worse in its performance than the parent ship (fig. 5.19e). For the mean of all routes (fig. 5.19f), this difference is lower (approx. 2%), but still opposite to the results in calm water. Even if both *performance assessments* had different measures of merit and without considering the possibility of insufficient precision or false assumptions in any of two methods (calm water resistance and operational simulations), this comparison shows clearly that operational aspects are worth to consider in ship design.

When including the newly designed subvariants in this comparison for $\lambda = 25$, the differences become slightly larger. From the evaluation in calm water, subvariant 2388.2_3223 appears to be the best configuration (see e.g. fig. C.3 in app. C). For the operational simulation between Melbourne and Djibouti, the best performance is attained by subvariant 2388.2_3211 which has, according to the operational simulation, a performance about 6%

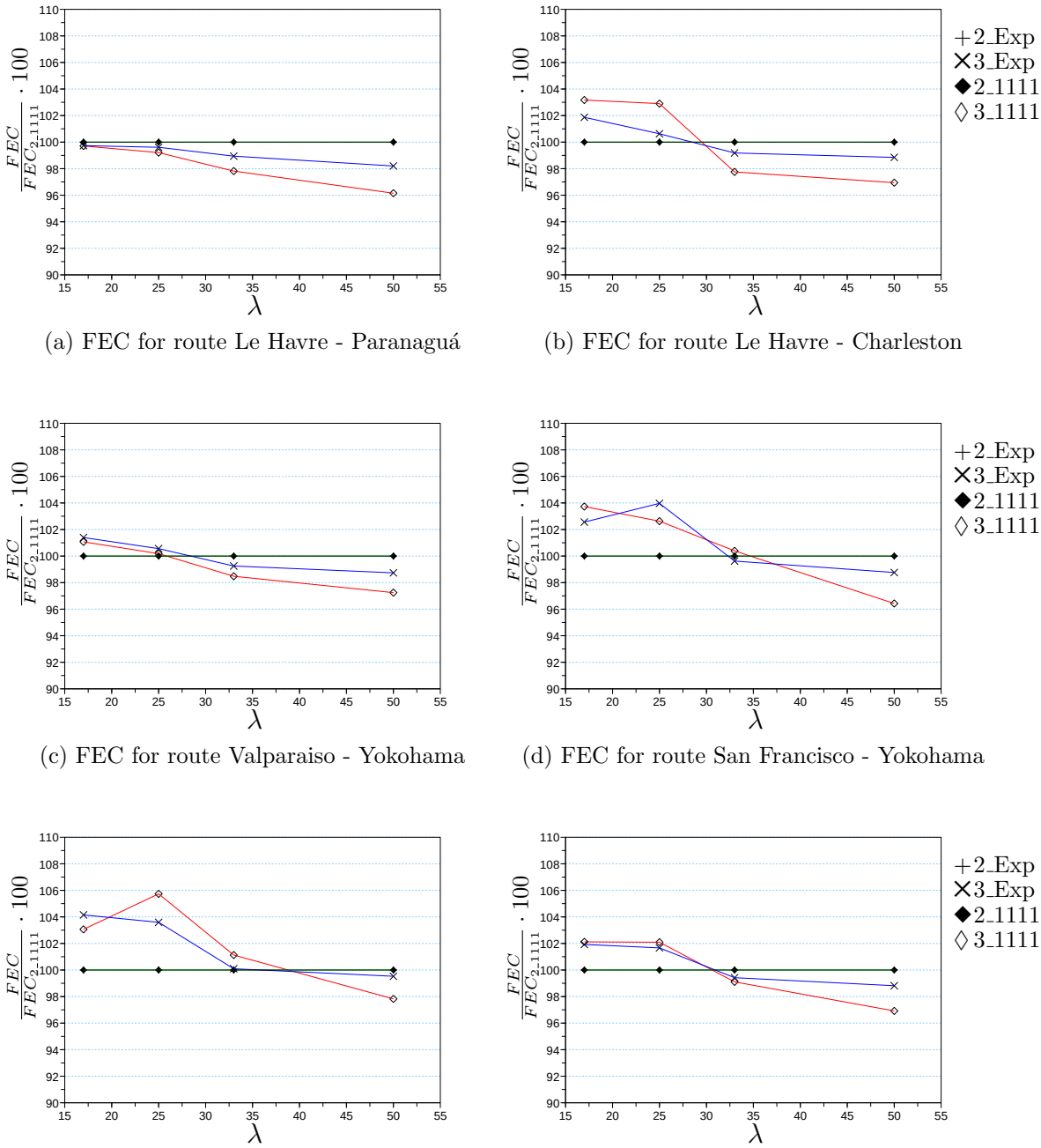

(a) FEC for route Le Havre - Paranaguá

(b) FEC for route Le Havre - Charleston

(c) FEC for route Valparaiso - Yokohama

(d) FEC for route San Francisco - Yokohama

(e) FEC for route Melbourne - Djibouti

(f) mean FEC of all routes

Figure 5.18.: Comparison of relative FEC of Mod. 2388 from operational simulations recalling experimental (2_Exp and 3_Exp) and numerical data (2_1111 and 3_1111) for all considered routes and mean values for all routes as function of the scaling factor λ. Note that values for (sub)variants 2388.2_Exp and 2388.2_1111 are used as reference and are constants (100%)

better than subvariant 2388.2_3223. For the mean of all routes, this difference is reduced to approx. 2%, due to the good performance of subvariant 2388.2_3223 in calm weather routes. When comparing results of the best subvariant (2388.2_3211) with variant 2388.3, differences become approx. 10% for the route Melbourne-Djibouti and 5% for the mean of all routes.

Considering that only a small design exploration has been performed here, it can be expected that greater improvements can be achieved by the application of an optimization strategy with a large number of designs.

5.5. Operational Simulations with Variable Speed and Variable Floating Condition

5.5.1. Simulation Setup

The simulations with variable speed and floating condition were made analogous to the description made in section 4.7. The main difference is the number of floating conditions calculated with potential CFD. For the present case, only three floating conditions for each velocity and subvariant were calculated. Results have been extensively described in section 5.2.2 and, as in the previous chapter, response surfaces (in this case response planes) were defined. Due to the small differences between the calculated and simulated floating conditions (defined in table 4.7), approximation errors due to the definition of the response planes are kept minimal.

5.5.2. Results

As in the previous chapter, since seakeeping data for off-design floating conditions was not included in the viscous CFD calculations, results for these floating conditions are obtained by means of corrections with help of strip theory calculations and offer therefore a higher uncertainty than results from simulations with fixed floating condition. Figures 5.20a to 5.20f show the relative fuel equivalent costs FEC for each route and subvariant as a function of ship size. The following tendencies can be observed:

- In contrast to the results from operational simulations with fixed floating condition, subvariant 2388.2_3223 has the worst performance, without exception, for all routes and all ship sizes. This is addressed by the high added resistance in waves and the poor calm water performance of this model.

- The opposite statement can be made for subvariant 2388.2_3211, showing for every route and ship size the best performance, without exception.

- In general terms, it can be observed, when compared to fixed floating condition results, that the influence of ship size in the performance ranking is significantly smaller. This can be also observed for the results in the previous chapter.

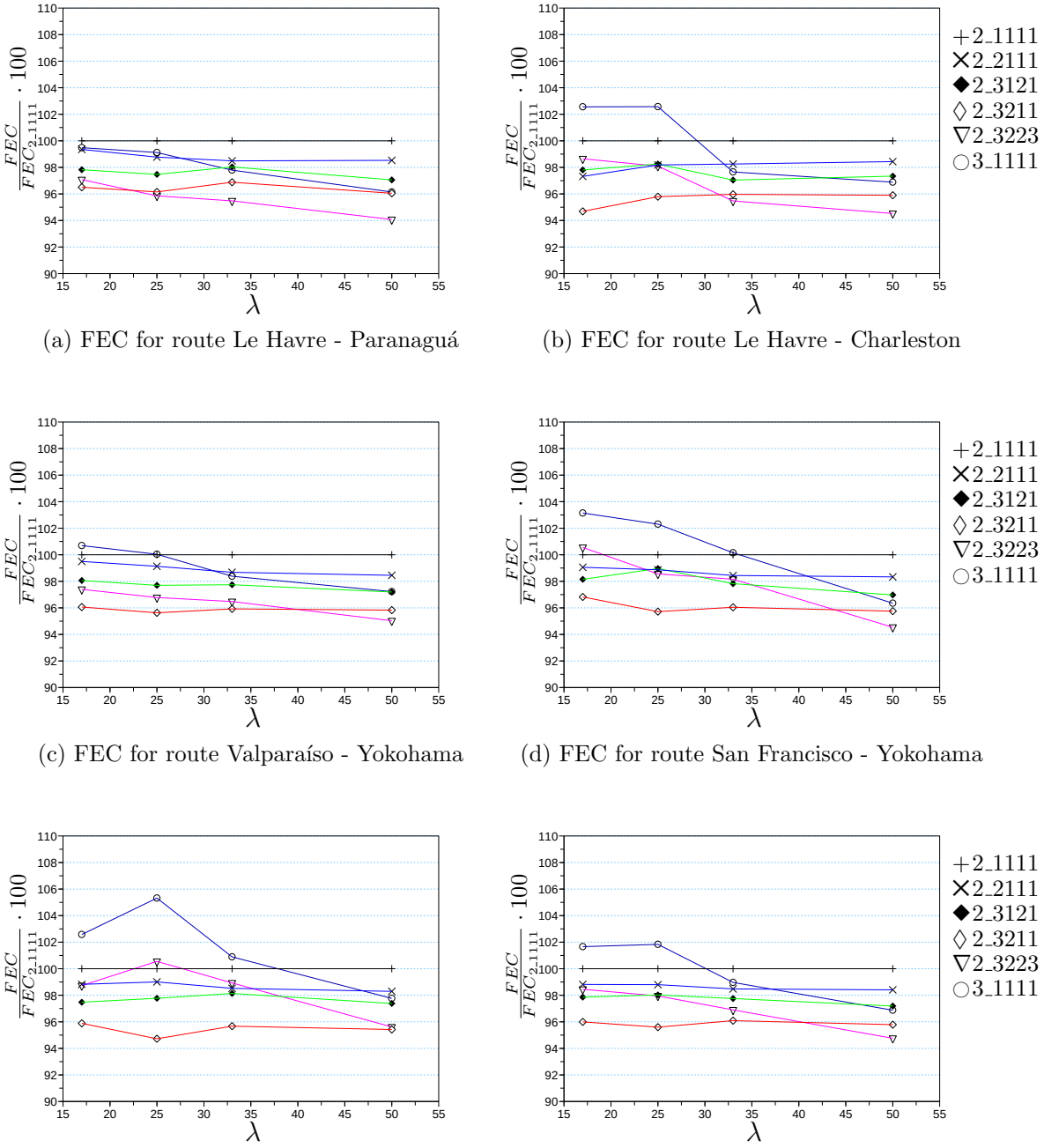

(a) FEC for route Le Havre - Paranaguá

(b) FEC for route Le Havre - Charleston

(c) FEC for route Valparaíso - Yokohama

(d) FEC for route San Francisco - Yokohama

(e) FEC for route Melbourne - Djibouti

(f) mean FEC of all routes

Figure 5.19.: Relative FEC of Mod. 2388 with different bulbous bows for all considered routes and mean relative FEC as function of the scaling factor λ from simulations with fixed floating condition

- The maximal FEC gain, when compared to the parent ship 2388.2, is found for the route between Melbourne and Djibouti for $\lambda = 25$ and is only of approx. 2.5%. For the same route and ship size, subvariant 2388.2_3223 shows approx. 7.5% higher fuel equivalent costs than the parent ship. When considering that this subvariant (2388.2_3223) presents the lowest calm water resistance at *design conditions* (design draft and design speed), a difference in performance of 10% is obtained between those subvariants. This would represent an economic loss of 10% of the Fuel Equivalent Costs when choosing the best configuration considering only the calm water performance at design conditions instead considering operational and weather aspects by means of an operational simulation. Even if this difference applies for a single example and a route with significant weather influence, it depicts clearly the evident disadvantage (or economic risk) of designing hull forms only for design conditions.

The presented operational simulations with variable speed and variable floating condition show the importance of considering off-design floating conditions, despite the drawback of unavailability of numerical seakeeping data for floating conditions other than design draft.

An evident change can be observed when comparing attained results to fixed floating condition simulations: the influence of the calm water resistance becomes higher, being the change in the rankings along ship size considerably less. This is shown by the evidently smaller number of "crossings" between the lines of FEC along the scaling factor λ. Where, for fixed floating condition simulations, a ship with a less pronounced bulbous bow was suitable for rather smaller ship sizes and a more pronounced one for larger sizes, variable floating condition simulations show a predominance of rather less pronounced bulbous bows as best configurations (lowest FEC) along all ship sizes studied. This recalls both the advantage of such a bulb in off-design floating conditions and its better seakeeping performance (i.e. lower added resistance in waves), at least in the form as it has been modeled here.

5.6. Conclusions about Application Case

The presented example case represents the general form of application of the proposed design methodology, integrating different numerical methods, a parametric geometry variation approach and operational simulations to improve the performance of a ship in an early design stage.

Different methods have been applied to model the operation of the ship. Unavoidably, some of these methods make assumptions of limited applicability. If these assumptions have also consequences in the relative rankings between different designs remains an open question. In this context, two aspects should be exposed:

- The consideration of a wide range of both floating conditions and velocities in the viscous CFD calculations in regular waves would have been of great advantage. Since this was not the case, and although this would increase the required computational

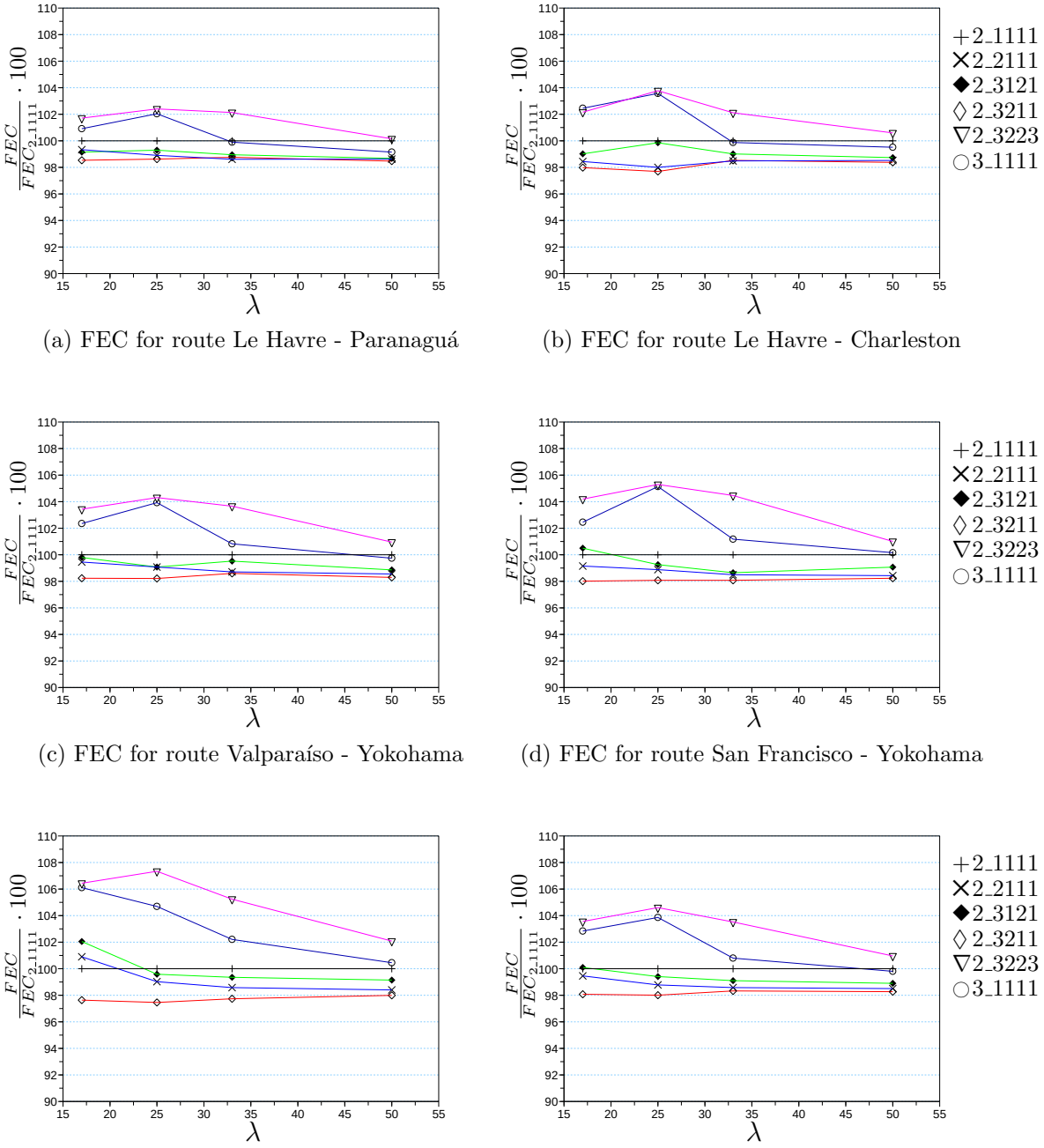

(a) FEC for route Le Havre - Paranaguá

(b) FEC for route Le Havre - Charleston

(c) FEC for route Valparaíso - Yokohama

(d) FEC for route San Francisco - Yokohama

(e) FEC for route Melbourne - Djibouti

(f) mean FEC of all routes

Figure 5.20.: Relative FEC of Mod. 2388 with different bulbous bows for all considered routes and mean relative FEC as function of the scaling factor λ from simulations with variable floating condition

resources considerably, this aspect and the influence of the assumption made shall be investigated in the future.

- The criterion for the slamming occurrence has been taken from the proposal by Ochi [89]. This methodology was defined for bulbless ships, and its applicability for ships with bulbous bows is clearly restricted. A deeper study of this aspect, e.g. by means of viscous CFD calculations without the need of any empirical criterion, would certainly bring more accurate predictions for this aspect.

Notwithstanding to this, the applicability of the presented design methodology has been demonstrated. Beginning with an extensive design exploration, the calm water resistance was evaluated by means of a potential CFD solver, leading to the choice of four designs for the evaluation of their seakeeping performances with a viscous CFD method. By means of two different operational simulation modes (fixed and variable floating condition), design variants with best performance were identified for each route and ship size considered.

For both simulation modes considered, subvariants 2388.2_3223 and 2388.2_3211 showed the best performance. Subvariant 2388.2_3223 achieved best performance in simulations with fixed floating condition, especially for calm weather routes and large ship sizes. This outcome can be expected, taking account of the advantageous calm water resistance of this subvariant. For rough weather routes and smaller ship sizes, and also for all simulations with variable floating condition, subvariant 2388.2_3211 showed the best performance. The bulbous bow of this subvariant is 30% larger than the baseline bow and part of its volume has been moved in forward direction (15% inner translation), remaining the vertical translation and the radial scaling unchanged. Within the bulbous bows considered in this design study, subvariant 2388.2_3211 can be placed, in both geometrical and hydrodynamic aspects, in the middle-field. The fact that this bulbous bow could be identified as the best configuration, shows the importance of including off-design conditions in early stages of ship design. In the same manner, this outcome points out the danger of designing and optimizing ships for a single condition (e.g. design speed, design draft and calm weather) leading, potentially, to designs of poor performance in waves and under off-design conditions.

If, for any reason, the consideration of weather aspects is not possible for the design of a bulbous bow, the choice of rather conservative bulbous bow sizes, with good performance in off-design speeds and off-design floating conditions, is recommended. Additionally, the consideration of the absolute size of the ship for the design of the bulbous bow is recommended, contrary to the common practice of considering scale-independent aspects only (such as Froude number and form coefficients).

6. Summary and Outlook

6.1. Summary

The presented study presents a design methodology considering the simulation of the operational life of the ship, including weather factors and off-design floating conditions. Different methods are integrated within a simulation environment to achieve this purpose, remarking the application of potential and viscous CFD methods for the evaluation of resistance and motions in waves.

Two different application cases were included in this investigation. In a first stage, operational simulations recalling existing experimental data were undertaken, discussing the applicability of the presented operational approach for design purposes. In a second stage, a general application case presents similar operational simulations, being all hydrodynamic characteristics recalled from numerical calculations. Of special interest are the ship responses and added resistance in waves, which are recalled from viscous CFD computations. For this application case, further designs were generated by a partially parametric approach and were included in the design study. Finally, the performance of each design for a given route and ship size was assessed and best configurations were identified.

The applied methods, especially those regarding hydrodynamic aspects, are well established and widely spread both in research and industry applications. Nevertheless, some of them have been applied in this investigation either in a novel form or in combination with other methods. In the case of viscous CFD methods, their application within a design study, intended to be applied in an early design stage, is new. The use of rather coarse meshes and simple setups emphasize the preliminary character of these computations in the design process. The combination of results from intensive CFD calculations with results from simple, computationally inexpensive methods such as strip theory, has been demonstrated. Although this has been already undertaken by other authors in the past, their use within operational simulations is new. Further studies in this issue shall be undertaken in the future.

The presented study demonstrates the practicability of an integrated approach for hydrodynamic ship (or specifically bulbous bow) design including resistance, responses in waves and off-design conditions in a single platform, considering realistic operational conditions and showing the possibility of identifying designs performing better under those conditions.

6.2. Outlook

The present study can be regarded as a further step towards the integration of all relevant methodologies involved in ship design, taking account of weather (especially seaway) and operational aspects for design evaluation.

Many aspects, which came to light during this investigation, brought also new questions with them. Due to the modular character of the simulation platform, further studies can be realized with a significantly reduced effort. An important prerequisite for this would be a more comprehensive validation of the simulation platform by studying a large number of existing ships under operation, where measured data can be compared with.

Detailed information about motions and forces in waves were available for head seas only. As a matter of fact, these are considered especially relevant for the added resistance in waves, but not necessarily critical for the security of the ship. Security-relevant situations (e.g. parametric rolling, wave-riding or reduction of stability), especially in following and quartering seas, with the subsequent voluntary speed loss, were not considered. Although it can be expected that the performance loss when including these aspects will not induce relevant *relative* differences between the studied variants and subvariants, this aspect shall be studied in the future.

Additional aspects, such as the inclusion of route optimization into the simulations is also a task showing the possibility of combining different approaches towards higher transport efficiency. Investigations related to this task are been undertaken at the moment by Balloch [10]. The consideration of security- or pollution-related tasks, combined with a more complex measure of merit able to include these aspects, can lead to a further step into the integration of all relevant aspects in ship design, being a potentially valuable contribution into concepts such as “holistic ship design” or “simulation-based ship design”.

The presented *general application case*, in all its simulation modes, has shown the practicability of the proposed method when recalling essential data alone from numerical methods. The inclusion of parametrically generated subvariants showed the ability of the methodology of helping the designer to identify economically convenient solutions along the design process. A higher automatization grade within all steps performed, together with a massive parallelization, can make this method a viable approach for practical applications in industry in the future.

Bibliography

[1] *Amazon Web Services (AWS) website.* `http://aws.amazon.com`. – last visited: may 2009

[2] *ECMWF ERA-40 data portal.* `http://data-portal.ecmwf.int/data/d/era40_daily`. – last visited: feb. 2010

[3] *HLRN Supercomputing Service.* `https://www.hlrn.de/home/view/Service`. – last visited: nov. 2009

[4] *IIHR - Hydroscience and Engineering website - experimental validation data.* `http://www.iihr.uiowa.edu/~shiphydro/efd.htm`. – last visited : 06.07.2010

[5] *International Marine Coatings - Hull Roughness Penalty Calculator.* `http://www.international-marine.com/newbuilding/brochures/HRPCFolder&Paper.pdf`. – last visited: feb 2007

[6] *OpenFOAM user manual.* `http://www.openfoam.com`. – last visited: jan. 2010

[7] *SciLab (Digiteo).* `http://www.scilab.org`. – last visited: 07.2008

[8] W.S. Atkins Consultants: MARNET-CFD - Best Practice Guidelines for Marine Applications of Computational Fluid Dynamics. 2003. – Tech. report

[9] Abt, C. ; Harries, S.: A New Approach to Integration of CAD and CFD for Naval Architects. In: *6th International Conference on Computer Applications and Information Technology in the Maritime Industries (COMPIT2007)*, 2007

[10] Balloch, M.: *Integration of Hydrodynamic Ship Design and Route Optimization using Long-Term Simulations: an Application Example for Different Bulbous Bow Variants*, Universitá di Genoa, MSc thesis, 2010

[11] Bertram, V.: Numerical Investigation of Steady Flow Effects in Three-Dimensional Seakeeping Computations. In: *22nd Symposium on Naval Hydrodynamics*, 2000

[12] Bertram, V. ; Thiart, G.: Fully 3-d ship seakeeping computations with a surge-corrected Rankine panel method. In: *Jour. of Marine Science and Technology* 3 (1998), no. 2, pp. 94–101

[13] Bertram, V. ; Veelo, B. ; Söding, H. ; Graf, K.: Development of a Freely Available Strip Method for Seakeeping. In: *COMPIT'06 (5th International Conference on Computer Applications and Information Technology in the Maritime Industries)*, 2006

[14] Bertram, V. ; Yasukawa, H.: Rankine source methods for seakeeping problems. In: *STG Jahrbuch* 90 (1996), pp. 411–425

[15] Bertram, V. ; Yasukawa, H.: Investigation of Global and Local Flow Details by a Fully Three-Dimensional Seakeeping Method. In: *23th Symposium on Naval Hydrodynamics*, 2001, pp. 355–367

[16] Blume, P.: Über die Effektivität von Bugwülsten unter Seebedingungen / HSVA. 1981 (1513). – Tech. report

[17] Blume, P. ; Kracht, A.: Prediction of the Behavior and Propulsive Performance of Ships with Bulbous Bow in Waves. In: *SNAME Transactions* 93 (1985), pp. 79–94

[18] Boese, P.: Eine einfache Methode zur Berechnung der Widerstanderhöhung eines Schiffes im Seegang. In: *Schiffstechnik* 17 (1970), no. 86, pp. 29–32

[19] Boulougouris, E. ; Papanikolaou, A.: Hullform Optimization of a High Speed Wave Piercing Monohull. In: *Ninth International Marine Design Conference (IMDC'06)*, 2006

[20] Buxton, I.: Fuel costs and their relationship with capital and operating costs. In: *Maritime Policy & Management* 12 (1985), Jan., no. 1, pp. 47–54

[21] Campana, E. ; Peri, D. ; Tahara, Y. ; Stern, F.: Shape optimization in ship hydrodynamics using computational fluid dynamics. In: *Computer methods in applied mechanics and engineering* 196 (2006), pp. 634–651

[22] Carrica, P. ; Wilson, R. ; Noack, R. ; Stern, F.: Ship motions unsing single-phase level set with dynamic overset grids. In: Elsevier (ed.): *Computers & Fluids* vol. 36, 2007, 1415-1433

[23] Carrica, P. ; Wilson, R. ; Stern, F.: Unsteady RANS simulation of the ship forward speed diffraction problem. In: *Computers & Fluids* 35 (2006), July, pp. 545–570

[24] Couwenberg, M.: *shipFoam contribution*. CFD-Online forum. `http://www.cfd-online.com/Forums/openfoam-solving/57774-hydrostatic-pressure-gravity-2.html`. – last visited: aug. 2008

[25] Cura Hochbaum, A. ; Pierzynski, M.: Flow Simulation for a Combatant in Head Waves. In: *Proceedings of the CFD Workshop Tokyo 2005*, 2005

[26] Cura Hochbaum, A. ; Vogt, M.: Numerische Simulation der Schiffsbewegungen in Wellen von vorme mit einem RANSE-Verfahren / HSVA-Report. 2002 (1648). – Tech. report

[27] Dallinga, R. P. ; Daalen, E.V. ; Grin, R. ; Willemstein, T.: Scenario Simulations in Design for Service. In: *Proceedings PRADS 2004*. Travemünde, Germany, 2004

[28] Dunlap, G. D. ; Shufeldt, H. H.: *Dutton's Navigation and Piloting*. Naval Institute Press, 1975

[29] Faltinsen, O. ; Minsaas, K. ; Liapis, N. ; Skjordal, S.: Prediction of Resistance and Propulsion of a Ship in a Seaway. In: *Proc. 13th. Symposium on Naval Hydrodynamics*. Tokyo, Japan, 1980, pp. 505–529

[30] Ferziger, J. H. ; Peric, M.: *Computational Methods for Fluid Dynamics*. Springer, 2002

[31] Geittner, M.: *Betriebssimulation von Frachtschiffen mit Windzusatzantrieb*, Technical University of Berlin, Design and Operation of maritime Systems, MSc thesis, 2007

[32] Gentaz, L. ; Guillerm, B. ; Alessandrini, B. ; Delhommeau, G.: Three-dimensional free surface viscous flow around a ship in forced motion. In: *Proceedings of the 7th International Conference on Numerical Ship Hydrodynamics*. Nantes, 1999

[33] Gerritsma, J. ; Beukelmann, W.: Analysis of the Resistance Increase in Waves of a Fast Cargo Ship. In: *International Shipbuilding Progress* 19 (1972), pp. 285–293

[34] Greitsch, L. ; Eljardt, G.: Simulation of Lifetime Operating Conditions as Input Parameters for CFD Calculations and Design Evaluation. In: *Numerical Towing Tank Symposium*. Cortona, 2009

[35] Greitsch, L. ; Eljardt, G. ; Krueger, S.: Operating Conditions Aligned Ship Design and Evaluation. In: *First International Symposium on Marine Propulsors*. Trondheim, Norway, 2009

[36] Grigoropoulos, G.J. ; Loukakis, T.A. ; Perakis, A.N.: Seakeeping Standard Series for Oblique Seas (a Synopsis). In: *Ocean Engineering* 27 (2000), pp. 111–126

[37] Grim, O.: Berechnung der durch Schwingungen eines Schiffskörpers erzeugten hydrodynamischen Kräfte. In: *STG Jahrbuch* 47 (1953), pp. 277–299

[38] Gui., L. ; Longo, L. ; Metcal, B. ; Shao, J. ; Stern, F.: Forces, Moment, and Wave Pattern for Surface Combatant in Regular Head Waves -Part 1: Measurement Systems and Uncertainty Analysis. In: *Experiments in Fluids* 31 (2001), no. 6, pp. 674–680

[39] Gui., L. ; Longo, L. ; Metcalf, B. ; Shao, J. ; Stern, F.: Forces, Moment, and Wave Pattern for Surface Combatant in Regular Head Waves-Part 2: Measurement Results and Discussions. In: *Experiments in Fluids* 32 (2002), no. 1, pp. 27–36

[40] Harries, S.: *Parametric design and hydrodynamic optimization of ship hull forms*, Technische Universität Berlin, PhD thesis, 1998. – ISBN: 3-933346-24-X

[41] Harries, S. ; Abt, C. ; Heimann, J. ; Hochkirch, K.: Advanced hydrodynamic design of container carriers for improved transport efficiency. In: *Design and Operation of Container Ships, RINA*, 2006

[42] Hermans, A. J.: Slowly moving hull forms in short waves. In: *Journal of Engineering Mathematics* 25 (1991), February, no. 1, pp. 63–75

[43] Hinnenthal, J.: *Robust Pareto - Optimum Routing of Ships utilizing Deterministic and Ensemble Weather Forecasts*, Technical University of Berlin, PhD thesis, 2007

[44] Hino, T. (ed.) ; NMRI Report 2005 (Veranst.): *Proceedings of the CFD Workshop Tokyo 2005.* 2005

[45] Hochkirch, K. ; Bertram, V.: Slow Steaming Bulbous Bow Optimization for a Large Containership. In: *COMPIT 2009*, 2009

[46] Hollenbach, U.: Estimating Resistance and Propulsion for Single-Screw and Twin-Screw Ships. In: *Schiffstechnik* 45 (1998), pp. 72–76

[47] Hollenbach, U. ; Friesch, J.: Efficient hull forms. What can be gained? In: *International Conference on Ship Efficiency*, 2007

[48] Hollenbach, U. ; Klug, H.: Optimising Hull Forms for Design- and "Off-Design"-Conditions. In: *STG-Sprechtag "Verbesserung der Propulsions- und Manövriereigenschaften von Schiffen"*. Emden, September 2008

[49] Holtrop, J.: A Statistical Re-Analysis of Resistance and Propulsion Data. In: *International Shipbuilding Progress* 353 (1984), pp. 272–276

[50] Holtrop, J. ; Mennen, G.: An Approximate Power Prediction Method. In: *International Shipbuilding Progress* 329 (1982), pp. 166–170

[51] Irvine, M. ; Longo, J. ; Stern, F.: Pitch and Heave Tests and Uncertainty Assessment for a Surface Combatant in Regular Head Waves. In: *Journal of Ship Research* 52 (2008), pp. 146–163

[52] ITTC: Report of the Seakeeping Commitee. 1978. – Tech. report

[53] ITTC: Report of the Resistance and Flow Commitee (20h ITTC). San Francisco, California, 1993. – Tech. report

[54] ITTC: Report of the Resistance and Flow Commitee (21h ITTC). Trondheim, Norway, 1996. – Tech. report

[55] ITTC: ITTC Recommended Procedures and Guidelines - ITTC 1978 Performance Prediction Method. 1999 (7.5-02-03-01.4). – Tech. report

[56] ITTC: Report of the Resistance Commitee (22h ITTC). Seoul and Shanghai, 1999. – Tech. report

[57] ITTC: Report of the Resistance Commitee (23h ITTC). Venice, Italy, 2002. – Tech. report

[58] Jasak, H.: OpenFOAM: Open source CFD in research and industry. In: *International Journal of Naval Architecture and Ocean Engineering* 1 (2009), no. 2, pp. 89–94

[59] Jensen, G.: *Berechnung der stationären Potentialströmung um ein Schiff unter Berücksichtigung der nichtlinearen Randbedingung an der freien Wasseroberfläche*, Technical University of Harburg-Hamburg, PhD thesis, 1988

[60] Jensen, G. ; Mi, Z.-X. ; SÃ¶ding, H.: Rankine Methods for the Solution of the Steady Wave Resistance Problem. In: *Sixteenth Symposium on Naval Hydrodynamics*, 1986

[61] Joosen, W.P.A.: Added Resistance of Ships in Waves. In: *6th Symp. on Naval Hydrodynamics*. Washington D.C., 1966, pp. 12

[62] Journee, J.M.J. ; Adegeest, L.J.M.: Theoretical Manual of StripTheory Program "SEAWAY for Windows" / TU Delft, Amarcon. 2003 (Rep. 1370). – Theoretical manual

[63] Kihara, H. ; Naito, S. ; Sueyoshi, M.: On the Practical Prediction of Added Resistance Using Nonlinear Slender Body Theory. In: *4th Osaka Colloquium on Seakeeping Performance of Ships*, 2000, pp. 115–129

[64] Kihara, H. ; Naito, S. ; Sueyoshi, M.: Numerical Analysis of the Influence of Above-Water Bow Form on Added Resistance using Nonlinear Slender Body Theory. In: *Journal of Ship Research* 49 (2005), pp. 191–206

[65] Kodama, Y. (ed.): *Proceedings of the CFD Workshop Tokyo 1994*. Japan, 1994

[66] Kracht, A.: Der Bugwulst als Entwurfselement im Schiffbau. In: *STG Jahrbuch* 70 (1976), pp. 139–159

[67] Kracht, A.: Weitere Untersuchungen über die Anwendung von Bugwülsten / VWS. 1979 ((811/78)). – Tech. report

[68] Kracht, A.: Einfluss des Bugwulstes auf den Leistungsbedarf eines Schiffes im Seegang / VWS. 1984 (988/84). – Tech. report

[69] Kracht, A.: Untersuchung des Einflusses teilgetauchter Bugwülste auf die erforderliche Antriebsleistung / VWS. 1984 (989/84). – Tech. report

[70] Kracht, A.: *Vorlesungsskript Schiffshydrodynamik I und II.* 2005. – Lessons material for ship hydrodynamics, held at TU Berlin

[71] Kring, D. ; Huang, Y.-F. ; Sclavounos, P. ; Vada, T. ; Braathen, A.: Nonlinear Ship Motions and Wave-Induced Loads by a Rankine Method. In: *Twenty-First Symposium on Naval Hydrodynamics*, 1997

[72] Larsson, L. ; Broberg, L. ; Kim, K.J. ; Zhang, D.H.: New Viscous and Inviscid CFD Techniques for Ship Flows. In: *Proc. 5th Int. Conf. on Numerical Ship Hydrodynamics*, 1990

[73] Larsson, L. (ed.) ; Stern, F. (ed.) ; Betram, V. (ed.): *Gothenburg 2000 - A Workshop on Numerical Ship Hydrodynamics.* Sweden, 2000

[74] Larsson, L. ; Stern, F. ; Betram, V.: Benchmarking of Computational Fluid Dynamics for Ship Flows: The Gothenburg 2000 Workshop. In: *Journal of Ship Research* 47 (2003), pp. 63–81

[75] Lewis, E. (ed.): *Principles of Naval Architecture.* vol. 3. SNAME, 1989

[76] Lewis, F.M.: The inertia of the water surrounding a vibrating ship. In: *SNAME Transactions* 37 (1929), pp. 1–20

[77] Luquet, R. ; Ducrozet, G. ; Gentaz, L. ; Ferrant, P. ; Alessandrini, B.: Applications of the SWENSE Method to seakeeping simulations in irregular waves. In: *9th International Conference in Numerical ShipHydrodynamics*, 2007

[78] MAN B&W (ed.): *Ship Propulsion - Basic Principles of Ship Propulsion (MAN B&W).* MAN B&W, 2006. `http://www.manbw.com`

[79] MAN B&W (ed.): *MAN B&W Marine Engine Programme 2007.* MAN B&W, 2007. `http://www.manbw.com`

[80] Maruo, H.: The Excess Resistance of a Ship in Rough Seas. In: *International Shipbuilding Progress* 4 (1957), no. 35, pp. 337–345

[81] Matsumoto, K. ; Naito, S. ; Takagi, K. ; Hirota, K. ; Takagishi, K.: Beak-Bow to Reduce the Wave Added Resistance at Sea. In: *PRADS'98, Practical Design of Ships and Mobile Units*, 1998

[82] Minoura, M. ; Naito, S.: Stochastic Sea Climate Simulation Based on Hindcast Data. In: *Proc. ISOPE* vol. III. San Francisco, California, 2006, pp. 94–101

[83] Naito, S.: Propulsive Performence of Ships in Actual Seas. In: *7th Osaka Colloquium on Seakeeping and Stability*, 2008

[84] Nakos, D. ; Kring, DF. ; Sclavounos, P.: Rankine panel methods for time-domain free surface ows. In: *Proceedings of the Sixth International Conference on Numerical Ship Hydrodynamics*, 1994

[85] Nowacki, H.: *Economic and technical issues in hull form development.* 1985. – Lessons material for ship theory, held at TU Berlin

[86] Nowacki, H.: Developments in Marine Design Methodology: Roots, Results and Future Trends. In: Erikstad, S. O. (ed.): *10th International Marine Design Conference (IMDC 2009)* vol. 1. Trondheim, Norway : Tapir Academic Press, 2009, pp. 47–80

[87] Nowacki, H. ; Holbach, G. ; Papanikolaou, A. ; Zaraphonitis, G.: Concept and Hydrodynamic Design of a High-Speed SWATH Passenger/Car Ferry for the Mediterranean Sea. In: *Jahrbuch der Schiffbautechnischen Gesellschaft* 84 (1990), pp. 171–181

[88] Ochi, M.: Wave Statistics for the Design of Ships and Ocean Structures. In: *SNAME Transactions* 86 (1978), pp. 47–76

[89] Ochi, M. K.: Prediction of Occurrence and Severity of Ship Slamming at Sea. In: *Proceedings of 5th Symposium on Naval Hydrodynamics.* Bergen, Norway, 1964, pp. 545–596

[90] Ogilvie, T.: Recent Progress Towards the Understanding and Prediction of Ship Motions. In: *Proc. of the 6th Symposium on Naval Hydrodynamics*, 1964

[91] Olivieri, A. ; Pistani, F. ; Avanzini, A. ; Stern, F. ; Penna, R.: Towing Tank Experiments of Resistance, Sinkage and Trim, Boundary Layer, Wake, and Free Surface Flow Around a Naval Combatant INSEAN 2340 Model / Iowa Institute of Hydraulic Research, The University of Iowa. 2001 (421). – Tech. report

[92] Orihara, H. ; Miyata, H.: Evaluation of added resistance in regular incident waves by computational fluid dynamics motion simulation using an overlapping grid system. In: *Journal of Marine Science and Technology* 8 (2003), pp. 47–60

[93] Oschmann, P.: *Betriebssimulation innovativer und konventioneller Hauptmaschinenkonzepte: ein Vergleich für unterschiedliche Szenarien und Schiffstypen*, Technical University of Berlin, Design and Operation of maritime Systems, MSc thesis, 2009

[94] Papanikolaou, A.: *Added Resistance in Waves.* – Presentation held at TU Berlin, May 2010 (unpublished)

[95] Papanikolaou, A.: On integral-equation-methods for the evaluation of motions and loads of arbitrary bodies in waves. In: *Journ. Ingenieur-Archiv* 55 (1985), pp. 17–29

[96] Pedersen, B. P.: *A Comparative Study of Methods for Predicting Added Resistance in Waves*, Technical University of Denmark, MSc thesis, 2006

[97] Raven, H.C.: *A Solution Method for the Nonlinear Ship Wave Resistance Problem*, Delft Univ. Techn., PhD thesis, 1996

[98] Sakamoto, T. ; Baba, E.: Minimization of Resistance of Slowly Moving Full Hull Forms in Short Waves. In: *Proceedings of the 16th Symposium on Naval Hydrodynamics*. Berkeley, USA, 1986, pp. 598–612

[99] Salvesen, N.: Added Resistance of Ships in Waves. In: *Journal of Hydronautics* 12 (1978), no. 1, pp. 24–34

[100] Sato, Y. ; Miyata, H. ; Sato, T.: CFD simulation of 3-dimensional motion of a ship in waves: application to an advancing ship in regular heading waves. In: *Jour. of Marine Science and Technology* 4 (1999), pp. 108–116

[101] Schmode, D. ; Bertram, V. ; Tenzer, M.: Simulating Ship Motions and Loads using OpenFOAM. In: *STG Conference "CFD in Ship-Design"*. Hamburg, 25. sept. 2009. – unpublished

[102] Schneekluth, H.: Kriterien zur Bugwulstverwendung. In: *STG Jahrbuch* 69 (1975), pp. 1–1

[103] Sclavounos, P.D. ; Nakos, Y. D.E.and H. D.E.and Huang: Seakeeping and Wave Induced Loads on Ships with Flare by a Rankine Panel Method. In: *Proceedings of the Sixth International Conference on Numerical Ship Hydrodynamics*, 1994

[104] Söding, H.: Bewegungen und Belastungen der Schiffe im Seegang / Technical University of Hamburg-Harburg. 1982. – course material

[105] Söding, H.: A Method for Accurate Force Calculations in Potential Flow. In: *Ship Technical Research* 40 (1993), no. 4, pp. 176–186

[106] Söding, H. ; Bertram, V.: Schiffe im Seegang. In: *Handbuch der Werften* XXIV (1998), pp. 151–189

[107] St. Denis, M. ; Pierson, W.J.: On the Motion of Ships in Confused Seas. In: *SNAME Transactions* 61 (1953), pp. 280–357

[108] Tampier, G.: *SimOship - General Description and Usage*. TU Berlin, 2008. – User Manual

[109] Tampier, G. ; Clauss, G. ; Siekmann, H.: Betriebssimulation von Frachtschiffen mit Windzusatzantrieb. In: *Jahrbuch der Schiffbautechnischen Gesellschaft* 101 (2008), pp. 320–335. – ISBN: 978-3-8167-7798-4

[110] Weymouth, G. ; Wilson, R. ; Stern, F.: RANS Computational Fluid Dynamics Predictions of Pitch and Heave Ship Motions in Head Seas. In: *Journal of Ship Research* 49 (2005), no. 2, pp. 80–97

[111] Wilson, R. ; Paterson, E. ; Stern, F.: Unsteady RANS CFD Method for Naval Combatants in Waves. In: *22nd Symposium on Naval Hydrodynamics*, 1998, 532-549

[112] Xing-Kaeding, Y.: *Unified Approach to Ship Seakeeping and Maneuvering by a RANSE Method*, Technische Universität Hamburg-Harburg, PhD thesis, 2006

[113] Zaraphonitis, G. ; Papanikolaou, A. ; Mourkoyannis, D.: Hull-Form Optimization of High Speed Vessels with Respect to Wash and Powering. In: *Eighth International Marine Design Conference (IMDC'03)*. Athens, 2003

Index

Appendix

A. Mesh Generation with snappyHexMesh

A.1. General Aspects

The OpenFOAM meshing utility `snappyHexMesh` generates grids starting from an initial, so-called *background mesh* (e.g. a block structured, Cartesian mesh) and a definition of the geometry in `.stl`-format. In a first step, the utility maps the surface and conforms the mesh to it by an iterative process of refining the mesh and adjusting point positions to match the surface contained in the `stl`-file. In a further step, a boundary layer of cells can be inserted by moving the generated mesh back. A sample of these steps for a simple geometry is shown in fig. A.1. At a first look, clear advantages due to its non-interactive

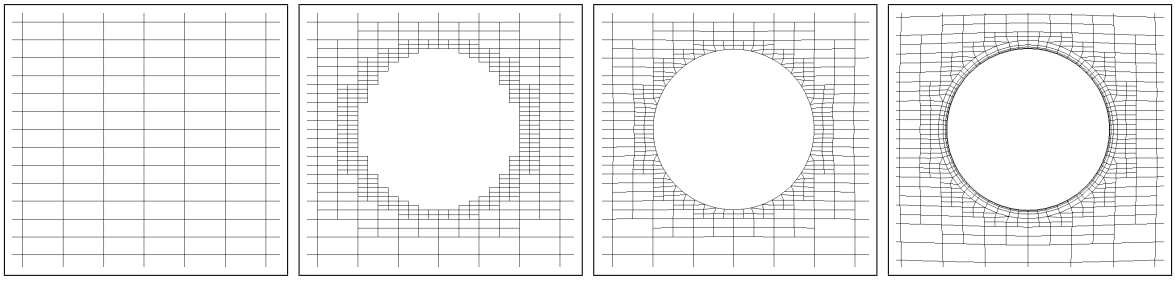

(a) Background grid (b) Refinement, removal (c) Mapping (d) Added Layers

Figure A.1.: `snappyHexMesh` steps of mesh generation

approach, compared to manual mesh generation, are evident, and it suggests an almost ideal suitability for its use within automatized generation of large amounts of variants, even if topological changes are necessary. Notwithstanding these advantages, it must be recalled that this tool is by far not fully developed and different problems appear. While some of these problems can be solved very easily, there are certain ones which cannot be solved at all yet. Some of these aspects will be briefly discussed and solutions for some of the problems will be shown.

The mesh generation for viscous CFD calculations of a ship in regular waves must be done very carefully and several aspects must be considered when doing this with the `snappyHexMesh` utility. First, it must be considered that `snappyHexMesh` starts from a background mesh. This mesh is normally created with the `blockMesh` utility and, for a typical ship hydrodynamics case, it is a rectangular box. In this case, the orientation, grading, fineness and aspect ratio of the cells of the background mesh play an important role in final mesh quality.

From the example in figures A.2 and A.3, different mesh quality improvement methods will be described. In these figures, the typical steps within the creation of such a mesh is shown for a cube. Figures A.2a and A.3a show the background mesh. The only difference between both figures is that in the latter, the background mesh was rotated in 30°.

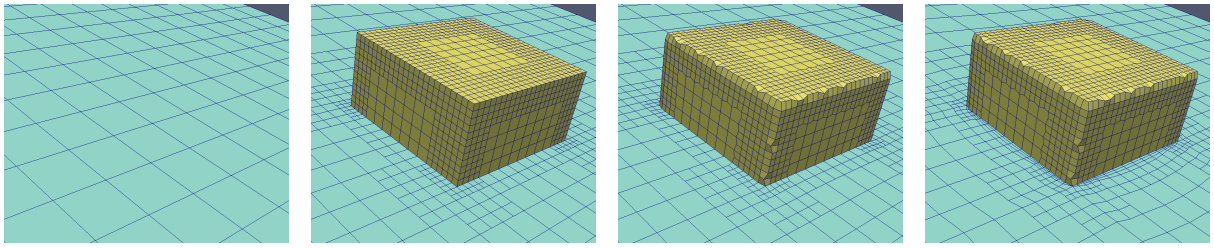

(a) Background grid (b) Refinement, removal (c) Mapping (d) Added Layers

Figure A.2.: Mesh generation for a cube. Note the unsharp edges after mapping despite of good pre-mapping edge

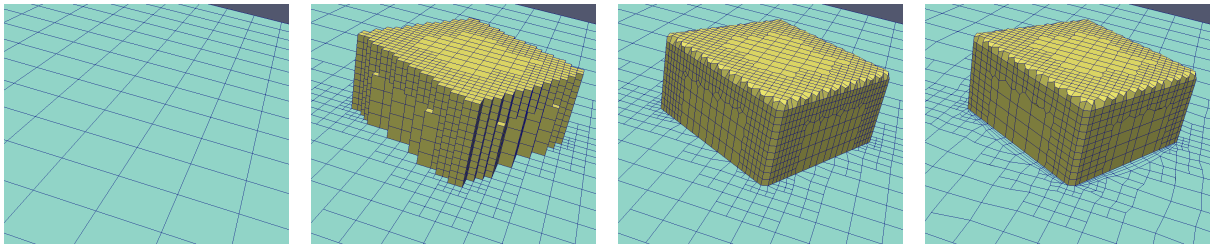

(a) Background grid (b) Refinement, removal (c) Mapping (d) Added Layers

Figure A.3.: Mesh generation for a cube not orthogonal to the background mesh. The edge quality gets even worse

Edges

The detection of edges is not implemented in the utility and it shall be its most important deficiency. This leads to massive quality losses in edges and makes the tool not suitable for many industrial applications. Fortunately, sharp edges in a typical ship are only present at the deck line and at the transom. For the deck line the problem is evidently not relevant, while for the transom only refinement can help to improve, at least partially, the transom edge. Even for the example case in figure A.2, where the cube to be meshed matches the cells exactly and, theoretically, no mapping would be necessary, the edges are mapped erroneously (compare figs. A.2b and A.2c). In detail, and compared to the mapped mesh in fig. A.3c, a small difference can be observed in the edge quality. Thus, orthogonality between the background mesh and the object to be meshed is recommended, when possible.

First Cell Layer After Mapping

Observing fig. A.3c in detail, a first layer containing half-hexaedral elements (wedges) can be observed. When possible, orthogonality between the geometry and the background geometry shall be attempted to avoid the presence of such cells. For complex geometries, this is not a trivial process and improvements can be only achieved with more complex, geometry-adapted background meshes. Further investigations shall be undertaken in this task.

Refinement and Boundary Layer Cells

Within `snappyHexMesh`, refinement regions can be declared. These can be linked to a surface (from the `.stl` file) or to a box-shaped region. A refinement level declares the refinement of a single cell in **all** directions, resulting into eight new cells. This addresses a new problem, since in many cases refinement in only one or two directions is needed, resulting into large amounts of cells and a subsequent reduction of the time step. This problem can be eliminated by the creation of an already refined background mesh or a directional refinement after the execution of `snappyHexMesh`.

For a selected surface, a cell layer of hexaedral elements parallel to the surface can be created. This is usually very convenient for boundary layer flows, diminishing the numerical quality loss of the results. An important problem can be observed here and no solution is yet present: when the layer is added, sharp edges and surface bounds are not extruded, resulting a zero thickness at these edges. This can be clearly observed in figures A.2d and A.3d.

Another problem in the boundary cell layer arises from the declaration of refinement levels and can be observed in both figs. A.2d and A.3d. Since a minimal and a maximal value for the refinement is given, the utility applies the most convenient refinement level (within max. and min.) depending of the achieved mesh quality. In the example case, a higher refinement near the edges can be observed. This leads to non-uniform boundary layer cells, which is usually not desired. Although theoretically convenient, the

feature must be switched off by entering the same value for the minimal and the maximal refinement level.

Mapping High Aspect Ratio Cells

For a typical ship mesh, high aspect ratio cells are for some regions convenient. This is usually the case for coarse meshes, where, in an attempt of saving both cells and time step size, a low number of cells in longitudinal direction is desired while keeping a good resolution in vertical direction to obtain a good definition of the free surface. This results in high aspect ratios and long, flat cells. This circumstance showed to be problematic for the `snappyexMesh` utility, and it seems to deliver optimum results only for aspect ratios near to one (cubes). This problem is solved easily by scaling the mesh down in the desired direction and rescaling it back after the execution of snappyHexMesh. An example of this is shown in figure A.4

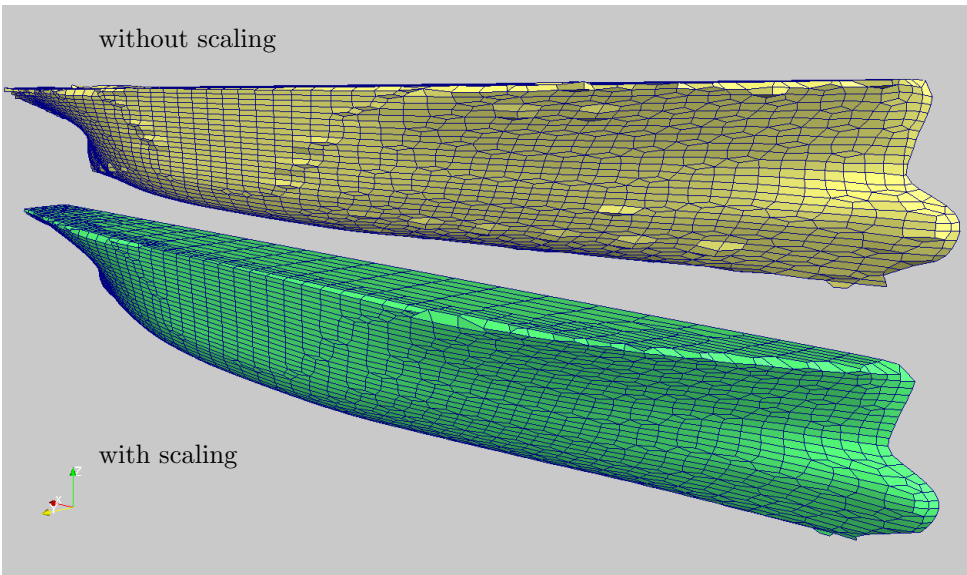

Figure A.4.: Mesh example with and without scaling during the execution of `snappyHexMesh`

A.2. Mesh Generation for Application Case

Applying all principles described in the previous section, the mesh generation took place in several steps. For convenience, two regions, one near the ship geometry (called *ship box*) and another for the rest of the domain (called *outer box)* were generated separately and stitched afterwards together. This has several advantages:

- savings in computational resources and increase maximum number of cells meshed for a given RAM memory

- time savings for large amounts of meshes for different subvariants, since the outer box remains unchanged
- independent refinement of regions. An example is the transom region near the free surface: since this region had to be refined additionally by `snappyHexMesh`, additional directional refinement would be highly inconvenient.

The complete meshing process comprises thus following steps:

- Shipbox and scaling of `.stl`-file
- `snappyHexMesh` in scaled box
- rescaling
- Generation of outer box
- stitch both boxes (trick - stackable boxes!)
- refinement in vertical and longitudinal dir for wave orbits
- additional vertical refinement at the free surface

These steps are shown for the presented application case in figures A.5, A.6 and A.7.

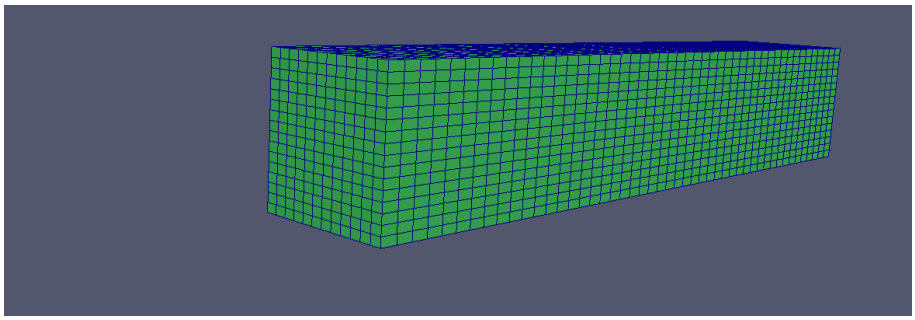

(a) Down-scaled background grid

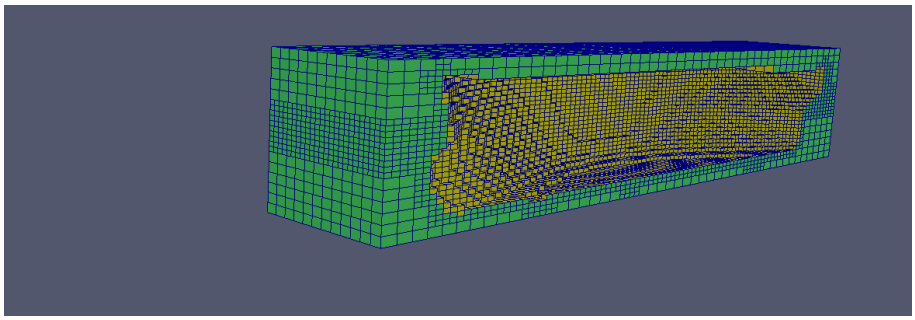

(b) Refinement and removal of cells

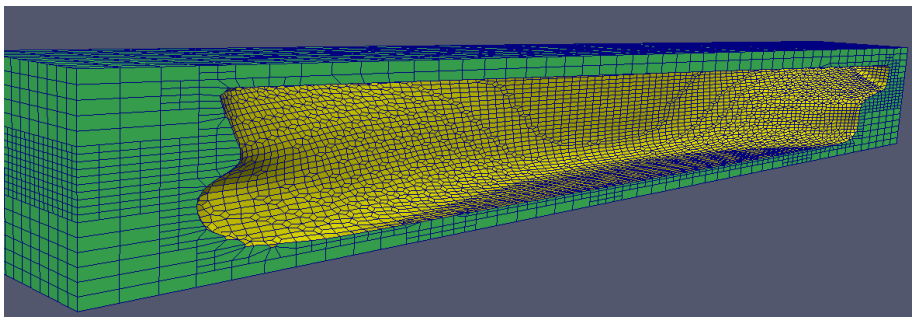

(c) Rescaled mesh after mapping

Figure A.5.: Meshing of the ship box

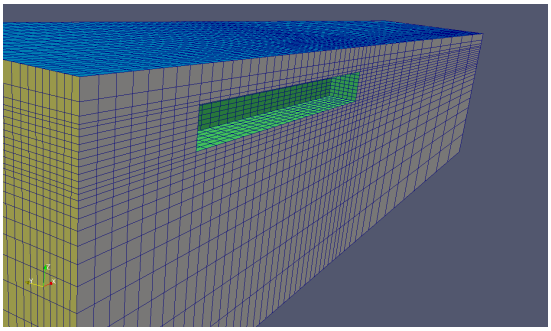

(a) Empty outer box

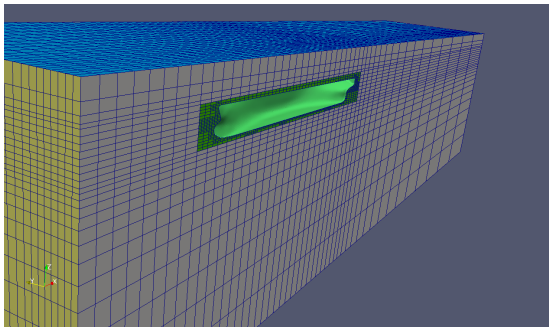

(b) Inserted ship box

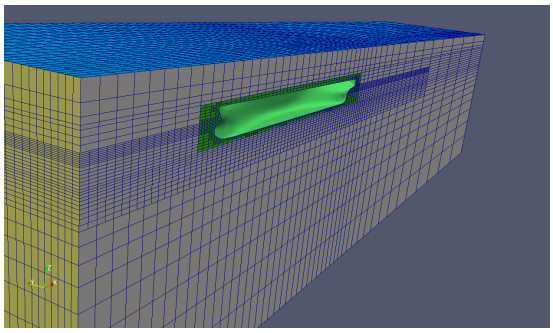

(c) Directional refinement near the free surface

Figure A.6.: Meshing of the outer box and stitching both meshes

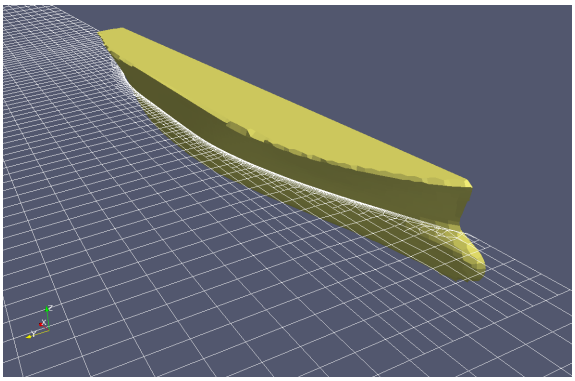

(a) 100k cells

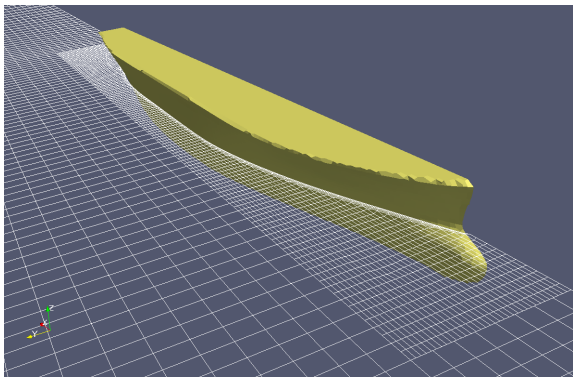

(b) 200k cells

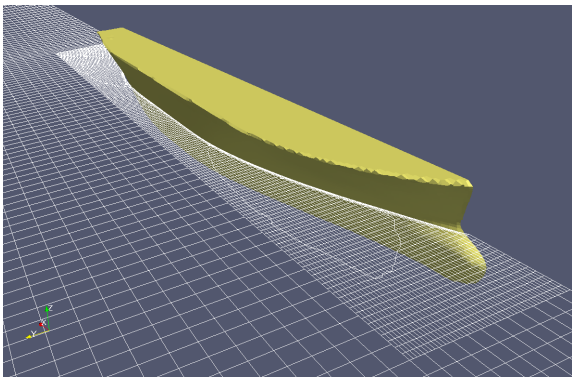

(c) 400k cells

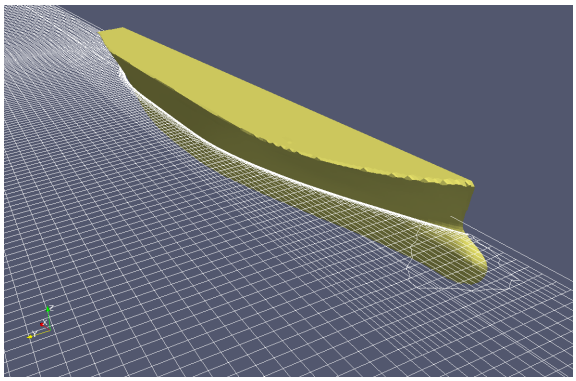

(d) 800k cells

Figure A.7.: Meshes with different refinement levels

B. Wave Resistance for Different Floating Conditions and Speeds: Definition of Response Surfaces

F_n	$i(T_{AP})$	$j(T_{FP})$	$10^3 \cdot C_W$		
			2388.0	2388.2	2388.3
0.200	2	2	0.777	0.272	0.385
	2	3	0.699	0.275	0.561
	3	3	1.017	0.665	0.890
	3	4	1.103	0.588	0.862
	4	2	1.345	0.767	0.862
	4	4	1.165	0.801	0.862
	4	6	1.106	0.596	0.908
	6	6	0.984	0.558	0.924
0.225	2	2	1.056	0.513	0.383
	2	3	0.935	0.320	0.480
	3	3	1.201	0.585	0.735
	3	4	1.174	0.562	0.896
	4	2	1.497	0.878	0.830
	4	4	1.411	0.588	0.734
	4	6	1.283	0.786	1.050
	6	6	1.163	0.755	0.898
0.250	2	2	1.227	0.825	0.620
	2	3	1.363	0.821	0.905
	2	4	4.204	0.496	0.838
	3	3	1.382	0.810	0.894
	3	4	1.326	0.814	0.917
	3	6	1.123	0.720	1.055
	4	2	1.709	1.207	1.106
	4	4	1.616	0.831	0.906
	4	6	1.102	1.077	1.364
	6	6	1.331	1.009	1.310

Table B.1.: Wave resistance coefficients calculated with FS-Flow for variants 2388.0, 2388.2 and 2388.3

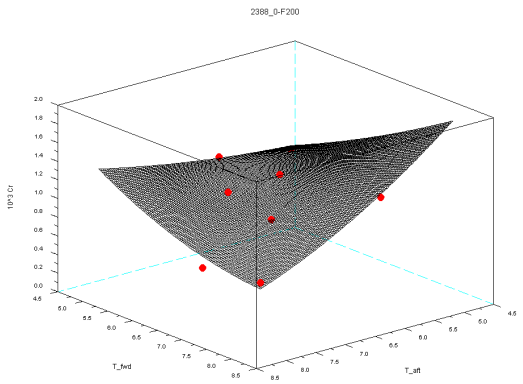

(a) 2388.0 at $F_n = 0.200$

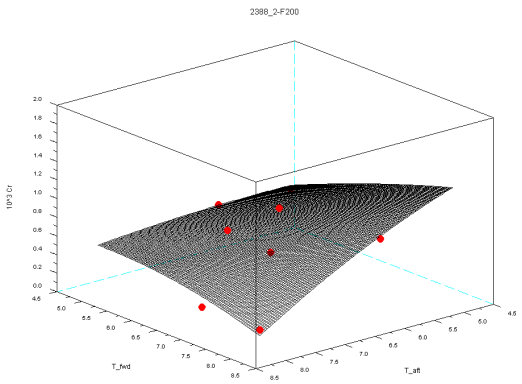

(b) 2388.2 at $F_n = 0.200$

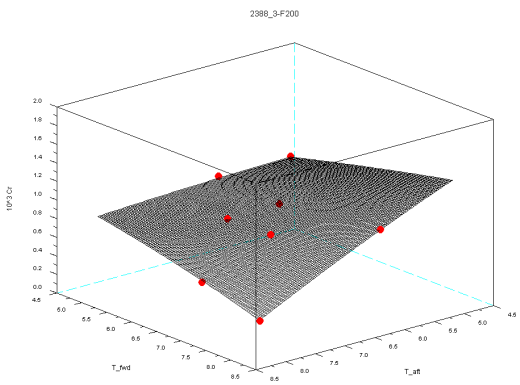

(c) 2388.3 at $F_n = 0.200$

$c_W(F_n, T_{AP}, T_{FP}) = \sum c \cdot T_{AP}^i \cdot T_{FP}^j$					
			c		
F_n	i	j	2388.0	2388.2	2388.3
0.200	0	0	-5.3923E-03	-1.6563E-03	-1.2756E-03
	0	1	1.3526E-03	3.9836E-04	4.4064E-04
	1	0	1.1609E-03	1.7580E-04	2.8776E-04
	1	1	-2.6194E-04	-1.2190E-05	-5.3196E-05
	2	2	6.8229E-07	-4.5764E-07	-1.6972E-07

Figure B.1.: Polynomial response surfaces and coefficients for the wave resistance coefficient c_W for variants 2388.0, 2388.2 and 2388.3 for $F_n = 0.200$

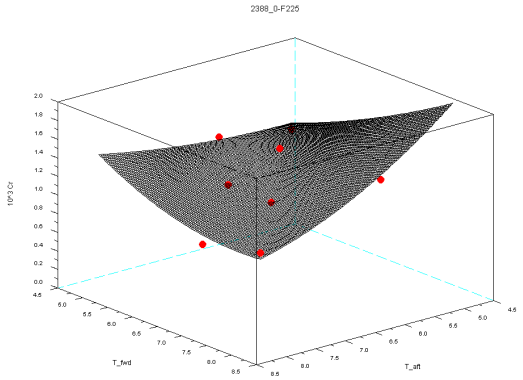

(a) 2388.0 at $F_n = 0.225$

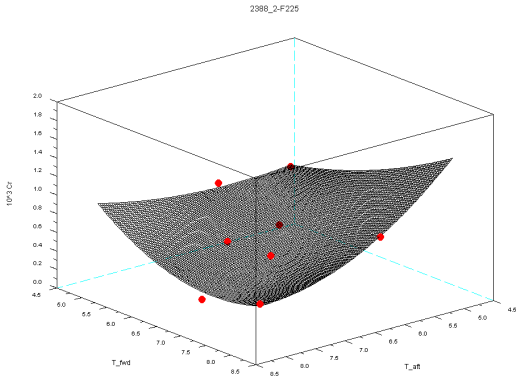

(b) 2388.2 at $F_n = 0.225$

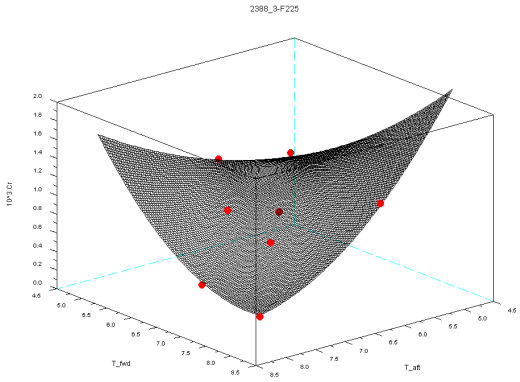

(c) 2388.3 at $F_n = 0.225$

$c_W(F_n, T_{AP}, T_{FP}) = \sum c \cdot {T_{AP}}^i \cdot {T_{FP}}^j$					
			c		
F_n	i	j	2388.0	2388.2	2388.3
0.225	0	0	-4.8254E-03	-5.5224E-03	-1.1679E-02
	0	1	1.3451E-03	1.5355E-03	2.7324E-03
	1	0	1.1426E-03	1.3524E-03	2.5499E-03
	1	1	-2.7677E-04	-3.6272E-04	-6.0520E-04
	2	2	8.8908E-07	1.4896E-06	2.0899E-06

Figure B.2.: Polynomial response surfaces and coefficients for the wave resistance coefficient c_W for variants 2388.0, 2388.2 and 2388.3 for $F_n = 0.225$

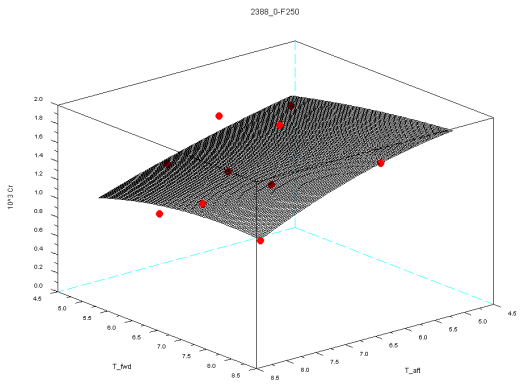

(a) 2388.0 at $F_n = 0.250$

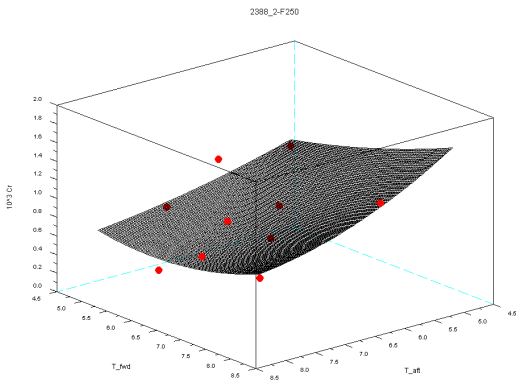

(b) 2388.2 at $F_n = 0.250$

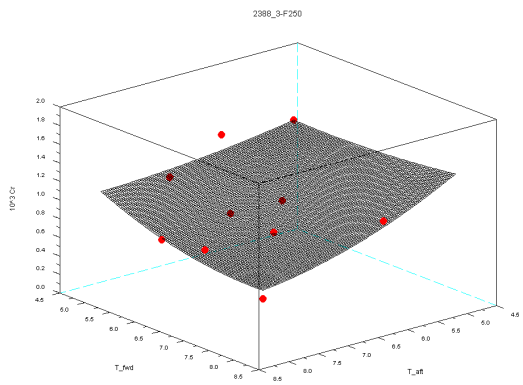

(c) 2388.3 at $F_n = 0.250$

$c_W(F_n, T_{AP}, T_{FP}) = \sum c \cdot T_{AP}^i \cdot T_{FP}^j$					
			c		
F_n	i	j	2388.0	2388.2	2388.3
0.250	0	0	2.5771E-03	-1.2578E-03	-5.9903E-04
	0	1	-1.4904E-04	7.5844E-04	5.7989E-04
	1	0	-4.0316E-04	4.5406E-04	4.8872E-04
	1	1	8.2847E-05	-1.6888E-04	-1.5402E-04
	2	2	-5.3199E-07	7.8641E-07	6.4139E-07

Figure B.3.: Polynomial response surfaces and coefficients for the wave resistance coefficient c_W for variants 2388.0, 2388.2 and 2388.3 for $F_n = 0.250$

C. Systematic Variation of Bulbous Bow for Potential CFD Calculations: Additional Tables and Figures

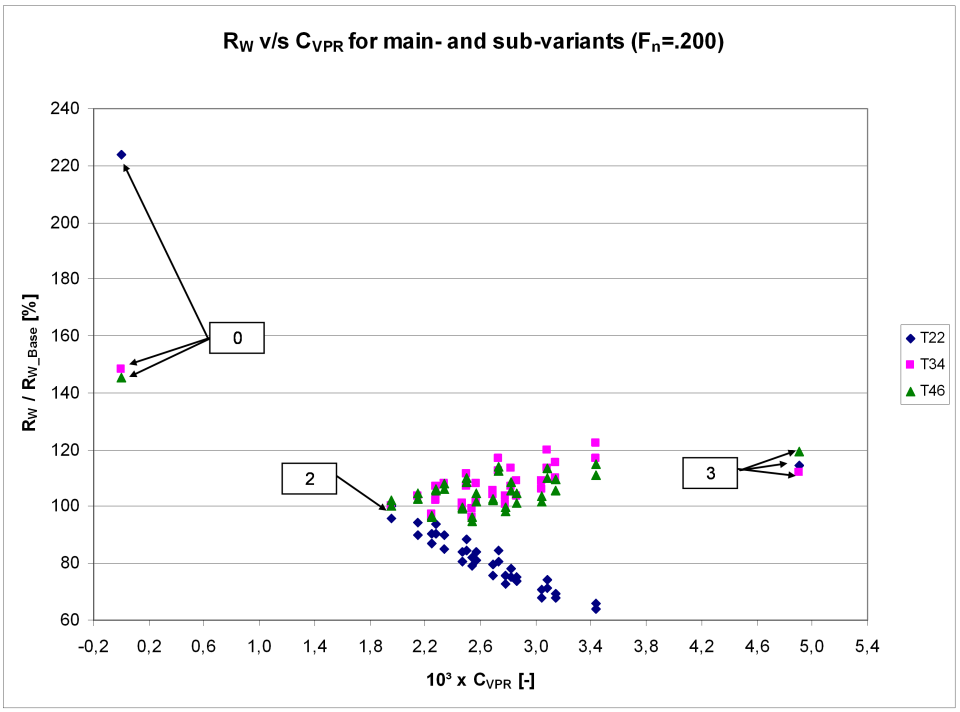

Figure C.1.: Wave resistance (as percentage of baseline) over bulb volume parameter $C_{\nabla PR}$ at $F_n = 0.200$ for main- and subvariants

$F_n = 0.200$				$C_{\nabla PR}$	C_{LPR}	C_{ABT}	$L^3_{PR}/$	$R_W/R_{W-1111} \cdot 100$		
i(δx_{tt})	j(δx_{ti})	k(δz_{tt})	l(S_r)	$\cdot 10^3$	$\cdot 10^2$	$\cdot 10^2$	∇_{PR}	T_{22}	T_{34}	T_{46}
1	1	1	1	1.96	2.68	7.78	1.692	100.0	100.0	100.0
1	1	1	2	2.14	2.68	8.57	1.545	94.2	103.5	102.7
1	1	1	3	2.34	2.68	9.41	1.416	89.7	107.8	105.9
1	1	2	1	1.96	2.68	7.78	1.692	95.7	100.3	102.2
1	1	2	2	2.14	2.68	8.57	1.545	89.7	103.8	104.9
1	1	2	3	2.34	2.68	9.41	1.416	84.9	107.9	108.0
1	2	1	1	2.28	2.68	7.78	1.454	93.9	102.2	106.3
1	2	1	2	2.50	2.68	8.57	1.324	88.4	107.0	109.9
1	2	1	3	2.73	2.68	9.41	1.212	84.7	112.7	114.0
1	2	2	1	2.28	2.68	7.78	1.454	90.2	106.9	105.4
1	2	2	2	2.50	2.68	8.57	1.324	84.5	111.6	108.7
1	2	2	3	2.73	2.68	9.41	1.212	80.4	117.0	112.5
2	1	1	1	2.25	3.09	7.78	2.238	90.5	95.8	96.2
2	1	1	2	2.46	3.09	8.57	2.043	84.3	99.6	99.0
2	1	1	3	2.69	3.09	9.41	1.872	79.6	104.0	102.4
2	1	2	1	2.25	3.09	7.78	2.238	86.7	97.5	97.0
2	1	2	2	2.46	3.09	8.57	2.043	80.4	101.2	99.5
2	1	2	3	2.69	3.09	9.41	1.872	75.5	105.7	102.7
2	2	1	1	2.57	3.09	7.78	1.959	83.8	101.7	104.6
2	2	1	2	2.82	3.09	8.57	1.785	78.1	107.2	108.8
2	2	1	3	3.08	3.09	9.41	1.633	74.3	113.6	113.7
2	2	2	1	2.57	3.09	7.78	1.959	81.3	107.9	101.8
2	2	2	2	2.82	3.09	8.57	1.785	75.4	113.4	105.5
2	2	2	3	3.08	3.09	9.41	1.633	71.3	119.8	110.0
3	1	1	1	2.54	3.49	7.78	2.860	82.0	96.2	96.4
3	1	1	2	2.79	3.49	8.57	2.610	75.6	100.7	99.7
3	1	1	3	3.04	3.49	9.41	2.392	71.0	106.0	103.8
3	1	2	1	2.54	3.49	7.78	2.860	79.0	99.2	95.0
3	1	2	2	2.79	3.49	8.57	2.610	72.6	103.6	98.0
3	1	2	3	3.04	3.49	9.41	2.392	67.7	109.0	101.8
3	2	1	1	2.86	3.49	7.78	2.540	75.3	103.6	104.6
3	2	1	2	3.14	3.49	8.57	2.315	69.6	109.8	109.4
3	2	1	3	3.43	3.49	9.41	2.118	65.9	117.0	114.9
3	2	2	1	2.86	3.49	7.78	2.540	73.8	109.2	101.4
3	2	2	2	3.14	3.49	8.57	2.315	67.9	115.3	105.8
3	2	2	3	3.43	3.49	9.41	2.118	63.9	122.4	111.0

Table C.1.: Bulb parameters and wave resistance (as percentage of baseline) of subvariants for $F_n = 0.200$

$F_n = 0.225$				$C_{\nabla PR}$	C_{LPR}	C_{ABT}	$L_{PR}^3/$	$R_W/R_{W-1111} \cdot 100$		
i(δx_{tt})	j(δx_{ti})	k(δz_{tt})	l(S_r)	$\cdot 10^3$	$\cdot 10^2$	$\cdot 10^2$	∇_{PR}	T_{22}	T_{34}	T_{46}
1	1	1	1	1.96	2.68	7.78	1.692	100.0	100.0	100.0
1	1	1	2	2.14	2.68	8.57	1.545	95.0	102.2	101.6
1	1	1	3	2.34	2.68	9.41	1.416	90.1	105.1	103.6
1	1	2	1	1.96	2.68	7.78	1.692	96.9	98.0	102.7
1	1	2	2	2.14	2.68	8.57	1.545	91.5	100.0	104.4
1	1	2	3	2.34	2.68	9.41	1.416	86.2	103.2	106.5
1	2	1	1	2.28	2.68	7.78	1.454	94.8	100.0	105.0
1	2	1	2	2.50	2.68	8.57	1.324	89.5	103.2	107.2
1	2	1	3	2.73	2.68	9.41	1.212	84.5	107.1	109.8
1	2	2	1	2.28	2.68	7.78	1.454	92.0	103.0	105.1
1	2	2	2	2.50	2.68	8.57	1.324	86.3	105.9	107.2
1	2	2	3	2.73	2.68	9.41	1.212	81.0	109.4	109.7
2	1	1	1	2.25	3.09	7.78	2.238	92.6	95.4	96.7
2	1	1	2	2.46	3.09	8.57	2.043	86.9	97.7	98.3
2	1	1	3	2.69	3.09	9.41	1.872	81.4	100.5	100.2
2	1	2	1	2.25	3.09	7.78	2.238	89.7	96.1	97.9
2	1	2	2	2.46	3.09	8.57	2.043	83.7	98.3	99.4
2	1	2	3	2.69	3.09	9.41	1.872	78.0	101.0	101.4
2	2	1	1	2.57	3.09	7.78	1.959	86.8	99.9	103.7
2	2	1	2	2.82	3.09	8.57	1.785	80.9	103.7	106.5
2	2	1	3	3.08	3.09	9.41	1.633	75.5	108.3	109.8
2	2	2	1	2.57	3.09	7.78	1.959	84.6	106.3	102.0
2	2	2	2	2.82	3.09	8.57	1.785	78.4	110.3	104.6
2	2	2	3	3.08	3.09	9.41	1.633	72.8	115.0	107.5
3	1	1	1	2.54	3.49	7.78	2.860	85.8	95.8	97.0
3	1	1	2	2.79	3.49	8.57	2.610	79.6	98.7	99.2
3	1	1	3	3.04	3.49	9.41	2.392	73.7	102.3	101.8
3	1	2	1	2.54	3.49	7.78	2.860	83.2	98.9	96.3
3	1	2	2	2.79	3.49	8.57	2.610	76.7	102.0	98.3
3	1	2	3	3.04	3.49	9.41	2.392	70.7	105.8	100.7
3	2	1	1	2.86	3.49	7.78	2.540	79.7	101.5	104.0
3	2	1	2	3.14	3.49	8.57	2.315	73.4	105.9	107.3
3	2	1	3	3.43	3.49	9.41	2.118	67.7	111.1	111.2
3	2	2	1	2.86	3.49	7.78	2.540	78.1	108.2	101.8
3	2	2	2	3.14	3.49	8.57	2.315	71.5	112.9	104.9
3	2	2	3	3.43	3.49	9.41	2.118	65.7	118.4	108.6

Table C.2.: Bulb parameters and wave resistance (as percentage of baseline) of subvariants for $F_n = 0.225$

$F_n = 0.250$				$C_{\nabla PR}$	C_{LPR}	C_{ABT}	$L^3_{PR}/$	$R_W/R_{W-1111} \cdot 100$		
i(δx_{tt})	j(δx_{ti})	k(δz_{tt})	l(S_r)	$\cdot 10^3$	$\cdot 10^2$	$\cdot 10^2$	∇_{PR}	T_{22}	T_{34}	T_{46}
1	1	1	1	1.96	2.68	7.78	1.692	100.0	100.0	100.0
1	1	1	2	2.14	2.68	8.57	1.545	96.9	100.7	100.9
1	1	1	3	2.34	2.68	9.41	1.416	95.9	101.8	102.1
1	1	2	1	1.96	2.68	7.78	1.692	98.0	97.6	102.1
1	1	2	2	2.14	2.68	8.57	1.545	94.6	98.1	103.3
1	1	2	3	2.34	2.68	9.41	1.416	91.4	99.1	104.7
1	2	1	1	2.28	2.68	7.78	1.454	96.9	98.7	103.4
1	2	1	2	2.50	2.68	8.57	1.324	93.5	100.0	104.6
1	2	1	3	2.73	2.68	9.41	1.212	92.3	101.8	106.0
1	2	2	1	2.28	2.68	7.78	1.454	95.0	100.7	103.8
1	2	2	2	2.50	2.68	8.57	1.324	91.4	101.2	105.1
1	2	2	3	2.73	2.68	9.41	1.212	88.0	102.6	106.6
2	1	1	1	2.25	3.09	7.78	2.238	95.4	95.9	97.9
2	1	1	2	2.46	3.09	8.57	2.043	91.8	96.8	98.8
2	1	1	3	2.69	3.09	9.41	1.872	88.5	98.0	99.9
2	1	2	1	2.25	3.09	7.78	2.238	93.5	96.3	98.8
2	1	2	2	2.46	3.09	8.57	2.043	89.7	97.0	99.7
2	1	2	3	2.69	3.09	9.41	1.872	86.1	98.2	100.9
2	2	1	1	2.57	3.09	7.78	1.959	91.8	99.1	103.3
2	2	1	2	2.82	3.09	8.57	1.785	88.0	101.2	105.0
2	2	1	3	3.08	3.09	9.41	1.633	84.5	103.8	106.9
2	2	2	1	2.57	3.09	7.78	1.959	90.3	104.5	101.9
2	2	2	2	2.82	3.09	8.57	1.785	86.2	106.8	103.5
2	2	2	3	3.08	3.09	9.41	1.633	82.5	109.5	105.3
3	1	1	1	2.54	3.49	7.78	2.860	91.1	96.9	98.6
3	1	1	2	2.79	3.49	8.57	2.610	87.2	98.4	99.9
3	1	1	3	3.04	3.49	9.41	2.392	83.4	100.3	101.5
3	1	2	1	2.54	3.49	7.78	2.860	89.3	99.7	98.0
3	1	2	2	2.79	3.49	8.57	2.610	85.2	101.4	99.3
3	1	2	3	3.04	3.49	9.41	2.392	81.3	103.5	100.8
3	2	1	1	2.86	3.49	7.78	2.540	87.3	101.2	103.8
3	2	1	2	3.14	3.49	8.57	2.315	83.1	103.8	106.0
3	2	1	3	3.43	3.49	9.41	2.118	79.3	108.4	108.5
3	2	2	1	2.86	3.49	7.78	2.540	86.0	106.4	102.3
3	2	2	2	3.14	3.49	8.57	2.315	81.7	109.3	104.3
3	2	2	3	3.43	3.49	9.41	2.118	77.7	112.7	106.7

Table C.3.: Bulb parameters and wave resistance (as percentage of baseline) of subvariants for $F_n = 0.250$

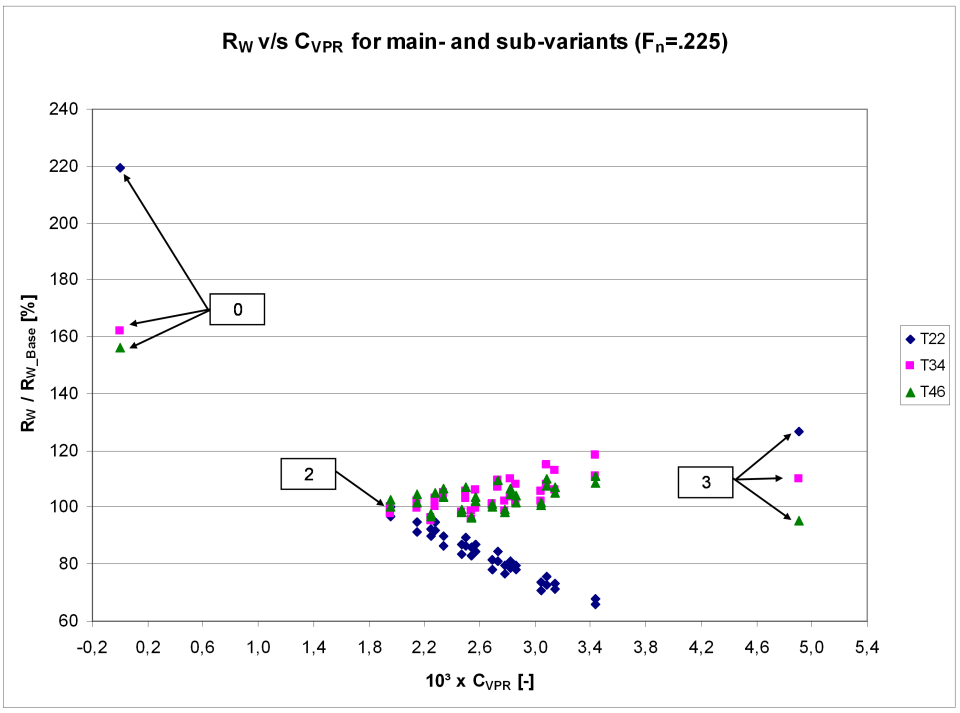

Figure C.2.: Wave resistance (as percentage of baseline) over bulb volume parameter $C_{\nabla PR}$ at $F_n = 0.225$ for main- and subvariants

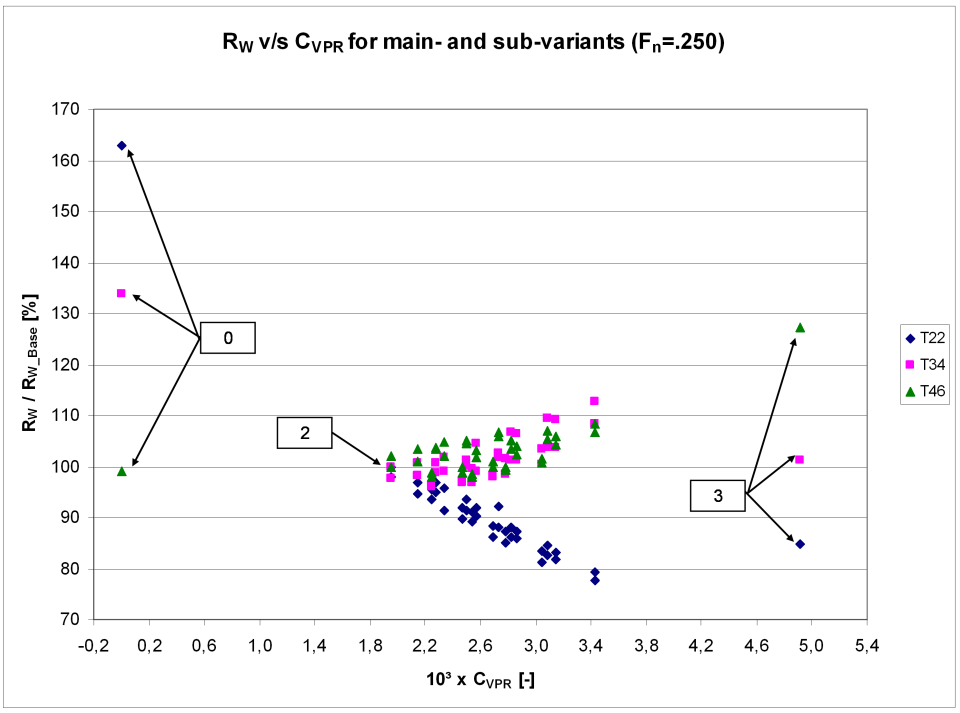

Figure C.3.: Wave resistance (as percentage of baseline) over bulb volume parameter $C_{\nabla PR}$ at $F_n = 0.250$ for main- and subvariants

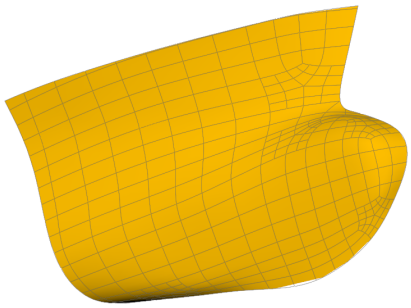

2388.2-1111

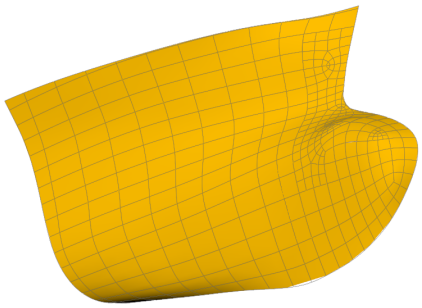

2388.2-2111

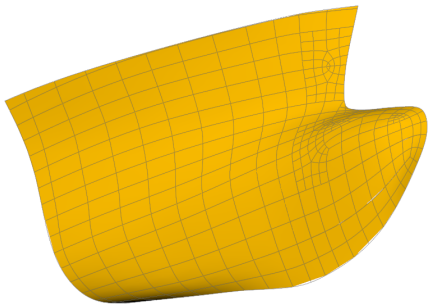

2388.2-3121

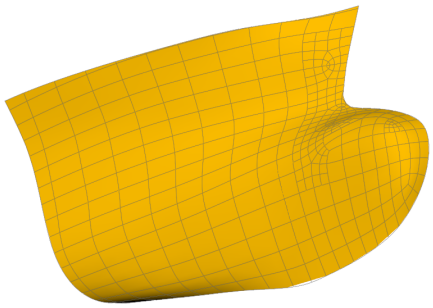

2388.2-3211

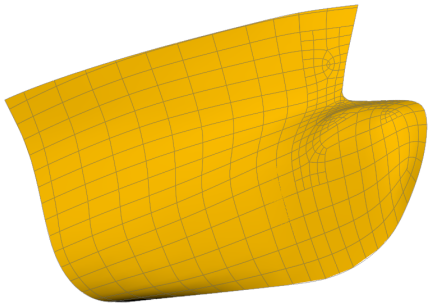

2388.2-3223

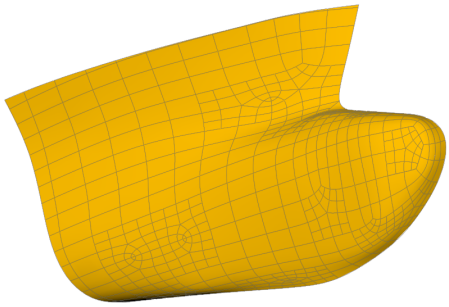

2388.3-1111

Figure C.4.: foreship surface of selected subvariants compared to optimization baseline 2388.2. From left, upper side: variant 2388.2-1111 (baseline), subvariants 2388.2-2111, 2388.2-3121, 2388.2-3211, 2388.2-3223 and variant 2388.3

D. Additional Tables and Diagrams for Chapter 4

	P_B [kW]				n [RPM]	
Engine	L_1	L_2	L_3	L_4	L_1, L_2	L_3, L_4
Ships with $\lambda = 17$:						
MAN 9 S26 MC6	3600	2880	3060	2430	250	212
as percentage of L_1	100%	80%	85%	68%	100%	85%
FE 2388-17.0	3713	2970	3156	2506	169	143
FE 2388-17.2	3512	2810	2985	2371	166	141
FE 2388-17.3	3463	2770	2944	2338	166	141
Ships with $\lambda = 25$:						
MAN 6 S60 MC6	12240	7800	9240	5880	105	79
as percentage of L_1	100%	64%	75%	48%	100%	75%
FE 2388-25.0	12219	7787	9224	5870	134	101
FE 2388-25.2	11564	7369	8730	5555	132	99
FE 2388-25.3	11406	7269	8610	5479	132	99
Ships with $\lambda = 33$:						
MAN 8 S80 MC6	29120	18640	21760	13920	79	59
as percentage of L_1	100%	64%	75%	48%	100%	75%
FE 2388-33.0	28457	18216	21265	13603	114	85
FE 2388-33.2	26947	17249	20136	12881	112	84
FE 2388-33.3	26583	17016	19864	12707	111	83
Ships with $\lambda = 50$:						
MAN 14 K108 ME-C6	97800	77980	93100	74760	94	90
as percentage of L_1	100%	80%	95%	76%	100%	96%
FE 2388-50.0	111119	88600	105779	84941	90	86
FE 2388-50.2	104539	83353	99515	79911	89	85
FE 2388-50.3	95110	75835	90539	72704	87	83

Table D.1.: Engine characteristics for base engines and fictive engines for all ships

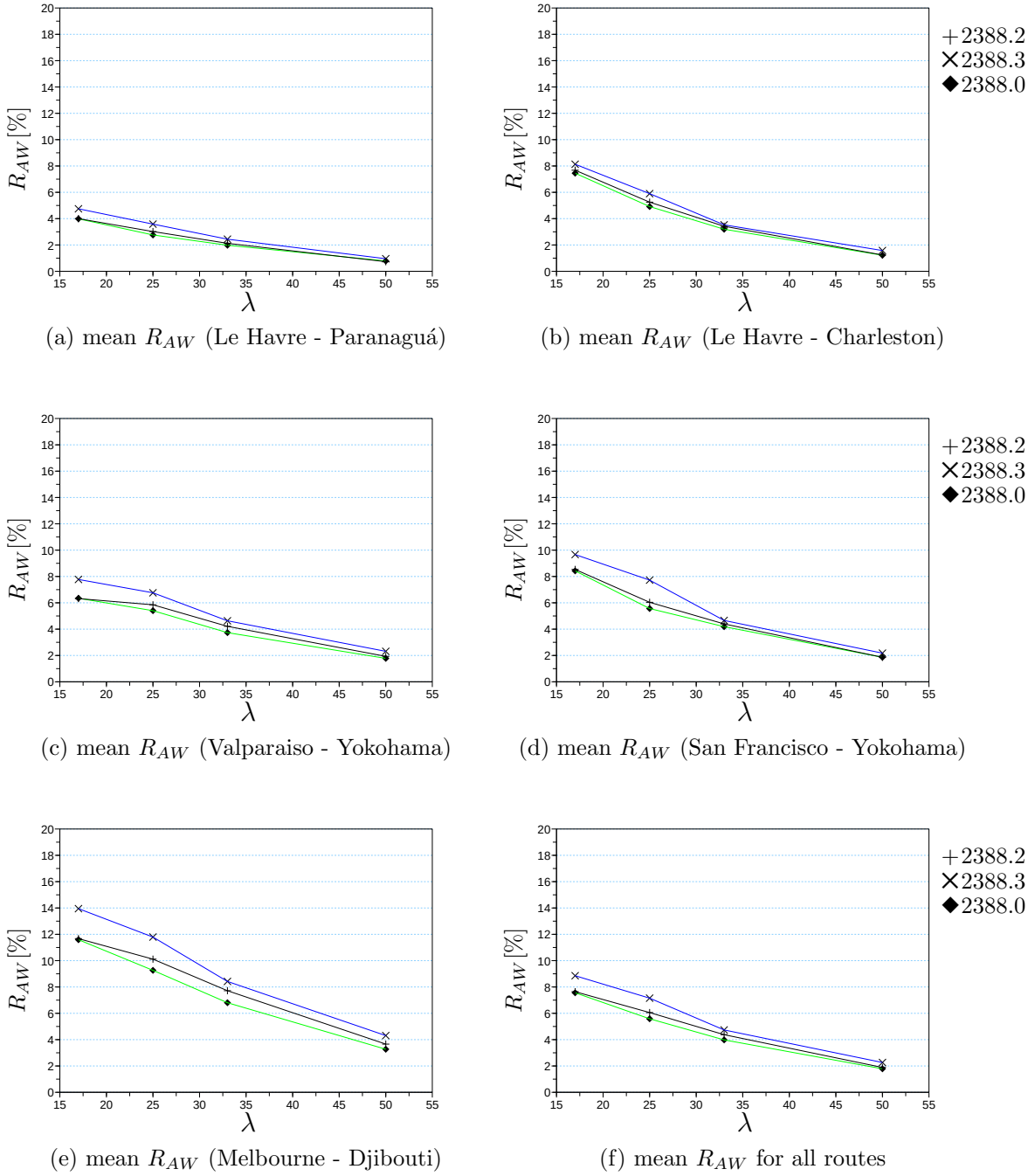

(a) mean R_{AW} (Le Havre - Paranaguá)

(b) mean R_{AW} (Le Havre - Charleston)

(c) mean R_{AW} (Valparaiso - Yokohama)

(d) mean R_{AW} (San Francisco - Yokohama)

(e) mean R_{AW} (Melbourne - Djibouti)

(f) mean R_{AW} for all routes

Figure D.1.: Relative mean R_{AW} of variants 2388.0, .2 and .3 for all considered routes and mean relative mean R_{AW} of all routes as function of the scaling factor λ from simulations with fixed floating condition

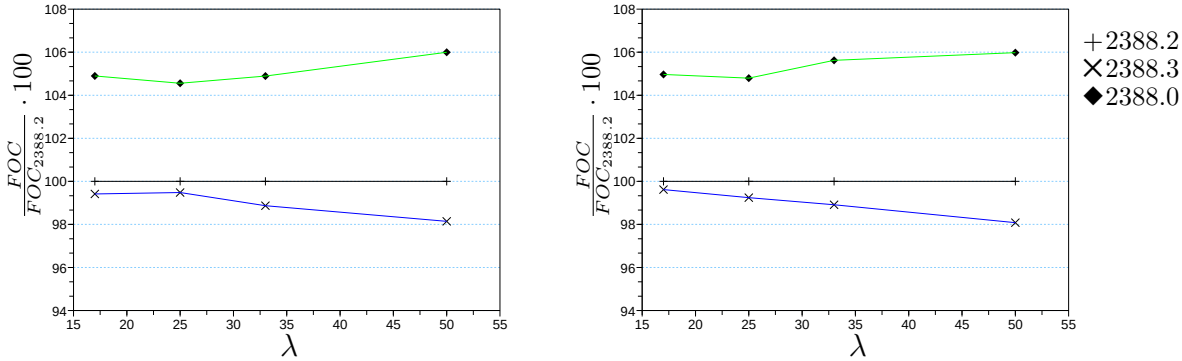

(a) FOC for route Le Havre - Paranaguá (b) FOC for route Le Havre - Charleston

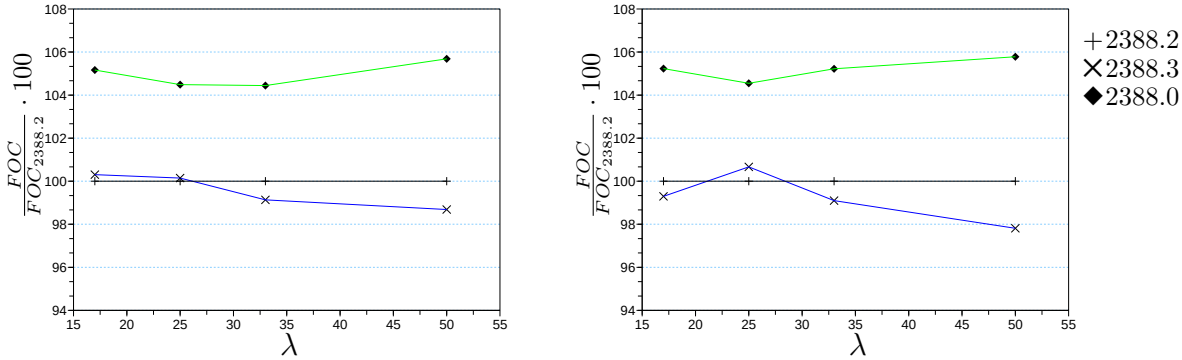

(c) FOC for route Valparaiso - Yokohama (d) FOC for route San Francisco - Yokohama

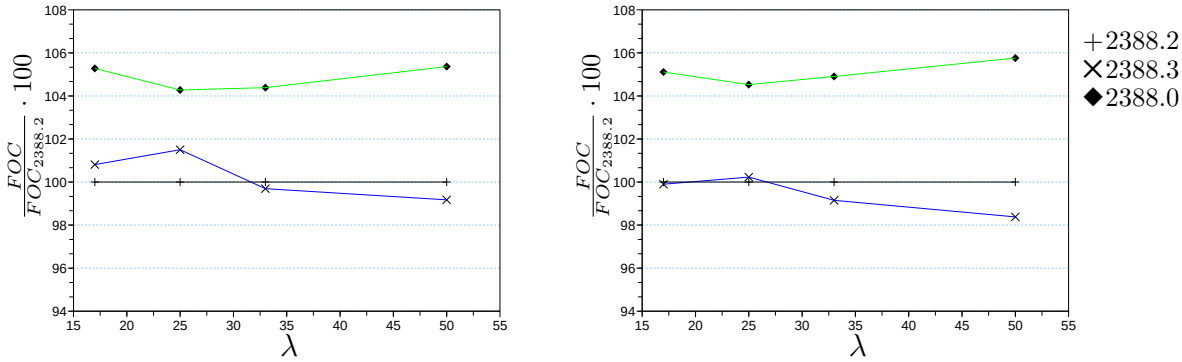

(e) FOC for route Melbourne - Djibouti (f) mean FOC of all routes

Figure D.2.: Relative FOC of variants 2388.0, .2 and .3 with fixed speed and fixed floating condition for all considered routes and mean relative FOC of all routes as function of the scaling factor λ from simulations with fixed floating condition

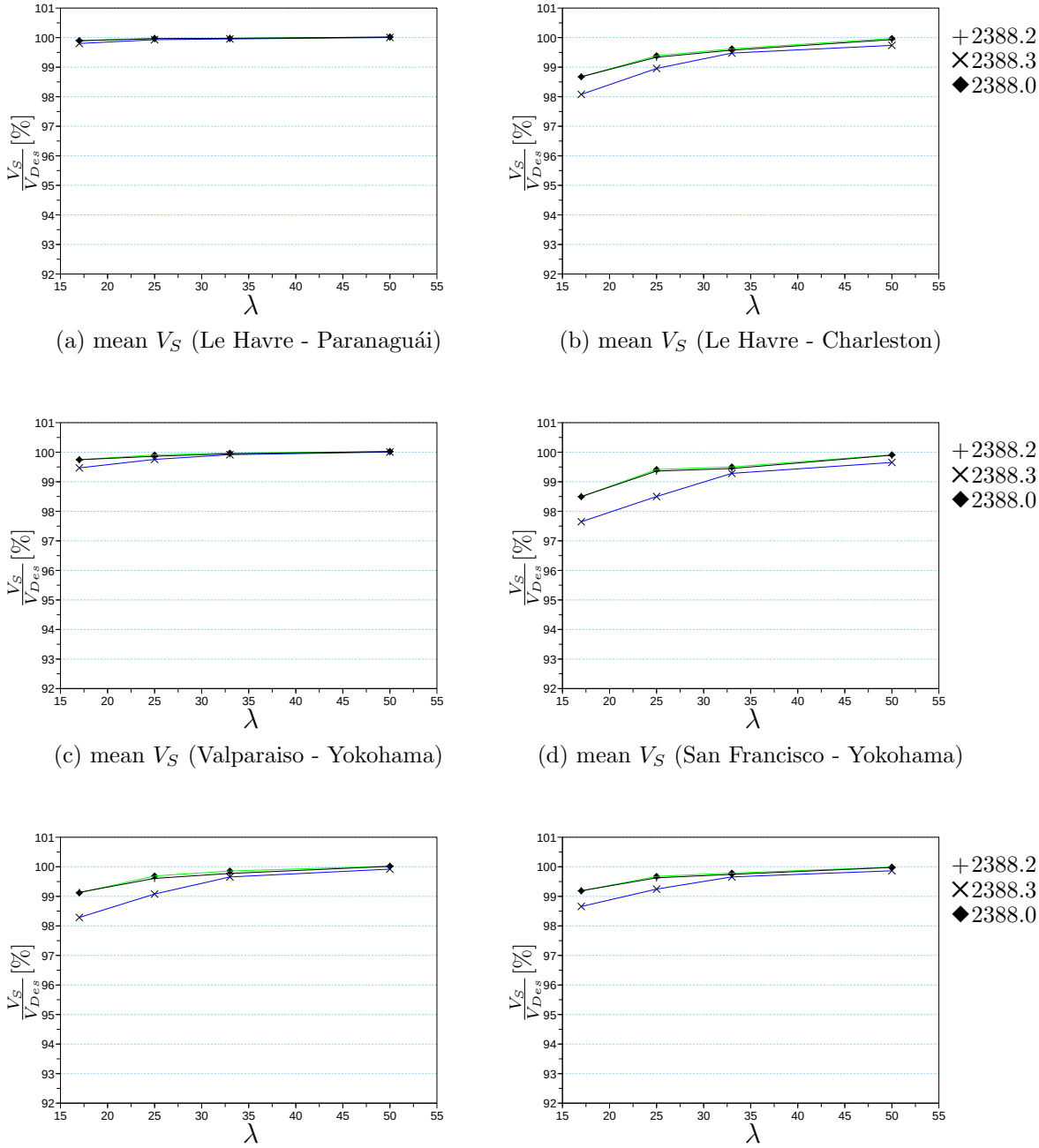

(a) mean V_S (Le Havre - Paranaguái)

(b) mean V_S (Le Havre - Charleston)

(c) mean V_S (Valparaiso - Yokohama)

(d) mean V_S (San Francisco - Yokohama)

(e) mean V_S (Melbourne - Djibouti)

(f) mean V_S for all routes

Figure D.3.: Mean velocity of variants 2388.0, .2 and .3 for all considered routes and mean value of all routes as function of the scaling factor λ from simulations with fixed floating condition

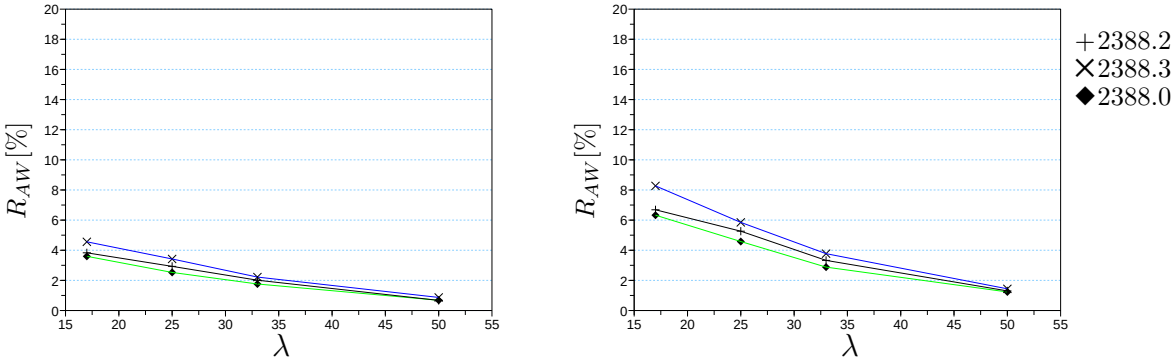

(a) mean R_{AW} (Le Havre - Paranaguá) (b) mean R_{AW} (Le Havre - Charleston)

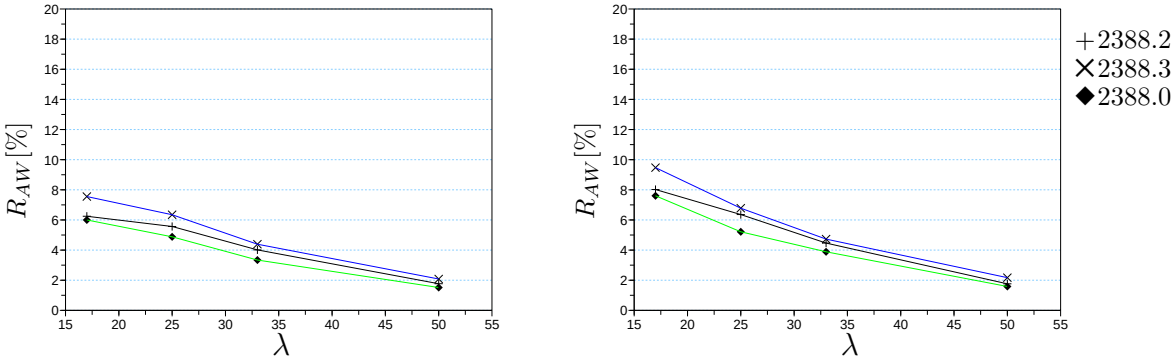

(c) mean R_{AW} (Valparaiso - Yokohama) (d) mean R_{AW} (San Francisco - Yokohama)

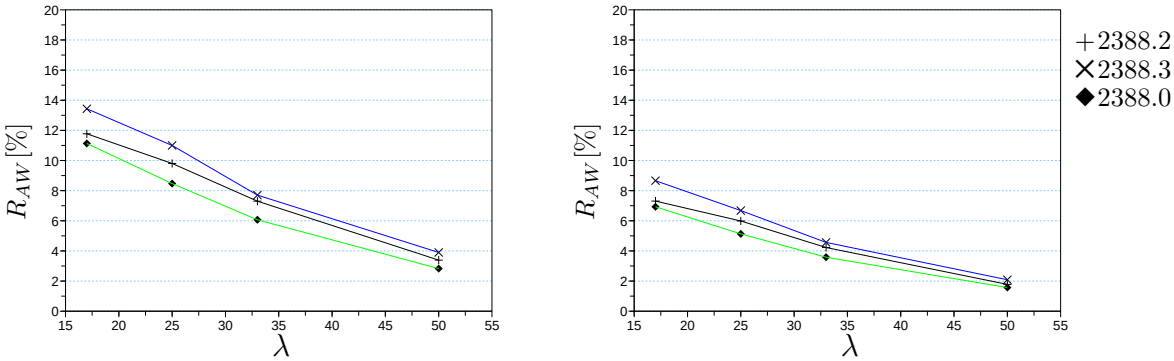

(e) mean R_{AW} (Melbourne - Djibouti) (f) mean R_{AW} for all routes

Figure D.4.: Relative mean R_{AW} of variants 2388.0, .2 and .3 for all considered routes and mean relative mean R_{AW} of all routes as function of the scaling factor λ from simulations with variable floating condition

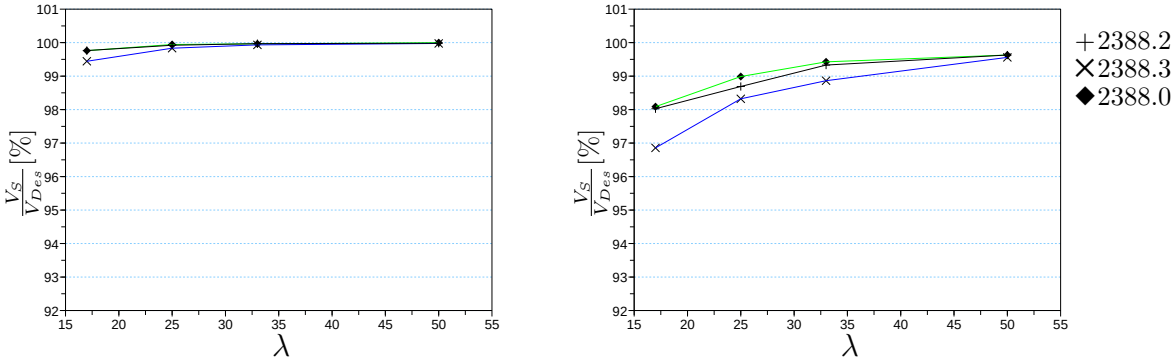

(a) mean V_S (Le Havre - Paranaguái) (b) mean V_S (Le Havre - Charleston)

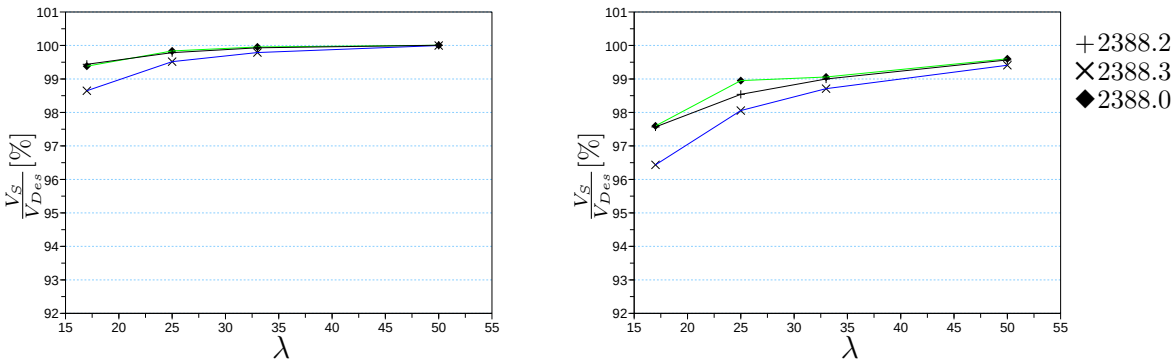

(c) mean V_S (Valparaiso - Yokohama) (d) mean V_S (San Francisco - Yokohama)

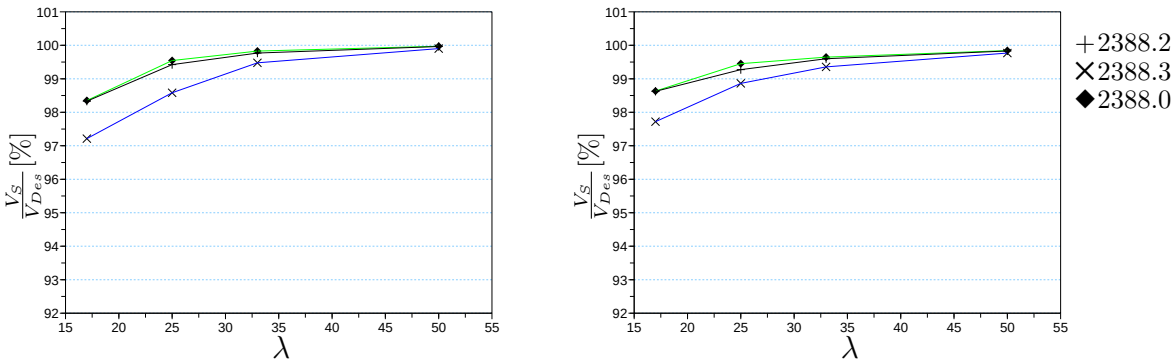

(e) mean V_S (Melbourne - Djibouti) (f) mean V_S for all routes

Figure D.5.: Mean velocity of variants 2388.0, .2 and .3 for all considered routes and mean value of all routes as function of the scaling factor λ from simulations with variable floating condition

E. Additional Tables and Diagrams for Chapter 5

	P_B [kW]				n [RPM]	
Engine	L_1	L_2	L_3	L_4	L_1, L_2	L_3, L_4
Ships with $\lambda = 17$:						
MAN 9 S26 MC6	3600	2880	3060	2430	250	212
parametrized	100%	80%	85%	68%	100%	85%
FE 2388-17.2-1111	3250	2600	2763	2194	163	138
FE 2388-17.2-2111	3230	2584	2746	2180	163	138
FE 2388-17.2-3121	3160	2528	2686	2133	162	137
FE 2388-17.2-3211	3140	2512	2669	2120	162	137
FE 2388-17.2-3223	3080	2464	2618	2079	161	137
FE 2388-17.3-1111	3135	2508	2665	2116	162	137
Ships with $\lambda = 25$:						
MAN 6 S60 MC6	12240	7800	9240	5880	105	79
parametrized	100%	64%	75%	48%	100%	75%
FE 2388-25.2-1111	11230	7156	8478	5395	131	99
FE 2388-25.2-2111	11080	7061	8364	5323	131	99
FE 2388-25.2-3121	10930	6965	8251	5251	130	98
FE 2388-25.2-3211	10850	6914	8191	5212	130	98
FE 2388-25.2-3223	10560	6729	7972	5073	130	98
FE 2388-25.3-1111	10780	6870	8138	5179	130	98
Ships with $\lambda = 33$:						
MAN 8 S80 MC6	29120	18640	21760	13920	79	59
parametrized	100%	64%	75%	48%	100%	75%
FE 2388-33.2-1111	27600	17667	20624	13193	112	84
FE 2388-33.2-2111	27300	17475	20400	13050	111	83
FE 2388-33.2-3121	26700	17091	19952	12763	111	83
FE 2388-33.2-3211	26500	16963	19802	12668	110	82
FE 2388-33.2-3223	25650	16419	19167	12261	110	82
FE 2388-33.3-1111	26300	16835	19653	12572	111	83
Ships with $\lambda = 50$:						
MAN 14 K108 ME-C6	97800	77980	93100	74760	94	90
parametrized	100%	80%	95%	76%	100%	96%
FE 2388-50.2-1111	105500	84120	100430	80646	89	85
FE 2388-50.2-2111	104000	82924	99002	79499	89	85
FE 2388-50.2-3121	101900	81249	97003	77894	88	84
FE 2388-50.2-3211	101200	80691	96337	77359	88	84
FE 2388-50.2-3223	98000	78139	93290	74913	87	83
FE 2388-50.3-1111	100500	80133	95670	76824	88	84

Table E.1.: Engine characteristics for base engines and fictive engines for all subvariants

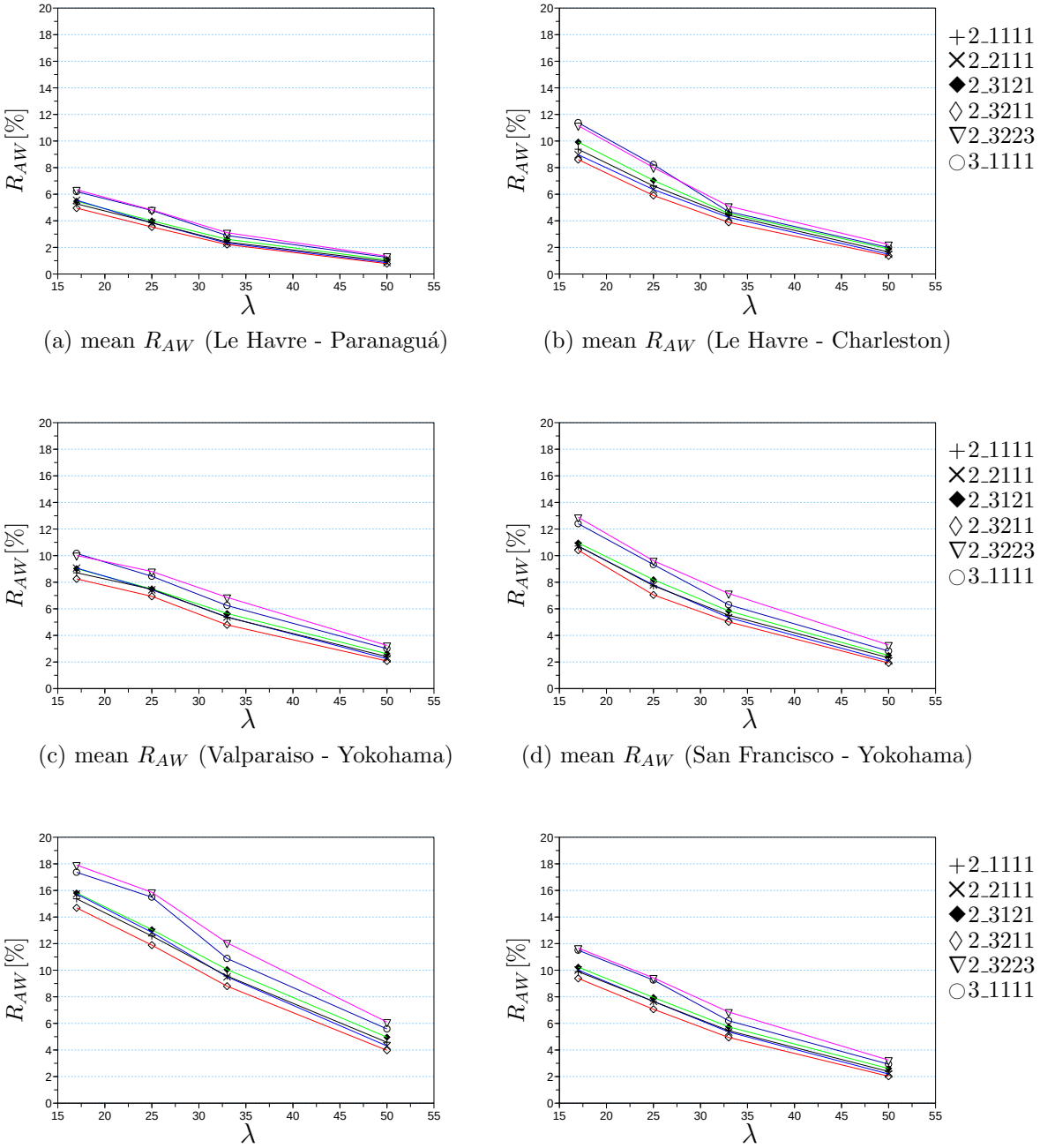

(a) mean R_{AW} (Le Havre - Paranaguá)

(b) mean R_{AW} (Le Havre - Charleston)

(c) mean R_{AW} (Valparaiso - Yokohama)

(d) mean R_{AW} (San Francisco - Yokohama)

(e) mean R_{AW} (Melbourne - Djibouti)

(f) mean R_{AW} for all routes

Figure E.1.: Relative mean R_{AW} for Mod. 2388 with different bulbous bows for all considered routes and mean relative mean R_{AW} of all routes as function of the scaling factor λ from simulations with fixed floating condition

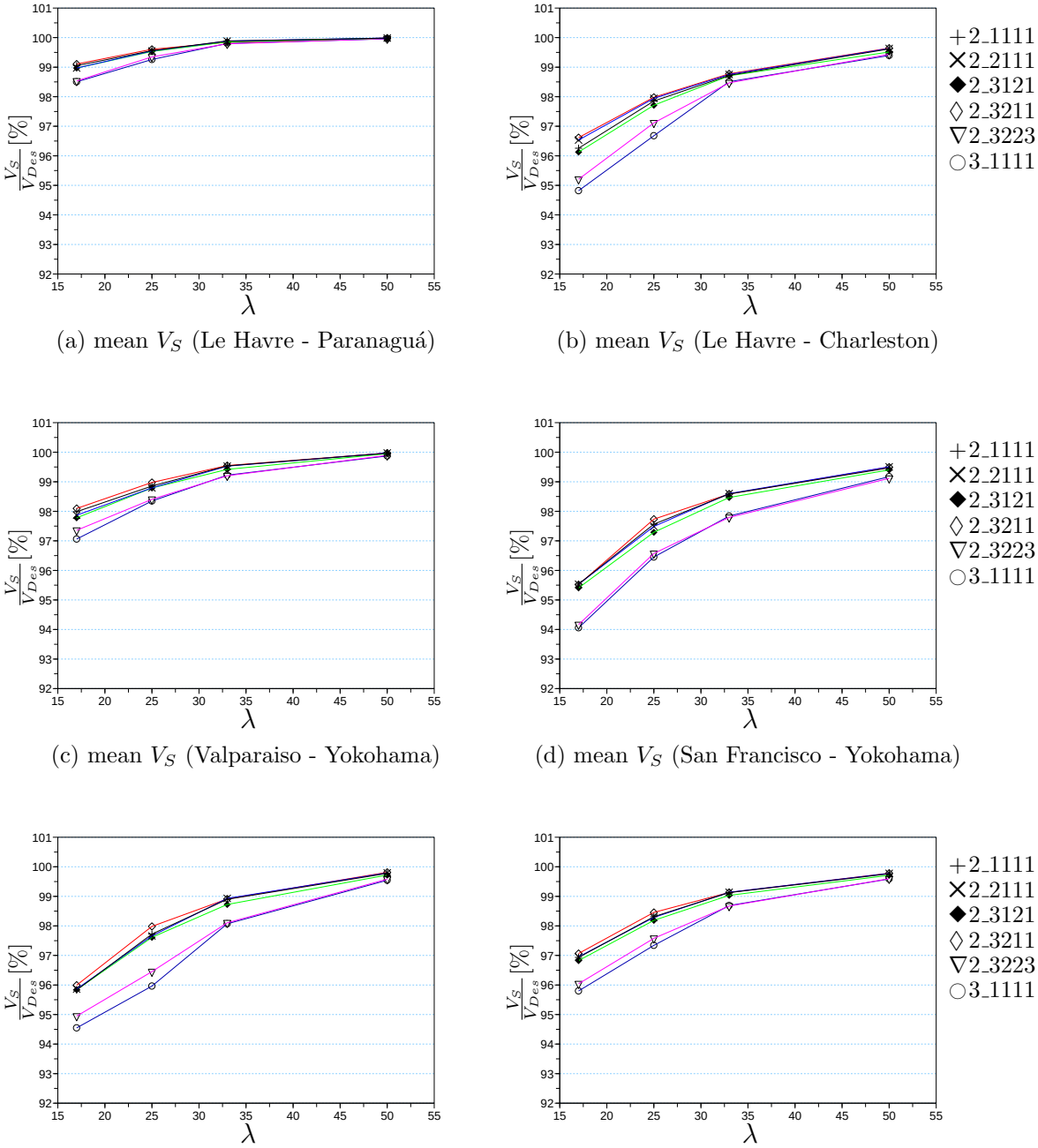

(a) mean V_S (Le Havre - Paranaguá)

(b) mean V_S (Le Havre - Charleston)

(c) mean V_S (Valparaiso - Yokohama)

(d) mean V_S (San Francisco - Yokohama)

(e) mean V_S (Melbourne - Djibouti)

(f) mean V_S for all routes

Figure E.2.: Mean velocity for Mod. 2388 with different bulbous bows for all considered routes and mean value for all routes as function of the scaling factor λ from simulations with fixed floating condition